

Integrated microfluidic devices for rapid DNA amplification applicable to diagnostics and pathogen detection in food



Georgia D. Kaprou

Department of Biology

University of Crete

This dissertation is submitted for the degree of

Doctor of Philosophy

VITA

KAPROU GEORGIA Chemical Engineer, MSc Biotechnology, PhD student

 <https://www.linkedin.com/in/kaprougeorgia>, gdkaprou@gmail.com / (+30)6982478305

EDUCATION

PhD Student, University of Crete, School of Science and Engineering, Greece 2013 - present

Department of Biology, Biosensors Laboratory

Dissertation: “Integrated microfluidic devices for rapid DNA amplification applicable to diagnostics and pathogen detection in food”

Academic Supervisor: Prof. E. Gizeli

Research Supervisor: Dr. A. Tserepi

Main focus: Design, fabrication and evaluation of microfluidic modules with integrated microheaters for nucleic acid amplification suitable for integration in lab on chip platforms addressing food safety, environmental issues and medical diagnostics.

MSc in Biotechnology, University of Edinburgh, United Kingdom 2011 - 2012

Master Thesis: ‘Artificial ecosystem selection of a bacterial community for growth on and degradation of the liquid by-product from Biochar production’

Supervisor: Dr. A. Free

Diploma in Chemical Engineering, National Technical University of Athens, Greece 2004 - 2010

Majored in Food Science and Biotechnology

Diploma Thesis in Applied Biotechnology: ‘Application of stem cells in neurodegenerative diseases’ (grade 10/10)

Supervisor: Prof. F. Kolisis

PROFESSIONAL EXPERIENCE

Research Associate-PhD student 01/2013 – 08/2018

National Centre for Scientific Research “Demokritos”, Institute of Nanoscience and Nanotechnology, Athens

My PhD research is mainly conducted at N.C.S.R. Demokritos in collaboration with the Biosensor’s Lab, Biology Dept, Univ. of Crete. Both institutes are partners in the following projects: **LoveFood** (<http://love-food-project.eu/doku.php>), **LoveFood2market** (<http://lovefood2market.eu/>) & “SYNERGASIA II”, “**LambSense**: Converging Lamb wave sensors with microtechnologies towards an integrated Lab-on-chip for clinical diagnostics” 11SYN-5-502.

Participation in a research program (research associate) 10/2010 - 08/2011

National Hellenic Research Foundation, Unit of Biomedical Applications, Institute for Biological Research and Biotechnology

Study of stem cells: culture and differentiation into different cell types (i.e. umbilical cord stem cells differentiated in bone cells)

Distillery-Winery of Thrace S.A., Komotini, Greece 07 - 08/2008

Q. C. of raw materials & final products

Main duties: Alcohol determination by measuring the density of the distillate & Volatile acids determination by steam distillation followed by titration

National Technical University of Athens – Quality Control of liquefied gases: Collection of gas samples from various gas stations located in the Northern part of Greece 04/2007

LANGUAGES

Greek, English: C2, **French**: B2

*I would like to dedicate this thesis to my loving parents **Manto** & **Demetris**, my siblings **Elpida-Sofia** & **Panos** and my adorable niece **Manto***

*Θα ήθελα να αφιερώσω την εργασία μου στους αγαπημένους μου γονείς **Μαντώ** και **Δημήτρη**, στα αδέρφια μου **Ελπίδα-Σοφία** και **Πάνο** και στην αξιολάτρευτη ανιψιά μου **Μαντώ***

Declaration

I hereby declare that except where specific reference is made to the work of others, the contents of this dissertation are original and have not been submitted in whole or in part for consideration for any other degree or qualification in this, or any other University. This dissertation is the result of my own work and includes nothing which is the outcome of work done in collaboration, except where specifically indicated in the text.

Georgia D. Kaprou

Heraklion, 2018

Acknowledgements

I would like to express gratitude to my supervisors **Dr. A. Tserepi** for welcoming me into the microfluidics team (INN, NCSR Demokritos) and guiding me into the Lab-on-a-Chip field in which I have found my passion and **Prof. E. Gizeli** (Biosensors Lab, Biology Dept., University of Crete) welcoming me into the Biosensors Lab and introducing me to the amazing world of Acoustic Biosensors. Thank you both for your warmth, the countless opportunities, for your generosity, and for being such a positive influence in my life for giving me the opportunity to do my Ph.D. thesis in your labs and your invaluable guidance throughout my PhD, supporting me both scientifically and otherwise.

I would also like to extend my appreciation to **Dr. G. Kokkoris** for performing the numerical calculations which were indispensable and also for being such a great office-mate, and **Dr. G Papadakis** for providing his support and deep knowledge on the biological protocols for the evaluation of the μ devices.

I would like to express my gratitude to **Dr. P. Petrou** and **Dr. S. Kakabakos** for helping and providing useful advice as well as accommodating us in their lab. I would like to extend special thanks to **Dr. D. Moschou** for the expertise transfer especially during my first year, the guidance and insights throughout my PhD and **Dr. S. Chatzandroulis** for the advice and valuable discussions.

Furthermore, I would like to acknowledge **Dr. E. Gogolides** for the support and guidance. I especially thank **Mrs. I. Kefala** and **V. Papadopoulos** for their enormous help with the numerical calculations. Also, I would like to thank all the members of the microfluidics lab and especially **Dr. K. Tsougeni** and **Dr. K. Ellinas** for their help and encouragement.

I would also like to thank **Dr. M. Eck** and **Dr. G. Jobst** from Jobst Technologies GmbH for providing the micropumps, plastic chips, and docking station as well as **Dr. D. Rabus** from Sensor, SAS for providing the SAW chips as well as for their contribution for the LoC platform development.

Very special thanks go to Institute Pasteur and more specifically to **Mrs. A. Hamiot** and **Dr. B. Depuy** for the guidance provided for the biological protocols.

This work would not have been possible without the financial support of the EU projects LoveFood ‘Love wave fully integrated Lab-on-Chip platform for food pathogen detection’ (FP7-ICT) and LoveFood2Market ‘A portable MicroNanoBioSystem and Instrument for ultra-fast analysis of pathogens in food: Innovation from LOVE-FOOD lab prototype to a pre-commercial instrument’ (H2020-EU.2.1.1. - INDUSTRIAL LEADERSHIP - Leadership in enabling and industrial technologies - Information and Communication Technologies (ICT)).



Table of Contents

Table of Contents	ix
Abstract	xiii
Περίληψη	xv
Preface-Structure & Novelties of the work	xvii
List of Figures	xix
List of Tables	xxxi
Abbreviations	xxxiii

Chapter 1 Microfluidics for Life Sciences	1
1.1 Introduction-Why microfluidics? Advantages of miniaturization	1
1.2 Materials-Technology-Fabrication methods	3
1.2.1 Silicon and glass technologies	4
1.2.2 Polymer technologies	7
1.2.3 PCB technology	17
1.2.4 Paper technology.....	20
1.2.5 Sealing.....	23
1.3 Applications	25

Chapter 2 DNA amplification methods & DNA amplification in microfluidic devices 41	
2.1 Introduction	41
2.2 PCR	43
2.3 HDA	44
2.4 RCA.....	45
2.5 RPA	46
2.6 LAMP	47
2.7 DNA amplification in μ -fluidic devices	48

Chapter 3	Biosensors-Detection Schemes	57
3.1	Introduction-General Concepts of Biosensing	57
3.2	Classification of Biosensors	61
3.3	Acoustic wave biosensors	63
3.3.1	Quartz crystal microbalance (QCM).....	64
3.3.2	SAW sensors.....	65
3.3.3	SAW sensors coupled with microfluidics.....	66
3.4	Motivation-Objectives-Novelty of this work	70
Chapter 4	Instrumentation and characterization methods.....	75
4.1	Instrumentation.....	75
4.1.1	Instrumentation for Device Fabrication	75
4.1.2	Surface modification equipment	78
4.2	Characterization equipment.....	79
4.2.1	Testing-Validation equipment	81
4.2.2	DNA amplification equipment.....	86
Chapter 5	Design, fabrication and characterization of DNA amplification devices with integrated microheaters.....	89
5.1	Introduction	89
5.2	Design-Numerical calculations	90
5.2.1	Comparison of fixed-loop CF and SC devices in terms of energy consumption 91	
5.2.2	Re-circulation (Closed-Loop) μ PCR	94
5.2.3	Static PCR & isothermal amplification microdevices	96
5.3	Material selection	98
5.4	Fabrication of DNA amplification microdevices	98
5.4.1	μ heaters	98
5.4.2	Fabrication of DNA amplification μ -devices	103
5.5	Sealing of DNA amplification microdevices	107
5.6	Characterization of DNA amplification microdevices.....	108
5.6.1	Electrical characterization of microheaters.....	108
5.6.2	Thermal behaviour of the microdevices	112
5.6.3	Characterization of Microfluidics	117
5.7	Wall passivation of μ -fluidic devices.....	118
5.8	Conclusions	123

Chapter 6	Evaluation of the DNA amplification microdevices.....	125
6.1	Introduction	125
6.2	Closed-loop continuous flow μ -PCR	127
6.3	Static μ -PCR.....	130
6.3.1	Static μ PCR on PCB	130
6.3.2	Static PCR on PMMA/PCB	131
6.4	Fixed-loop, continuous flow μ -PCR device	140
6.5	HDA μ -device	151
6.6	RPA μ -device	154
6.7	LAMP μ -device.....	156
6.8	Conclusions	160
Chapter 7	QCM-D - Surface functionalization for selective DNA capturing.....	163
7.1	Introduction	163
7.2	Experimental	165
	Acoustic detection protocol	166
7.3	Results and Discussion.....	167
7.4	Conclusions	173
Chapter 8	DNA amplification microdevices in integrated systems	175
8.1	Introduction	175
8.2	Modular integration of the HDA μ device	176
8.3	Integrated platform performing RPA and on-chip detection	183
8.4	Compact, integrated platform for on-chip sample preparation using the LAMP method and SAW detection	187
8.5	Conclusions	199
Chapter 9	Epilogue	201
9.1	Conclusions	201
9.2	Suggestions for future work	203

Abstract

This PhD thesis focuses on the development of low cost and low energy consumption DNA amplification Printed Circuit Board (PCB)-based microdevices, enabling their use even in low resource settings, suitable for integration in Lab-on-a-Chip (LoC) platforms addressing pathogen detection employed in food safety, medical diagnostics, and environmental monitoring.

Both high integrability and low fabrication cost were achieved by selecting PCB as the main substrate and developing fabrication processes compatible with PCB manufacturing. Besides the integration of microfluidics with electronic components such as sensors, PCB allows also the integration of copper microheaters providing the thermal zones necessary for DNA amplification. Therefore, low-cost, mass production amenable DNA amplification microdevices are feasible with the implementation of commercially available, PCB compatible materials and processes proposed for the fabrication of the microdevices within the established PCB industry, thus addressing one of the microfluidics bottlenecks which is their commercialization.

In this thesis, both static and continuous flow DNA amplification microdevices were fabricated and validated employing numerous amplification (isothermal and non-isothermal) methods such as Polymerase Chain Reaction (PCR), Recombinase Polymerase Amplification (RPA), Helicase Dependent Amplification (HDA) and Loop-mediated Amplification (LAMP). Amplification protocols much faster than in conventional thermocyclers (up to more than 20 times) were demonstrated within the developed DNA amplification microdevices, from 2 min –one of the fastest ever reported- to 30 min. The design of the DNA microdevices (based on numerical calculations) assures also low energy consumption (324 J to 4320 J) which can be translated to the independent operation/performance of 65 to 1000 reactions (depending on the DNA amplification method) with a regular power bank of 10.000 mAh (9V).

Such DNA amplification microdevices were for the first time integrated with Surface Acoustic Wave (SAW) biosensors; a LoC platform based on SAW acoustic detection is

demonstrated in this work, performing cell capturing, lysis and DNA amplification on a single chip for the detection of viable Salmonella cells (stemming from artificially spiked milk) within less than 6 h.

In parallel, further improvement of the LoC platform was achieved by investigating methods for wall passivation to prevent biomolecule adsorption on the surface of the microfluidic devices and promote DNA amplification. Bovine Serum Albumin (BSA) 1% proved to better passivate wall surfaces by inhibiting biomolecule adsorption. Similarly, surface functionalization of acoustic sensors (Quartz Crystal Microbalance with Dissipation, QCM-D) for selective DNA binding in complex samples was investigated, paving the way to employ the developed platform with complex matrices. The use of a blocking buffer prior passing the sample improves the discrimination potential between contaminated and control samples when Avidin-Biotin conjugate detection is used.

Περίληψη

Η παρούσα διδακτορική διατριβή επικεντρώνεται στην ανάπτυξη μικροαντιδραστήρων για την ενίσχυση δεσοξυριβονουκλεϊνικών οξέων (DNA) με βάση το υπόστρωμα τυπωμένου κυκλώματος (Printed Circuit Board, PCB) με χαμηλό κόστος και χαμηλή κατανάλωση ενέργειας, επιτρέποντας τη χρήση τους ακόμη και σε περιοχές με χαμηλούς πόρους, κατάλληλες για ολοκλήρωση σε πλατφόρμες μικροεργαστηρίων σε ψηφίδα (Lab-on-a-Chip, LoC) με εφαρμογή στην ασφάλεια τροφίμων, στα ιατρικά διαγνωστικά και στην περιβαλλοντική παρακολούθηση για την ανίχνευση παθογόνων.

Επιτεύχθηκε ταυτόχρονα μεγάλος βαθμός ολοκλήρωσης και χαμηλό κόστος κατασκευής των μικροδιατάξεων αυτών με την επιλογή του PCB ως το κυρίως υπόστρωμα και την ανάπτυξη διαδικασιών κατασκευής συμβατών με την τεχνολογία PCB. Εκτός από την ολοκλήρωση των μικροευστονικών δικτύων με ηλεκτρονικά στοιχεία όπως οι αισθητήρες, το PCB επιτρέπει επίσης την ολοκλήρωση μικροθερμαντικών στοιχείων χαλκού που παρέχουν τις θερμικές ζώνες που είναι απαραίτητες για την ενίσχυση του DNA. Ως εκ τούτου, η χαμηλού κόστους μαζική παραγωγή μικροδιατάξεων ενίσχυσης DNA είναι εφικτή με την χρήση των προτεινόμενων εμπορικά διαθέσιμων υλικών και μεθόδων συμβατών με την τεχνολογία PCB για την κατασκευή των μικροδιατάξεων αυτών στην καλά εδραιωμένη βιομηχανία PCB, αντιμετωπίζοντας έτσι ένα από τα εμπόδια σχετικά με τις μικροευστονικές διατάξεις που είναι η εμπορική αξιοποίησή τους.

Στην παρούσα διατριβή, κατασκευάστηκαν μικροδιατάξεις ενίσχυσης DNA στατικού θαλάμου και συνεχούς ροής και ελέγχθηκαν χρησιμοποιώντας πολυάριθμες μεθόδους ενίσχυσης (ισοθερμικές και μη ισοθερμικές) όπως η αλυσιδωτή αντίδραση πολυμεράσης (Polymerase Chain Reaction, PCR), Recombinase Polymerase Amplification (RPA), Helicase Dependent Amplification (HDA) και Loop-mediated Amplification (LAMP). Πρωτόκολλα ενίσχυσης DNA πολύ ταχύτερα σε σχέση με αυτά που διενεργούνται σε συμβατικούς θερμοκυκλοποιητές (μέχρι 20 φορές) διεξήχθησαν εντός των μικροδιατάξεων ενίσχυσης DNA, με συνολική διάρκεια από 2 λεπτά - μία από τις ταχύτερες που αναφέρθηκαν ποτέ - έως 30 λεπτά. Ο σχεδιασμός (βάση αριθμητικών υπολογισμών) των μικροαντιδραστήρων DNA εξασφαλίζει επίσης χαμηλή κατανάλωση ενέργειας (324 J έως

4320 J) η οποία μπορεί να μεταφραστεί στην ανεξάρτητη διεξαγωγή από 65 μέχρι 1000 αντιδράσεων (αναλόγως της μεθόδου ενίσχυσης DNA) με χρήση συνήθους μπαταρίας ισχύος 10.000 mAh (9V).

Τέτοιοι μικροαντιδραστήρες ενίσχυσης DNA ολοκληρώθηκαν για πρώτη φορά με ακουστικούς βιοαισθητήρες (Surface Acoustic Wave, SAW). Στην εργασία, παρουσιάζεται μια πλατφόρμα μικροεργαστηρίου σε ψηφίδα LoC βασισμένη στην ακουστική ανίχνευση SAW, εντός της οποίας διεξάγεται η δέσμευση και λύση κυττάρων, και η ενίσχυση του βακτηριακού DNA σε ένα και μόνο θάλαμο για την ανίχνευση ζώντων κυττάρων Σαλμονέλλας (που προέρχονται από τεχνητό εμβολιασμό στο γάλα) μέσα σε λιγότερο από 6 ώρες.

Παράλληλα, επιτεύχθηκε περαιτέρω βελτίωση της πλατφόρμας LoC με διερεύνηση μεθόδων παθητικοποίησης των τοιχωμάτων μικροκαναλιών για την πρόληψη προσρόφησης βιομορίων στην επιφάνεια των μικροδιατάξεων για τη βελτίωση της ενίσχυσης DNA. Διάλυμα 1% αλβουμίνης Βόιου ορού (Bovine Serum Albumin, BSA) παρατηρήθηκε ότι παθητικοποιεί με βέλτιστο τρόπο τα τοιχώματα και συνεπώς αναστέλλει την προσρόφηση βιομορίων. Παρομοίως, διερευνήθηκε η επιφανειακή ενεργοποίηση των ακουστικών αισθητήρων (Quartz Crystal Microbalance with Dissipation, QCM-D) για επιλεκτική δέσμευση DNA σε πολύπλοκα δείγματα, ανοίγοντας το δρόμο για να χρησιμοποιηθεί η αναπτυγμένη πλατφόρμα με πολύπλοκες μήτρες δειγμάτων. Η χρήση παρεμποδιστικού ρυθμιστικού διαλύματος πριν την εισαγωγή του δείγματος προς ανάλυση στον βιοαισθητήρα βελτιώνει τη διαχωριστική ικανότητα μεταξύ μολυσμένων και μη δειγμάτων όταν χρησιμοποιείται η ανίχνευση μέσω ειδικής πρόσδεσης Αβιδίνης-Βιοτίνης.

Preface-Structure & Novelties of the work

Advances in microfluidics and biosensors technologies are driving a revolution in various fields such as food safety, environmental monitoring and biomedical research, through the development of the so called Lab-on-Chip (LoC) devices, which could eventually lead to timely diagnosis and thus the prevention of various outbreaks which cause an immense economic burden worldwide. Such LoC platforms are often suitable for low-resource and remote settings providing timely diagnosis of potential health and environmental threats, thus leading to the prompt and efficient prolepsis and/or treatment. The clever integration of microfluidic devices and sensors, automated and precise fluid handling and signal detection in a compact, portable and low cost platform describes the essence of a successful LoC. The ultimate goal of the present thesis is the development of such **an automated bioanalytical platform integrating various modules focusing on DNA amplification and Surface Acoustic Wave detection for the rapid and sensitive detection of foodborne pathogens**. The outline of the present thesis follows the milestones achieved in the course of the experimental work; the chapters are categorized in accordance with the track towards the development of the suggested bioanalytical platform.

More specifically, **Chapter 1** introduces us in the Microfluidics field and the relevant microfabrication technologies employed for the fabrication of microfluidic devices. **Chapter 2** is an introduction to the various nucleic acid amplification methods describing the state-of-the-art in nucleic acid amplification microdevices. As for **Chapter 3**, it reviews the Biosensors field giving greater emphasis on Surface Acoustic Wave sensors and states the objectives of the present thesis. **Chapter 4** describes the experimental instrumentation and methods followed towards the realization of the objectives. **Chapter 5** summarizes the design (aided by numerical calculations regarding temperature uniformity and energy consumption), fabrication (patterning of microfluidics, heaters and robust sealing) characterization (electrical and thermal characterization of μ heaters and fluidic characterization) and discusses concerns encountered and solved during this work. **Chapter 6** concerns the evaluation tests performed for the various DNA amplification microdevices performing numerous amplification methods. **Chapter 7** regards the investigation and evaluation of various surface

modification schemes for selective DNA binding on an acoustic biosensor, a Quartz Crystal Microbalance sensor. The highlight of the present thesis is **Chapter 8** reporting and evaluating the integrated microfluidic platforms for the detection of foodborne pathogens. Finally, **Chapter 9** epitomizes the essential conclusions of the current PhD thesis regarding the DNA amplification efficiency of the various microfluidic devices developed and emphasizes the successful operation of the developed integrated diagnostic platforms. Furthermore, future prospects and suggestions on the evolution of the DNA amplification microdevices and their integration in diagnostic platforms are discussed.

The novelty of the present thesis lies on:

- The seamless fabrication of DNA amplification microdevices on commercially available PCB substrates with integrated Cu resistive microheaters lying at very close distance to the microfluidic network where the amplification takes place, thus offering great thermal contact and low power consumption.
- The validation of the PCB-based DNA amplification devices with four different DNA amplification methods, namely Polymerase chain reaction (PCR), Helicase dependent amplification (HDA), Recombinase amplification method (RPA) and Loop-mediated amplification method (LAMP)
- A novel sealing method using a commercially available and PCB compatible polyimide-based coverlay used in an ultimately different way than the manufacturer offering robust and irreversible sealing of microdevices withstanding both high pressure and temperature (patent pending).
- The proposed fabrication methods which are PCB compatible thus allowing for mass production in the PCB industry reliably and with excellent reproducibility at very low cost.
- Monolithic integration of the microfluidic components, heating elements and other electronic components such as sensors on a common PCB substrate.
- The integration of the aforementioned DNA amplification microdevices with acoustic biosensors incorporated in a surface acoustic wave (SAW) chip.
- Development of a fast and sensitive LoC platform for pathogen detection in complex samples based on SAW sensor employing a label-free detection scheme.

List of Figures

Figure 1 a) Glass wet etching-bulk micromachining, b) microchannels etched by wet etching in glass [12].....	4
Figure 2 Illustration of the etch profile, a) with and without stirring, using an isotropic wet chemical etchant [17] b) anisotropic wet chemical etchant [16].	5
Figure 3 a) Chemical, b) Physical etching [12]	5
Figure 4 Illustration of a surface micromachining process [17]	6
Figure 5 SEM image of a fully released SiC floating membrane realised using PECVD SiC as a structural material and polyimide as a sacrificial layer	7
Figure 6 Classification of plastics [19]	8
Figure 7 Steps involved in the fabrication of polymeric microfluidics	10
Figure 8 (1) Embossing, (2) injection moulding, (3) thermoforming and (4) PDMS casting process.....	13
Figure 9 Device fabrication process: photographs of 4-device arrays (left) and SEMs of the post and channel structure of a device (right) illustrate results of each replication step Patterned SU8 photoresist on a silicon wafer served as a mould to create a negative replica in PDMS (a) to permit pouring and curing of epoxy (b) to create the durable epoxy master mould (c). The master mould formed the microfluidic features in the COC plate under load and elevated temperature through hot embossing (d) [31].....	14
Figure 10 Additive manufacturing classification based on the feedstock type.....	16
Figure 11 a) Four mixing units, b) fluorescent image of the mixing progress within the 3D-printed micromixer.....	17
Figure 12 Paper microfluidics a) photolithography technique, b) an example of a wax-printed 384-zone paper plate after the application of several dyes [62]	21
Figure 13 Bonding methods a) UV-curable adhesive application using capillarity-mediated resin introduction (indirect) [64], b) liquid phase solvent bonding (direct) [65].....	24
Figure 14 Schematic of the process flow for bonding between a PMMA and a PDMS substrate [67].....	26
Figure 15 Segmentation of rapid diagnostics [69]	28
Figure 16 Images/schematics of microfluidics-based PoC tests.....	33

Figure 17 Global PoC diagnostics market forecast.....	36
Figure 18 Microfluidics for PoN testing: roadmap.....	37
Figure 19 Companies that have developed and marketed microfluidic devices for diagnostic applications [87].....	38
Figure 20 a) PCR principle PCR comprising 3 steps: 1: Denaturation (dsDNA unwinds) @95°C, 2: Annealing @ 55°C (primers bind to specific regions on the template), 3: Extension @72°C (DNA polymerase synthesizes the amplicon) [117], b) Schematic diagram of HDA principle 1: A DNA helicase (red star) unfolds the dsDNA which are bound by SSB (grey circles). 2: primers (yellow-green rhombus) bind to the targeted dsDNA region. 3: A DNA polymerase (purple square) synthesizes the amplicon. 4: Amplicons continue to the next amplification round [121].....	45
Figure 21 Principle of RCA method [123].....	46
Figure 22 Schematic of the RPA method [131].....	47
Figure 23 LAMP amplification method [123].....	49
Figure 24 a) i. Schematic illustration of centrifugal LAMP microdevice. ii. Detailed structure of one unit of the microdevice. iii. Assembled microdevice. iv. Schematic illustration of the disassembled microdevice showing four layers[158] b) i. RPA Lab-on-a-disc showing top and bottom plates made of polycarbonate, strip sensors, adhesive layer, and the metal heater. ii. Section of the disc featuring the chambers for cell lysis, isothermal amplification, metering, dilution, and detection. iii. Schematic illustration of the experimental setup [160] c) NASBA μ -fluidic chip for cell concentration, cell lysis and RNA extraction, NASBA amplification and detection[163] d) RCA digital μ -fluidic chip and assay layout. Positions of droplets with reaction mixes are depicted. Mixing of two droplets is illustrated with green arrows with double arrowheads. Mixing of single droplets is illustrated by green arrows with single arrowhead. Magnetic particle transfer between droplets is indicated with red arrows [167], e) i. Polymer-based microfluidic chip with multiple reaction chambers, a toe warmer, and Styrofoam cups; ii. Vent holes on the sides of the Styrofoam cup control the air supply to initiate and maintain the oxidation reaction in the toe warmer; the number of holes controls the temperature of the reaction chamber, f) well-based PCR chip for NA amplification [141], g) closed-loop PCR chip for NA amplification [172], h) continuous flow PCR chip for NA amplification [148].....	54
Figure 25 (a) Illustration of a biosensor comprising a bioreceptor layer on a transducer layer, which captures its target during biorecognition event followed by signal transduction.	

(b) Affinity based biosensors such as antigen-antibody, nucleic acid hybridization involving ribo—(RNA), deoxyribo—(DNA), peptide (PNA), and locked (LNA) nucleic acids, and aptamer based biosensors. (c) Catalytic biosensors involving catalytic probe such as probe-enzyme complex, which converts substrate into a product after binding an analyte leading to signal transduction. (d) Labeled biosensors involve labeling of bioreceptor or probe via various modes, such as covalent bonding, avidin biotin interaction, intercalation, electrostatic attraction. These labeled biosensors are commonly coupled with optical and electrochemical transduction. (d) Label-free biosensors directly transduces biorecognition event by converting a physical change such resistance, mass, and reflectance into electrical signal using techniques such as electrochemical impedance spectroscopy (EIS), quartz crystal microbalance (QCM), and surface plasmon resonance (SPR), respectively [179].....	58
Figure 26 Schematic of biosensor classification schemes	59
Figure 27 SAW propagation: a) Schematic of Rayleigh wave, having both surface-normal and surface-parallel components with respect to propagation direction, b) Schematic of shear-horizontal (SH) Love wave, an added guiding layer keeps most of SH vibration close to surface [198].....	64
Figure 28 Schematic of a SAW sensor	65
Figure 29 a) Love-wave device coupled with a PDMS microfluidic chip forming a microchannel connected to a syringe pump [211], b) schematic of a SAW sensor chip integrated with a PDMS multi-channel microfluidic module [206].....	68
Figure 30 Brass docking station a) with magnets b) screws for applying the force needed, c) PMMA microfluidic module attached to the docking station [205].....	69
Figure 31 a) multi-channel flow cell attached to a polystyrene fluidic connector, b) Picture of SAW docking station with spring for uniform pressure onto the flow cell seals on top of the SAW chip [205]	70
Figure 32 Photograph of (a) the biotesting system and (b) the Love-wave device [223].....	70
Figure 33 a) Karl-Suss MJB 3 STD Mask Aligner, b) Thermo Scientific Heraeus Series 6000 Incubator	76
Figure 34 a) LPKF ProtoMat S series, b) DREMEL® Workstation (220), c) IKA RH basic KT/C Hotplate-magnetic stirrer	77
Figure 35 Carver 3850-Hydraulic heated press	78
Figure 36 a) Nextral Alcatel NE330 RIE, b) Expanded Plasma Cleaner, c) PlasmaFlo Gas Flow	79

Figure 37 a) Fluke 62 MAX Infrared Thermometers, b) Flir A325sc thermal camera, c) FLIR T197214 Close-up Lens (2x)	80
Figure 38 a) GBX Digidrop Contact Angle Measurement System, b) JSM-7401F FEG scanning electron microscope	81
Figure 39 Victor ³ _{TM} , PerkinElmer, plate reader	82
Figure 40 a) Q-Sense E4 Quartz Crystal Microbalance (QCM-D), b) standard gold-coated sensor crystal comprising a quartz disk and three electrodes (one of which consists the active electrode or in other words the sensing area)	83
Figure 41 a) LabSmith liquid handling components, b) Gilson's MINIPULS® 3 peristaltic pump	84
Figure 42 Temperature controllers a) 1 st version, b) 2 nd version	85
Figure 43 2 nd edition of temperature controller under operation	86
Figure 44 a) thermocycler peqStar, b) iClycler, c) Gel electrophoresis system, d) UV transilluminator	87
Figure 45 Unit cells of the a) CF and b) SC devices utilized in the numerical calculations. Dimensions are in mm. c) The material stack of the devices; d is the thickness of the polymeric substrate where the microchannels are fabricated. Dimensions are in μm	93
Figure 46 Energy consumption in CF and SC devices for different substrate thicknesses ...	94
Figure 47 a) The temperature distribution on a cross section at the middle height of the microfluidic channel with the volumetric flow rate equal to i) 30 $\mu\text{l}/\text{min}$ and ii) 60 $\mu\text{l}/\text{min}$. b) image of the same microdevice using an an IR camera.....	96
Figure 48 Numerical control results for thick (1.6mm) PCB, thin (0.8mm) PCB and thin PCB with external Cu layer	97
Figure 49 i) & ii) Caplinq® Al-metalized polyimide sheet, lithographic masks for aluminium resistors with iii) 1000 nm Al thickness (Caplinq®), iv) 300 nm Al thickness (Goodfellow®), realised microheaters on v) plain AL-metalized polyimide sheet vi) AL-metalized polyimide sheet laminated on a rigid PCB substrate.....	99
Figure 50 Fabrication process flow of PI/Al microheaters	100
Figure 51 Fabrication process flow of microheaters on Cu clad	101
Figure 52 a) realised μ -heaters on cu clad, b) realized μ -device on cu clad under operation	102
Figure 53 a) schematic of heater, b) 3D representation of multilayer PCB heater, c) backside of realised heater, d) front side of realised heater	103
Figure 54 Fabrication process flow of the DNA amplification μ -devices	103

Figure 55 Dry photoresist - Pyralux® PC1025 (Dupont®)	105
Figure 56 Fabrication process flow of the microfluidic network by means of lithography..	105
Figure 57 CNC milling process flow	106
Figure 58 Products used for sealing microfluidic devices: a) Polyimide silicon adhesive tape 7176, b) Kapton with silicon adhesive tape7270, c) Clear Polyolefin StarSeal (PCR), d) LF Coverlay	108
Figure 59 Electrical characterization set-up.....	109
Figure 60 Change in resistance for various temperatures (Al heater 300nm)	110
Figure 61 Change in resistance for various temperatures (Al heater 1000nm)	110
Figure 62 Change in resistance for various temperatures (Cu heater on PCB)	112
Figure 63 μ PCR device with microheaters integrated in PCB. a) Back side of the device, b) CAD design of the heaters	113
Figure 64 Back-side of the device. A meandering microheater is shown defining the extension zone.....	114
Figure 65 Thermal image of the back-side of the device between the extension and denaturation zones	114
Figure 66 Image of the back-side of the μ PCR device. The two black lines denote the extent of the transition zone between the extension and denaturation zone.....	115
Figure 67 Image of the front side of the μ PCR device. The two black lines denote the transition zone between denaturation and extension zone.....	115
Figure 68 Image of the front side of the device. The two black lines denote the transition between extension and annealing zone	116
Figure 69 a) custom-made PMMA chip holder, b) Fluidic interconnections (fittings, ferrules, tubing).....	118
Figure 70 Frame-Seal incubation chambers.....	119
Figure 71 Schematic of the process flow for evaluating each modification relatively to hindering biomolecules adsorption	120
Figure 72 Images of the PCB substrates with different modifications while the reaction is over	121
Figure 73 Table with modifications corresponding to the readings of the OD reader.....	121
Figure 74 % Reduction of protein adsorption on PCB surface implementing various surface modifications.....	122
Figure 75 1% BSA solution effect on protein adsorption on different substrates (PCB, LF, PC)	123

Figure 76 Recirculation μ devices. a) μ -device with chambers, b) μ -device with meandering channels.....	127
Figure 77 a) Setup for PCR with circular on-chip-pumping. b) Close-up picture of the on-chip pump with integrated μ PCR channel assembled within the docking station and attached by thermal paste to the 3-temperature-zone PCB heater	128
Figure 78 μ -PCR device operating with a peristaltic micropump from Jobst Technologies GmbH, Germany.....	129
Figure 79 a) Engraved μ -PCR device used in 2T-PCR protocols, b) agarose gel electrophoresis products of on-chip amplification lane 1: DNA ladder, lane 2: on-chip amplification of 8ng short <i>Salmonella</i> DNA, lane 3: of 0.8ng, lane 4: thermocycler amplification of 8ng short <i>Salmonella</i> DNA, c) agarose gel electrophoresis products of on-chip amplification of negative sample and 0.5ng genomic <i>Salmonella</i> DNA.....	131
Figure 80 a) PMMA fluidic with 4 u-shaped chambers, b) PMMA fluidic with 6 u-shaped fluidics, c) PMMA fluidic on top of a thin PCB μ -heater with external Cu layer, d) PMMA fluidic attached to a thick PCB μ -heater	132
Figure 81 2T-PCR temperatures for optimal amplification efficiency	133
Figure 82 Number of 2T-PCR cycles vs. amplification efficiency.....	133
Figure 83 Experimental set-up for temperature measurements	134
Figure 84 2T-PCR ramping protocol without chip holder (40s@95°C, 60s@55°C)	135
Figure 85 2T-PCR ramping protocol without chip holder (35s@95°C, 50s@55°C)	135
Figure 86 2T-PCR ramping protocol with chip holder (35s@95°C, 55s@55°C)	136
Figure 87 2T-PCR ramping protocol with chip holder (40s@95°C, 80s@55°C)	136
Figure 88 Graph representing the 3 cycles of the 2-T PCR protocol followed. The blue line corresponds to power consumption whereas the red line to the temperature profile.....	138
Figure 89 a) agarose gel image comparing the product amplification achieved on chip with the conventional thermocycler, b) agarose gel for various genomic <i>Salmonella</i> DNA concentrations	139
Figure 90 Amplification efficiencies for different DNA concentrations for the μ PCR device and the thermocycler.....	139
Figure 91 Schematic of a continuous flow μ -PCR device (green: μ -fluidic network, khaki: PCB substrate, orange: Cu μ -resistors	141
Figure 92 a) Design of the microheaters, b) design of the microfluidic mask, c) design of the μ PCR device comprising the microheaters and the microfluidic network	142

Figure 93 Sequence of the 250-bp DNA fragment from the exon 20 of the BRCA1 gene. Enclosed in the dashed blue lines, the 157bp amplicon is depicted. Forward primer is highlighted in red color whereas the reverse primer in green.....	143
Figure 94 Image of a continuous flow μ PCR device (non-sealed for clearly viewing the microchannel), employing 30 cycles, fabricated on a PCB substrate with embedded microheaters.....	145
Figure 95 Images of agarose gels depicting DNA ladder (on the left of each image) and 153 bp DNA amplicons (on the right of each image) from the μ PCR device, operating at different flow rates (2.5-15 μ l/min). The negative signal (no DNA template in the cocktail) is also shown in one of the images. No amplification was observed with a flow rate of 20 μ l/min was used.	148
Figure 96 Gel image loaded with PCR products from Plasmid DNA i) supplemented with 1 set of primers, ii) supplemented with two set of primers	150
Figure 97 Gel image loaded with PCR products from <i>Salmonella</i> genomic DNA amplification	151
Figure 98 a) Schematic of an inclined view of the isothermal DNA amplification device, showing the discrete layers of the device, b) polymeric substrate with embedded Cu microheaters (before microfluidic patterning), c) fabricated device before sealing (meandering microfluidic network and meandering microheaters), d) fabricated device after sealing.....	153
Figure 99 Gel electrophoresis image depicting the 113 bp fragments amplified in a microfluidic device (lane 1) and in an eppendorf tube placed in a thermocycler (lane 2) using the HDA isothermal method	153
Figure 100 Gel electrophoresis image depicting the 100 bp ladder (lane 1) and the 88 bp fragments amplified in a microfluidic device (lane 2) using the HDA isothermal method	154
Figure 101 RPA μ -devices: a) 3 U-shaped channels on PMMA, b) 3 meandering channels on PMMA	155
Figure 102 Agarose gel electrophoresis of on-chip amplified RPA product from 1ng genomic <i>Salmonella</i> DNA.....	155
Figure 103 a) meandering PCB amplification device patterned by means of photolithography, b) Gel electrophoresis image depicting the 228bp RPA amplification product for the conventional thermocycler (left) and the PCB device (right) performed at 39°C for 1h.....	156

Figure 104 Figure Lamp μ -devices: a) 6 square-shaped wells on PCB substrate, b) 3 meandering engraved channels on PCB substrate, c) 6 square-shaped well device on PCB substrate sealed with kapton adhesive, d) 4 U-shaped channels on PMMA.....	157
Figure 105 Comparison of LAMP products, lane 1: on-chip positive sample, lane 2: on-chip negative sample, lane 3: i-Cycler positive sample.....	158
Figure 106 Gel electrophoresis images: a) Comparison of LAMP-on chip products of serial dilutions of <i>Salmonella</i> DNA template: lanes L1, L2, L3 and L4 show the products corresponding to 25.000, 2500, 250 and 25 cells respectively, b) LAMP products, lane 1: i-Cycler positive sample, lane 2: on-chip positive sample on passivated PCB, lane 3: on-chip positive sample on untreated PCB	159
Figure 107 Gel electrophoresis image of DNA amplicons for 1000 cells using 0.04% Triton after 30 min of LAMP performed at 65°C within the i-Cycler (lane 2) for 1000 cells using 0.04% Triton after 30 min of LAMP performed at 65°C within the chip (lane 3), for 1000 cells using 0.004% Triton after 30 min of LAMP performed at 65°C within the chip (lane 4)	160
Figure 108 Schematic of the steps followed for the detection of PCR products using whole blood as template sample. A constant flow rate of 20 μ l/min was used for all steps. The sensors can be re-used several times by cleaning the sensors surface by gentle rubbing with a cotton stick. Real time measurements of the amplitude and phase changes were recorded using an Agilent Network Analyzer.	167
Figure 109 Gel electrophoresis image depicting the 524bp amplicons corresponding to the BRCA gene fragment.....	167
Figure 110 Working principle of the PLL-g-PEG surface modification, enabling the ds DNA to bind/interact with the sensors surface while repelling proteins	168
Figure 111 Bar charts showing the measured acoustic signal changes (D and F) and the acoustic ratio ($\Delta D/\Delta F$) caused by the PCR reactions. The bars with the solid colour filling represent the positive samples whereas the bars with the dashed filling represent the negative/control samples.....	169
Figure 112 Schematic for the detection scheme followed to verify the presence of amplified DNA targets a) immobilization of streptavidin/neutravidin layer on the sensors surface. b) blocking/passivation buffer is loaded before the introduction of the PCR reactions. c) i. a positive PCR reaction with ds biotinylated primers and ii. a negative amplification reaction with DNA template but containing biotinylated primers for another target is used as a control.....	169

Figure 113 Real time plots of the three basic steps of the assay. (1) Modification solution (Neutravidin (200 µg/ml)/Streptavidin (20µg/ml) is added in the sensing system with a flow rate of 20µl/min followed by rinsing (2) blocking/passivation buffer is added followed by buffer rinsing with a flow rate of 20µl/min (3) PCR reaction is added followed by buffer rinsing with a flow rate of 20µl/min leading to dissipation shift of 100 Hz approx. On the left panel results regarding the positive PCR are depicted; the right panel shows the results regarding a negative/control PCR (with blood template, but Salmonella primers) leading to a slight change of 20Hz approx. in the dissipation signal. The frequency follows the same trend. Note that frequency data is divided by the harmonic number (7 th harmonic used, i.e., F/7).....	170
Figure 114 Bar charts showing the measured acoustic signal changes (D and F) and the acoustic ratio ($\Delta D/\Delta F$) caused by the PCR mixture in the QCM sensing system modified with streptavidin. Blue colour represents the experiment with the passivation/blocking (wp) step whereas the red colour without (wop). The solid filling represents the positive samples whereas the dashed one the negative/control samples.	171
Figure 115 Bar charts showing the measured acoustic signal changes (D and F) and the acoustic ratio ($\Delta D/\Delta F$) caused by the PCR mixture in the QCM sensing system modified with streptavidin. Blue colour represents the experiment with the passivation/blocking (wp) step whereas the purple colour without (wop). Red colour represents the results obtained with the low template concentration of 0.25µl per reaction with passivation/blocking step. The solid filling represents the positive samples whereas the dashed one the negative/control samples.	173
Figure 116 Integrated microfluidic device for DNA amplification and enzymatic digestion	176
Figure 117 a) Picture of the LoC Green arrows show the direction of liquid flow. The microfluidic device shown has three ports. Port 1 is the inlet to the µHDA. Port 2 is the inlet for the restriction enzyme, which merges with the outlet of the µHDA at the entrance of the SAM micro-mixer (see also Fig. 97). Port 2 is closed in this case. Port 3 is the exit from the micro-mixer. The sample starting position and the exit from the acoustic sensor (waste) are also shown labelled in red, b) Graph presenting the comparison of the acoustic ration indicative of the amplification efficiency within the integrated platform and conventional thermocycler. 15c and 30c are the control reactions for 15 and 30 min respectively. 15s and 30s are the samples containing DNA template.	177

Figure 118 a) Optical image of the cell capture, thermal lysis and DNA purification PMMA module on top of a PCB substrate with 3 embedded heaters, b) design of the PCB microheaters with respect to the cell capture / lysis chip, c) DNA amplification device (μ HDA) with meandering microchannels fabricated by means of CNC	179
Figure 119 Schematic of pumps and valves connected to integrated sample preparation LoC.	179
Figure 120 Agarose gel electrophoresis of <i>Salmonella</i> products from milk spiked with <i>Salmonella</i> bacteria: Off-chip PCR products: (a) Lanes 1 and 2 correspond to cell lysate from 5000 <i>Salmonella</i> cells. Lanes 3 and 4 correspond to purified <i>Salmonella</i> DNA from fraction of the initial cell lysate of 5000 <i>Salmonella</i> cells (1 μ l of sample per 15 μ l of reaction, 40 cycles), (b) Lane 5 corresponds to cell lysate from 500 cells and lane 6 corresponds to purified <i>Salmonella</i> DNA from fraction of the initial cell lysate of 500 cells (1 μ l of sample per 15 μ l of reaction, 35 cycles), (c) Lane 7 corresponds to cell lysate from 100 cells and lane 8 corresponds to purified <i>Salmonella</i> DNA from fraction of the initial cell lysate of 100 cells (1 μ l of sample per 15 μ l of reaction, 40 cycles). ..	181
Figure 121 Agarose gel electrophoresis image of on-chip amplified DNA originating from 500 cells after integration of a bacteria cell capture and lysis microchip, the DNA purification microchip and a HDA microchip	182
Figure 122 a) 3 μ -fluidic chips for RPA amplification on PMMA, b) PCB substrate with 3 embedded resistive μ -heaters, c) multilayer μ -fluidic card fabricated on PET enabling fluidic interconnections among the 3 modules, d) front side of the stack structure comprising the chips assembled, e) back side of the stack	184
Figure 123 Acoustic monitoring of the RPA reaction addition over the neutravidin modified biochip surface (Data acquired by G. Papadakis)	186
Figure 124 a) the disposable plastic card on top of the SAW biochip with two isothermal DNA amplification micro-chambers; and an extended path at the other end that flows over the 4-sensors of the acoustic biochip, b) the PMMA docking station housing one acoustic biochip and the plastic card with the 2 amplification chambers. The plastic card lies above a PCB, where a microheater is fabricated for on-chip heating, (c) schematic representation of the device surface upon addition of a positive sample that contains ds DNA amplicons, cell lysates and LAMP ingredients (left); and as before but for a negative sample, i.e., only the LAMP ingredients (right), d) Normalized amplitude changes for the detection of 10^3 whole <i>Salmonella</i> cells with the LoC system. Each red point represents one of the 19 acoustic measurements [253].	188

Figure 125 Image of the pre-treatment chip.....	189
Figure 126 Image of SAW chip, SENSEOR SAS & GmbH, France.....	190
Figure 127 Types of microfluidic cards developed by Jobst Technologies GmbH and assembly with the pre-treatment chips.....	191
Figure 128 a) Front and b) back side of the docking station developed by Jobst Technologies, GmbH. The sample preparation microfluidic chip is shown with red dye flowing through. c)-d) Two pieces of the opened docking station.....	192
Figure 129 a) LoC platform, b) Picture of the electronic box developed by Sensor SAS, GmbH, France and electronic components inside it	193
Figure 130 Operation Protocol for the LoC	193
Figure 131 SAW functionalization step.....	194
Figure 132 Sample introduction step in the sample preparation chamber	195
Figure 133 Example of LAMP products analysed by gel electrophoresis: lane1: ladder, lane2 positive benchtop control sample w.cells, lane3: positive on chip sample w.cells, lane 4: negative control sample on chip (no captured bacteria), lane 5: negative benchtop control, lane 6: positive benchtop control w. purified <i>Salmonella</i> DNA.....	196
Figure 134 SAW detection step	197
Figure 135 Real-time binding curves of LAMP products flowing sequentially over the 4 channels of the SAW sensors of the LoC. The green and red lines correspond to changes in phase (dB) for the negative and positive samples respectively.	198
Figure 136 Normalized amplitude changes for the detection of 10^3 whole <i>Salmonella</i> cells with the LoC platform. Each red point represents one of the 16 acoustic measurements.	198

List of Tables

Table 1 Common polymer properties [19]	9
Table 2 Polymers used in additive manufacturing of microfluidic devices	16
Table 3 Commercialized 3D printers suitable for microfluidic devices fabrication	17
Table 4 Description of the main advantages and drawbacks for different fabrication techniques of paper-based microfluidic devices [62]	22
Table 5 Overview of thermoplastic bonding technique for microfluidic device [64]	27
Table 6 Rapid diagnostic tests in the market	29
Table 7 Representative examples of μ -PCR devices [140]	51
Table 8 Fully integrated μ -fluidic devices for PoC testing [156]	52
Table 9 Bibliographic TCR values for different thickness of Al thin films [231]	111
Table 10 Theoretical and measured TCR values for Cu and Al films with different thicknesses	111
Table 11 Set-point temperatures and achieved ones (measured with a thermocouple) for different TCRs	117
Table 12 Comparison of the temperatures acquired from the temperature controller, IR camera, and thermocouple	117
Table 13 List of surface modification	119
Table 14 Protocols followed for 2T PCR. Setpoints and duration for each step and measured residence time	134
Table 15 Ramping rates for heating & cooling and duration of 2T-PCR protocols with and without chip holder	137
Table 16 Power requirements of the microheaters for achieving PCR-relevant temperatures	146
Table 17 Residence time in each zone, total PCR duration, 1-cycle duration of the PCR reaction and relative band intensity versus the volumetric flow rate through the μ PCR	148
Table 18 DNA amplification microdevices designed, fabricated and evaluated for efficient DNA amplification	161
Table 19 Operational protocol of integrated HDA-based lab-on-chip platform	180

Table 20 Operational protocol for the LoC validation	185
Table 21 Summary of integrated platforms developed	199
Table 22 Cumulative table with the developed and validated DNA amplification microdevices	202
Table 23 Cumulative table with the developed integrated LoC platforms	203

Abbreviations

AM: additive manufacturing

bp: base pair

CAD: computer aided design

CE: capillary electrophoresis

CF: continuous flow

CLIA: Clinical Laboratory Improvement Amendments

COC: cycloolefin copolymer

ds: double stranded

HDA: Helicase Dependent Amplification

ICAN: isothermal and chimeric primer initiated amplification of nucleic acid

LAMP: Loop Mediated Amplification

LPCVD: low-pressure chemical vapor deposition

LoC: Lab-on-a-Chip

MDA: Multiple Displacement Amplification

MEMS: MicroElectro-Mechanical System

μCP: microcontact printing

μFN: microfluidic networks

μTAS: micro Total Analysis Systems

NASBA: nucleic acid sequence-based amplification

NEAR: Nicking and extension amplification reaction

NIH: National Institute of Health

PC: Polycarbonate

PCB: printed circuit board

PCR: Polymerase Chain Reaction

PDMS: Polydimethylsiloxane

PE: polyethylene
PEEK: Polyether ether ketone
PET: Polyethylene terephthalate
PI: polyimide
PMMA: Poly(methyl methacrylate)
PoC: point-of-care
QCM: quartz crystal microbalance
RCA: Rolling circle Amplification
RIE: reactive ion etching
RPA: Recombinase Polymerase Amplification
SAW: surface acoustic wave
SDA: strand displacement amplification
SL: Stereolithography
ss: single stranded
STL: surface tessellation
Tg: glass transition temperature
Tm: melting temperature
UV: Ultraviolet

Chapter 1 Microfluidics for Life Sciences

In this chapter, a comprehensive definition of microfluidics is given along with the essential advantages of microfluidics. Microfluidic-related fields such as micro-electromechanical systems (MEMS), Lab-on-a-Chip (LoC) and micro Total Analysis Systems (μ TAS) are discussed in conjunction with the respective materials and technologies used in these fields such as silicon and glass, polymer, PCB and paper technology. Furthermore, microfluidic-based applications are presented in combination with the developed and in some cases commercialised devices presented in the literature. Great emphasis is given in biomedical applications (Point of Care, PoC diagnostics) where nucleic acid amplification is indispensable. Last, LoC related challenges and market (commercialization) prospects are discussed.

1.1 Introduction-Why microfluidics? Advantages of miniaturization

Definition and history

Microfluidics is the science and technology of systems manipulating and processing minute amounts of fluids (microliters or nanoliters), employing channels with microscale [1]. It deals with the precise control and manipulation as well as the behaviour of particles and fluids within microchannels in the scale of tens to hundreds of micrometres [2] employing microdevices fabricated with technologies first introduced by the semiconductor industry and later further developed by the field. The fluid phenomena that govern liquids at the microscale are noticeably different from those dominating the macroscale [3].

Microfluidics is a rapidly growing area that has captured great scientific and technological interest. Microfluidics is also considered as a useful tool for chemical, biological and medical applications in miniaturized platforms called Lab-on-a-Chip (LoC), or micro Total Analysis Systems (μ TAS) [3]. The concept of μ TAS was proposed by Manz et al in 1990 [4]

suggesting the incorporation of sample pretreatment, separation, and detection in a single chip. Although, the first analytical microdevice fabricated on silicon, which was a gas chromatographic analyzer, was presented by Terry in 1979 [5]. In 1993 the first micromachined accelerometer (ADXL50) was commercialized by Analog Devices [6].

Advantages of microfluidics

Promoted by the precise manipulation and control of biological particles and its neighbouring microenvironment, this alluring technology holds remarkable advantages compared to conventional macro-scale platforms (e.g. centrifuge, and flow cytometry etc.). Microfluidics is, at its heart, an enabling technology, with an essential goal of enhancing the performance and capabilities of end products [7]. Microfluidics assets include (i) low cost, (ii) fast sample processing, (iii) high sensitivity, (iv) reduction of costly reagent and sample volumes, (v) enhanced portability, (vi) high integration, automation potentially leading to reduced human intervention and error (vii) disposability, (viii) low power consumption, (ix) parallel sample processing leading to high-throughput, and (x) online monitoring and analysis.

Microfluidic flow related phenomena

Microfluidic flow exhibits unique phenomena that can be leveraged to develop microscale devices capable of performing bio-physical processes. Miniaturization is able to expand the capability of existing technologies (i.e. separation) and techniques (i.e. chemical synthesis). This can mainly be attributed to laws of scale for heat transport, diffusion and surface per volume ratio which allow for dramatic increase in throughput [8]. Microfluidic devices possess numerous advantages over conventional devices. As such, mixing time can be reduced to milliseconds in a micro-mixer, heat exchange can be tenfold higher compared to full-scale devices due to the decrease in linear dimensions, surface-catalysed reactions are significantly enhanced due to the increased surface to volume ratio [9]. Accurate manipulation such as separation, focusing, and fractionation of bio-particles is an essential capability of microfluidics. For instance, separation of cells [10] or microparticles or in general biomolecules according to their particular biophysical signatures such as shape, size, deformability, density allows for a broad spectrum of applications such as biological sample preparation (e.g., blood), enrichment or isolation of target cells [11].

Furthermore, high heat transfer ability allows rapid cooling and heating of reaction volume within the microstructured channels and/or chambers. Another crucial advantage of microfluidic devices is their ability to use small reactant volumes. As a result, the amount of expensive and hazardous reagents required is reduced. The aforementioned reduction of reactants leads to the elimination of environmental pollutants produced rendering the microfluidic devices environmental friendly. Moreover high surface-to-volume ratios present in microfluidic devices increase the catalytic efficiency and generally improve processes which depend on interfacial interactions [9].

1.2 Materials-Technology-Fabrication methods

Since the advent of ‘planar’ technology in microelectronics in late 1950s, the improvement of micromanufacturing techniques and the miniaturization limits have never stopped. Silicon was initially proposed for its semi-conducting properties well as the exceptional quality of its oxide. Silicon was also employed for the development of mechanical functions such as micro-motors. Over the last two decades, MEMS popularity has been a driving force for developing new types of microsystems combining mechanical and electrical functions with microfluidic functions (i.e. pumps, valves, microchannels). The introduction of new manufacturing processes and materials was also encouraged in microtechnologies. The glass technology which was enormously employed initially, combining wet etching and thermal bonding is restricted by drawbacks in terms of integration and aspect ratio. Despite the fact that silicon etching is much more established, especially with deep reactive ion etching (DRIE), its incompatibility with capillary electrophoresis (CE) and electrokinetic pumping - both widely used in LoC- renders it a crucial disadvantage preventing its use. Microtechnologies gained versatility by opening up to polymers and their wide range of properties. The microstructuring process has become more flexible, both with micromoulding techniques and the employment of thick photoresists (i.e. SU-8), thus avoiding the expensive etching step and/or the use of aggressive chemicals. In general, the employment of polymers opened up new prospects in terms of micromanufacturing processes, cost and integration. In this section the state-of the-art of the various manufacturing technologies will be described [12].

1.2.1 Silicon and glass technologies

1.2.1.1 Bulk micromachining

Bulk micromachining refers to the method in which structures are defined in the substrate itself. A generic approach of glass wet etching is depicted in Fig. 1. Once the substrate is cleaned, the protective material that will be used during the etching step is deposited (1). A photoresist is spin-coated (2). Using a mask with transparent and opaque areas the resist is exposed to ultraviolet radiation (UV), (3) followed by development (4) where the exposed areas are wiped out (positive resist, see Fig. 1) or endure (negative resist), depending on photoresist's polarity. Next, the protective layer is etched (5) thus removing the resist from the substrate (6). The glass etching step follows (7). Finally, the mask is removed from the substrate (8).

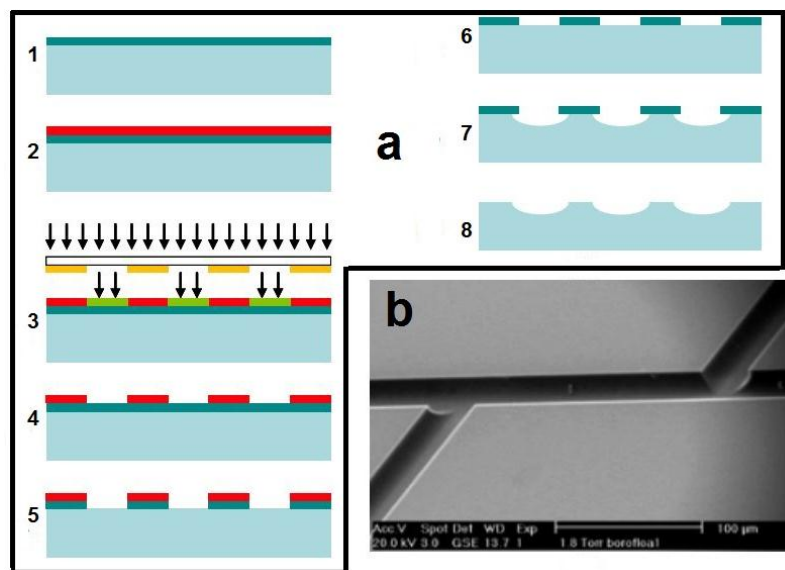


Figure 1 a) Glass wet etching-bulk micromachining, b) microchannels etched by wet etching in glass [12]

The etching process is crucial in bulk micromachining and it is divided in two categories namely wet and dry etching. As for wet etching, it is subdivided in two categories isotropic where the etching rate is the same in all directions and anisotropic where the etching rate differs depending for example on the crystallographic orientation of the substrate material (see Fig. 2).

Wet etching

Typical examples of silicon (wet) etchants are a mixture of hydrofluoric acid, nitric acid and ethanol [13], hydrofluoric acid for glass [14]. The main disadvantage of isotropic wet etching is the difficulty in controlling the profile as depicted in Fig. 2a [15-17]. Anisotropic silicon wet etching (Fig. 2b) [16] is performed in solutions such as potassium hydroxide (KOH) or tetramethylammonium hydroxide (TMAH). This technique is suitable for very thin membrane as well as suspended structures fabrication.

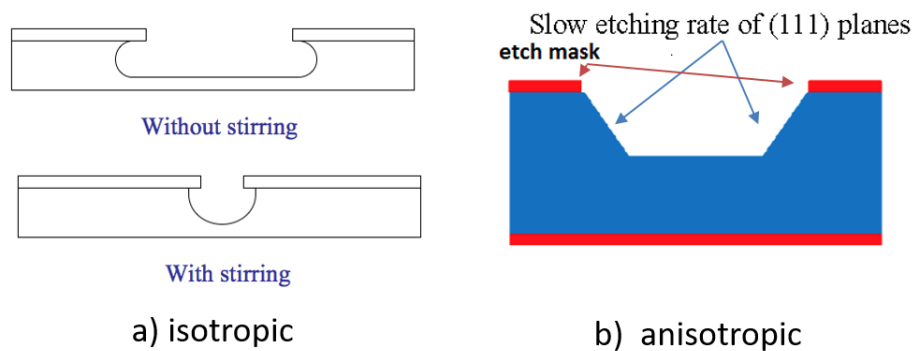


Figure 2 Illustration of the etch profile, a) with and without stirring, using an isotropic wet chemical etchant [17] b) anisotropic wet chemical etchant [16].

Dry etching

Another etching technique is dry etching where substrates get exposed to ionized gases. Two major dry etching phenomena are depicted in Fig. 3.

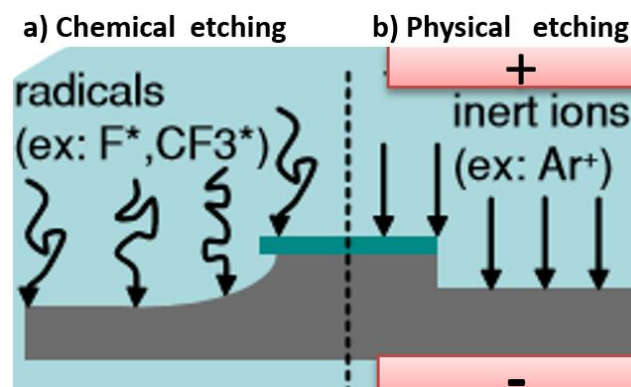


Figure 3 a) Chemical, b) Physical etching [12]

The physical phenomenon resembles to sandblasting at the atomic scale where the sand is substituted by inert species such as neon, helium, argon in an ionized form. Fundamentally, inert species are created in plasma and are accelerated by the electric field generated between two electrodes. The substrate is located to the cathode. In this case the etching is anisotropic, not selective and comparatively slow. The chemical modification is the outcome of the interaction between radicals created from reactive gases (i.e. SF_6 , CF_4) in a plasma form and the substrate's surface. In this case, two competitive phenomena are present, etching and deposition. The dominance of each phenomenon depends on the various parameters used during the process (concentration of gases employed, temperature and pressure). The main advantage of this chemical etching, although it is isotropic, is that it offers higher rates and better selectivity. An alternative to these two types of dry etching is reactive ion etching (RIE) combining the advantages of chemical and physical etching by employing reactive ions accelerated by an electric field. Reactive ionic etching offers faster etching rates, satisfactory selectivity and exceptional anisotropy.

1.2.1.2 Surface micromachining

Another method is surface machining [17] (Fig. 4) in which deposition or growth of thin layers on top of a substrate is used followed by selective etching of them. Contrary to bulk machining, the thin extra layer and not the substrate is employed as a structural material. Typically, the process commences with the sacrificial layer (i.e. silicon oxide deposition by low-pressure chemical vapour deposition (LPCVD)) deposition. Once this first layer is treated by photolithography the deposition of the structural layer follows, usually consisting of LPCVD polycrystalline silicon, and the accesses are defined. At last, etching of the sacrificial layer is performed and the structure is released. This technology can be employed for the fabrication of thin suspended structures.

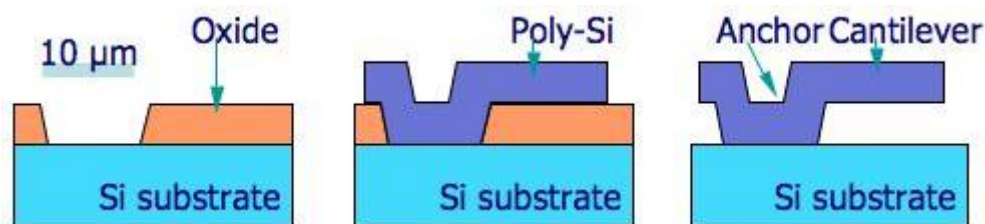


Figure 4 Illustration of a surface micromachining process [17]

Polymers could also be employed as a sacrificial mask layer. They might be deposited directly by spin coating at relatively low temperature. In addition, some polymers are photosensitive. For instance, a 2–4 μm thick layer of polyimide was employed to make the structure depicted in Fig. 5 [18]. Polyimide not only withstands temperatures of up to 400 °C but it is also chemically resistant. The deposited layer is structured by means of oxygen plasma using an aluminium mask.

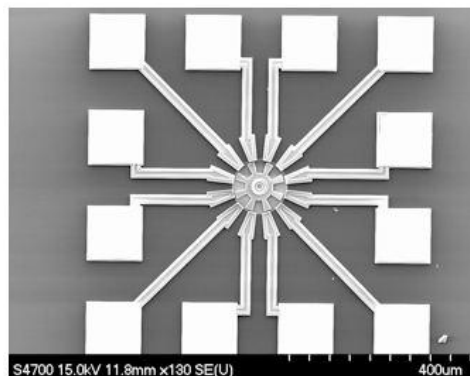


Figure 5 SEM image of a fully released SiC floating membrane realised using PECVD SiC as a structural material and polyimide as a sacrificial layer

1.2.2 Polymer technologies

Numerous polymer-based materials have been employed for micro-manufacturing of different devices. Practically, polymers are long chains produced during a polymerization process. These chains could be either in a partially crystalline or an amorphous arrangement. The behaviour of polymers is governed mainly by the bond type existing between the chains. Thermoplastics, such as polycarbonate (PC) or PMMA, are composed of chains that are poorly bonded together. These polymers soften once they are heated and harden when they are cooled down. A typical characteristic of thermoplastic materials is their solubility in organic solvents. On the contrary, thermosetting polymers are cross-linked, insoluble in organic solvents and they must be structured before the process of cross-linking. For instance, rubber and epoxy resins after vulcanization belong in this category of polymer materials. In Fig. 6 the classification of plastics is presented [19].

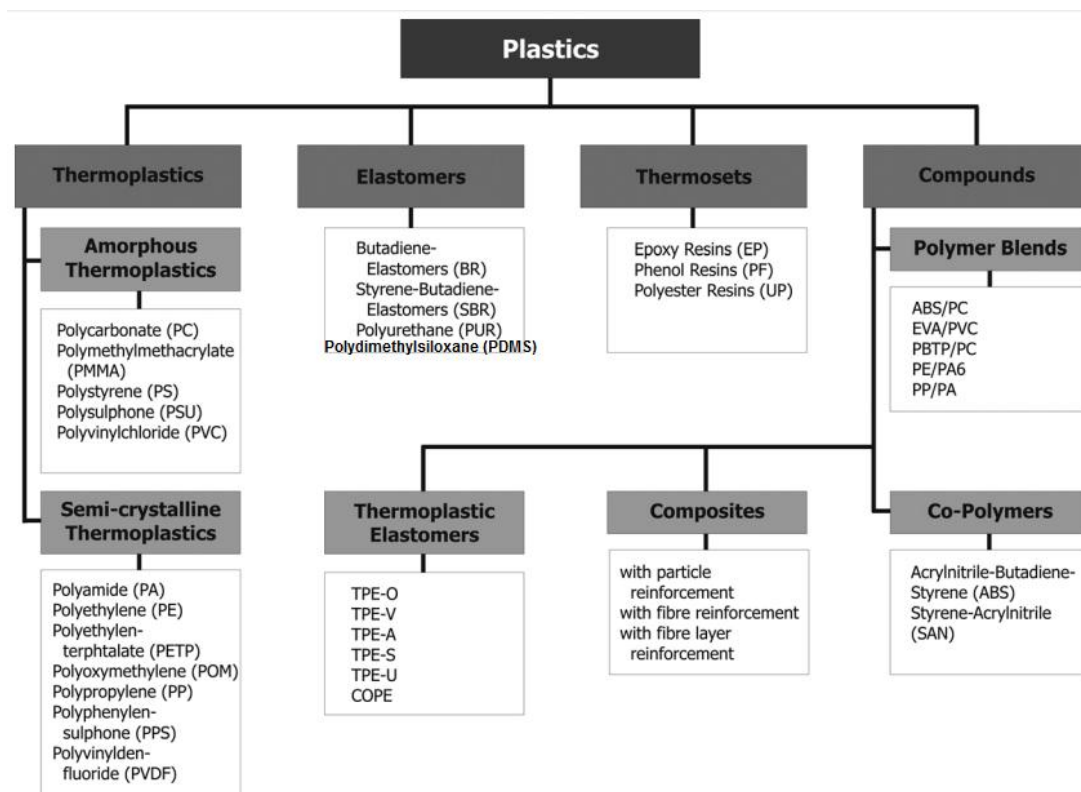


Figure 6 Classification of plastics [19]

Polymers are generally defined by the glass transition temperature (T_g), the melting temperature (T_m) and the decomposition temperature. In Table 1 properties of (such as T_g , T_m , thermal expansion coefficients and structure) commonly used polymers in the microfabrication of devices are presented in comparison with monocrystalline silicon and amorphous glass. These values might vary from one supplier to another thus they are given just for guidance. More relevant information on the polymer-based materials, could be found in well-established text books, such as Young and Lovell [20] and Ward [21].

There is an immense choice of various polymer based materials thus it is easy to apprehend the tremendous interest in incorporating these materials in microfabrication. For instance, polyetheretherketone (PEEK) withstands temperatures of 250 °C and is extremely chemically resistant, while thermoplastics, such as PMMA, PC or cycloolefin copolymer (COC), are optically transparent.

Table 1 Common polymer properties [19]

Name		Tg (°C)	Tm (°C)	Thermal expansion coefficient (ppm K ⁻¹)	Structure
COC TOPAS 5013	Cycloolefin copolymer	140	/	nd	Amorphous
PMMA	Polymethylmethacrylate	105	/	70-77	Amorphous
PC	Polycarbonate	150	/	66-70	Amorphous
PS	Polystyrene	100	/	30-210	Amorphous
POM	Polyoxymethylen	-15	160	80-120	Semi-crystalline
PFA	Perfluoralkoxy copolymer	nd	310	nd	Semi-crystalline
PVC	Polyvinylchloride	90	/	50-180	Amorphous
PP	Polypropylene	-20	170	100-180	Semi-crystalline
PET	Polyethylene terephthalate	80	265	20-80	Semi-crystalline
PEEK	Polyetheretherketone	150	340	50-110	Semi-crystalline
PA	Polyamide	50	260	80-95	Semi-crystalline
PVDF	Polyvinylidenefluoride	40	210	80-140	Semi-crystalline
PI	Polyimide	350	/	30-60	Amorphous
LCP Vectra A950	Liquid crystal polymer	/	280	0-30	Semi-crystalline
Crosslinked SU-8		200	/	50	Amorphous
Crosslinked PDMS Sylgard 184	Polydimethylsiloxane	-128	/	310	Amorphous
Borofloat glass		525	/	3.25	Amorphous
Silicon		/	1414	2.5	crystalline

These polymers are insulators in terms of electricity but they can be modified with proper powders to make them electrical conducting or to modify their magnetic properties. Other advantageous properties of polymers are biocompatibility, biodegrade-ability (i.e. polycaprolactone (PCL)) [22] as well as low cost -which is one of the essential driving forces for moving towards polymers- (i.e. PMMA is 10–100 times cheaper compared to glass).

1.2.2.1 Replication-based techniques

In 2004 Hecke et al presented a great review on the thermoplastics micro-moulding [23]. One of the first micro-moulding examples was presented in 1970 by a Princeton Group [24]. This group reproduced the micrometric patterns by rolling a nickel matrix onto a vinyl tape. In the middle of 1990s the first applications were published. The techniques used were well adapted from established plastic replication technologies [25]. Fig. 7 shows the various steps involved in the replication manufacturing process for micro-fluidic elements.

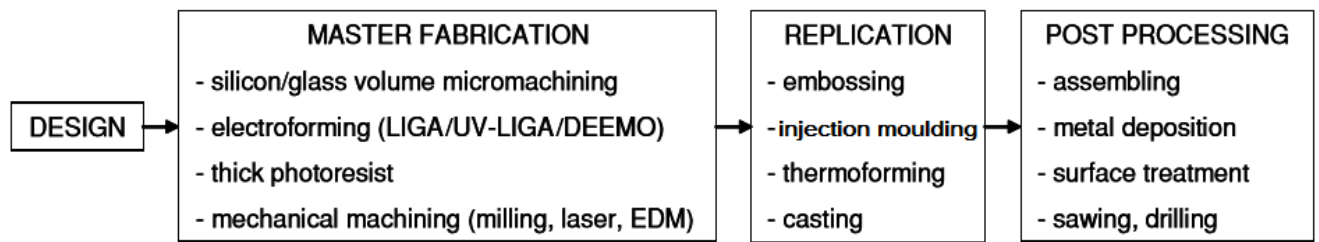


Figure 7 Steps involved in the fabrication of polymeric microfluidics

1.2.2.2 Master fabrication

The replication process starts with the manufacturing of the master that will be employed as a negative for the actual replication. Several conditions should be met relatively to the master fabrication such as: i) low roughness, ($<100\ 100\ \text{nm RMS}$) so as the master removal is facilitated, ii) a slight inclination (if compatible with the application) [23] iii), use of hard and ductile material withstanding several moulding cycles. As a matter of fact, the type of the master material depends both on the replication process and the type of plastic to be used.

i. LIGA technique

One of the best known techniques developed at Forschungszentrum Karlsruhe (FzK) is LIGA, the German acronym for Galvanoformung und Abformung, namely lithography, electroforming and moulding [26]. The master manufacturing process when employing the LIGA technique is described below. The process starts with (a) a thin metal layer deposition (used as an electrode during the electrolytic deposition), followed by x-ray lithography of a thick PMMA layer. Since x-rays are poorly absorbed, quite thick structures could be obtained (tens of μm) with exceptional aspect ratios. However, although exceptional resolution is achieved, this lithography is not cost efficient since synchrotron radiation is required. Once the PMMA is patterned, the electrolytic growth (b) of the metal is implemented, followed by (c) the resist dissolution releasing the master. Nickel or nickel-based alloys (NiCO, NiFe) are commonly employed.

ii. 3D silicon machining

Techniques for 3D silicon machining have also been employed for master fabrication. The trapezoidal architecture achieved by anisotropic wet etching enhances mould removal and the process offers a very low roughness although the geometry is limited. The DRIE process could be employed to achieve straight structures with an exceptional aspect ratio though roughness would be higher for higher etching rates. Since silicon is fairly fragile, it could be mounted on top of another supportive layer or it could be employed as an intermediary, (like the PMMA layer in the LIGA), in order to fabricate a metal master. The DEEMO (deep etching, electroplated, moulding) technique consists of silicon etching by DRIE, followed by the growth of a metal layer by means of electroforming before employing it for replication. The use of conventional photoresists for electrolytic growth of the master is an alternative to the costly x-lithography and the roughness produced during DRIE process. However, the absorption of UV of most typical resists is too high, thus just a few tens or a hundred microns thick layers could be employed [27]. SU-8 is an epoxy-based negative resist produced by Shell Chemical. It is made photosensitive by adding triarylsulfonium salt. SU-8 was developed by IBM around the 1990s, and it can be employed to achieve structures larger than a millimetre thick offering aspect ratios that were only feasible by x-lithography. Since the process cost was dramatically reduced by using a traditional aligner rather than a synchrotron, it is usually called the UV-LIGA or the ‘poorman’s’ LIGA. SU-8 could also be employed on a silicon substrate as a master. Despite such a structure being suitable for prototyping, it cannot withstand many (just a few tens) thermal cycles, whereas metal components can withstand thousands. This can be attributed to the difference between the thermal expansion coefficients of silicon and SU-8 and silicon (factor of ten) [28].

iii. Milling techniques

Conventional milling techniques could also be employed for resolutions in the order of 50–100 μm . For example, masters could be fabricated with CNC (Computer Numerical Control) machining, though the roughness measured on the walls is relatively high (approx. 200 nm). Less rough structures could be achieved with diamond cutters, where the smallest possible diameter for this type of tool is 200 μm thus restricting usage [23]. Steel tools could be employed for smaller dimensions, compromising though the surface condition. At last, laser machining seems to be a quite promising alternative both in terms of resolution and the

material that could be processed [29]. Furthermore, these techniques offer good control over the angle of the walls, which is hard to achieve or even impossible with the other previously mentioned methods.

1.2.2.3 Replication techniques

Hot embossing

Hot embossing is the replication technique most commonly employed in microtechnology. As depicted in Fig. 8(1), a thermoplastic sheet is treated under heat (above its T_g) and vacuum. Following, the assembly is cooled down and the formed structure is detached from the mould.

Injection moulding

On the other hand, for industrial usage the most frequently employed and best known technique is injection moulding depicted in Fig. 8(2). The so-called variotherm process which is mainly used for macroscopic structuring consists of the following steps. First of all, the tool along the microstructured master is heated above the T_g of the thermoplastic and put under vacuum. Afterwards, the polymer is heated and injected. Finally, the formed part is stripped off the mould after being cooled down. What makes the cycle of variotherm process much shorter than the embossing cycle and thus favourable for most macroscopic format production is the fact that the polymer is constantly heated above its T_g . Nonetheless, embossing machinery is much simpler, rendering it more convenient for small and medium production and for research purposes.

Thermoforming

Last but not least, thermoforming, depicted in Fig. 8(3), is another replication technique used at the macroscopic scale [12]. A thermoplastic thin layer is clamped into the tool under vacuum, and the temperature is increased. Then a pressurized gas brings the thermoplastic film in contact with the patterned mould. Finally, the assembly is cooled and the mould is withdrawn. Thermoforming cannot be employed to achieve large aspect ratios due to the inability of the polymer to be heated extensively. Controlled heating is needed to prevent the permeability increase once the gas blows it into contact with the master.

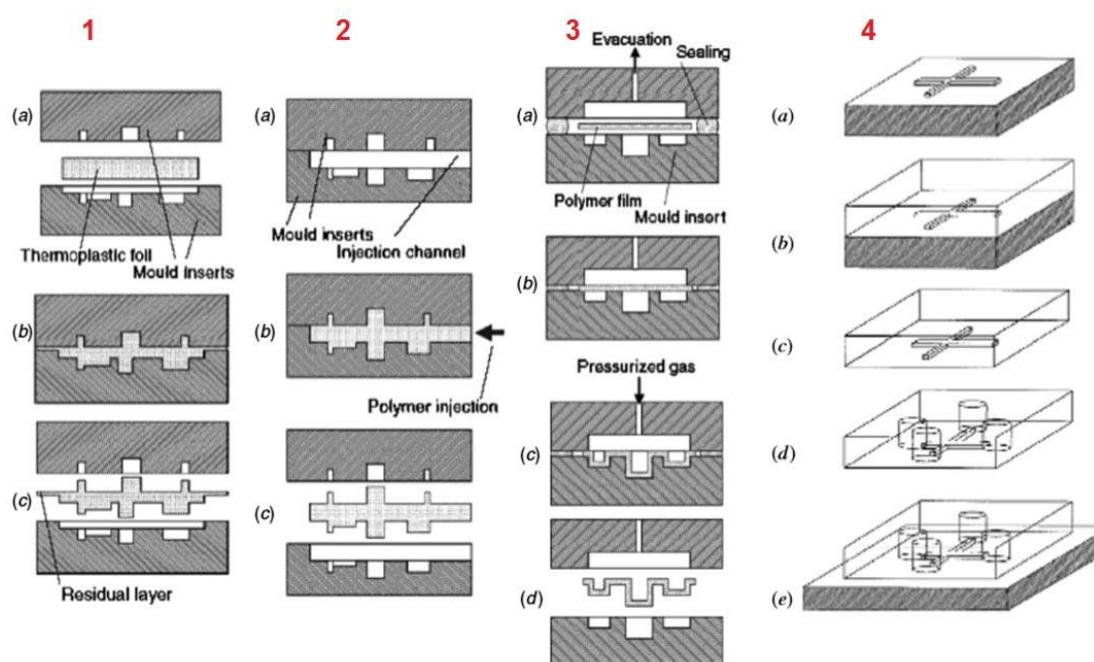


Figure 8 (1) Embossing, (2) injection moulding, (3) thermoforming and (4) PDMS casting process

Casting

The most common replication technique employed in microfluidics currently is undoubtedly PDMS casting (Fig. 8(4)) [30]. The process initiates by the mould manufacturing, usually by means of bulk silicon machining or by thick SU-8 photolithography (a). A mixture of silicone rubber and a cross linking agent is poured on the mould (b). After cross linking, PDMS is simply detached from the substrate (c), holes (inlets/outlets) are created, usually with a part holder (d), which is then transferred onto another piece of PDMS (e).

G M Whitesides initially proposed this moulding method for advanced lithography techniques such as micromoulding in capillaries' (MIMIC), 'microcontact printing' (μ CP) [31, 32], IBM also employed the same method for 'microfluidic networks' (μ FN) [33]. The main advantage of casting technology is its ease of implementation since neither tooling is needed nor process development for conditions fine-tuning (temperature, pressure). The mould is destroyed less rapidly than in the aforementioned techniques since the thermal cycle is frequently lower and peeling off is straightforward considering PDMS is an elastomer. This attribute also facilitates the formation of a conform contact to another substrate (i.e. glass or silicon plate, another PDMS piece). This property renders it extremely easy to seal PDMS systems since what is needed is to cover the open structure with an adequately flat substrate

to create a reversible assembly due to Van der Waals forces. Excellent transparency, biocompatibility, and the exceptional replication quality (nanometric scales) of PDMS are some of its key characteristics. All these assets indicate that PDMS is a suitable material for laboratories that do not own advanced technological equipment.

In Fig.9 the fabrication process of a device (master fabrication and replication) employing hot embossing on COC is depicted.

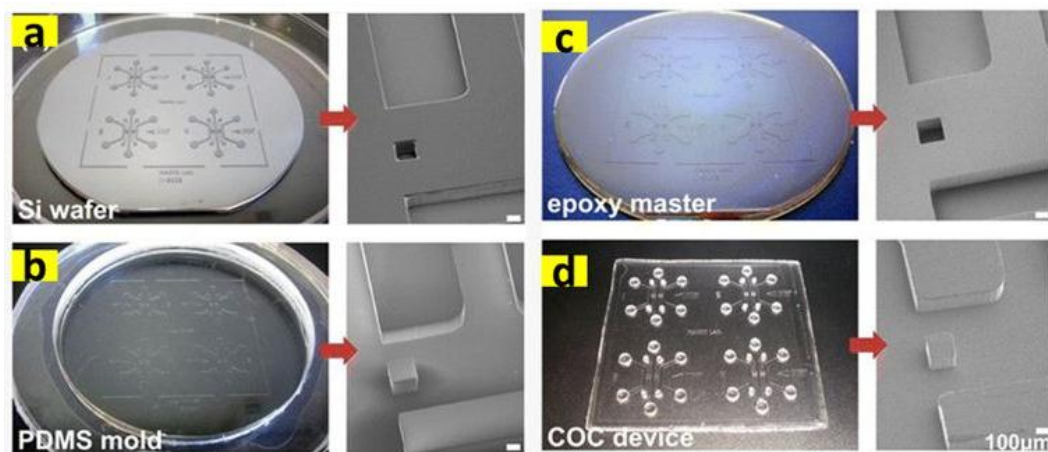


Figure 9 Device fabrication process: photographs of 4-device arrays (left) and SEMs of the post and channel structure of a device (right) illustrate results of each replication step. Patterned SU8 photoresist on a silicon wafer served as a mould to create a negative replica in PDMS (a) to permit pouring and curing of epoxy (b) to create the durable epoxy master mould (c). The master mould formed the microfluidic features in the COC plate under load and elevated temperature through hot embossing (d) [31].

1.2.2.4 Direct methods

3D printing

In the past decade, a relatively new technology has witnessed enormous growth, namely 3D printing and it has achieved to penetrate many different aspects of our lives. Currently, cutting edge 3D printers can fabricate objects in the micrometre scale. Thus, the fabrication of microfluidic devices employing 3D printing has been made feasible. The highest resolution achieved at the moment is at the nanometre scale, and still continues to drop.

Taking into account that the geometric complexity is not a consideration for 3D printing, innovative 3D lab-on-a-chip and microfluidics systems that are otherwise infeasible to fabricate with conventional 2D microfabrication technologies have started to break through. 2D microfabrication techniques are enormously constrained by the complex 3D structures, thus limiting researchers' ability to fabricate complex 3D flow routes with irregular cross sections and of various sizes and directions. Luckily, the rapid advancement of 3D printing technology, also referred as additive manufacturing (AM) technology, made it possible to circumvent this problem [32].

Stereolithography

In 3D technology, the structure to be fabricated is sliced into various 2D cross sections, and thus, the fabrication becomes a simple layer-by-layer fabrication process. Stereolithography (SL) technology is the precursor of 3D printing, initially introduced by the US company 3D Systems. In stereolithography, a polymeric resin is treated with UV light to shape a 2D cross section of a single layer of the end device. Following, a similar procedure takes place successively to build up the remaining layers of the desired 3D structure, and the uncured resin can be removed, leading to the final structure [33]. Compared to soft lithography and other conventional fabrication techniques which are tedious and slow, stereolithography provides an automated fabrication technique of 3D geometries which is more cost-efficient, faster and more convenient [34]. Various stereolithographic approaches can be found in the literature [35-37].

Unlike conventional manufacturing technologies, AM technology is the outcome of the development of computer aided design (CAD) technologies. The process of 3D printing initiates with the design of a CAD file to specify the geometry of the part to be fabricated, which in turn is converted to a surface tessellation (STL) file providing a polygonal representation of the surface geometry. Afterwards, the file is transferred to a computerized system, where the digital representation is "sliced" into virtual horizontal layers of different thicknesses by specialized computer software. The manufacturing platform then builds each layer individually. Each successive layer is located on top of the previous one. This bottom-up build process is repeated until the module is completed. In 3D printing technology, there is no constrain in product design for manufacturing and assembly thus; the freedom provided enormously advances product innovation. A straightforward approach for AM processes

classification is according to the type of feedstock material employed [38]. By utilising this approach, AM processes can be classified into solid-based processes, liquid-based processes and powder-based processes as shown in Fig. 10.

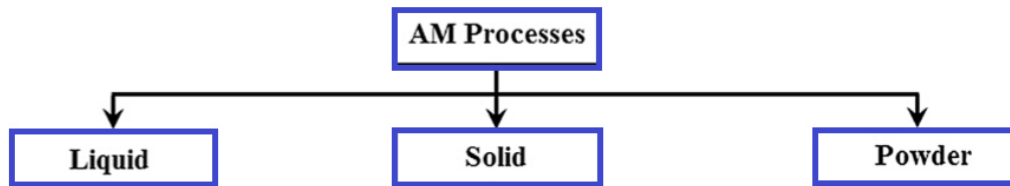


Figure 10 Additive manufacturing classification based on the feedstock type

Polymeric materials, paper laminates and waxes were the first materials employed for AM processes. At a later time, attempts have been focused in enhancing mechanical properties by introducing composites, ceramics and metals. For example, different lightweight structures [39, 40] and composites have been introduced to fabricate functional products employing AM technologies [41]. The selection of materials for AM is highly dependent on the fabrication technique. Table 2 presents examples of polymers and their properties employed in additive manufacturing of microfluidic devices. Nevertheless, many AM technologies suffer from the limited choice of materials available for the production of functional devices in terms of biocompatibility, transparency, mechanical endurance. In Fig. 11 an example of a 3D printed micromixer is depicted.

Table 2 Polymers used in additive manufacturing of microfluidic devices

Type	Glass transition temperature T_g (°C)	Transparent?	Biocompatible?	Example
ABS	~105	No	No	MakerBot ABS filament
Acrylate/epoxy	45–200	Choice of transparent or non-transparent	Choice of biocompatible or non-biocompatible	–
E-Glass	NA	Yes	NA	EnvisionTEC
E-Guard	~109	Yes	Yes	EnvisionTEC
E-Shell 300, 600 Series	86–160	Choice of water clear, rose clear, red, and blue	Class IIa biocompatible	EnvisionTEC
MED610	52–54	Yes	Yes	Stratasys
PLA	45–60	No	No	MakerBot PLA filament
RGD720	48–50	Yes	No	Stratasys
Veroclear RGD810	52–54	Yes	No	Stratasys

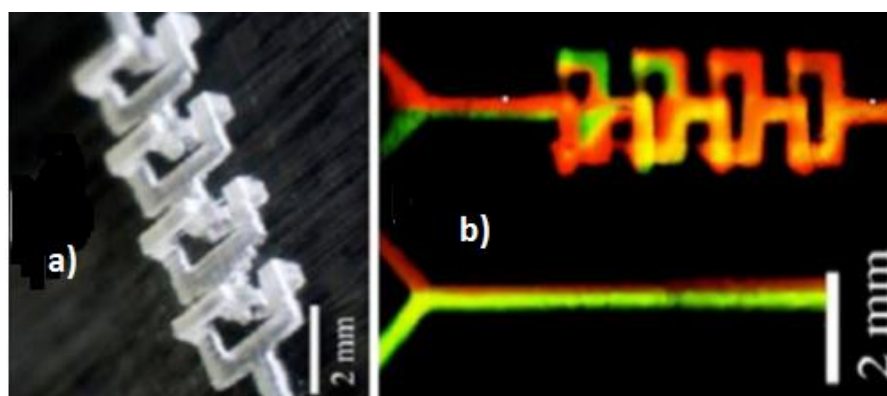


Figure 11 a) Four mixing units, b) fluorescent image of the mixing progress within the 3D-printed micromixer

Widespread employment of 3D printing is foreseen for future advancements in lab-on-a chip and microfluidic engineering technology. Table 3 presents commercially available 3D printers applicable to microfluidics fabrication [32].

Apart from the aforementioned methods for polymeric substrates patterning, plasma etching [42] (more information can be found in 1.2.1) and direct milling [43] is used.

Table 3 Commercialized 3D printers suitable for microfluidic devices fabrication

Type	Brand	Model	Price (\$)	Material	Max size (mm)	Layer thickness (μm)	Speed (mm/s)
FDM	Ultimaker	Ultimaker 2	2499	PLA, ABS, U PET	$210 \times 210 \times 205$	20	30–300
FDM	Cubify	CubePro	2799	PLA, ABS, NYLON	$285.4 \times 270.4 \times 230$	70–300	15
FDM	Lulzbot	TAZ	2200	PLA, ABS, NYLON	$298 \times 275 \times 250$	75–350	200
FDM	Airwolf	AW3D HD	2995	PLA, ABS, NYLON	$304.8 \times 203.2 \times 304.8$	60	150
FDM	Cubify	Cube	999	PLA, ABS	$152.5 \times 152.5 \times 152.5$	70	15
FDM	Type A	Series 1	2749	PLA, ABS	$305 \times 305 \times 305$	50–250	50–250
FDM	Afinia	H800	1899	PLA, ABS	$254 \times 203.2 \times 203.2$	100	30
DLP	EnvisionTEC	Perfactory Micro	~12,000	E-material (proprietary)	$60 \times 45 \times 100$	50	0.007
DLP + SL	MiiCraft	MiiCraft+	1200	ProBV-003 (Proprietary)	$43 \times 27 \times 180$	5–200	2.7×10^{-5}
SL	FormLabs	Form 1+	3299	UV resin	$125 \times 125 \times 165$	25–200	~0.0085
SL	B9Creator	V1.2 HD	4595	Castable resin	$57 \times 32 \times 203$	30	~0.003 – 0.006
SL	Kudo3D	Titan 1	2999	UV resin	$190.5 \times 109.22 \times 254$	~100	0.019
SL	Cubify	Project 1200	4900	UV resin, FTX visijet	$42.9 \times 149.9 \times 26.9$	30	~0.004

1.2.3 PCB technology

Recently, there is an increasing interest in using printed circuit boards (PCB) as (rigid or flexible) substrates for the development of microfluidic devices [44–46]. The well-established PCB technology, industrially available for the mass production of electronic circuits and

consumer electronics, as well as the low cost of the substrates makes it highly appealing. Moreover, the integration possibilities for electronics, microfluidics, sensors and actuators offered by the use of PCB are enormous.

PCBs are typically composed of interchanging planar insulating layers of laminates –such as the flame retardant laminate sheet (FR4) which is fiberglass interwoven with an epoxy resin- and layers of conducting metal. The most commonly used metal is copper that may be present in many layers, also of different thickness.

Various implementations of PCB technology to microfluidic applications have been proposed in the literature for the formation of microfluidic patterns and their sealing, for creating enclosed microchannels and microchambers. Most of these implementations demand PCB process flow modification, and some type of pre/post-processing to realize an enclosed microfluidic system. Below, a description of the current state-of-the-art on microfluidics/LoC fabrication and sealing based on PCB technology follows.

PCB patterning

Very early work on microfluidics fabrication using PCB technology proposed the use of copper as a material for the formation of microfluidic networks. By using lithography followed by etching of the outer copper layer, 3-sided channels (copper on sidewalls, FR4 on bottom) were patterned [44, 47], followed by sealing of the channel with a planar cover board (i.e. made of glass using epoxy resin to form fully enclosed microchannels. Another means of sealing microchannels patterned on copper (by lithography and wet etching) was based on spin-coating of a UV-curable adhesive that bonds to a cover glass to create enclosed microchannels [48]. In addition, etching of an outer copper layer to form the microchannels (copper on sidewalls, FR4 on bottom) was used on two PCBs, which after alignment and lamination (with epoxy resin) form a fully enclosed microfluidic network [45, 49]. This technique can be repeated as many times as necessary for an arbitrary number of layers on which the microfluidic network extends.

Metalized polyimide films

Fabrication of microfluidic channels has been also reported on flexible metalized polyimide films (also implemented in the current PCB technology), a photosensitive type (e.g. PI2732, DuPont) which can be patterned by means of lithography and a non-photosensitive type (e.g.

PI2611, DuPont) which can be patterned by dry etching techniques. The sealing process that was followed uses n-methyl-2-pyrrolidone solvent (NMP is a swelling agent) in order to treat and swell the surface of partly imidized polyimide and allow higher interdiffusion with the polyimide cover layer [50]. A non-photosensitive type of polyimide, Pyralux™, was microstructured by means of plasma etching (O_2/SF_6) and the device was sealed using a polyolefin cover with a pressure sensitive poly (dimethyl) siloxane (PDMS) adhesive [51]. Similarly, another device was fabricated using the same patterning method and materials, but the sealing was performed using a commercially available Kapton® PI tape with a silicon adhesive [52].

Polymers for PCB patterning

Furthermore, an extensively used epoxy resist, SU-8, has been used to form microchannels/microchambers on top of PCB. On the PCB, the electrical components were fabricated and then the PCB was coated with an SU-8 layer to aid the adherence of the fluidics which were patterned on a subsequent layer of SU8 [46]. After the UV treatment, bake and development of the SU8, the device was sealed with a thicker layer of SU8 by means of BETTS (Bonding, UV-Exposure and Transferring Technique in SU-8) process [53]. The described device served mixing purposes. In another case, the electrical components have been formed on the PCB by Cu etching. Then with the aid of an SU-8 layer, the surface of the PCB was planarized and resistors (Pt) were fabricated by Pt sputtering followed by lift off process. The microfluidics were then patterned on a second layer of SU-8. Afterwards, a thin layer of PMMA was spin-coated on the surface of the SU-8 channels. Finally, the device was sealed with a thicker plate of PMMA by thermal bonding with a thermal press [54].

Dry film photosensitive resists

Very recently, dry film photosensitive resists (DFR) such as TMMF or 1002F were used for planarization, encapsulation and creation of the microfluidic network and sealing on PCB substrates. More specifically, TMMR S2000 also called TMMF S2000 when sold as a dry resist from Tokyo Ohka Kogyo Co., Ltd [55]. The 1002F polymer has been used to planarize and encapsulate surface mounted components on top of a PCB surface by casting the 1002F polymer and using a hot press and UV exposure. A second layer of 1002F was used for the fluidic patterning. Similarly, a heated press was used to make a planar layer of the 1002F

polymer, and after UV lithography the fluidics were patterned. The sealing of the device was achieved with a lamination process at 110°C using a tape or thin layer of cured 1002F polymer [56, 57].

To facilitate mass production of microfluidic devices, researchers have proposed materials with which PCB manufacturers are mostly familiar, such as the polyimide-based laminated dry film resists that have been implemented recently as patterning layers on top of commercial PCBs. For example, micromixers of various geometries have been fabricated, after sealing them with thin polyolefin films [58, 59]. In addition, short microchannels on multilevel PCB stacks have been fabricated by standard PCB processing, however due to their small channel length, they do not develop high pressures during fluidic operation [60]. Methods and materials for fabrication of PCB-based microfluidic devices for performing DNA amplification have been also described in US2013/0210080 A1.

In most of the previously mentioned works, with the exception of the work of Pagel and co-workers [45, 49], cover sheets and adhesive materials not commonly used in the PCB technology have been implemented (glass, PMMA, SU-8, TMMF, 1002F, PDMS, etc.) for the formation of microchannels and sealing purposes. Therefore, the introduction of new materials and modified processes in the PCB industry is required to allow upscaling of PCB-based microfluidics fabrication. Specifically, for sealing microfluidic channels/chambers/networks, even in the work of Pagel and co-workers, a non-standard PCB technology step has been proposed: an epoxy resin to cover the PCBs, by means of dipping and withdrawing the boards from the resin solution, and letting them dry, thus using a complicated and time-consuming process. In other works [51, 52], materials based on PI such as Kapton® tapes or polyolefin tapes with a silicon pressure sensitive adhesive have been used, and they often lead to sealed microfluidic devices of low robustness and fabrication throughput, especially when employed for applications where high temperatures are required for performing biological reactions.

1.2.4 Paper technology

“Paper-based microfluidics” or “lab on paper,” a blossoming research field first introduced in 2007 by the Whitesides Group of Harvard University (Fig. 12) [61]. It provides a novel system for fluid handling and fluid analysis for several applications including medical

diagnostics, food testing and environmental monitoring. Paper has become an attractive substrate for microfluidic chips due to: (1) its ubiquity and extremely low cost of cellulosic material; (2) its compatibility with many biochemical and biomedical applications; and (3) its ability to transport liquids through capillary forces without the aid of external forces [62].

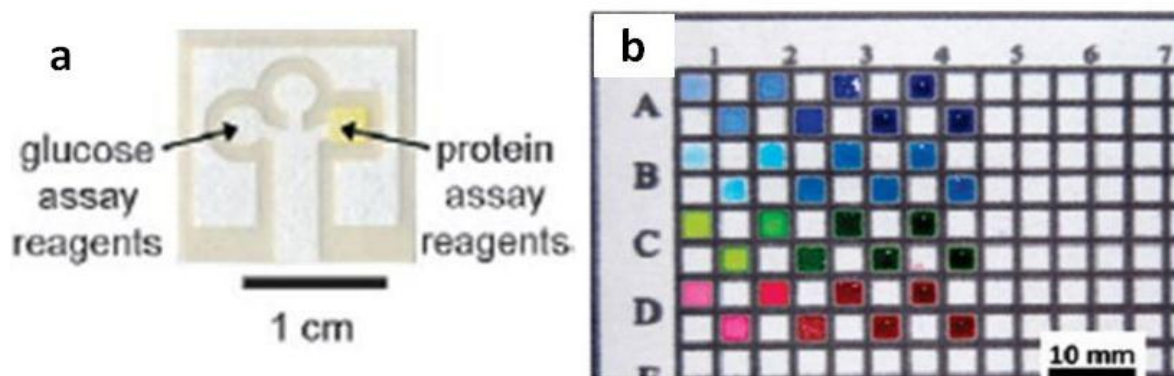


Figure 12 Paper microfluidics a) photolithography technique, b) an example of a wax-printed 384-zone paper plate after the application of several dyes [62]

As for the fabrication techniques of paper-based microfluidics, 10 have been reported in the literature: (1) photolithography, (2) ink jet etching, (3) plotting with an analogue plotter, (4) (5) wax printing (Fig. 12b), (6) plasma treatment, (7) paper cutting, (8) ink jet printing, (9) laser treatment, (10) flexography printing and (11) screen printing. The underlying fundamental principle of these fabrication techniques is the patterning of hydrophobic-hydrophilic contrast on a piece of paper for creating micron-scale capillary channels on paper. An exception to this principal is the cutting technique. Paper is first shaped in the desired pattern by cutting assisted by a computer controlled plotter cutter followed by the encasing of the shaped paper with sticky tape, serving as a backing for creating paper-based microfluidic devices [62]. In table 4 a description of the main advantages and drawbacks for different fabrication techniques of paper-based microfluidic devices is presented. The detection methods accompanying paper-based microfluidics are electrochemistry, electrochemiluminescence and colorimetry.

Table 4 Description of the main advantages and drawbacks for different fabrication techniques of paper-based microfluidic devices [62]

Fabrication techniques	Advantages	Drawbacks
Photolithography	High resolution of microfluidic channels (channel width is as narrow as 200 μm ; the barrier is sharp)	Requires expensive equipment; requires an extra washing step to remove un-crosslinked polymer; devices are vulnerable to bending
Plotting	Patterning agent (PDMS) is cheap; devices are flexible	Deteriorated barrier definition; cannot be readily applied to high throughput production
Ink jet etching	Requires only a single printing apparatus to create microfluidic channels by etching and to print bio/chemical sensing reagents	Creation of microfluidic channels requires 10 times of printing; the printing apparatus must be customized; not suitable for mass fabrication
Plasma treatment	Uses very cheap patterning agent (AKD); dramatically reduces the material cost	Requires different masks for creating different microfluidic patterns on paper
Wax printing	Produces massive devices with simple and fast (5-10 min) fabrication process	Requires expensive wax printers; requires an extra heating step after wax deposition
Ink jet printing	Uses very cheap AKD; produces massive devices fast (<10 min) and simply; requires only a desktop printer to produce devices and to print sensing reagents	Requires an extra heating step after AKD deposition; requires modified ink jet printers
Flexography printing	Allows direct roll-to-roll production in existing printing houses; avoids the heat treatment of printed patterns	Requires two prints of polystyrene solution; requires different printing plates; print quality relies on the smoothness of paper surface
Screen printing	Produces devices with simple process	Low resolution of microfluidic channels (rough barrier); requires different printing screens for creating different patterns
Laser treatment	High resolution (minimum pattern size of about 62 μm)	Microfluidic channels do not allow lateral flow of fluids; requires extra coating for liquid flow

Besides the advantages of paper-based microfluidics, they also possess several limitations. (i) The sample retention and sample evaporation during transport result in the low efficiency of sample delivery (less than 50% of the total volume reaches the detection zones) within paperfluidic channels of the device. In case the sample volume is tiny or the sample is expensive, sensors with low volume and more efficient sample delivery are preferable. (ii) Some patterning hydrophobic agents build inadequately hydrophobic barriers which are incapable of withstanding samples of low surface tension. When the surface tension of a liquid is lower than a critical value liquid can penetrate the hydrophobic areas of the device too. Thus, guided liquid transportation is ineffective. This is due to the lowering of the surface free energy stemming from the paper hydrophilization which leaves unblocked pores in the paper. (iii) The analysis of samples of very low concentration are hindered due to the

high limit of the detection (LOD) offered by the conventional colorimetric methods integrated into the paper-based microfluidic devices, rendering the current paper-based devices insufficient [62].

1.2.5 Sealing

Another crucial issue of microfluidic devices is: sealing. Sealing processes are very important in microfluidics fabrication, and indeed sealing of LoC devices is considered by experts as one of the important practical challenges [63] and an obstacle for the commercialization of microfluidics, since it has great impact on the manufacturing cost and the performance of the final devices. The microfluidics society (academia, research, industry) lacks suitable materials in order to seal inexpensively, easily, irreversibly, robustly, and massively, devices with long microchannels (where high pressures are expected to develop especially at high temperatures). There are numerous considerations that must be taken into account while selecting and implementing a bonding method depending on the functional requirements of the end microfluidic device. Bonding strength is a critical issue. On one hand there are applications that require interfacial bonding energies equal to the cohesive strength of the bulk substrate material. On the other hand, there are applications that benefit from comparatively weak and reversible bonding. Bond interfaces should assure suitable chemical or solvent compatibility in order to prevent degradation while employed, without compromising the robustness (dimensional control, lack of deformation) of the microfluidic network during the bonding process. Other crucial considerations relative to the bonding interfacing include material compatibility, optical properties, surface chemistry as well as homogeneity channel's sidewalls. Furthermore, there are manufacturability and interconnects compatibility which can also restrict the selection of bonding methods according to the microfluidic applications. For instance, the employment of thin laminating film to seal microstructures may prove to be inadequate when thicker sealing layer is needed to support large fluidic connections or reservoirs.

Microfluidic bonding techniques could be divided into two categories: indirect or direct. Indirect bonding (Fig. 13a) comprises the employment of an adhesive layer to seal two substrates and create encapsulated microfluidic networks fabricated in one of the two substrates. Contrary, direct bonding (Fig. 13b) methods makes no use of additional materials to the interface. Although direct bonding could be considered as a form of adhesive bonding,

(in this case the bulk polymer itself holds the role of the adhesive), it is notable to have the ability to provide enclosed microstructures with homogeneous sidewalls, while indirect bonding (involving an intermediate adhesive) results in inhomogeneous channels with different mechanical, optical and chemical properties compared to the main bulk polymer.

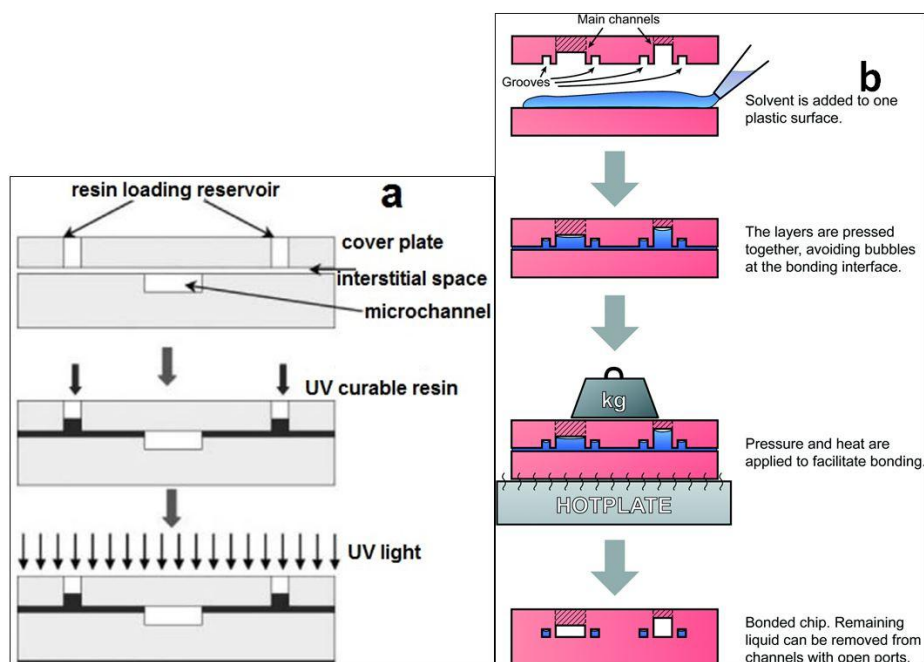


Figure 13 Bonding methods a) UV-curable adhesive application using capillarity-mediated resin introduction (indirect) [64], b) liquid phase solvent bonding (direct) [65]

Generally, bonding forces between surfaces derive from either charge interactions or molecular entanglement. Electrostatic or chemical (covalent) bonding, van der Waals forces, acid-base interactions, are the main driving forces in charge interactions resulting in bonding between two surfaces whereas molecular entanglement occurs by mechanical interlocking of surface diffusion. For instance, thermoplastic bonding methods such as solvent bonding, thermal fusion bonding, localized welding, and surface modification and treatment bonding are usually obtained by molecular entanglement. Charge interactions lead to adhesive bonding. During thermoplastic bonding process, efficient interaction or intermixing is mostly favoured between high interfacial compatibility polymer chains. This is mainly attributed to the fact that polymers employ the same internal bond structures. In most cases, high bond strength can be achieved at high temperature. This is because polymer entanglement and

interaction at the bonding interface are enhanced with increased temperature. Nonetheless, unlike macro-scale, bonding methods in micro-scale should be adapted and fine-tuned for the challenging task of sealing, so as to avoid excessive deformation of the channel cross-sections within the microfluidic networks. Thus, extreme heating leading to melting of thermoplastic are often undesired. High surface wettability is advantageous to boost more intimate contact between surfaces in low temperature bonding process. With regard to most thermoplastic polymers, they are formed from hydrocarbons with extra atomic components such as oxygen and nitrogen, leading to low-energy hydrophobic surfaces thus with poor wettability, hindering the strength of bonds which might be easily formed. To surpass this limitation, various direct and indirect bonding techniques have been proposed for thermoplastic microfluidics that stem from techniques developed for conventional thermoplastic manufacturing. Table 5 presents some of these methods [64].

Over the last years, numerous PDMS bonding techniques have been presented in the literature since there was an increasing interest on multilayer PDMS microdevices. Oxygen plasma bonding is the prevailing method for bonding PDMS layers despite the additional fabrication time and the high cost. Alternative methods include corona discharge, uncured PDMS adhesive, partial curing and cross-linker variation. Both uncured and partially cured PDMS adhesive exhibited double the average bonding strength compared to Oxygen plasma. [66]. In 2009 another low cost sealing method for microdevices was proposed by Vlahopoulou *et al.* The process is performed at a low temperature and relies on the surface modification of an organic substrate using a silane solution. This method (Fig. 14) is generic and can be applied on structured or plain organic polymeric substrates (such as PMMA, PS - an intermediated PDMS layer is required), glass, Si and epoxy-type polymers results in irreversible bonding [67].

1.3 Applications

Microfluidics is a particularly relevant field for the development of LoC devices, since microfluidics is an enabling technology of analysing and manipulating fluid flow of sub-millilitre scale structures. The manipulation of fluids is ruled by many different physical phenomena such as surface tension, wetting, electrowetting, electrophoresis, electroosmosis. Moreover, thermophoresis, dielectrophoresis, magnetophoresis and acoustic streaming are

some physical principles which fluid manipulation can rely on. During the past two decades, numerous miniaturized bio -MEMS have been developed and commercialised. Such microdevices are enhancing the way many significant chemical and biological analyses are performed in chemical diagnostic laboratories, research centres and industry. The development and progress of the technologies involved was facilitated by a synergistic combination of disciplines including molecular biology, material science, microfabrication, engineering, (bio-)chemistry. A significant number of these new technologies and devices use sophisticated microfabrication processes previously developed and employed by the semiconductor industry [2]. Microfluidics used in LoC offers the ability to perform various analytical steps, including sample pre-treatment, reaction, and detection, on a microchip in an effective and automatic format. Thus, the development of LoC devices hold a critical role in the progression of various fields of research ranging from diagnostic devices to extra-terrestrial research, where automation, cost-effectiveness and short duration of analysis are key parameters.

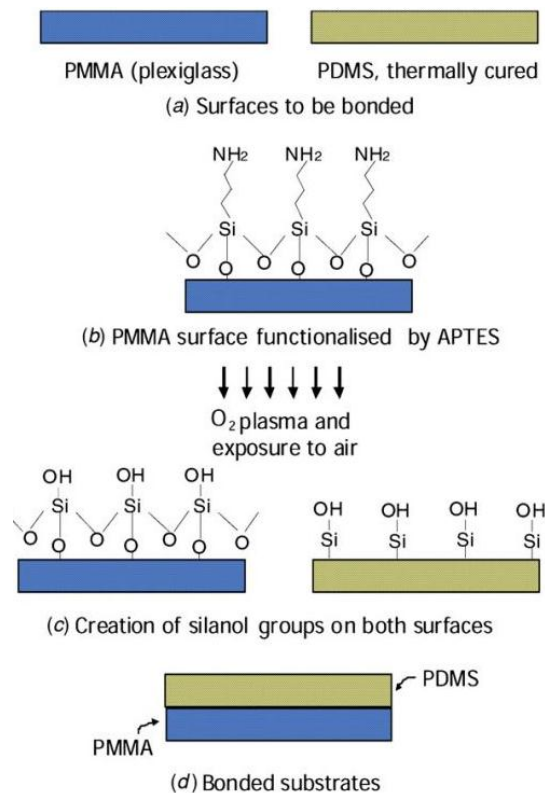


Figure 14 Schematic of the process flow for bonding between a PMMA and a PDMS substrate [67]

Table 5 Overview of thermoplastic bonding technique for microfluidic device [64]

Bonding method	Bonding strength	Bonding quality	Process complexity	Bonding time	Cost	Advantage	Limitation	Suitable material
Adhesive printing bonding	high	fair	medium-high	short-medium	low-medium	Low temperature, high bond strength, low channel clogging, controllable adhesive thickness	Scarification channel (contact printing) or printing mask (screen printing) required	PMMA, COC
Adhesive interstitial bonding	high	fair	low	short	low-medium	Simple, fast, low temperature, high bond strength, low channel clogging, low cost	Adhesive loading reservoirs or flush adhesive out of channel needed	PMMA
PDMS-interface bonding	medium	low	medium	long	medium	Low temperature, compatible with PDMS microfluidics	PDMS layer may squeeze into channel	PMMA
Lamination film bonding	medium	fair	low	short	low-medium	Simple, fast, low cost, low temperature, no adhesive clogging	Lamination film may embedded inside channel	PMMA, PC, PS, PET
Thermal fusion bonding	medium	fair	low	long	low-medium	Simple, homogeneous channel, compatible with various material	Channel deformation from un-optimized process condition	PMMA, PC, PSnylon, COC, PSU
Solvent bonding	high	fair	low	short	low-medium	Simple, fast, low temperature, high bond strength, low cost	Soften polymer surface may collapse channel from un-optimized process	PMMA, PC, COC
Solvent bonding with sacrificial material	high	good	high	medium	low-medium	High bond strength, low cost, low channel collapse and clogging	Sacrificial material need applied into channel before bonding and removed after bonding	PMMA
Localized welding	medium	fair	medium-high	medium	medium	Low temperature, localized bonding	(ultrasonic welding) or metal layer (microwave welding) are required	PMMA, PEEK
Surface treatment bonding	medium-high	good	medium	medium	medium-high	Low temperature bonding, low channel deformation	Surface chemistry changed after treatment	PMMA, PC, COC PS, PET

Point-of-Care diagnostic devices

A 2007 report from National Institutes of Health (NIH) [US Department of Health and Human Services, National Institutes of Health. Point-of-Care Diagnostics Testing, Fact Sheet. Bethesda, MD, USA (2007)] indicates that point-of-care (PoC) testing holds the potential to initiate a paradigm shift from curative to predictive, preventive and personalized medicine [68]. PoC testing promotes a conversion from conventional lab-based diagnostic tests to near-patient settings, allowing physicians to make decisions relative to diagnosis and treatment with timely diagnostic information. In the meanwhile, the ease of use of PoC devices empowered patients since it allows them to personally monitor their own health quantitatively at home. Thus, the requirement for sample transport and result collection from/to lab facilities

is being obsolete. Healthcare delivery will emphasize patient-centred, personalized approaches promoting wellness and effectiveness treatment-wise. Due to these emerging needs in the healthcare industry, the development of cost-effective and easy-to-handle medical devices (combined with data-sharing tools) providing information both rapidly and accurately at the PoC will become essential. The segmentation of PoC diagnostics is depicted in Fig. 15 [69].



Figure 15 Segmentation of rapid diagnostics [69]

Microfluidic devices applications have proliferated at an enormous speed due to the existing well-established knowledge stemming from the microelectronics field and have shown to hold great promise in a diverse range of biological applications including, nucleic acid amplification (i.e. PCR) [70, 71], cell sorting [72, 73], immunohybridization reactions [74] and enzymatic assays [75].

In the next table (Table 6) existing rapid diagnostic tests and the respective fields and needs they address are presented [69]. Historically, the first point-of-care test, that was commercialised, was a paper based strip test measuring the glucose in urine [76].

Table 6 Rapid diagnostic tests in the market

Test	Application
Urinalysis	Metabolic disorders: Human chorionic gonadotropin (pregnancy), (pH, glucose, protein, ketone, leukocytes, nitrite, blood, urobilinogen, bilirubin, specific gravity), albumin to creatinine ratio, and ascorbic acid
	Drug abuse: Alcohol, amphetamines, barbiturates, benzodiazepines, buprenorphine, cocaine, ketamine, methamphetamines, methadone, morphine/opiates, oxycodone, phencyclidine, propoxyphene, 9-tetrahydrocannabinol (marijuana), and tricyclic antidepressants
Immunoassays	Infectious diseases: C. difficile, Cytomegalovirus, dengue fever, E. coli, enterics, epstein barr virus, mononucleosis, giardiasis, herpes simplex virus, HIV, Lyme disease, malaria, measles, S. aureus, methicillin-resistant Staphylococcus aureus (MRSA), mumps, rubella, syphilis, toxoplasmosis, tuberculosis, varicella zoster, West Nile virus, hepatitis B/C, Chagas disease, chlamydia, cholera, hantavirus, leishmaniasis, leptospirosis, Listeria, and H. pylori
	Respiratory diseases: Influenza (flu), Legionnaire's disease, pneumonia, respiratory syncytial virus, streptococcal pharyngitis, and Streptococcus pneumonia
	Cardiovascular condition: acute kidney injury, acute coronary syndrome, dyslipidemia, heart failure, oral anticoagulation, shortness of breath, and venous thrombosis
	Oncology: Bladder, colon cancer, and colorectal cancer
	Women's health: Osteoporosis, ovulation, and preeclampsia

Veterinary diagnostics	Canine: Blood, urobilinogen, bilirubin, protein, nitrite, ketones, glucose, pH, density, leukocytes, heartworm (<i>Dirofilaria immitis</i>), parvovirus, Giardia, Lyme disease, distemper virus, coronavirus, Ehrlichia, Leishmania, adenovirus, rotavirus, pancreatic lipase, relaxin, blood group typing, Borrelia, Brucella, c-reactive protein, Leptospira, progesterone, rabies, rheumatoid factor, and vaccination status
	Feline: Blood, urobilinogen, bilirubin, protein, nitrite, ketones, glucose, pH, density, leukocytes, immunodeficiency virus, leukemia virus, heartworm (<i>Dirofilaria immitis</i>), Ehrlichia, Leishmania, Giardia, parvovirus, infectious peritonitis, <i>Toxoplasma gondii</i> , relaxin, blood group typing, Borrelia, chlamydia, coronavirus, panleukopenia, progesterone, and vaccination status
	Bovine: Alpha toxin, Brucella, Chlamydophila, Clostridium perfringens, coronavirus, Cryptosporidium, rotavirus, <i>E.Coli</i> K99, Cryptosporidium parvum, epsilon toxin, foot-and-mouth disease virus, IgG, Leptospira, Mycobacterium bovis, Neospora, progesterone, rabies, parainfluenza-3, and rotavirus
	Swine: Aujeszky's disease, <i>Clostridium perfringens</i> , <i>Cryptosporidium</i> , epidemic diarrhoea virus, rotavirus, alpha toxin, foot-and-mouth disease virus, progesterone, and transmissible gastroenteritis virus
	Equine: Borrelia, rotavirus, Clostridium perfringens, IgG, pregnant mare serum gonadotropin, progesterone, tetanus, and troponin
	Avian: Influenza, Chlamydophila, infectious bursal disease, and Newcastle disease
	Small ruminants: Foot-and-mouth disease virus
Food and beverage safety tests	Mycotoxins: Aflatoxins, deoxynivalenol (vomitoxin), fumonisins, zearalenone, ochratoxin, T-2 and HT-2 toxin, patulin, ergot alkaloids)
	Food pathogens: <i>E.Coli</i> O157:H7, <i>Listeria</i> , <i>Staphylococcus aureus</i> , and <i>Salmonella Enteritidis</i>
	Food allergens: Almond, brazil nut, casein, cashew/pistachio, coconut, hazelnut, lupin, macadamia nut, mustard, peanut, sesame, soy, walnut, whole egg, β -lactoglobulin, total milk, crustacea, and gliadin/gluten

	Genetically modified organisms: Bulk grain, seed and leaf, toasted meal, and corn Comb 7 Traits
	Veterinary drug residues: Chloramphenicol, nitrofurantoin AMOZ/ AOZ/AHD, clenbuterol, ractopamine, beta agonists, dexamethasone, ciprofloxacin, quinolones, β -Lactam antibiotics, flunixin, aminoglycoside, amphenicol, enrofloxacin, macrolide, sulphonamide, tetracycline, and melamine
	Beverage: Methanol contamination, acetic acid, citric acid, D-glucose, D-fructose, lactose, milk (lactic acid, urea), and wine (acetic acid, total acidity, glucose, fructose, L-lactic acid, L-malic acid, and sucrose)
	Pesticide residues: Organophosphates, thiophosphates, and carbamates
	Seafood analysis: Amnesic shellfish poisoning (ASP), marine biotoxins (okadaic acid), histamine, and sulphite residues
	Species identification: Pork, horse, beef, fish, goat, poultry, rabbit and sheep
Environmental monitoring devices	Water testing: Algae, alkalinity, aluminium, ammonia, arsenic, bleach, boron, bromine, cadmium, calcium hardness, carbon dioxide, chelant, chloride, chlorine, chromate, chromium, conductivity, copper, cyanuric acid, cyanide, detergents, dissolved oxygen, faecal streptococci, E.Coli and faecal coliforms, filming amine, fluoride, formaldehyde, glutaraldehyde, hardness, hydrazine, hydrogen peroxide, iodine, iron, lead, magnesium, manganese, molybdate/molybdenum, morpholine, nickel, nitrate, nitrite, oil in water, organophosphate, dissolved oxygen, ozone, quaternary ammonium compounds, peracetic acid, pH, phosphate, phosphonate, polyphosphates, polyquat, potassium, Pseudomonas aeruginosa, salinity, silica, sulphate, sulphide, sulphite, turbidity, total dissolved solids, tannin/lignin, toluidine PS biocide, and zinc
	Soil: Humus, organic matter, pH, and plant tissue macronutrient (texture)
Biothreat detection	Anthrax, plague, tularaemia, ricin, botulinum toxin, Staphylococcal enterotoxin B, orthopox, Brucella, abrin, biological warfare simulants, nerve (G&V series), Category A-C biothreat agents, and blister (HD) agents, acids, bases, aldehydes and oxidisers

The description of a perfect microfluidic-based PoC device would resemble one envisioned by Gervais et al. in a 2011 article [77] and also meet the ASSURED criteria:

- Affordable by those at risk of infection
- Sensitive with very few false-negatives
- Specific with very few false-positives
- User-friendly tests that are simple to perform and require minimal training
- Rapid, to enable treatment at first visit, and Robust, for example not requiring refrigerated storage
- Equipment-free
- Delivered to those who need it

An ideal PoC device would be minimally invasive, employing minute unprocessed sample volumes (i.e. less than a finger prick [25 μ l]) stemming directly from a patient. The addition of the sample should trigger the initiation of the analysis. As for sampling, it should be automated -completed by the chip- and accurate, with the capability of employing larger volumes of sample if needed. The PoC device should also be capable of multiplex analysis (i.e. proteins, nucleic acids, cells) yielding quantitative results within very short time (i.e. 5min). The analytes used should be detected with extreme selectivity and sensitivity thus minimising or even eradicating the possibility for false-positives. Negative controls should also be incorporated. Cross-contamination between samples coming from either different patients or different (consecutive) runs should be eliminated. The ideal limit of detection – sensitivity- should be in the pico or even to femtomolar range, enabling/admitting the detection of species present in very low concentrations, while not compromising the robustness and repeatability to measure analyte in the micromolar quantities. As for the structural material of the PoC device, it would be biocompatible, low cost and preferably transparent –enabling the observation-. Furthermore, it should have low power consumption, with autonomous power supply (i.e. long life battery) with no recharging requirement for years. The PoC device should not be affected by common solutions such as water or organic ones and it should remain solid, durable and secure when exposed to medium hardships (i.e. fall, liquid spillage). As for the storage conditions, it should be durable in a wide range of temperatures for years. It should also be used in hospital settings, remote/low resource settings and at home by inexperienced patients. Lastly, the PoC device should have a low cost. Several microfluidic-based diagnostics already presented in the literature are depicted in Fig. 16.

For example, the Piccolo Xpress® chemistry analyzer (Fig. 16c) allows healthcare practitioners to perform routine multi-chemistry panels using 0.1cc of whole blood, serum or plasma. From sample to complete panel results 3 simple steps are required and approximately 12 minutes. The system uses patented single-use reagent discs which contain up to 14 chemistry tests related to electrolytes, lipids and kidney function [78]. The GeneXpert Dx System (Fig. 16e) automates and integrates sample preparation, nucleic acid amplification, and detection of the target sequence in simple or complex samples using real-time Polymerase Chain Reaction (PCR). The system is suited for in vitro diagnostic and research based applications that require hands-off processing of patient samples and provides both summarized and detailed test results data in tabular and graphic formats. The GeneXpert system can only be used with the GeneXpert cartridge [79]

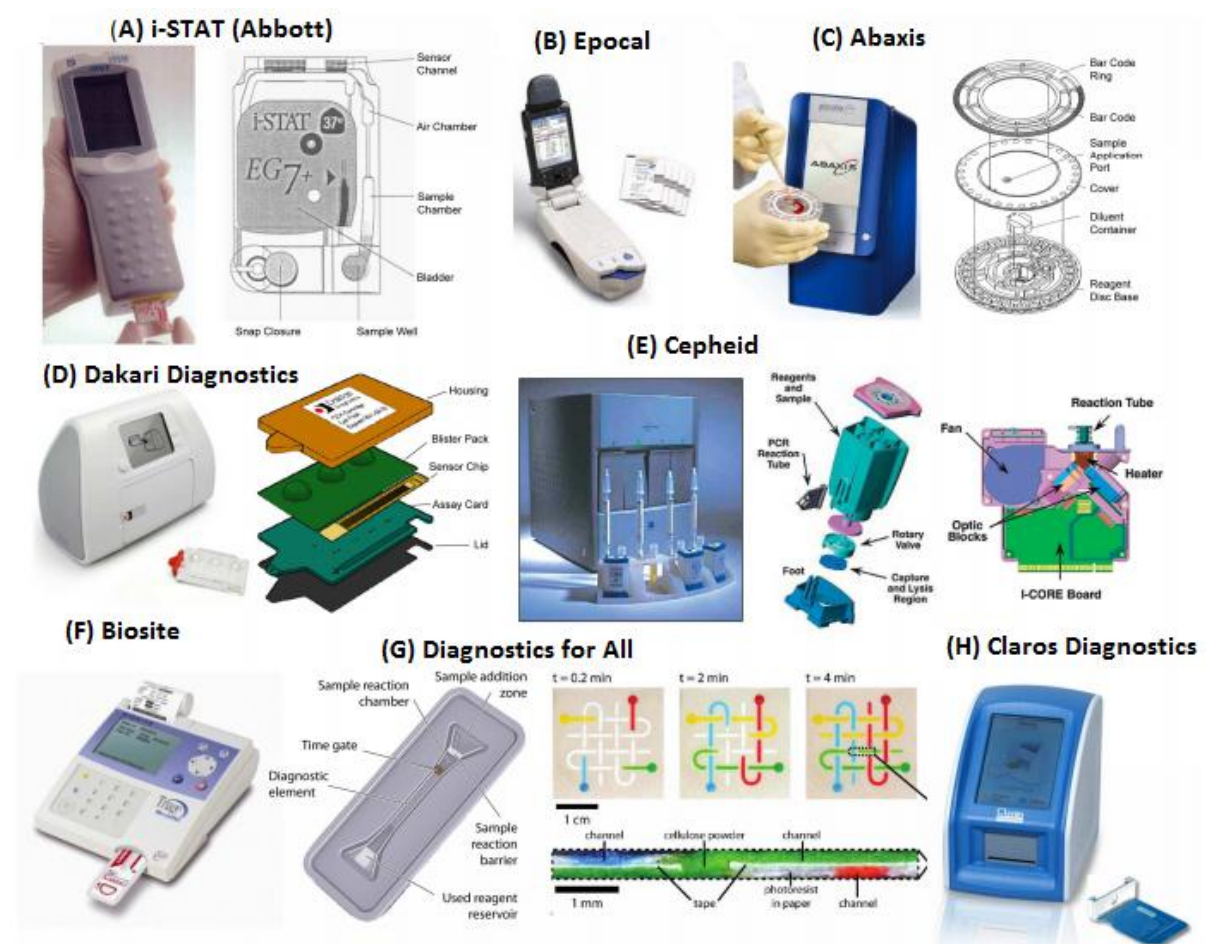


Figure 16 Images/schematics of microfluidics-based PoC tests

The cost of the PoC device is a particularly important characteristic given the heterogeneous healthcare needs across the world. While in developed countries (USA, Europe) the leading killer diseases are cancers and heart diseases, in developing countries, infectious diseases (e.g., HIV/AIDS, malaria, lower respiratory infections, tuberculosis and measles) are the dominant cause of death. With proper diagnosis and treatment most of the deaths caused by these infectious diseases could be prevented [80, 81]. For the fast diagnosis of these diseases chemical or biological assays (i.e. ELISA) are involved, as well as other assays relying on lab instrumentation, such as flow cytometers, that are usually unavailable in developing countries.

PoC/LoC challenges

Although there is a tremendous progress in the field of microfluidics and there are myriads of assays developed in the biology and medicine field, PoCs are still facing challenges. One drawback is linked with the sheer complexity of the idealized LoC approach. Although many complex biochemical processes employed in various diagnostic procedures have been performed on-chip, the majority of them are impossible without the usage of expensive and bulky external parts, such as: valves, pumps, and switches enabling fluid manipulation and a variety of optical detectors and sensors for signal measurement. Even with the new approaches available -with miniaturized components- the integration of all these in an automated device of a small footprint is extremely challenging. Since various components must be designed in a manner that mutual compatibility is achieved, this process could be proved extremely demanding as the complexity of the designed PoC is analogous to the components to be integrated. In a scenario where the envisioned final device is poorly-described at the early stages of the design, no matter how appealing the individual components may be, the integrated, end product device may never be accomplished since the technical requirements can differ enormously for each assay step or component.

Although there is an enormous number of papers presenting in detail the use of various materials, microfabrication technologies as well as surface modifications in MEMS/LoC relevant to sample processing, fluid handling, integration, detection and biological interactions in the microscale, this area still faces challenges. In order to overcome the aforementioned challenges, the existing work and its findings should be leveraged with transformative technologies so as to offer low-cost and high-throughput manufacturing

process for robust, user-friendly integrated microfluidic platforms suitable for performing complex biochemical reactions in short times with high accuracy.

Market

According to the market report from Markets and Markets in 2016, PoC diagnostics market is estimated to reach USD 40.5 Billion by 2022 from USD 23 (see Fig. 17).16 Billion in 2016, at a CAGR of approximately 10% during the forecast period as shown in Fig. 8. As for the market dynamics, the key drivers are: 1) the high prevalence of infectious diseases in developing countries, 2) the increasing Incidence of lifestyle diseases, 3) the rising usage of home-based PoC devices, 4) the growing government support, 5) private investments and venture capital activities, 6) the technological advancements and new product launches, 7) the growing number of regulatory approvals for novel immunoassay techniques, 8) the shortage of skilled laboratory technicians, 9) the increasing preference of PoC testing and 10) the rising number of CLIA-Waived PoC Tests (All facilities in the US performing laboratory testing employing human specimens to assess, diagnose, prevent or treat are regulated under the Clinical Laboratory Improvement amendments of 1988 (CLIA) [82]. However, certain challenges still exist in integrating the microfluidics technology into existing workflows. Some of the main restraints are: 1) product recalls, 2) pricing pressures due to reimbursement cuts and budget constraints hampering profits and 3) stringent and timely regulatory policies which significantly increasing gestation period for product launches and 4) reluctance from the industry towards changing the existing norms.

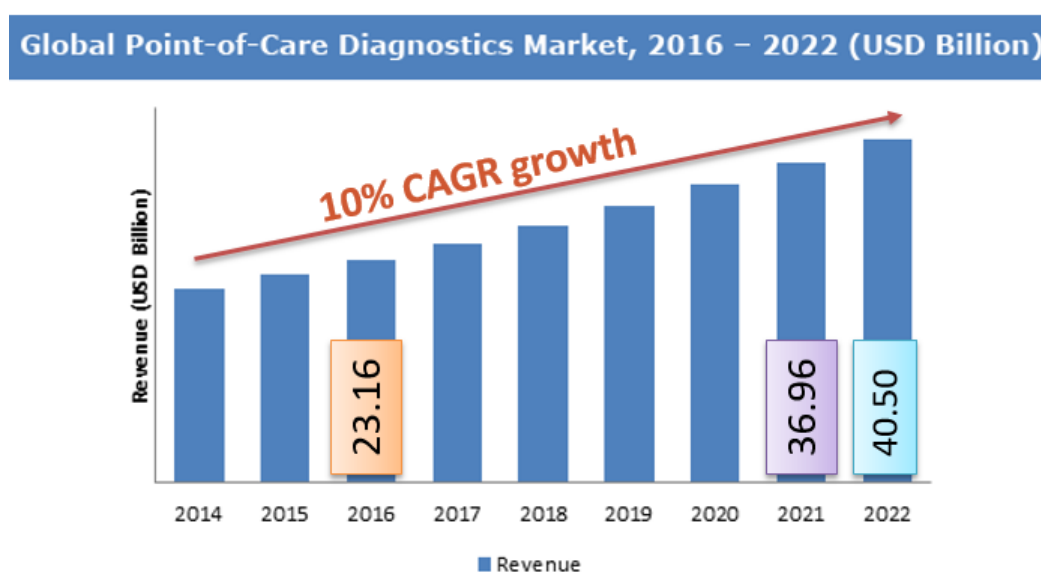


Figure 17 Global PoC diagnostics market forecast

Since the appearance of PoC testing and albeit the constant technology improvements, both diagnostics companies as well as technology developers have put great effort to integrate and automate complicated steps on microfluidic devices. These tests, generally involve molecular analysis, hence requiring bulky equipment or manual intervention from an experienced operator for sample preparation. Nonetheless, 2015 was a major turning point for the PoC industry since the first ever DNA/RNA-based test was CLIA waived by the US FDA. That indicated they are adequately integrated, and user friendly thus allowing being run by inexperienced people promoting their use in decentralised areas. More specifically, in January 2015, the ALERE i Flu A&B Test was the first ever molecular test to be CLIA-waived, followed by Alere i Strep A, Roche's Cobas LIAT Strep A, Flu A&B and Flu/RSV and Cepheid's GeneXpert Flu/RSV Xpress. The roadmap of microfluidics for PoC testing is depicted in Fig. 18. In the near future there will be (if not already here) a transition towards PoC testing not only in hospitals but also in doctor's clinics for molecular diagnostics addressing seasonal diseases (e.g. influenza). Thus PCR-based tests which exhibit much greater sensitivity compared to immunoassays and in addition they are capable of differentiating strains of the same disease will become promising candidates [83].

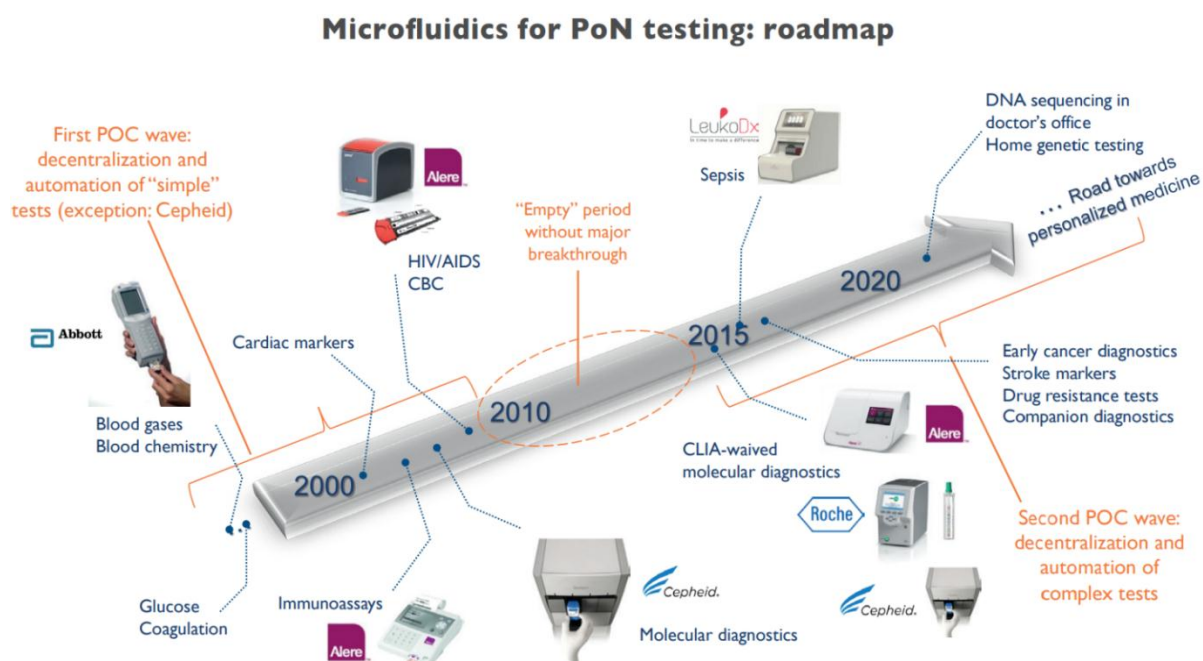


Figure 18 Microfluidics for PoN testing: roadmap

Some of the key players in PoC diagnostics market are: Abbott Laboratories, Inc. (U.S.), Alere Inc. (U.S.), Roche Diagnostics Limited (Switzerland), Siemens AG (Germany), Becton, Dickinson and Company (U.S.), Beckman Coulter, Inc. (U.S.), PTS Diagnostics (U.S.), Johnson & Johnson (U.S.), Instrumentation Laboratory (U.S.), and Nova Biomedical (U.S.), bioMerieux (U.S.) Danaher Corporation (U.S.), Trinity Biotech PLC (Republic of Ireland), OraSure Technologies Inc (U.S.) [84-86]. In Fig. 19 companies that have developed and marketed microfluidic devices for diagnostic applications are illustrated.

In the next few years, the microfluidics industry could experience additional growth booms. More specifically, cancer diagnostics, treatment planning, and follow-up show great potential and hold promise with the increasing use of microfluidic technologies not only at sample preparation level (e.g. circulating tumour cells isolation or DNA in liquid biopsies) but also at diagnostics level (e.g. molecular diagnostics for oncology analysing these cells and DNA molecules).



Figure 19 Companies that have developed and marketed microfluidic devices for diagnostic applications [87]

Additionally, Brice Sagot, Founder & CEO of KnowMade admits that oncology is the main field targeted by patent applicants regarding the domain of microfluidic technologies for diagnostic applications [Microfluidic Technologies for Diagnostic Applications Patent Landscape report, KnowMade, January 2017]. The most prevalent diagnostic technique in patents in this domain is nucleic acid amplification. Another microfluidics application with high potential is organs-on-chip. It could enable predictive models for drug and compound testing thus becoming a multi-billion-dollar market [88].

To sum up, one of the most tremendous challenges engineering and science is asked to deal with is the development of technologies, in order to improve the health and safety of people especially in poor regions. Over the past two decades, microfluidics research has offered sophisticated tools for fluid handling, sample processing and detection. The remaining challenge is the integration of such components into a single device, preferably not requiring complicated instruments to be operated. Typically, these components rely on large equipment

such as computers and syringe pumps thus rendering these platforms ill-suited for remote and low-resource settings.

Nucleic-acid based testing

Nucleic acid testing holds great promise for rapid, specific and sensitive diagnosis both for genetic and infectious disease as well as pathogen detection. The complex nature of biological samples in combination with the low presence of nucleic acid targets in most of them points out the need for nucleic acid amplification in order to obtain adequate sensitivity with the existing technology of biosensors leading to a reliable answer/result.

There are several considerations regarding nucleic acid amplification methods especially when they are to be employed in a Lab-on-Chip or Point-of-care platforms. The leading consideration is the type of amplification template. The existing amplification methods offer the possibility of amplifying varied targets namely dsDNA, ssDNA and RNA. DNA is preferred due to its high stability where appropriate. The use of DNA is more likely to enhance sensitivity in stored and/or transported samples even in suboptimal conditions [89], a characteristic that can be attributed to the persistence of the DNA molecule. On the contrary, the lability of RNA restricts the detection only to viable amplification samples. The main difference between DNA and RNA is that after cell death RNA is degraded while the more stable DNA remains detectable even in a non-viable pathogen [90]. Another major consideration is the operating temperature. Apart from PCR, there also some isothermal amplification methods (RCA) requiring an initial heating step at an elevated temperature (95°C approx.) in order to promote dsDNA separation. This extra heating step not only adds complexity on the heating control mechanism but also augments the power consumption. However, there are numerous isothermal methods that do not require the additional heating steps since specific enzymes are used for dsDNA displacement, and thus they are performed at a single temperature (for example: RPA, LAMP, HDA). The reaction temperatures needed in the isothermal methods vary and range from 30°C to 65°C. The higher the temperature, the higher is the power consumption. The reaction temperature should be carefully chosen in order to maximize the amplification efficiency and simultaneously increase the specificity by eliminating the non-specific primer binding [91, 92] (the higher the temperature the higher the specificity). In the following chapter, more details will be given relatively to nucleic acid amplification methods and their implementation in microfluidic devices.

Chapter 2 DNA amplification methods & DNA amplification in microfluidic devices

Nucleic acid (DNA/RNA) amplification is a powerful tool that has had a critical impact on research and diagnostic industries in the past three decades. The complex nature of biological samples in combination with the low presence of nucleic acid targets in most of these applications points out the need for sufficient nucleic acid amplification in order to obtain adequate sensitivity with the existing technology of biosensors leading to a reliable answer/result. In this chapter some of the most common nucleic acid amplification methods are described as well as the integration of nucleic acid microdevices in LoC systems.

2.1 Introduction

Since 1985 when polymerase chain reaction (PCR) was first reported, a new field has evolved relative to laboratory testing relying on detecting nucleotide sequences in various biological samples. While PCR still remains the most acknowledged method, it requires sample thermocycling for the separation of the dsDNA into two ssDNA strands as well as for subsequent DNA replication. Nevertheless, there is a constant and novel development of alternative isothermal DNA amplification methods which eliminate the need of thermocycling [93]. All these amplification technologies have made immense contribution to the advancement of molecular biology, thus leading to a deeper understanding of the pathology as well as to the accurate diagnosis of diseases [94]. The nucleic acid replication in vivo involves various diverse enzymatic activities, and the accurate replication mechanism relies on the nature of the template [95]. On the other hand, in vitro nucleic acid replication is comparatively simpler and it often requires a single enzyme or enzymatic activity. Formation of nucleic acids in vivo is complex due to the need of single-stranded (ss) template generation in order to commence the replication process. Thus, to achieve localized unfolding and denaturation of double stranded (ds) DNA in vivo, diverse enzymes are required. As for the

in vitro amplification, the formation of single-stranded replication templates is less complicated and is typically accomplished through thermal denaturation. When thermal denaturation is required, thermostable enzymes are preferred. DNA polymerase -the enzyme used in PCR- is responsible for replicating the targeted DNA with the aid of diverse proteins. Recently, these proteins were identified thus enabling the development of novel in vitro isothermal nucleic acid replication methods [96] which mimic the aforementioned in vivo mechanisms. As a result, numerous isothermal amplification methods have been developed relying on enzymatic processes for the generation of replication templates. [97].

There are several considerations regarding nucleic acid amplification methods especially when they are to be employed in a Lab-on-Chip or a Point-of-care platform. The leading consideration is the type of amplification template. The existing amplification methods offer the possibility of amplifying various targets namely dsDNA, ssDNA and RNA. DNA is preferred due to its high stability where appropriate. The use of DNA is more likely to enhance sensitivity in stored and/or transported samples even in suboptimal conditions [89], a characteristic that can be attributed to the persistence of the DNA molecule. On the contrary, the lability of RNA restricts the detection only to viable amplification samples. The main difference between DNA and RNA is that after cell death RNA is degraded while the more stable DNA remains detectable even in a non-viable pathogen [98]. Another major consideration is the operating temperature. Apart from PCR, there are some isothermal amplification methods (RCA) requiring an initial heating step at an elevated temperature (95°C approx.) in order to promote dsDNA separation. This heating step not only adds complexity on the heating control mechanism but also augments the power consumption. On the contrary, there are numerous isothermal methods that do not require the additional heating steps since specific enzymes are used for dsDNA displacement, and thus they are performed at a single temperature (such as RPA, LAMP, HDA). The reaction temperatures in the isothermal methods vary and range from 30°C to 65°C. The higher the temperature, the higher the power consumption is. The reaction temperature should be carefully chosen in order to maximize the amplification efficiency and simultaneously increase the specificity by eliminating the non-specific primer binding [91, 92] (the higher the temperature the higher the specificity).

There are several types of isothermal nucleic acid amplification methods [99] namely strand displacement amplification (SDA) [100, 101], rolling-circle amplification (RCA) [102, 103], nucleic acid sequence-based amplification (NASBA) [104, 105], helicase dependent

amplification (HDA)[106, 107], recombinase polymerase amplification (RPA) [108, 109], loop mediated isothermal amplification (LAMP) [110, 111], single primer isothermal amplification (SPIA) [112], nicking and extension amplification reaction (NEAR) isothermal and chimeric primer initiated amplification of nucleic acid (ICAN) [113], and multiple displacement amplification (MDA) [114, 115].

The most widespread of these DNA amplification methods are described in the sections that follow.

2.2 PCR

PCR technology has become one of the most influential and revolutionary discoveries of the molecular biology leading to a Nobel prize for Mullis in 1993. Due to the great impact of PCR in combination with the thermostable Taq DNA polymerase (the enzyme responsible for the PCR), the pair was declared as the first “Molecule of the Year” by Science in 1989. PCR has been a major player in nucleic acid analyses. It is an enzyme-mediated, temperature controlled amplification method. Since 1986 [116], it has become an indispensable tool in biology related fields. Briefly, the underlying mechanism is performed in 3 steps (Fig. 20a) [117]. Step 1 Denaturation: High temperature (approximately 95°C) is utilized to separate (denature) double stranded DNA into two single strands. Step 2 Annealing: Primers – synthetic single stranded DNA sequences- are utilized to recognize and bracket the region of interest (target) to be amplified. Each primer is complimentary to the start and end of the DNA target region of each single strand. This step requires a reduction of the temperature to approximately 55°C. Step 3 Extension: The complimentary strands are formed by the catalytic action of polymerase enzyme which best functions at 72°C. One PCR cycle comprises these three steps. PCR offers exponential amplification, thus after 20 cycles there is ideally a yield of over one million of copies. Lower yields can be attributed to poor temperature control, poor primer-template hybridization, reagent depletion, sample contamination and insufficient thermal cycling [118].

The success of PCR relies on its simplicity and its cost-effectiveness. Furthermore, it offers the potential for a single DNA molecule amplification (i.e., single-molecule PCR) [119] due to its extremely efficient exponential amplification. However, despite its many advantages,

the main drawback PCR bears is the need for thermal cycling which renders conventional PCR time-consuming.

2.3 HDA

The helicase-dependent amplification was initially described in 2004 [107]. HDA is based on the naturally occurring DNA replication process. A helicase enzyme unfolds the dsDNA target at a temperature of 37 °C circumventing the heat-assisted denaturation step of PCR. The MutL protein triggers the helicase unfolding, while the single-stranded binding (SSB) protein inhibits re-hybridization of the unfolded ssDNA template [120]. Afterwards, primers are allowed to bind on the separated ssDNA and subsequently a DNA polymerase synthesizes the desired amplicon.

The HDA principle is schematically presented in Fig. 20b. Million-fold copies of target DNA could be produced by this exponential reaction in 60 to 120 min. The advent of a heat-stable helicase from *Thermoanaerobacter tengcongensis* eliminated the need of MutL and SSB allowing for a reaction temperature in the range of 45°C to 65°C [121]. Recently, the performance of the HDA regarding the amplicon size was enhanced from initially up to 400 bp to >2000 bp [120]. As for the limit of detection, a sensitivity of 10 copies of bacterial genomic DNA was presented. The simplicity of the HDA is one of the major advantages over other amplification methods since some of them include more than one set of primers. Additionally, compared to other amplification methods the need for initial denaturation is eliminated. HDA offers the ability to detect both DNA and RNA. The efficiency/effectiveness of HDA was validated with varied samples, from blood [122], urine and vaginal swabs. Because of the aforementioned attributed, HDA is considered as promising candidate for LoC or PoC devices [123].

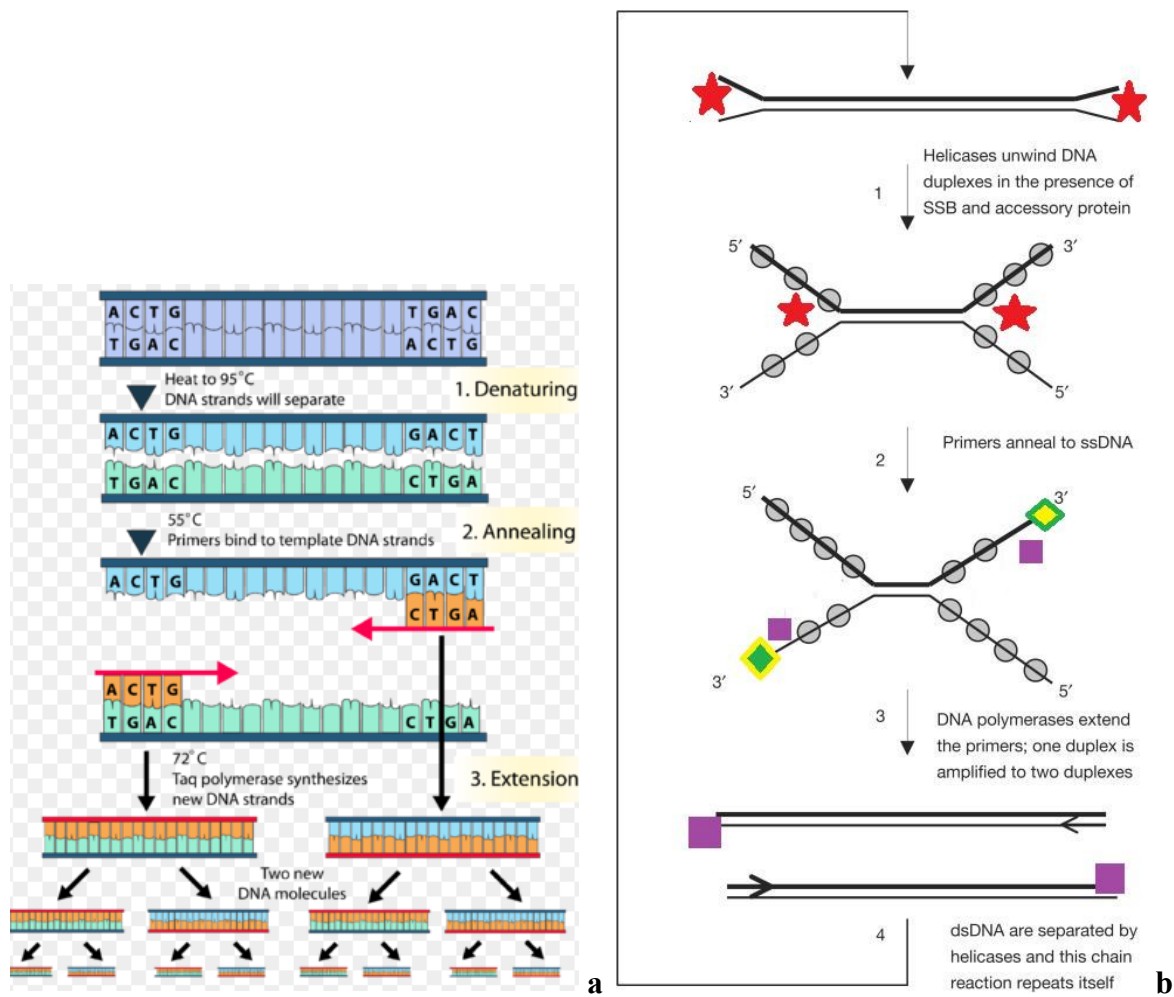


Figure 20 a) PCR principle PCR comprising 3 steps: 1: Denaturation (dsDNA unwinds) @95°C, 2: Annealing @ 55°C (primers bind to specific regions on the template), 3: Extension @72°C (DNA polymerase synthesizes the amplicon) [117], b) Schematic diagram of HDA principle: 1: A DNA helicase (red star) unfolds the dsDNA which are bound by SSB (grey circles). 2: primers (yellow-green rhombus) bind to the targeted dsDNA region. 3: A DNA polymerase (purple square) synthesizes the amplicon. 4: Amplicons continue to the next amplification round [121]

2.4 RCA

RCA was first described in 1998 [124]. RCA takes advantage of the excellent strand displacement activity of a Phi29 bacteriophage polymerase on targeted DNA templates. RCA allows for the amplification of a ssDNA to form a continuous concatenated product of up to 5×10^5 bases. So far different approaches have been reported to perform the reaction. Some of them are described in [125-127]. The padlock probes approach is one of the most successful

for linear DNA. Padlock probes are linear oligonucleotides comprising two target specific sequences, which have the ability to circularize upon hybridization and subsequent ligation as shown in Fig. 21 [123]. Specificity of detection is ensured by the dual recognition jointly with a ligation reaction. Subsequently, the circular padlock probe is used as template for the polymerase, which continuously synthesizes the product and unfolds the generated strand since it has a displacement activity. Furthermore, it is possible to employ extra primers binding the generated amplicon and thus resulting in hyper branching structures. The previously described reaction is called ramification amplification and it was initially described in 2001 by Zhang et al. [128]. As for the limit of detection, optimized RCA was able to detect less than 0.2 pg of genomic DNA stemming from *Listeria monocytogenes* [129].

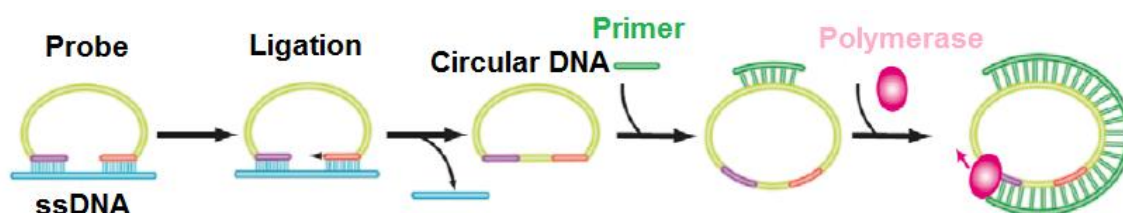


Figure 21 Principle of RCA method [123]

2.5 RPA

RPA reaction was first described (and patented) in 2006 by Piepenburg. Compared to other isothermal amplification methods, a single temperature typically being 37°C is required. The sensitivity of RPA is comparable to that of PCR. Both amplification and detection of less than 10 DNA copies have been demonstrated [130]. Apart from the low reaction temperature, RPA combines short reaction duration i.e. 15-30 min. These two main characteristics offer great potential for PoC tests. Essentially, RPA couples isothermal recombinase-driven primer annealing on the DNA template with the strand-displacement DNA formation. RPA amplifies DNA sequences by employing three proteins namely a recombinase, DNA polymerase and single-stranded DNA-binding proteins (SSBs). A RPA cycle initiates with the binding of a recombinase to the primers in the presence of ATP. After the formation of the recombinase-primer complex, it attaches to the ds DNA, making the 3'-ends of the primer accessible to DNA polymerase. ssDNA is created due to the displacement activity of the DNA polymerase. The stabilization of the ssDNA is aided by the SSBs enabling the accessibility of both strands

and thus leading to exponential amplification. The principle of the RPA method is depicted in Fig. 22 [131]. TwistDX (Cambridge, UK) made RPA kits commercially available.

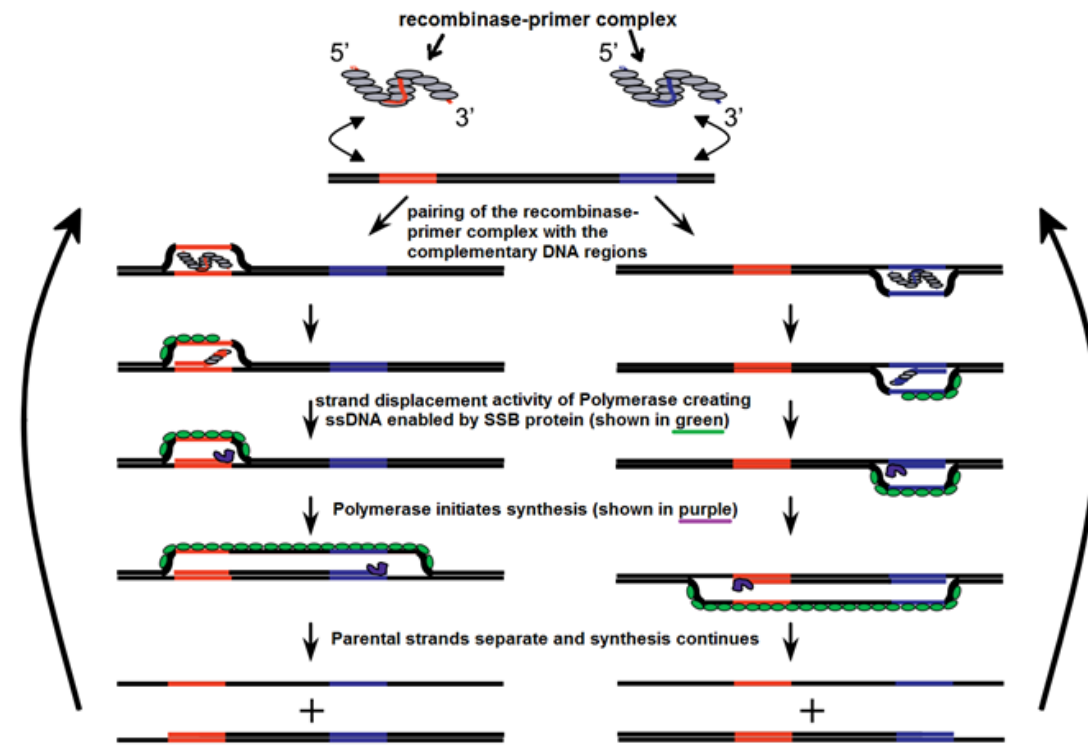


Figure 22 Schematic of the RPA method [131]

2.6 LAMP

The loop-mediated isothermal amplification LAMP was initially presented in 2000 and commercially exploited by the Japanese Eiken Chemical Co, Ltd. (Tokyo) [132]. LAMP is described as an extremely promising amplification tool suitable for microsystems. Fundamentally, LAMP reaction makes use of a strand displacement activity DNA polymerase and 4 or 8 specifically designed primers recognizing 6 or 8 distinct nucleic acid sequences on the DNA template under isothermal conditions (60-65°C). On average, the duration of the reaction is about 60 minutes, exhibiting a surprisingly high specificity [133]. Additionally, LAMP offers high amplification efficiency allowing the synthesis of huge amounts of DNA in a short time. As for the detection limit of LAMP is down to a few copies per reaction and thus is directly comparable to that of PCR. In order to perform the LAMP assay, a heating block or a water bath at a constant temperature is necessary. LAMP can also

be performed using RNA templates with the aid of a reverse transcriptase under the same working conditions (temperature 60-65°C) and without any additional time for the transcription [134].

There are various means of detecting LAMP amplification products such as gel electrophoresis, turbidity or directly with the naked eye. A major characteristic of LAMP is the synthesis of large amounts of DNA which yield pyrophosphate ion by-product rendering it visually observable since this by-product precipitates. The reaction is performed using a set of two specially designed inner and outer primer pairs and a DNA polymerase with strand displacement activity. LAMP steps are presented in Fig. 23 [123]. DNA template regions F3 and R3 are complementary to F3c and R3c respectively. The F2 region in the forward inner primer FIP is complementary to the F2c region followed by the F1c complementary to F1 of the target DNA. The design of the backward primer follows the same principle. Thus, these four primers recognize six specific nucleic acid sequences of the DNA template ensuring high amplification specificity. In addition, the generation of a stem-loop DNA for subsequent LAMP cycling is enabled by these primers including self-priming reactions. A DNA mixture, varying in the number of loops as well as the lengths of the stem loop, is formed as end products. LAMP is considered a promising candidate for point-of-care applications due to its ease of operation, high specificity and sensitivity [123].

2.7 DNA amplification in μ -fluidic devices

The integration of nucleic acid (NA) amplification methods in microfluidic devices represents a hugely promising concept for the development of simple, cheap and efficient diagnostic tools for food safety, environmental monitoring, and clinical applications. Such tools are anticipated to operate in resource-limited settings as point of care (PoC) diagnostics. The amplification process of the target NA sequence comprises a crucial/indispensable step for the development of sensitive and accurate detection assays.

μ PCR devices

The most popular method for NA amplifications for integration in microfluidic devices is PCR, though PCR is undoubtedly restricted by the thermal cycling needed to achieve the NA amplification. As a promising alternative, isothermal (performed at constant temperature)

amplification methods have emerged, thus greatly simplifying the implementation of such amplification methods in PoC diagnostics and devices to be employed in resource-limited settings [135].

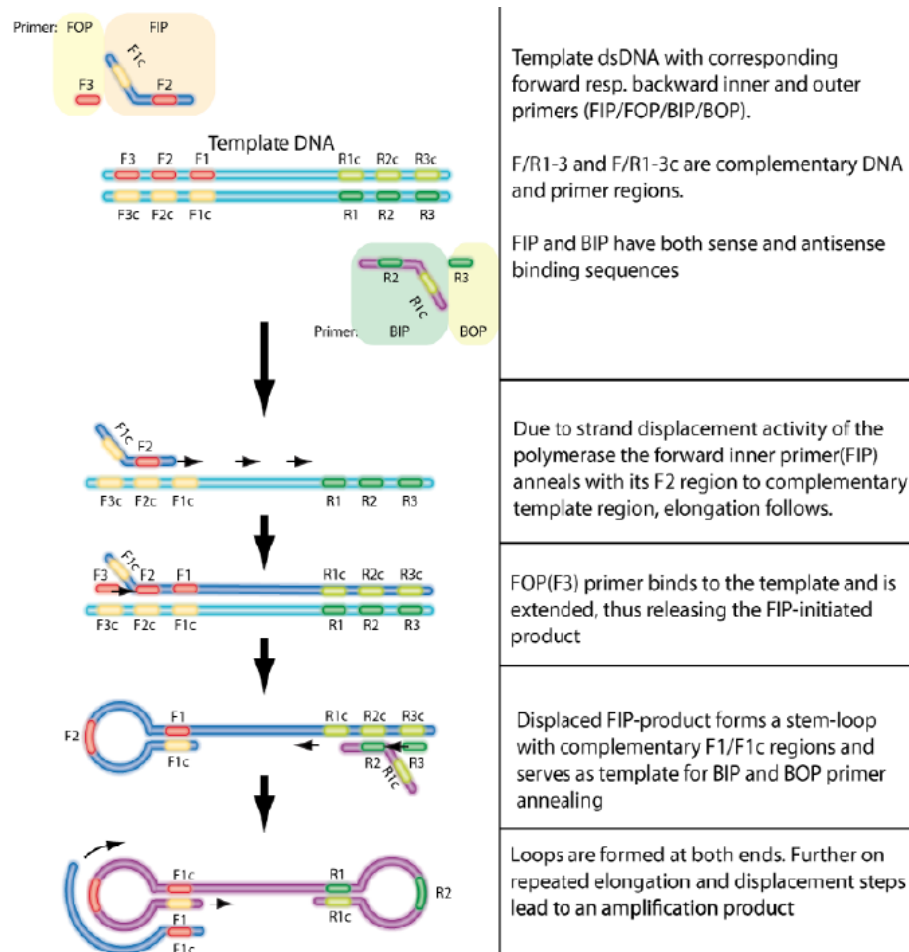


Figure 23 LAMP amplification method [123]

The most popular method for NA amplifications for integration in microfluidic devices is PCR, though PCR is undoubtedly restricted by the thermal cycling needed to achieve the NA amplification. As a promising alternative, isothermal (performed at constant temperature) amplification methods have emerged, thus greatly simplifying the implementation of such amplification methods in PoC diagnostics and devices to be employed in resource-limited settings [135].

The first integration of NA amplification in a microfluidic device was reported by Northrup et al., in 1993 [136] comprising a static well PCR device, mimicking a conventional

thermocycler. Though, many steps forward have been made since then. In 1999, PCR amplification performed in stationary droplets (digital PCR) was presented by Vogelstein and Kinzler [137]. Ten years later, the same method was implemented in continuous-flow droplet setup by Schaerli et al. [138] paving the way for innovative approaches addressing the ultrasensitive quantification of NA [139]. More specifically, digital PCR involves dividing a solution of the NA target mixed with the PCR amplification reagents into numerous discrete reactions where single DNA molecules are statistically confined. In a nut shell, μ -PCR devices can be categorized into two main types: well-based and continuous-flow (CF) PCR chips. In turn, CF μ -PCR devices can be subdivided into three categories i) fixed loop, ii) closed loop and iii) oscillatory. In table 7, an overview of μ -PCR devices is presented [140].

Table 7 Representative examples of μ -PCR devices [140]

Type	Material	Cycles *	Detection	Year & Ref.
Well-based	SU-8	Melting curve experiment 35 (199 bp, 90 min)	SYBR Green (melting curve) Electropherogram (off-chip)	(2004) [141]
	PDMS/Glass (droplet array)	40 (several amplicons, 65 min)	EvaGreen (real-time + melting curve)	(2009) [142]
	Silicon (droplet array)	45 (18–25 bp, 65 min + 66 min) micro RNA, RT-PCR	TaqMan probes (real-time)	(2011) [143]
	Polycarbonate	32 (243 and 96 bp, 45 min)	CE (on-chip)	(2016) [144]
Fixed-loop	Glass	20 (176 bp, 1.5–19 min)	Gel + EtBr (off-chip)	(1998) [145]
	Glass	20, 25, 30, 35 and 40 (230 bp, 17 min for 40 cycles)	SYBR Green (off-chip)	(2003) [146]
	PMMA	20 (990 bp, 57 min)	Gel + EtBr (off-chip)	(2009) [147]
	Pyralux	30 (90 bp, 5 min)	Gel + EtBr (off-chip)	(2014) [148]
	FEP tubing	40 (Plasmid clones and Escherichia coli 40 min)	TaqMan probes	(2014) [149]
Closed-loop	Ceramic	40 (209 bp, 27–70 min)	Electronic	(2003) [150]
	Teflon	35 (305 and 700 bp, 73 min)	Gel + EtBr (off-chip)	(2004) [151]
Oscillatory	Silicon/Pyrex	20–30 (only theoretical model)	Gel + EtBr (off-chip)	(2003) [152]
	Silicon	35 (Human papillomavirus, 15 min)	Gel + EtBr (off-chip)	(2005) [153]
	PDMS	12(–20) (Plasmid DNA, 3–4 min)	SYBR Green	(2007) [154]
	PDMS/Glass	30 (Hepatitis B virus, 23 min)	TaqMan probe	(2014) [155]

Integrated μ fluidic devices & commercially available NA amplification platforms

In table 8 below fully integrated μ -fluidic devices for PoC testing implementing NA amplification are presented [156].

Table 8 Fully integrated μ -fluidic devices for PoC testing [156]

Device type	Extraction	Amplification	Signal read-out	Target	Limit of detection	Detection time	Automation
Integrated chip	SE	PCR	Fluorescence	Virus	5000 copies of virus	—	No
Integrated chip	SE	LAMP	Fluorescence	Human gene	—	40 min	No
Integrated chip	SE	HDA	Lateral flow strip	Bacteria	10^2 CFU	60 min	No
Integrated chip	SE	—	Electrophoresis	Bacteria; virus	10^4 copies/mL	—	No
Integrated chip	PE	LAMP	Lateral flow strip	Virus	10^6 copies/mL	45 min	No
Integrated chip	MBE	PCR	Electrochemical sensor	Virus	10 TCID ₅₀	3.5 h	No
Integrated chip	MBE	PCR	Fluorescence	Virus	—	95 min	Yes
Integrated chip	MBE	—	Fluorescence	Virus	0.021 pfu/mL	1 h	No
Integrated chip	MBE	PCR	Fluorescence	Human gene	—	—	Yes
Integrated chip	SE	LAMP	Fluorescence	Human gene	0.01% (mutant)	1 h	No
Integrated chip	PE	SDA	Lateral flow strip	Bacteria	$\sim 5 \times 10^3$ genomic copies	<60 min	No
Integrated chip	MBE	—	Fluorescence	Virus	0.2 pfu/mL	—	Yes
Slipchip	SE	PCR	Capillary electrophoresis	Human gene	1 μ L whole human blood	60 min	Yes
Slipchip	—	PCR	Fluorescence	Bacteria	—	3 h	No
Pipette tip based device	PE	LAMP	Fluorescence	Bacteria; virus	2 copies of plasmids	90–160 min	No
Capillary-tube based device	PE	LAMP	Fluorescence	Human gene	—	150 min	No
CD	SE	LAMP	Fluorescence	Bacteria	10^2 CFU/mL	2 h	Yes
CD	SE	PCR	Fluorescence	Bacteria	2 CFU	3 h and 45 min	Yes
CD	MBE	PCR	Fluorescence	Virus	—	—	Yes
CD	SE	PCR	Fluorescence	Bacteria; virus	—	—	No
CD	SE	LAMP	Colorimetric read-out	Bacteria	10 bacterial cells	<65 min	Yes
CD	SE	LAMP	Lateral flow strip	Bacteria	50 CFU	80 min	Yes

Isothermal amplification microdevices

LAMP reaction can yield up to 10^9 amplicon copies ($t < 1$ h @ 60–65 °C) with a comparable detection limit to PCR [157]. LAMP is suitable for DNA amplification of pathogens since it can amplify a few hundred base pair long NA sequences. Additionally, LAMP is not inhibited in complex biological matrices contrary to PCR which is an enzymatic reaction. Colorimetric detection of LAMP products is achieved by using different dyes [157]. Such colorimetric assays coupled with centrifugal microfluidic devices have been used for foodborne pathogen detection such as *Escherichia coli* and *Salmonella Typhimurium*, offering also multiplexity (Fig. 24a) [158]. LAMP was also employed in paper microfluidics for the detection of *E. coli* [159].

Lutz et al. first demonstrated the integration of RPA in a centrifugal microfluidic device in 2010 [130]. The suggested μ -device contained pre-stored liquid and RPA reagents in dry form. It was employed for detection of the antibiotic resistance gene *mecA* of *S. aureus*. Four years later, Kim et al. demonstrated centrifugal microfluidic device performing not only lysis/DNA extraction, and isothermal RPA but also detection (see Fig. 24b). The device was used for *Salmonella* detection in spiked-milk samples within 30 min [160]. The centrifugal

microfluidic configuration was implemented in several RPA μ -devices offering improved multiplex analysis capabilities and compatibility with complex matrices [161, 162].

A microfluidic device integrating NASBA amplification with fluorescence detection of Norovirus in oysters was presented by Chung et al. [163] (Fig. 24c). Reinholt et al demonstrated a PMMA μ -fluidic device performing NASBA amplification using NA isolated from lysate samples for the detection of *Cryptosporidium parvum* in water samples [164]. More recently, NASBA amplification was integrated in a portable biomolecular platform for the rapid, and low cost detection of Zika virus [165].

Various μ -fluidic device configurations have been demonstrated for the implementation of RCA amplification such as rotary valveless μ -devices for the multiplex identification of five point mutations of the TP53 gene [166] and droplet-based devices (Fig. 24d) employing magnetic beads between droplets for the detection of synthetic *Pseudomonas aeruginosa* DNA[167]. In addition, μ -fluidic technology was merged with the RCA method for the identification specific protein markers on tumor- cell surfaces using nanoliters droplets [168].

In addition, HDA amplification method takes advantage of a simple design assay, rendering this method more appealing for the integration in LoCs. Numerous microfluidic devices implementing the HDA method have been demonstrated. For example Mahalanabis et al. demonstrated a μ -fluidic device integrating NA extraction, amplification and detection [169], whereas others require extra sample processing steps for the detection of infectious diarrhea (Fig. 24e) [170] or breast cancer [171].)

Non-isothermal amplification microdevices

Moreover a well-based PCR chip for NA amplification (Fig. 24 f) [141], g) and a closed-loop PCR chip for NA amplification (Fig. 24 g) [172], h) as well as a 30-cycle continuous flow PCR chip for NA amplification Fig. 24 h [148] were previously presented.

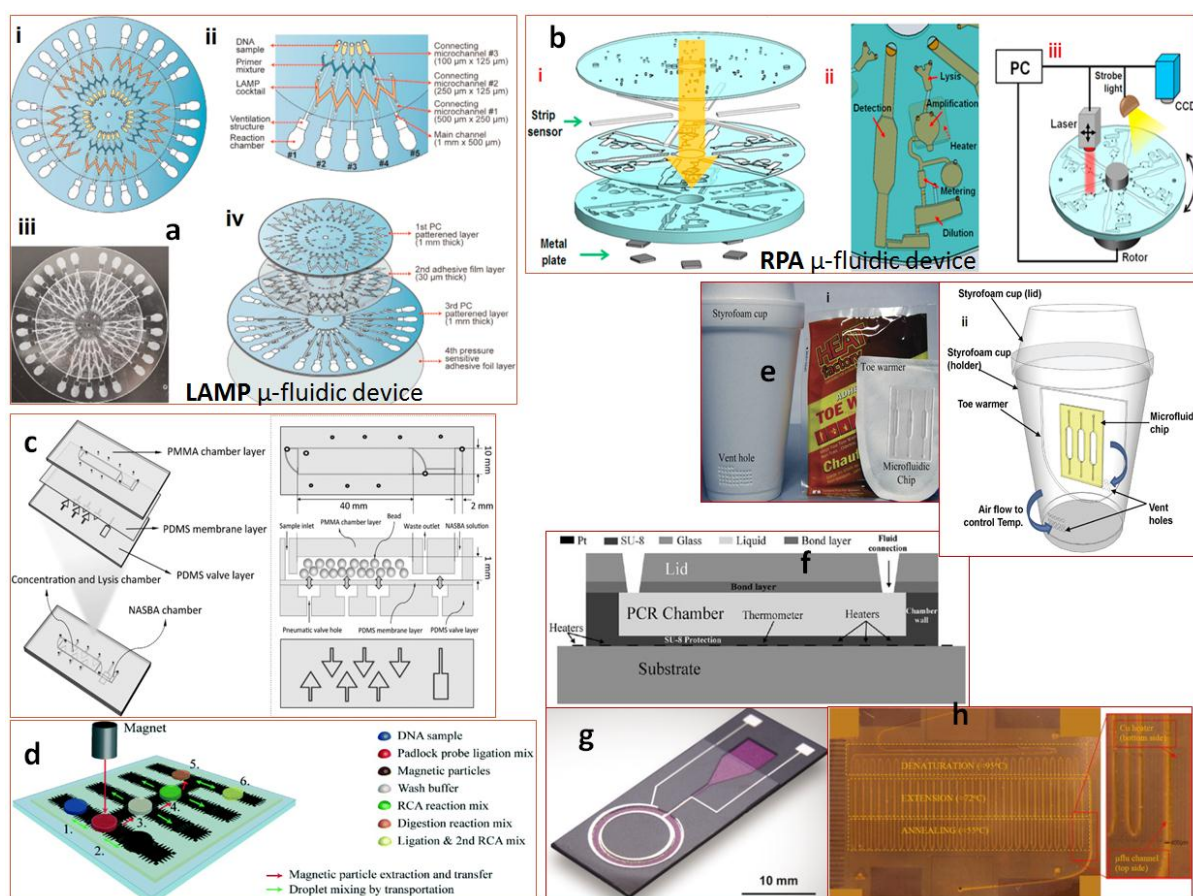


Figure 24 a) i. Schematic illustration of centrifugal LAMP microdevice. ii. Detailed structure of one unit of the microdevice. iii. Assembled microdevice. iv. Schematic illustration of the disassembled microdevice showing four layers[158] b) i. RPA Lab-on-a-disc showing top and bottom plates made of polycarbonate, strip sensors, adhesive layer, and the metal heater. ii. Section of the disc featuring the chambers for cell lysis, isothermal amplification, metering, dilution, and detection. iii. Schematic illustration of the experimental setup [160] c) NASBA μ -fluidic chip for cell concentration, cell lysis and RNA extraction, NASBA amplification and detection[163] d) RCA digital μ -fluidic chip and assay layout. Positions of droplets with reaction mixes are depicted. Mixing of two droplets is illustrated with green arrows with double arrowheads. Mixing of single droplets is illustrated by green arrows with single arrowhead. Magnetic particle transfer between droplets is indicated with red arrows [167], e) i. Polymer-based microfluidic chip with multiple reaction chambers, a toe warmer, and Styrofoam cups; ii. Vent holes on the sides of the Styrofoam cup control the air supply to initiate and maintain the oxidation reaction in the toe warmer; the number of holes controls the temperature of the reaction chamber, f) well-based PCR chip for NA amplification [141], g) closed-loop PCR chip for NA amplification [172], h) continuous flow PCR chip for NA amplification [148]

Several platforms employing isothermal NA amplification methods have been recently made commercially available. For example, Genie®II (OptiGene) and Illumigene® (Meridian Bioscience Inc.) are two platforms based on LAMP amplification. In addition, NucliSENS easyQ® (BioMérieux) and OligoC-TesT (Coris BioConcept) rely on NASBA whereas Twista® (TwistDx, UK) relies on RPA. Furthermore, AmpliVue® (Quidel Corporation) relies on HDA and BD Probetec™ ET System (Becton Dickinson, USA) exploits the SDA approach [135].

Chapter 3 Biosensors-Detection Schemes

In this chapter the general concepts of biosensing are given along with classification of the existing biosensors. More focus is given on acoustic wave biosensors, since these are the ones used in the present thesis. Existing Surface acoustic wave sensors coupled with microfluidics are described in detail. Finally, the motivation, the objectives and the novelty of this thesis is presented in the last subsection.

3.1 Introduction-General Concepts of Biosensing

Advancement in micro/nanotechnology-based sensing methods have been met with critical challenges in the development of diagnostic devices allowing for the simultaneous detection on a single platform of different types of biotargets for monitoring. The urgent need to rapidly characterise and detect microorganisms in several samples is imperative in various industries, such as environmental monitoring, food and agriculture, healthcare, and biodefense which are the key players [173-175]. The inability for culturing most of naturally occurring micro-organisms besides the demonstrated need compels a rapid, reliable, robust and sensitive platform, such as a LoC system. The Centre for Disease Control and Prevention (CDC) in the United States has compiled a list of various biological threat agents [176] including *Bacillus anthracis* (anthrax), *Yersinia pestis* (plague), *Francisella tularensis* (tularemia), *Variola major* (smallpox), *Coxiella burnetii* (Q fever), botulinum toxin (botulism), *Brucella* spp. (brucellosis), ricin, *Vibrio cholera* (cholera), *Shigella* and *Salmonella* spp. The aforementioned biological agents are transmitted via water, food, insect vectors or by direct contact [177, 178]. Microfabrication technology has paved the way for biosensors miniaturisation in response to augmented demand for their employment in medical and environmental diagnostic applications. Global Industry Analysts, Inc., have indicated that biosensors provide low-cost, low-power and compact devices both for and point-of-care medical and environmental monitoring applications.

Biological and biochemical processes play an extremely crucial role in biology, biotechnology and medicine. However, it is very challenging to directly convert biological data to electrical signal. Biosensors can overcome this difficulty. A biosensor can be regarded as a device comprising a biological recognition system (bioreceptor) and a transducer. The interaction between the analyte and the bioreceptor is designed to obtain an effect measured by the transducer, which in turn converts the acquired information into a measurable signal (i.e. electrical signal). Fig. 25 depicts the conceptual principle of biosensing. Biosensors can be classified either by their transducer or their receptor type (Fig. 26).

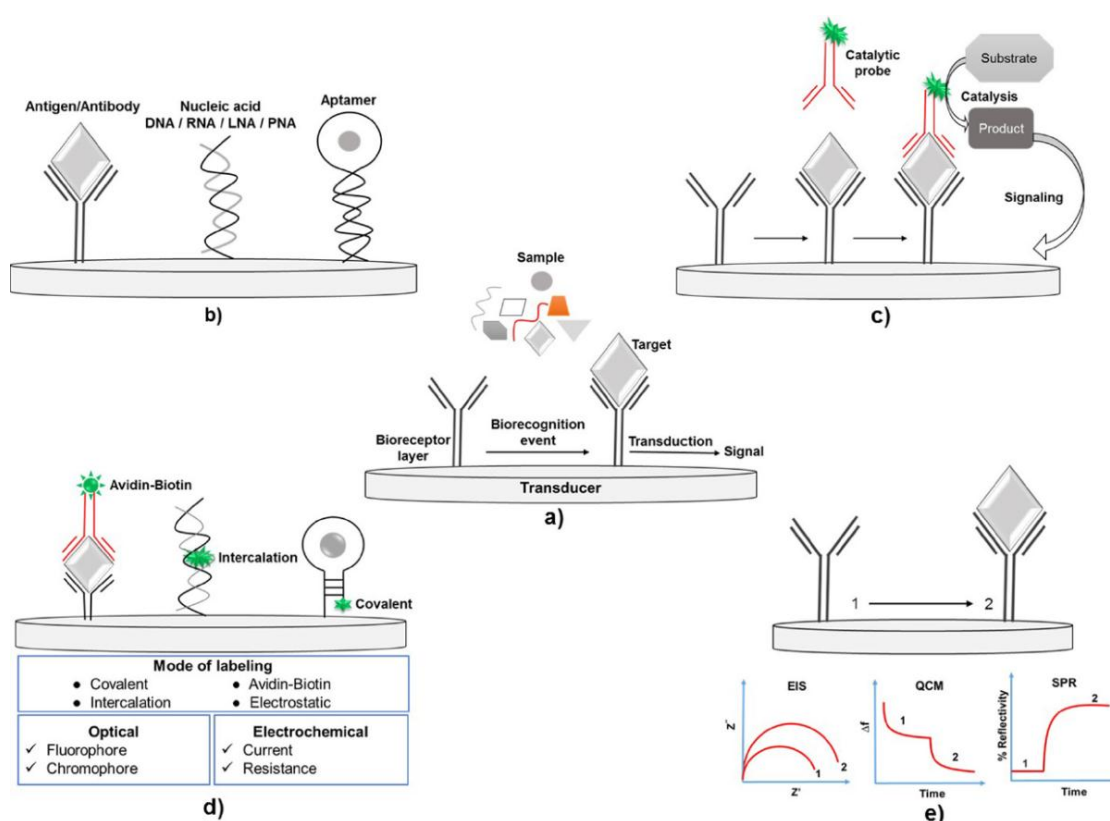


Figure 25 (a) Illustration of a biosensor comprising a bioreceptor layer on a transducer layer, which captures its target during biorecognition event followed by signal transduction. (b) Affinity based biosensors such as antigen-antibody, nucleic acid hybridization involving ribo—(RNA), deoxyribo—(DNA), peptide (PNA), and locked (LNA) nucleic acids, and aptamer based biosensors. (c) Catalytic biosensors involving catalytic probe such as probe-enzyme complex, which converts substrate into a product after binding an analyte leading to signal transduction. (d) Labeled biosensors involve labeling of bioreceptor or probe via various modes, such as covalent bonding, avidin biotin interaction, intercalation, electrostatic attraction. These labeled biosensors are commonly coupled with optical and electrochemical transduction. (d) Label-free biosensors directly transduces biorecognition event by converting a physical change such resistance, mass, and reflectance into electrical signal using techniques such as electrochemical impedance spectroscopy (EIS), quartz crystal microbalance (QCM), and surface plasmon resonance (SPR), respectively [179].

Bioreceptors are biological molecular species (such as enzymes, antibodies, nucleic acids or proteins), or living biological systems (such as whole organisms, tissue or cells) employing a biochemical mechanism for recognition. A bio-sensitive layer is part of sampling component. This layer can either comprise bioreceptors covalently bound to the transducer or contain bioreceptors. The most commonly used forms of bioreceptors in biosensing rely on 1) nucleic acid interactions, 2) antibody/antigen interactions, 3) cellular interactions (such as microorganisms, proteins) 4) enzymatic interactions and 5) interactions employing biomimetic materials (such as synthetic bioreceptors). Regarding transducer classification, traditional techniques comprise: 1) mass-sensitive measurements (such as surface acoustic wave, microbalance, 2) optical measurements (such as absorption, luminescence, surface plasmon resonance) 3) electrochemical [180]. The development of biosensors was first reported in the early 1960s. First Clark and Lyons described a biosensor in 1962. They managed to immobilize glucose oxidase (GOD) on an amperometric oxygen electrode surface semipermeable dialysis membrane in order to directly measure glucose concentration in a sample [181]. Recently, biosensors have seen a tremendous growth in various applications especially in biological/biomedical monitoring and environmental sensing applications.

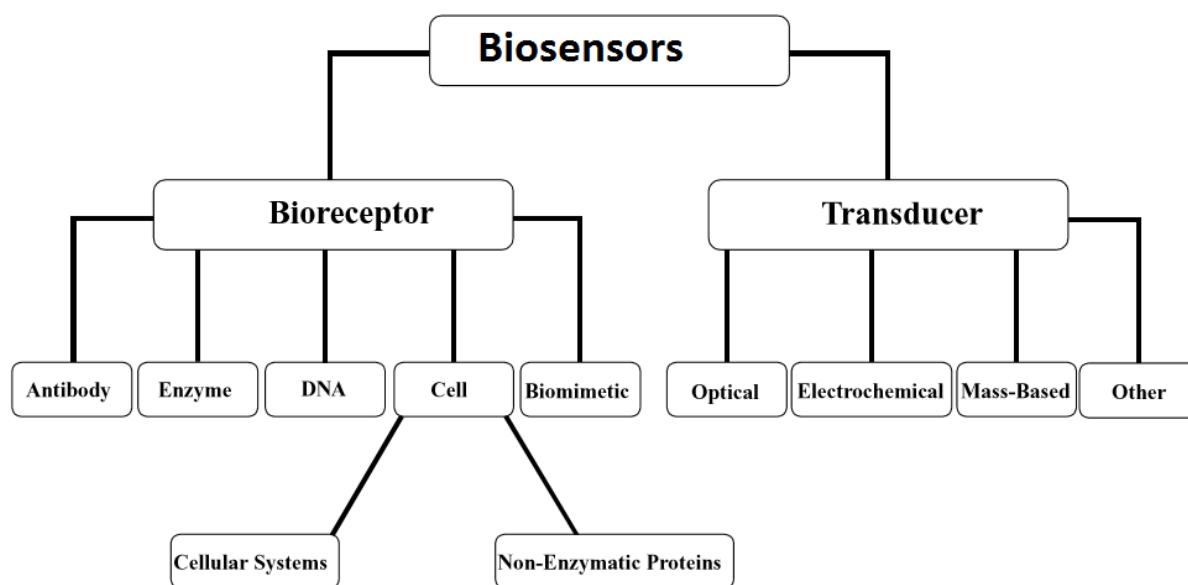


Figure 26 Schematic of biosensor classification schemes

Biorecognition elements

Enzyme-based biosensors are extremely popular with more than 2000 articles published in the literature possibly stemming from the need for glucose monitoring in blood [182, 183] as well as the ease of fabrication of such biosensors. The utilization of enzymes as the biological recognition element consisted the most common method in the development of the 1st generation of biosensor mainly due to their commercial availability and/or ease of isolation and purification from various sources. Among various oxidoreductases, horseradish peroxidase, alkaline phosphatase and glucose oxidase have been used in numerous biosensor studies [184-186]. During the last two decades, affinity biosensors have drawn great attention considering they provide information about binding of cell receptors to their ligands, antibodies to antigens and DNA/RNA to complementary sequences of nucleic acids. The detection of specific DNA sequences has been supported for detecting viral and microbial pathogens [187] since viruses are practically DNA or RNA composed within an outer capsid or coat of protein. Generally, the DNA biosensors use relatively short synthetic oligodeoxynucleotides for the detection of the target DNAs with the same length [188]. This system can be employed for repeated analysis due to denaturation ability of the nucleic acid ligands to reverse binding followed by regeneration [189].

Why DNA for diagnostics?

DNA detection of PoC platforms enables personalized healthcare. For instance, if the sequence of an individual's complete genome is known, the prescription can be pharmacogenomically adapted to the patient in order to provide a personalized treatment scheme maximizing its efficiency. Apart from the whole genome sequencing, tumor mutation profiling and highly specific disease markers identification is enabled by DNA-based diagnostics [190].

General DNA sensing technique for diagnostics

There is an increased demand for high-throughput DNA analysis platforms assisting diagnostics in clinical and research. The standard approach comprises the amplification of the DNA sample through PCR followed by fluorescence detection of the amplified DNA relying on their electrophoretic mobility on a gel substrate [191]. The aforementioned approach requires the employment of separate facilities for each step, including well-equipped

laboratories with highly trained operators. Another valuable approach for DNA sequencing is the utilization of fluorescence hybridization assays. These assays are based on the selective immobilization of ssDNA or RNA strands on a solid substrate. The immobilized ssDNA entities are complementary to the ssDNA to be hybridized. The probe DNA is labeled with fluorescent markers and supplemented to the chip which carries the immobilized test DNA. Hybridization events could be optically detected since probed DNA carries fluorescent tags.

Microfluidic DNA sensor for PoC diagnostics

The need of a complex tool-chain (i.e. PCR, electrophoresis, and fluorescence scanner) accompanied by the high cost of the hybridization assay tools consist the dominant reason for the restricted use of DNA-based diagnostics. In 2004 Gascoyne *et al.* [192] conducted a comparison of different methods along with DNA hybridization for detection of Malaria and it was demonstrated that significant advantages could be offered when using genetic detection methods contrary to microscopy assays once they are implemented in a microfluidic platform. Based on the success of the “standard” approach relative to DNA-based analysis, the development of DNA-based microfluidic diagnostics has mainly focused on imitating the standard approach, comprising PCR and gel electrophoresis, by incorporating the various steps into a microfluidic platform for PoC applications. Miniaturization is useful since the conventional macroscopic liquid handling causes sample dilution and the utilization of multiple instruments leads to sample loss and carries contamination risks [193].

3.2 Classification of Biosensors

Although various transducer methods have been proposed for the development of biosensor technology, electrochemical, optical and piezoelectric are the most prevalent methods [184-187]. Typically, biosensors associate with one of the following categories of signal transduction:

Optical-detection

Optical detection biosensors are the most diverse category of biosensors since they can be employed for numerous types of spectroscopy, such as fluorescence, absorption, Raman, SERS, phosphorescence, refraction, and dispersion spectrometry. Furthermore, different properties can be measured by these spectroscopic methods, such as energy, decay time,

amplitude, and polarization. For instance, amplitude is the most commonly measured property since it can readily be correlated to the analyte concentration [194]. Optical sensors make use of optical fibers or planar waveguides in order to direct light towards the sensing film. Propagating evanescent waves from waveguides can be employed to probe only the sensing film to diminish the optical background signal from the sample. Optical biosensors are attractive for simultaneous screening of numerous samples; however, miniaturization for bloodstream implants is challenging. Another complication is the requirement of a spectrophotometer in order to detect any signal changes in the majority of optical transduction methods.

Electrochemical

Electrochemical sensors detect and measure the electrochemical changes occurring upon chemicals interaction with a sensing surface of the detecting electrode. The current produced from reduction and oxidation reactions is measured by electrochemical biosensors. The concentration of the electroactive species present or its rate of consumption/production can be correlated to the current produced [194]. The electrical changes can rely on the voltage difference measured between the two electrodes (potentiometric), the current difference measured at a constant voltage (amperometric), or a change in the charge transport which is an inherent property of the sensing material (conductometric). Electrochemical biosensors seem to be more suitable for field monitoring applications (e.g. portable) and relatively easily miniaturized towards the development of an implantable biosensor. Based on their characteristics such as simplicity, high sensitivity, and cost competitiveness, the majority of the reported biosensors in the literature rely on electrochemical transducers [188].

Mass-sensitive

Measurement of small changes in mass is alternative form of transduction that has been employed for biosensors. The principle means of mass analysis is based on the use of piezoelectric crystals. Mass sensors produce a signal relying on the interaction of mass with the sensing film. Acoustic wave devices, fabricated by piezoelectric materials, consist the most common sensors, which upon voltage application to the crystal bend. In acoustic wave sensors, an oscillating voltage is applied at the resonant frequency of the crystal, and the change in resonant frequency is measured once the target analyte interacts with the sensing surface. The application of an electrical signal of a specific frequency can cause these crystals

to vibrate at a specific frequency. The oscillating frequency depends on the electrical frequency applied to the crystal as well as the crystal mass. Therefore, an increase in mass due to binding of chemicals causes a change in the oscillation frequency of the crystal, thus the resulting change can be measured electrically and employed to determine the additional mass of the crystal [180].

Thermal detection

Changes in temperature upon a reaction between a biomolecule and a suitable analyte are measured by thermal biosensors [195]. The change measured in temperature can be correlated to the amount of products formed or reactants consumed.

3.3 Acoustic wave biosensors

The term acoustic wave sensor can be used to indicate various significantly different devices. The common characteristic of these microdevices is the involvement of acoustic waves on their operating principle. The general operation principle of an acoustic wave sensor is a traveling wave in combination with a concrete/ specific structure producing a standing wave. The frequency of the wave is jointly determined by the dimensions of the specific structure and the velocity of the traveling wave. As a result, the measurand can cause a change in the wave velocity and/or an alteration in the amplitude of the traveling wave (degree of dampening).

As for the acoustic (traveling) waves, there are two main categories: bulk acoustic wave (BAW) – the wave propagates through the interior of the substrate- and surface acoustic waves (SAW) –the wave propagates on the surface of the substrate. In the case of BAW two types of waves can be propagated, longitudinal and shear waves where the vibration is parallel and perpendicular to the direction of the propagating wave, respectively. Shear waves have lower velocity than longitudinal.

SAW can be differentiated into Rayleigh and Love waves (Fig. 27), Lamb waves and surface transverse waves by vibration and propagation. As for SAW, Rayleigh waves are the most common. They are 2D waves (longitudinal and shear) and are restricted at the surface down to a penetration depth similar to the wavelength [196]. The wave consists of a shear and a longitudinal component normal to the surface. Rayleigh waves cannot be efficiently

employed in liquids due to the high acoustic losses when immersed. Lamb waves are linked with Rayleigh waves propagating in plates. They can be considered as being composed of two Rayleigh waves which propagate on each side of the plate. As for Love waves, they are guided acoustic modes propagating in a thin layer deposited on a substrate. The main disadvantages of Lamb sensors are the fabrication cost (membrane fabrication) and the device fragility. The high mass sensitivity of Love waves is explained by the concentration of the acoustic energy on the guiding layer [197].

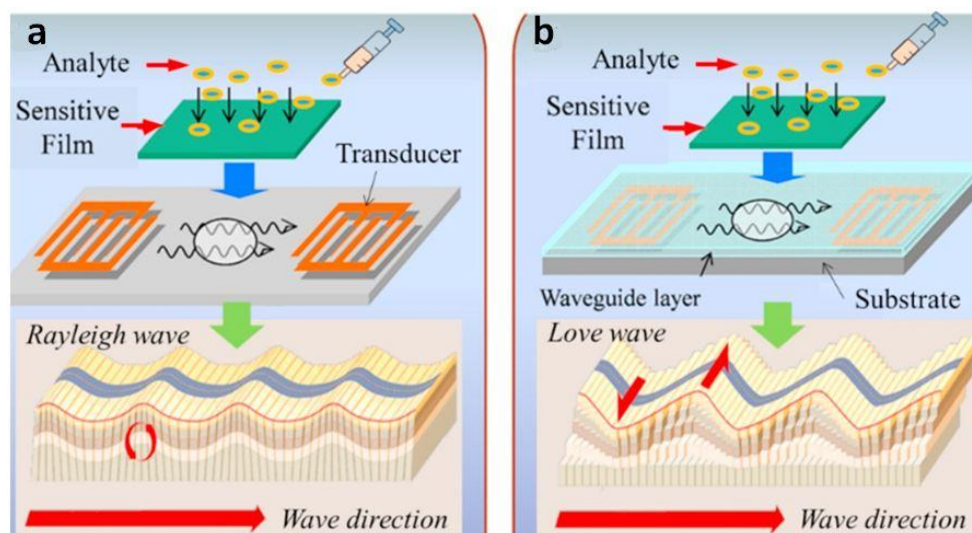


Figure 27 SAW propagation: a) Schematic of Rayleigh wave, having both surface-normal and surface-parallel components with respect to propagation direction, b) Schematic of shear-horizontal (SH) Love wave, an added guiding layer keeps most of SH vibration close to surface [198].

3.3.1 Quartz crystal microbalance (QCM)

Quartz crystal microbalance (QCM) sensor is the oldest sensor application of quartz crystal resonators. QCM sensors typically comprise a thin AT-cut quartz plate and circular electrodes on the two main parallel surfaces of the crystal. By applying an electrical high frequency signal to the electrodes, BAW are generated. When QCM are operated in thickness-shear mode they are called TSM sensors. The resonant frequencies of the sensor are inversely correlated to the thickness of the crystal. The fundamental frequencies of QCM range from 5-150 MHz. The main effect, applicable to all acoustic wave sensors, is the reduction of the resonant frequency which stems from the addition of mass in the form of film. Within a specific range, there is a linear correlation between the frequency shift Δf and

the added loading mass Δm . The properties of the film are unimportant. As for the sensitivity, $\Delta f/\Delta m$ is proportional to f^2 [199, 200].

In case of operation within a liquid, where thickness shear mode (TSM) is predominant, the frequency shift correlates with the viscosity and the density of the liquid. Therefore, TSM are well suited for studying fluid properties. These sensors can also be used for bio-chemical analysis by using bio-chemically active films as coating for the sensor surface.

3.3.2 SAW sensors

SAW sensors (Fig. 28) are made by a thick plate of piezoelectric material (ST-cut quartz, lithium tantalite or lithium niobate). Interdigital transducers (IDT) (comb-like structure configuration of electrodes) generate the surface waves. The distance between two consecutive fingers of the IDT is called pitch or period length, d . Once alternative current is applied to the IDT, the generation of acoustic waves takes place. These waves propagate along the axis, perpendicular to the IDT's fingers (in both directions). When constructive interference occurs (among the fingers), the maximum amplitude is obtained. Constructive is achieved when the synchronous or characteristic frequency $f_0 = v/d$ (v : SAW velocity in the material) is used. Typical characteristic frequencies for SAW sensors range from 30-500 MHz.

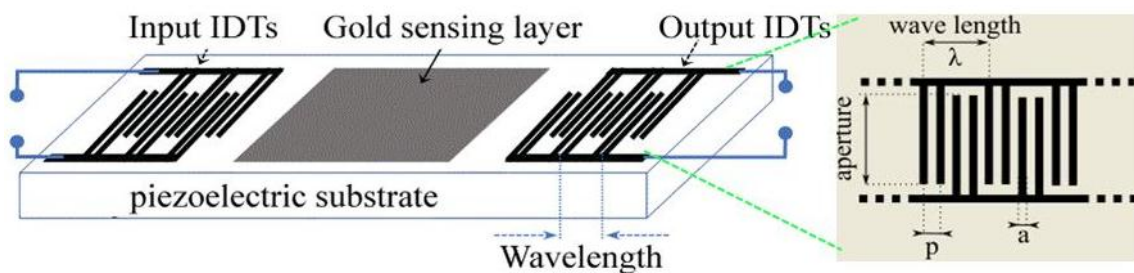


Figure 28 Schematic of a SAW sensor

Love Wave Sensors

As for Love wave sensors, a thin layer of a material with low acoustic wave velocity is deposited over a quartz plate where two IDTs are placed. The aforementioned thin layer (typically made by polymethacrylate or silicon dioxide) acts as a waveguide, thus keeping the vibration energy concentrated to the surface. Therefore, this type of sensor is extremely

sensitive (responsive) to surface perturbations and this attribute make it suitable for mass detection. Due to the shear mode vibrations, in-liquid operation is allowed. The first Love wave device for biosensor measurements was presented in 1992 by Gizeli *et al* [201] where the employment of a resonating polymer film (PMMA) enhanced the sensitivity (detection of biological materials such as proteins) . Bio-chemical analysis in solutions is where love wave acoustic sensors are mainly used [199, 202, 203]. Compared to Rayleigh and LAMB wave sensors, Love wave sensors have the advantage no losses in liquids and a better sensitivity to mass loading due to the concentration of the wave near the surface.

3.3.3 SAW sensors coupled with microfluidics

The newly introduced surface acoustic wave (SAW) technology in LoC platforms has revolutionized microfluidics. The numerous advantages granted by such SAW microfluidics such as simple fabrication, fast fluid actuation, high biocompatibility, versatility, compactness, contact-free particle manipulation and multiplex and sensitive sensing, enable SAW microfluidics to have a crucial role in various applications in chemistry, biology, biochemistry, medicine and engineering. Numerous SAW microfluidic devices demonstrated to date, for fluid mixing and transport, particle/cell focusing and sorting [204].

SAW microfluidic devices are not only employed for the aforementioned functions, but they are also excellent sensors. Since SAW devices possess a substantially smaller active mass and considerably higher operating frequency compared to those of QCMs, they exhibit a monumental increase in sensitivity. Moreover, by employing advanced photolithography technology (i.e. e-beam writing techniques), it is now feasible to fabricate SAW microfluidic devices reaching high operating frequencies up to the Gigahertz, and thus allowing for further increase in the sensitivity of SAW sensors.

SAW devices operating at the longitudinal mode have a substantial surface-normal displacement which leads to a rapid coupling of the acoustic wave energy within a liquid, thus causing excessive damping, and therefore poor sensitivity and high levels of noise for liquid biodetection. Higher sensitivity in liquids can be obtained with shear horizontal mode SAW devices which have considerably less dissipation of the acoustic energy within the liquid. Love wave SAW devices consisting of a standard SAW device integrated with a thin wave guide layer on top of the sensing surface -typically fabricated on polymer- of a few

hundred nanometers were developed offering further reduction of the base mass thus leading to improved sensitivity. [<https://www.intechopen.com/books/modeling-and-measurement-methods-for-acoustic-waves-and-for-acoustic-microdevices/acoustic-wave-based-microfluidics-and-lab-on-a-chip>]. Furthermore, polymeric guiding layers render SAW devices reusable without compromising their performance or sensitivity, simply by removing the deposited polymer-based film with acetone rinsing followed by film re-deposition. In addition, the planar geometry of the SAW devices offers the potential to be coupled with other components or micro-devices thus enabling the development of integrated platforms [205].

Biomarkers (protein and genetic) and whole cells are the main targets detected by Love wave sensors addressing diagnostic applications. Protein biomarker detection has the largest share in the Love wave sensors applications. More specifically, a SAW sensor chip was integrated with a PDMS multi-channel microfluidic module allowing for rapid and efficient multi-analyte (four biomarkers) detection of cardiac markers [206]. Additionally, a SAW biosensor coupled with a CMOS Si chip for the development of a portable system offering real time detection for the interleukin family of proteins in human serum was presented in 2008 [207]. A SAW chip biosensor system enabling marker-free detection of thrombin and antithrombin antibodies using double frequency measurement mode thus assuring reliable reference measurements has been presented [208]. In another work, an acoustic waveguide device was employed for measuring binding constants for immunological reactions where each device was mounted in a custom-made holder allowing liquid to be pumped through a flow cell which was tightly attached on SAW surface by a rubber gasket [209]. A Love-wave immunosensor device coupled with a PDMS microfluidic chip (Fig. 29 a) has been developed for real time detection of pathogenic microorganisms or toxins in a dynamic mode [210-212].

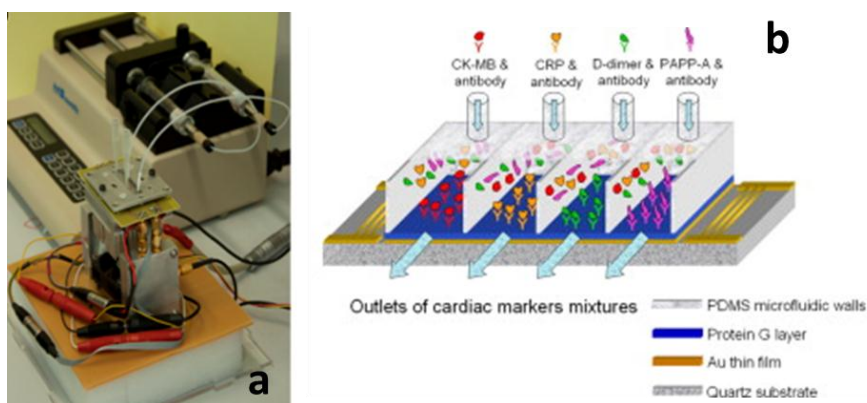


Figure 29 a) Love-wave device coupled with a PDMS microfluidic chip forming a microchannel connected to a syringe pump [211], b) schematic of a SAW sensor chip integrated with a PDMS multi-channel microfluidic module [206].

A novel multisensing approach relying on the integration of a parallel-channel microfluidic module with a SAW sensor chip has been presented (Fig. 29b). The microfluidic module was employed for compartmentalization of the SAW sensor chip surface into equal subareas so as to enable the delivery and the detection of multiple samples on the sensor. The fabrication was achieved by means of soft lithography of PDMS. A four-compartment module was successfully demonstrated with highly reproducible and reliable measurements offering good sensitivity for all four channels [213]. Additionally, a SAW sensor coupled with microfluidics) made of PDMS using soft lithography was employed for multi-sensing in order to quantitatively correlate the acoustic signal with the molecular weight of the bound proteins onto the sensors surface [214].

Furthermore, a SAW device integrated with a PDMS microfluidic channel was employed for the detection of specific binding between the pre-patterned -by means of Dip-Pen Nanolithography – functionalized lipids with their counterpart biomolecules exhibiting enhanced sensitivity thus making an excellent candidate for rapid, multiplex bioanalytical platform [215]. Also, a bacterial based (relying on cell degradation following heavy metals injection) Love wave sensor integrated with a PDMS microfluidic chip pressed and not glued on the Love-wave component, in order to preserve easy surface accessibility. for the rapid detection ($t < 60s$) of heavy metals was presented [216].

More recently, a detailed study on Love wave biosensors considering various parameters affecting their performance such as the operating frequency, microfluidic chip and type of

sample and target analyte was presented. In this study, various fluidic modules coupled with their corresponding docking stations for housing both the SAW device and the fluidic modules were evaluated. The docking stations were made of brass and the applied force for bringing together the two pieces of the docking station was realized either by using screws or magnets for a more uniform pressure across the sensing area (Fig. 30 a, b). The microfluidic module was fabricated on PMMA (Fig.30 c) and since PMMA is not flexible enough, tight sealing was ensured by using PDMS seals. More specifically, there are 8 channels over the 2 sensors. The aforementioned fluidic designs efficiently served both the sample transportation and manipulation within the various modules allowing the effective and automated handling of minute sample volumes.

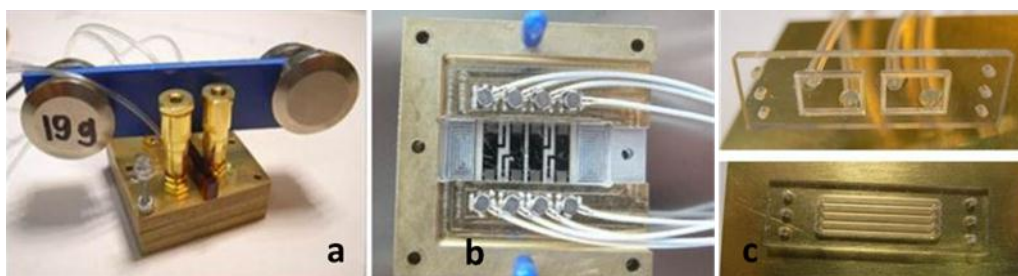


Figure 30 Brass docking station a) with magnets b) screws for applying the force needed, c) PMMA microfluidic module attached to the docking station [205]

An alternative microfluidic module comprising a fluidic connector made of polystyrene and a flow cell made (in direct contact with the SAW sensor) of PMMA connected with adhesive tape are presented in the same study (Fig. 31a). This fluidic design allows for multiple detection and offers design flexibility too. A similar docking station (Fig. 31b) is used with a modification using two springs for applying a constant force onto the SAW chip through the flow cell seals. A construction with screws was employed to adjust and optimise the pressure exerted in order to minimize the losses while still ensuring a leak free sealing. In both cases the main purpose was to achieve minimal signal distortion by testing a dual and array type Love wave devices along with a microfluidic module.

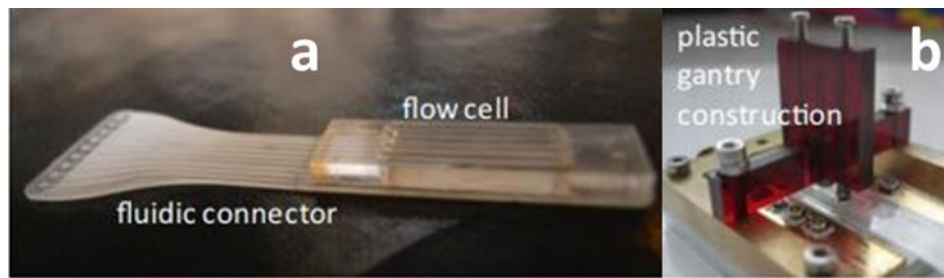


Figure 31 a) multi-channel flow cell attached to a polystyrene fluidic connector, b) Picture of SAW docking station with spring for uniform pressure onto the flow cell seals on top of the SAW chip [205]

Regarding integrated systems comprising surface wave sensors, a real-time, label-free sensing platform comprising a Love-wave microfluidic sensor with automated quantitative sample injection (Fig. 32 a,b) was developed for the rapid detection of prostate cancer based on the PSA biomarker [217].

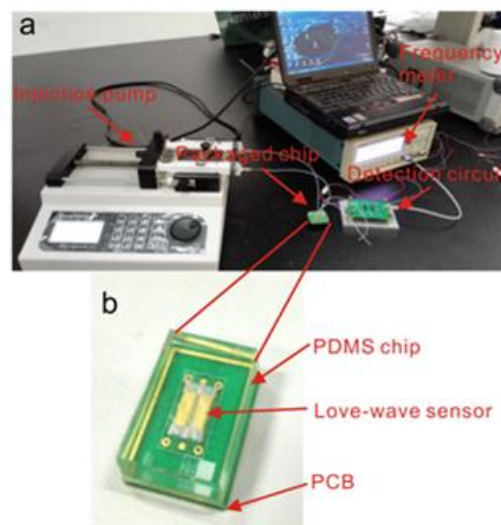


Figure 32 Photograph of (a) the biotesting system and (b) the Love-wave device [223]

3.4 Motivation-Objectives-Novelty of this work

Current diagnosis and analysis procedures are usually lengthy and costly, presenting a major bottleneck for timely and effective healthcare. Headlines reporting food-contamination outbreaks often reach the first page of newspapers globally. Victims of such events are obviously humans, but also the food industry and consumers' confidence to it and food-safety

measures. The need for introducing a paradigmatic change in food control and testing is now recognised as urgent within Europe and the USA. Therefore, rapid, reliable and cost-effective diagnostic tools at point-of-care are on high demand. Owing to miniaturization, LoC technology possesses high potential to enable enhanced biomedical and food-safety applications in terms of rapid and reliable analysis, low-cost, ease-of-operation and high-throughput. In this direction, efforts toward developing new LoC-based PoC systems for diagnosis is growing fast. Low-cost, automation, minimal sample pre-treatment, speed of analysis, portability and low-power consumption are the main characteristics for a commercially successful LoC.

The present thesis addresses the aforementioned challenge by providing an innovative method for food safety management: A simple (user-friendly), low cost and automated platform for the detection of food-pathogens validated for *Salmonella* detection in milk. The proposed concept overcomes the main problems of current methods, by providing a time-to-response of less than 6hrs, as opposed to the currently required 2-3 days, and a simple, automated and portable system, as opposed to current labor-intensive and lab-based methods.

The novelty of the present thesis lies in 1) the fabrication of DNA amplification microdevices on commercially available PCB substrates with **integrated Cu micro-rective heaters** lying at a very close distance to the microfluidic network where the amplification takes place thus offering great thermal contact and low power consumption. 2) In addition, the proposed fabrication methods are PCB compatible thus allowing for **mass production** in the PCB industry reliably and with excellent reproducibility at a very low cost. 3) Moreover, the employed PCB substrate is ideal for **monolithic integration** not only of the microfluidic components and the heating elements but also for other electronic components such as sensors. Therefore, the proposed amplification microdevices in combination with the suggested fabrication method are suitable components for Lab-on-a-Chip platforms. 4) Several DNA amplification microdevices have been designed, realized, characterized and validated with **four amplification methods** such as PCR, LAMP, HDA and RPA. 5) The most interesting and novel outcome of the present thesis is the integration of the aforementioned devices with an acoustic biosensor chip, a Love wave acoustic device leading to a simple, fast, user-friendly and mass amenable LoC system for food-pathogen detection.

Contrary to current systems, that allow the testing of one-sample-per-SAW, the integration of a single SAW (or Love wave) element with microfluidics module allows the analysis of multiple samples per acoustic channel, leading to the creation of a microfluidics-on-SAW platform. The proposed design of acoustic biochips incorporating an array of M multiple delay lines -first introduced by Mitsakakis, in combination with N microfluidic channels, provide a matrix able to detect $M \times N$ pathogens or samples. With the aforementioned novel design, the simultaneous detection of multiple genetic markers and bacteria at once is feasible.

More specifically, several of the DNA amplification microdevices constitute part of a fully or modularly integrated, low cost, low power consuming, mass production amenable lab-on-chip platform, performing pathogen detection in real samples such as *Salmonella* in dairy products. The nucleic acid amplification in the proposed platform is achieved either by using the HDA, the RPA or the LAMP method and the detection of the amplified products is performed through a SAW sensor. The use of the developed LoC platform apart from the food safety field can further extend to healthcare (disease diagnosis) as well as environmental monitoring.

The materials were carefully chosen, bearing in mind the requirements set from the DNA amplification module and the SAW sensor. More specifically, for the fabrication of the μ -amplification module, a polyimide-based dry resist, which is routinely used in the PCB industry as solder mask, was used for the formation of the microfluidic network. The patterning of the μ -fluidics was achieved either by UV-lithography or by means of micromilling. Note that both these processes are compatible with and used in the PCB industry. The fabrication of the embedded resistive μ -heaters was realized in PCB, thus enabling not only the efficient and simple integration of the two components (microfluidic network-microheaters) but also other electronics (such as temperature sensors). Since the aforementioned materials are commercially available, biocompatible, low cost and readily transferable to PCB production line, the processes employed are suitable for mass production of the developed microdevices and thus facilitate their potential commercial exploitation.

In other words, the introduction of suitable materials, already known and implemented in the PCB industry, however in a completely different role and application, are presented in this work for creating enclosed microfluidic devices/reactors where high temperatures are

achieved and where high pressures are developed during their operation (for example, in the case of devices involving long microchannels). The proposed fabrication methods secure robust sealing of devices operating even at high temperatures (nearly 100°C) and high pressures developed across excessively long (>1.5 m) microchannels. Thanks to the low cost and compact technologies involved as well as the low power consumption of the DNA amplification microdevices, the proposed devices are expected to provide competitive analytical μ -devices for direct application in LoC and PoC platforms suitable for field and low resource settings.

Chapter 4 Instrumentation and characterization methods

4.1 Instrumentation

In this chapter, the instrumentation used for the fabrication, the characterization and the evaluation of the DNA amplification microdevices is described.

4.1.1 Instrumentation for Device Fabrication

4.1.1.1 Patterning

Karl-Suss MJB 3 STD Mask Aligner (clean room, NCSR-Demokritos)

Lithography and UV exposures were performed on a Karl-Suss MJB 3 STD Mask Aligner using a broadband lamp which belongs to the NCSR Demokritos Clean Room. MJB 3 STD Mask (shown in Fig. 33a) Aligner has been designed for high resolution photolithography suitable for laboratory environment. It offers exquisite flexibility for irregularly shaped substrates handling of various thicknesses. It is also compatible with standard size wafers of up to 3" diameter. MJB 3 STD Mask Aligner is equipped with a 200W mercury short-arc lamp accompanied with a relatively easy to use and yet comparatively high resolution optical system. The primary exposure wavelengths are in the range of 350-500nm. The aligner is capable of performing exposure both in hard contact mode –when nitrogen pressure is applied to the substrate- and soft contact –when vacuum is applied to the substrate-. There is also a third option for performing proximity exposures. Under optimum conditions, it can achieve a space/line resolution of 1.5 μ m and alignment accuracies of 0.2 μ m.

Thermo Scientific Heraeus Series 6000 Incubator (RRP, NCSR-Demokritos)

The Heraeus Function Line drying oven (Fig. 33b) with natural convection is used for thermal processes: heated storage, heat treatment and thermal testing, and for conventional

drying processes with temperatures up to 250 °C. This incubator was mainly used for baking and drying the devices.



Figure 33 a) Karl-Suss MJB 3 STD Mask Aligner, b) Thermo Scientific Heraeus Series 6000 Incubator

Computer Numerical Control machining LPKF (INN, NCSR-Demokritos)

The system used for micromilling of either PCB or PMMA substrates in order to shape the desired structures (channels, wells, chambers) was an LPKF ProtoMat S series (depicted in Fig. 34a) installed in the National Technical University of Athens, in the Mechanical Engineering Department. LPKF equipment offers cost-effective, environmentally friendly equipment for each stage of the prototyping process, from design verification to structuring. The incorporated automatic tool change can accommodate up to 15 tools and includes drill bit inspection and automatic milling width adjustment. As a result, it enables automated production without manual intervention. It also offers, milling width adjustment providing a pre-defined tool penetration depth thus ensuring a consistent milling track width. The incorporated vacuum table secures the work piece flat across the entire working surface thus eliminating any substrate irregularities such as twisting and warping. It allows both flexible and rigid-flex PCBs to be machined with ease. LPKF CircuitPro software which is the latest powerful CAM and machine software accompanying LPKF systems combines data preparation and system control in one program providing exquisite precision and ease of use [218].

DREMEL® Workstation (220) (INN, NCSR-Demokritos)

DREMEL® Workstation is a combined Drill Press (see Fig. 34b) and Tool Holder. It is the perfect solution for stationary working with your Dremel. Drill vertically or in an angle, adjustable in increments of 15 degrees. Holds tool horizontally for polishing and sanding. It also possesses i) depth markings for consistent depth adjustment and ii) base markings (metric and inches). This equipment was used for drilling through hole for the in/outlet of the microdevices.

IKA RH basic KT/C Hotplate-magnetic stirrer (INN, NCSR-Demokritos)

IKA RH basic KT/C is a magnetic stirrer with (Fig. 34c) new heating and bushing according to DIN 12878 for connecting an electronic temperature controller technology for fast, accurate temperature control. It has a long life cycle due to foil heating and solid state switching for heat control. This equipment was used for preparing the buffer solutions such as Tris, TBE and the Na_2CO_3 developer solution for removing the photosensitive dry film.



Figure 34 a) LPKF ProtoMat S series, b) DREMEL® Workstation (220), c) IKA RH basic KT/C Hotplate-magnetic stirrer

4.1.1.2 Sealing equipment

Hydraulic heated press (INN, NCSR-Demokritos)

Carver 3850 (Fig. 35) is a manual, two column, and hydraulic lab press with 6" x 6" square platens. It possesses easy to-read dual scale analog gauge, reading in pounds force and metric

tons. The clamping force of the Carver 3850 Press is up 24,000 pounds, or 12 tons and comes with two fully threaded columns. This hydraulic heated press was used for the sealing process developed within this thesis for irreversible and robust sealing of microfluidic devices with extended microfluidic channels where biological reactions are accommodated employing high temperature (up to 100°C).



Figure 35 Carver 3850-Hydraulic heated press

4.1.2 Surface modification equipment

Nextral Alcatel NE330 reactive ion etching (RIE)

Plasma surface activation of substrates was conducted in a Nextral Alcatel NE330 (shown in Fig. 36a) reactive ion etching (RIE) installed in the clean room of NCSR Demokritos. It was mainly used for O₂ plasma activation in the experiments performed for surface passivation of the walls within the microfluidic devices.

Expanded Plasma Cleaner & Plasma FloTM (Biosensors Lab, Uni Crete)

Expanded Plasma Cleaner (Fig. 36b) is table-top plasma instrument used for surface cleaning and surface activation. The PlasmaFlo Gas Flow Mixer (Fig. 36c) serves the quantitative control of up to two process gases and monitoring of chamber pressure. Plasma cleaner was employed for cleaning the QCM sensors during the experiments of the surface functionalization of the QCM sensor in order to achieve specific binding of the desired products.



Figure 36 a) Nextral Alcatel NE330 RIE, b) Expanded Plasma Cleaner, c) PlasmaFlo Gas Flow

4.2 Characterization equipment

Infrared camera/thermometer

The Fluke 62 MAX and 62 MAX + Infrared Thermometers (shown in Fig. 37a) can determine the surface temperature by measuring the amount of infrared energy radiated by the target's surface. Note that the Japanese models indicate Celsius only. The main characteristics of the IR thermometer are described below. The temperature range is -30°C - 500°C . The optical resolution offered is 10:1 (distance: spot). The accuracy offered when the measured temperature is higher than 0°C , it is $\pm 1.5^{\circ}\text{C}$ or $\pm 1.5\%$ of the reading, whichever is greater. The response time is <500 ms (95 % of reading). The display resolution is 0.1°C . It also has an integrated laser beam to enable precise, accurate and repeatable measurements [219].

FLIR A325sc (see Fig. 37b) was designed from the ground up to deliver the accurate thermographic imaging and repeatable temperature measurements you needed in research and science applications, generating over 76,000 accurate temperature measurements in every image. FLIR A325sc's detector offers a resolution of 320×240 with a pitch of $25\mu\text{m}$. As for the frame rate, it is 60 Hz. The accuracy provided is $\pm 2^{\circ}\text{C}$ or $\pm 2\%$ of the reading [220]. In addition, a FLIR T197214 Close-up Lens was used for magnification (Fig. 37c). It offers a 2x

Magnification and is suitable for observations of objects down to 50 μm . The Field of View (FOV) is 16 x 12 mm and the working distance is 33 mm [221].

This thermal equipment was used for the characterization of the fabricated μ -heaters. It also assisted the verification of the correct/desired temperatures during the actual experiments.



Figure 37 a) Fluke 62 MAX Infrared Thermometers, b) Flir A325sc thermal camera, c) FLIR T197214 Close-up Lens (2x)

GBX Digidrop Contact Angle Measurement System (INN, Demokritos)

This system was employed for static contact angle measurements on treated and untreated surfaces. All contact angle measurements were performed with drops of 5 μl deionized water at ambient conditions. GBX Digidrop Contact Angle Measurement System could be used to monitor surface wetting properties with the incorporated Camera. Contact angle meter provides information regarding the bonding energy of the solid surface and surface tension of the droplet. Static, advancing, receding contact angles may be measured with this system. The maximum magnification offered is 10X. The accuracy of contact Angle provided is ± 0.7 degrees. The method of measurement is tangent at the triple-phase point. In Fig. 38a GBX Digidrop Contact Angle Measurement System is depicted. It was mainly used for characterizing the treated and untreated surfaces during the wall passivation experiments of the microfluidic devices.

JSM-7401F FEG scanning electron microscope (INN, NCSR-Demokritos)

Scanning electron microscopy (SEM) was utilised for the characterization of the morphology of plasma etched substrates, and the topography of the polyimide μ -channels (samples viewed at 45° tilt). The JSM-7401F (depicted in Fig. 38b), JEOL's highest resolution SEM, is a field emission scanning electron microscope (FESEM) incorporating a cold cathode field emission gun, ultra-high vacuum, and sophisticated digital technologies for high resolution, high quality imaging of micro structures. Using a patented Gentle Beam™ method, the JSM-7401F produces ultra-high resolution at low kV (0.1 kV) and enables observation of true surface structures while helping to reduce charging of non-conductive samples. It can handle samples up to 8" in diameter with its automatic, fully eucentric stage. Its unique graphical user interface controls condition setup, motor stage drive, imaging, and data filing, assuring stable and reliable operation. Using Windows® 2000 with superior networking as a host computer, the system facilitates the process from imaging to data processing under optimum conditions, allowing the operator to display real-time images, save the data in an external PC through the network, retrieve and manipulate the data [222]

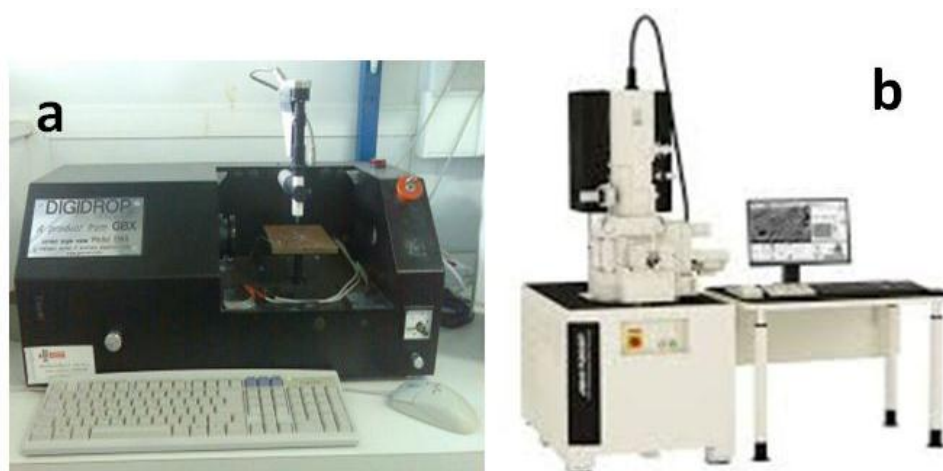


Figure 38 a) GBX Digidrop Contact Angle Measurement System, b) JSM-7401F FEG scanning electron microscope

4.2.1 Testing-Validation equipment

Victor³™, PerkinElmer, Inc, MA, USA (RRP-NCSR Demokritos)

VICTOR3 (Fig. 39) is a multilabel, multitask plate reader for all light-emitting and light-absorbing detection technologies including: fluorescence (top and bottom), luminescence,

absorbance (Absorbance: 405 nm, 450 nm and 492 nm), UV absorbance, time-resolved fluorometry, and fluorescence polarization. A wide range of high quality filters is factory installed. These filters cover the most common wavelengths used in fluorometric and photometric applications. It was used for measuring the OD during the passivation experiments with the various surface modifications for reducing the adsorption of biomolecules on the surface of the microfluidic devices.



Figure 39 Victor³_{TM}, PerkinElmer, plate reader

Q-Sense E4 Quartz Crystal Microbalance (QCM-D)

The Q-Sense E4 QCM with dissipation (Fig. 40a) is a real-time analytical instrument for studies of molecular events occurring on surfaces. The E4 measures mass and viscoelastic properties of molecular layers as they build up or change on the sensor surface. Areas of interest include materials, protein and surfactant research. It possesses 4 flow modules for parallel measurements. Since the 4 measurements are performed with the same measurement sequence, the data sets can easily be compared to each other. Mass, thickness, viscoelastic parameters, adsorption rates can easily be extracted from the analysis software. 4-sensor chamber enables higher throughput and simultaneous comparison of measurement parameters. Moreover, the removable flow module, one for each sensor, gives flexibility and simplifies cleaning. As for the Sensor Crystal (Fig. 40b), the measurement surface of the standard sensor crystal is gold, but the top layer can be almost any other material. Q-sense was used during the experiments of the surface functionalization of the QCM sensor in order to measure the specific binding of the desired PCR products.

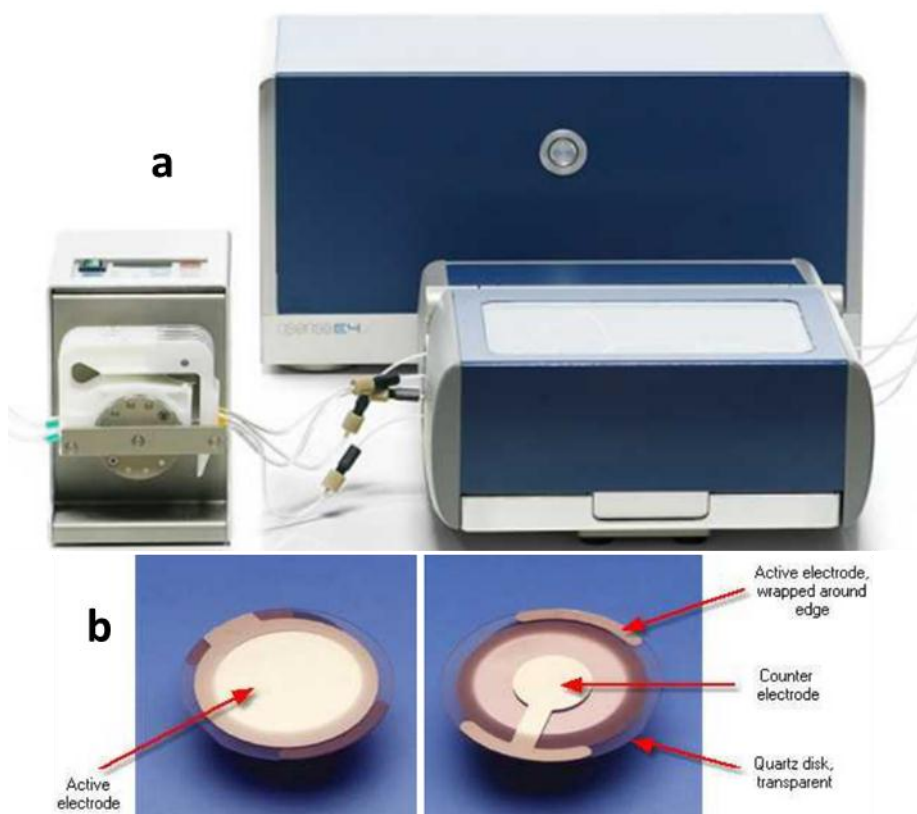


Figure 40 a) Q-Sense E4 Quartz Crystal Microbalance (QCM-D), b) standard gold-coated sensor crystal comprising a quartz disk and three electrodes (one of which consists the active electrode or in other words the sensing area)

Pumping systems

Three main systems were used for conducting the experiments according to the needs (i.e. level of integration and or automation, ease of use). These three pumping systems are described below. The following pumping systems were used for injecting/withdrawing the samples in the μ -devices with high precision and at a constant flow rate.

- LabSmith liquid handling system

Lab Smith system offers versatility since it is accompanied by a sophisticated software providing controlling of each component (syringe pumps and three-way valves). Each SPS01 syringe pump (Fig. 41a) consists of a glass barrel and a plunger. The volume of each syringe is 100 μ l. LabSmith valves are compatible with capillary or tubing via CapTite one-piece. As for the valves, two-position three-port automated valves (Fig. 41a) compatible with 360 μ m capillary, 1/32" tubing or 1/16" tubing were used for the assembly. The valves could be

connected to capillary or tubing via one-piece fitting (Fig. 41a). EIB200 interface controller (Fig. 41a) is required for communicating with PC. EIB200 interface controller can control more than 100 μ Devices for sequential operation and up to 10 μ Devices for simultaneous operation. It includes specialized software (uProcess), power supply, micro USB 2.0 cable, and flat ribbon connection cable [223].

- Peristaltic Pump (Biosensors Lab, Uni Crete)

Gilson's MINIPULS® 3 (shown in Fig. 41b,) is a peristaltic pump specifically designed to meet process laboratory liquid handling needs. It comes with interchangeable heads for delivering smooth, low pulse flows of biological and chemical fluids in 1, 2, 4, or 8 channels. The MINIPULS 3 peristaltic pump combines microprocessor speed control with a high-torque stepper motor. It is equipped with chemical-resistant pump heads with 10 stainless steel rollers to set the performance standard in producing smooth, low-pulse flow and reproducible flow rates at higher pressures. Standard flow rates range from 0.3 μ L/min to 30 mL/min at a maximum pressure of 0.5 MPa [224].

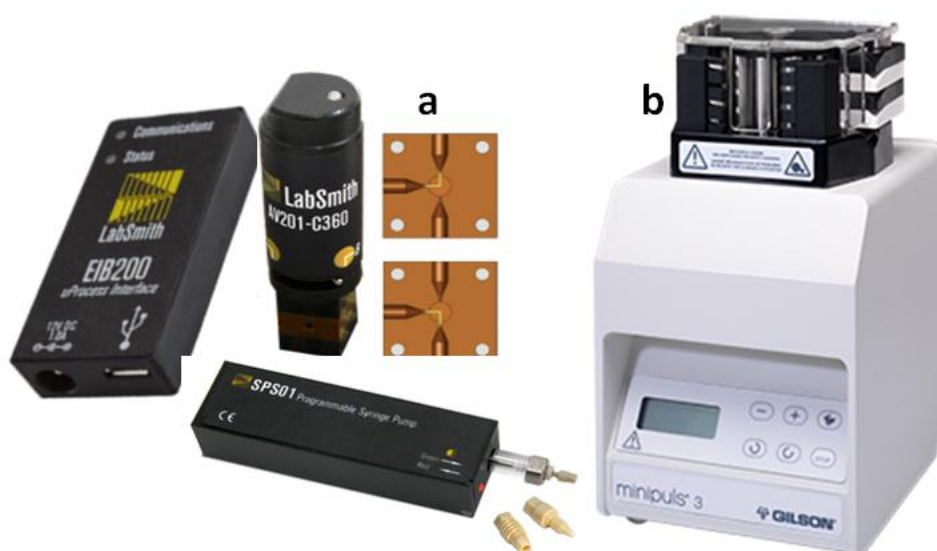


Figure 41 a) LabSmith liquid handling components, b) Gilson's MINIPULS® 3 peristaltic pump

Temperature controller unit

A custom-made temperature controller unit to drive the microheaters was designed by external collaborators. The circuit is able to control up to three microheaters (with room temperature resistance in the range 15-50 Ohm) necessary for the μ PCR (Fig. 42a).

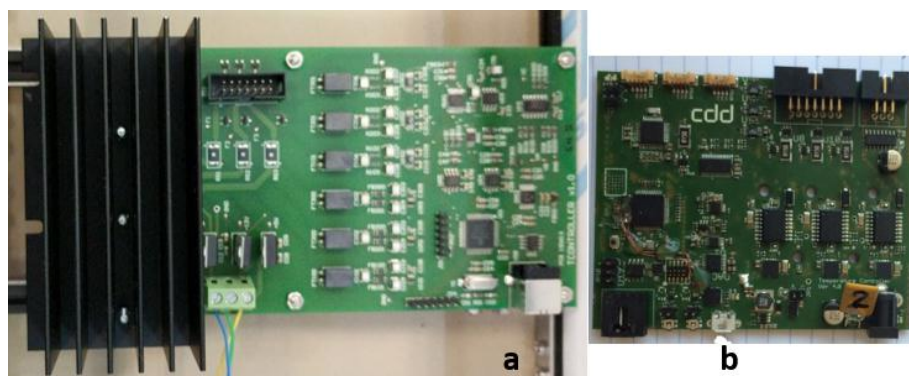


Figure 42 Temperature controllers a) 1st version, b) 2nd version

The control of each heater temperature is performed independently using a temperature control unit providing the voltage needed across each resistive microheater, whilst a small resistor is used to measure the current flowing through. Thus, the controller measures in real time the resistance of each microheater to derive its operating temperature through the temperature coefficient of resistance for copper (i.e. using the microheaters as temperature sensors), and the resulting value is used in a proportional-integral (PI) feedback control loop to stabilize the temperature of each microheater at a certain set value. Communication with a host PC is done using a USB serial port in order to set the operating parameters of the PCR (i.e. temperature at each zone) as well as log data during its operation (temperature over time). A second enhanced and more robust version of a temperature controller (Fig. 42b) was subsequently designed offering greater flexibility since the resistance value range improved (10-100 Ohm). Also the graphic user interface was improved providing real-time graphs for the temperature since a Resistance Temperature Detector (RTD) was integrated in the temperature controlling unit allowing for more precise logging of data while running an experiment. Last but not least the second unit was more compact thus more suitable for being integrated in a LoC platform. In Fig. 43 the second edition of the developed temperature under operation is illustrated.

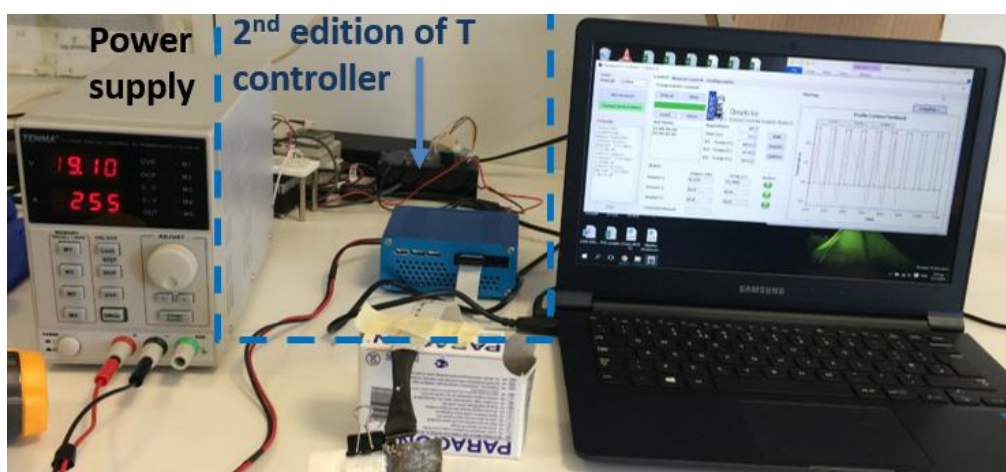


Figure 43 2nd edition of temperature controller under operation

4.2.2 DNA amplification equipment

Thermal cycler

Two different thermal cyclers were used for the benchtop experiments of nucleic acid amplification. PeqSTAR 2X thermal cycler from PeqLab, ISOGEN LIFE SCIENCE™ (shown in Fig. 44a), with two independent high speed 48 well blocks, was used in all the experiments conducted in the Biosensors' Lab (Biology department, university of Crete). This system has newly engineered thermoplate with impressive thermal characteristics, powerful Peltier elements with Long Life Technology, a revolutionary heat sink and cooling fans with magnetic bearing enabling rapid temperature change control of up to 5 °C/s. FlexGradient™ Technology, offers individually controlled temperature of the 8 rows, allowing to select between a perfect linear temperature gradient -ideal for PCR optimization, or independent lane control -ideal for the use of different primer pairs in the same run [225].

The iCycler™ thermal cycler (shown in Fig. 44b) from BIO-RAD (installed in the Institute of Radioisotopes and Radiodiagnostic Products, NCSR Demokritos) accommodates 96 wells and it features an intuitive touch-screen user interface to make running PCR easy. Thermal Gradients in the iCycler are formed from the front to the rear of the sample block resulting in eight specific temperatures for assay optimization. This innovative design allows for evaluation of the maximum assay components at each specific temperature [226]

These pieces of equipment were employed for running the DNA amplification control samples in conventional laboratory equipment to verify and compare the results with the μ -devices.

Gel Electrophoresis System

Sub-Cell® Horizontal electrophoresis system (shown in Fig. 44c) which includes 15- and 20-well combs, gel caster, 15 x 15 cm (W x L) UV-transparent tray, dual channel power supply (PowerPac™ Basic Power supply) was the System used for agarose gel electrophoresis [227].

UV transilluminator

The MiniBIS Pro (shown in Fig. 44d) is an easy to use, convenient and reliable gel doc system which addresses all visible dye applications and most common UV dyes. The MiniBIS Pro uses highly sensitive scientific camera to combine the demanding requirements of professional imaging with capabilities of an advanced life science research system. With its 16-bit, 1.3Mpixel camera and high quality optics that include a super bright lens, the MiniBIS produces sharp, clear images with minimal geometric and light distortion [228]. This equipment was used for visualizing the agarose gels.

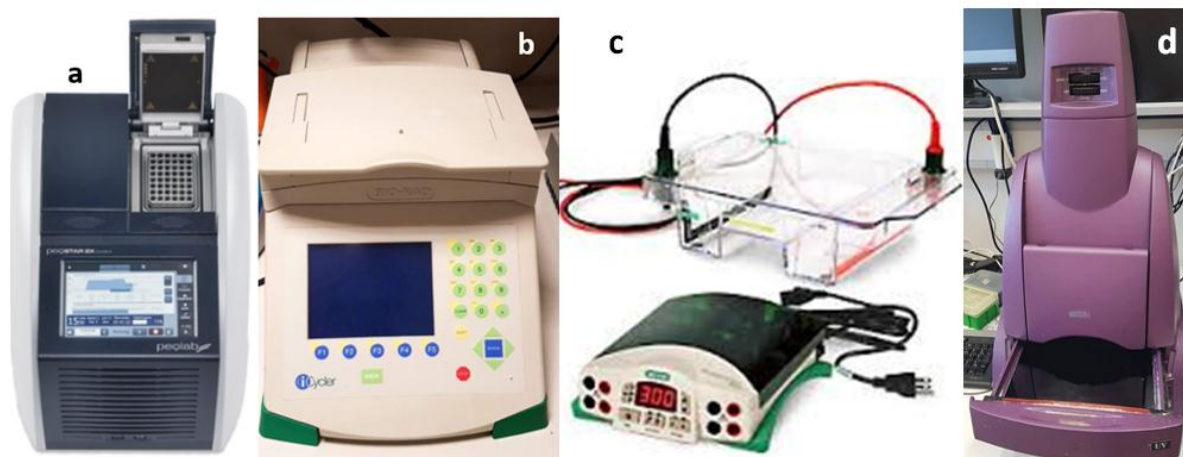


Figure 44 a) thermocycler peqStar, b) iCycler, c) Gel electrophoresis system, d) UV transilluminator

The two aforementioned pieces of equipment were used for verifying the DNA amplification of the desired products. It also assisted the semi-quantification of the DNA amplification efficiencies achieved with suitable image software (ImageJ).

Chapter 5 Design, fabrication and characterization of DNA amplification devices with integrated microheaters

The goal of this chapter is to introduce the design considerations taken into account and fabrications methods employed in order to develop efficient amplification microdevices suitable for integration in LoC platforms. Answers to the design-related issues (such as minimizing power consumption, achieving thermal uniformity across heated zones) were given through numerical calculations (conducted by G. Kokkoris team). Moreover, the materials chosen as well as the fabrication methods used for reliable and cost efficient microdevices are described in detail. The main achievement in this chapter is the development a robust sealing process (considered as one of the bottlenecks microdevices are dealing with) regarding microfluidic devices using commercially available products compatible with the PCB technology since this is the main substrate used for the fabrication of the amplification microdevices. The fabricated devices are characterized in term of leak-tightness and temperature behaviour. Last but not least, several surface modifications for wall passivation have been tested so as to minimize biomolecules adsorption in order to maximize the amplification efficiency.

5.1 Introduction

This chapter aims at familiarizing the readers with the steps involved in order to develop a microfluidic device. In order to have reproducible and functional microdevices, no circumventions of the established process steps should be done to ensure the fabrication of reliable and efficient microdevices.

The structure of the chapter is as follows: first numerical calculations are performed to guide the design of the envisioned microdevices bearing in mind geometrical characteristics in order to minimise the energy consumption and improve temperature uniformity which is

crucial for the efficiency of the DNA amplification microdevices. Numerical calculations give useful information for enhancing the performance of a microdevice and give a first estimation of its performance. More specifically, a comparison of SC and CF devices is presented in term of energy consumption leading to a conclusion regarding the thickness of the substrate. In case the substrate is thicker than $\sim 800\text{ }\mu\text{m}$, the energy consumption at the SC device exceeds the energy consumption at the CF microdevice. In addition, the distance between neighbouring μ heaters is numerically calculated in order to minimize thermal cross talk and increase temperature uniformity across each heater to increase the DNA amplification efficiency of the microdevice. The main finding is the incorporation of a solid Cu layer on top of each heater maximises the temperature uniformity reaching 100%.

Following, there is a description of the materials selected and the fabrication processes employed, bearing in mind cost, integrability, ease of fabrication, fabrication processes transferable to mass production. All these characteristics were met on PCB which is why we selected this material as the main substrate for the development of the DNA microfluidic devices.

Last, the characterization processes are described in order to ensure the efficient functionality of the fabricated microdevices prior validating them with real amplification protocols. The main characteristics studied are the thermal behaviour and the leak-tightness of the microdevice. Due to the high surface/volume ratio of the microdevices, we also investigated wall passivation using several agents. The most promising one proved to be BSA, thus the use of BSA was later incorporated in the biological protocols to minimise biomolecules adsorption which in turn leads to reduced amplification efficiency.

5.2 Design-Numerical calculations

To guide the DNA amplification microdevice design, both static chamber (SC) and continuous flow (CF) microdevices were simulated. All numerical calculations were performed by Dr. G. Kokkoris team.

Comparison is made in terms of energy consumption of devices fabricated on the same material stack, with identical sample volume and channel dimensions, and is implemented by a computational study coupling heat transfer in both solid and fluid, mass conservation of

species, and joule heating [236]. The conclusions drawn from the simulations were used as a guide for the devices realized and implemented for efficient DNA amplification.

As discussed in section 2.6, nucleic acid amplification microdevices are divided in two main categories: stationary chambers and continuous-flow devices. When more than one temperature is needed to perform the reaction (for example in case of PCR), in the case of the stationary chamber the whole device undergoes thermal cycling whereas in the case of the continuous flow device the thermal zones are maintained at a constant temperature and only the sample changes temperature as it moves through the heated zones. In case of an isothermal amplification reaction the type of the microdevice is irrelevant. Nevertheless, there are numerous parameters that should be taken into account such temperature uniformity across the heated areas in order to maximize the amplification efficiency and elimination of thermal cross talk between two neighboring heating zones. Thus the design of the μ -device can be greatly improved in terms of efficiency when it is based on numerical calculations. Numerical calculations were performed to demonstrate the advantages of thin polymeric substrates for PCR, in terms of power consumption, minimization of thermal cross-talk (thermal isolation) between neighbouring PCR zones and temperature uniformity of the zones.

5.2.1 Comparison of fixed-loop CF and SC devices in terms of energy consumption

To complement our experiments, SC and CF DNA amplification microdevices fabricated on polymeric substrates with embedded microheaters were simulated. Comparison is made in terms of energy consumption on devices fabricated on the same material stack, with identical sample volume and channel dimensions and is implemented by a computational study coupling heat transfer in both solid and fluid, mass conservation of species, and joule heating. The pros and cons of each configuration are compared and discussed and the conclusions drawn are used as a guide for the devices to be realized and implemented for efficient DNA amplification.

The objective of the computational study was the evaluation of the two most common types of μ PCR devices, i.e. the fixed-loop CF and SC devices, in terms of energy consumption. The comparison was performed for the same material stack, i.e. polymeric films (thin or thicker,

100 to 1000 μm) with metal layers for integration of microheaters, the same PCR protocol (time duration at each zone), and the same volume of PCR mixture. The computational study is performed at the unit cells of the devices under comparison. The unit cells of both the (fixed loop) CF and the SC devices are shown in Fig. 45. In the CF device, the sample moves through fixed temperature zones to achieve the required thermal cycling; the number of cycles is determined at the design/fabrication stage. In the unit cell of the CF device (Fig. 45a), one thermal cycle takes place. The fluid flows through a meander shaped microchannel, above three separate microheaters which impose the temperature set points dictated by the PCR protocol. The fluid volume of the unit cell is 0.53 μl . The unit cell of the SC device (Fig. 45b) includes one meander of the microheater. A fluid volume of 0.6 μl can be accommodated in the unit cell. The material stack for both devices is shown in Fig. 45c and is based on commercially available polymeric films with metal layers.

Results and discussion of the computational study

The conditions of the simulations are the same for both devices: a) the same stack of materials is considered for both devices; three separate numerical simulations are performed for substrate thickness (parameter d in Fig. 45) of 100 μm , 500 μm , and 1000 μm . b) The same volume of the PCR mixture to be amplified is assumed, i.e. 5.3 μl , corresponding to 10 unit cells for the CF and 8.83 unit cells for the SC device. c) The same PCR protocol and the same number of cycles (10) are considered for both devices. The chosen PCR protocol is 3s:4.2s:6.2s [denaturation (95°C), annealing (55°C), and extension (72°C) step duration, respectively] which allows for the temperature uniformity in the CF device. Calculations do not take into account the energy required for pumping, and the energy for preheating and final extension of the PCR mixture.

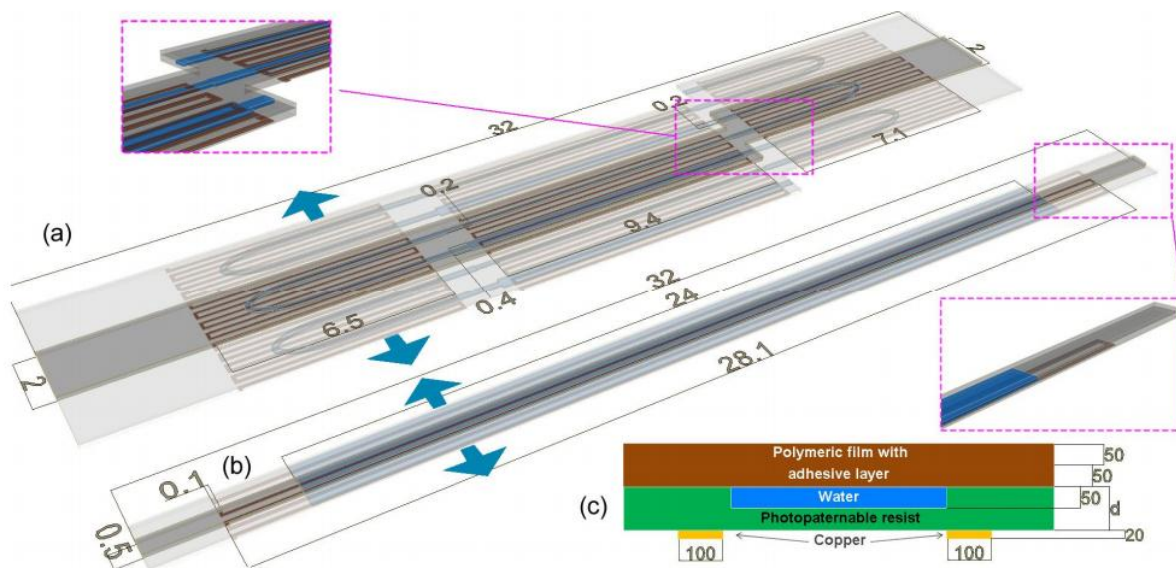


Figure 45 Unit cells of the a) CF and b) SC devices utilized in the numerical calculations. Dimensions are in mm. c) The material stack of the devices; d is the thickness of the polymeric substrate where the microchannels are fabricated. Dimensions are in μm

The result of the comparison is summarized in Fig. 46, where the effect of the substrate thickness on the energy consumption of both SC and CF devices is shown. The increase of the substrate thickness induces an increase of the energy consumption for both devices. However, the energy consumption for the SC device is more sensitive to the substrate thickness. The energy consumption for the SC device is significantly lower to that of the CF device, for substrate thickness less than 500 μm . If the substrate is thicker than $\sim 800 \mu\text{m}$, the energy consumption at the SC device exceeds the energy consumption at the CF device. The difference in the energy consumption can be explained by the heat losses to the ambient at each device; the SC device has lower heat losses due to the smaller (almost 4.5 times) area in contact to the ambient compared to the CF device. At low substrate thickness, the constant heat losses at the CF device exceed the energy required for the thermal cycling of the SC device. At greater substrate thickness, the thermal inertia of the SC device increases due to the increase of the thermal mass, and as a consequence the energy consumption for the SC device increases. This increase for substrate thickness greater than $\sim 800 \mu\text{m}$ is enough to exceed the small consumption increase for the CF device. For the CF device, the increase of the substrate thickness increases the distance of the microheaters to the microchannel and as a consequence a slightly greater temperature at the microheaters is required to achieve the set point temperatures in the microchannel.

The conclusion of the computational study, although it refers to μ PCR devices, can verify that isothermal DNA amplification methods are beneficial on the substrate mainly utilized (1.5 mm PCB) compared to a PCR taking place in a SC device (where temperature ramping is required). The energy consumption of a device for isothermal DNA amplification methods will be close (or even lower) to that of CF μ PCR device where no temperature ramping occurs. The mathematical model used for these numerical calculations is described in [229] and [52].

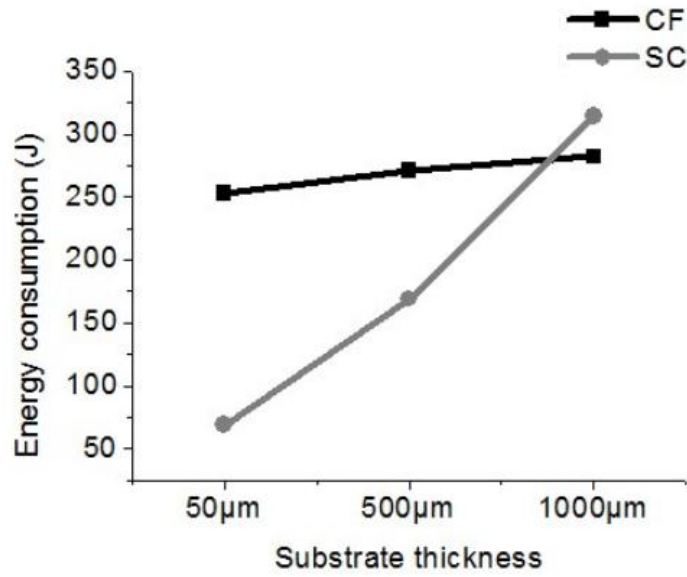


Figure 46 Energy consumption in CF and SC devices for different substrate thicknesses

5.2.2 Re-circulation (Closed-Loop) μ PCR

Model for the calculations of heat transfer and fluid flow in the closed-loop μ PCR device

The heat transfer equation in the moving DNA sample (PCR cocktail) and in the solid blocks of the unit cells as well as the momentum conservation and continuity equations in the microfluidic channel are numerically solved in 3d by a commercial code, namely COSMOL. It is considered that the temperature at each heater is equal to the pertinent set point, i.e. 369 K (96°C) for the heater below the denaturation chamber, 328 K (55°C) for the heater below the annealing chamber, and 348 K (75°C) for the heater below the extension chamber. Natural heat convection to the ambient (293 K) is considered for all boundary surfaces surrounded by air and periodic boundary are considered for boundary surfaces in touch with the other two μ PCR units. The no slip condition is imposed to the wall of the microfluidic

channel. The outputs of the calculations are the temperature distribution in the μ -PCR unit, the power requirements for heating during the operation of the unit, and the pressure drop in the microfluidic channel.

Results

a) Temperature uniformity in the chambers of the μ PCR device

The requirement for a high performance μ PCR device is uniform fluid (DNA sample) temperature in each one of the thermal zones (chambers in our design): The fluid temperature variation should be less than 3K in the denaturation, the annealing, and the extension chamber.

The temperature distribution at the middle height of the microfluidic channel of the μ -PCR unit is shown in Fig. 47a for two cases of volumetric flow rate (30 μ l/min and 60 μ l/min). It is obvious from Fig. 48a that there is no thermal cross talk between the chambers of the μ -PCR unit and that the temperature uniformity is high in all chambers. A quantitative calculation verifies Fig. 48a: It is calculated that more than 99% of the volume of each chamber is in the range $[T_{set} - 1\text{ K}, T_{set} + 1\text{ K}]$ (T_{set} is the set point for each chamber) when the volumetric flow rate is 30 μ l/min. This percentage drops to 96.5% for the case of a volumetric flow rate of 60 μ l/min. The temperature values are in K in all numerical calculations. The above mentioned results were also verified using an IR camera as shown in Fig. 47b.

b) The power requirements for heating during the unit operation are c.a. 1.1 W for both volumetric flow rates value which is in good agreement with the experimental value measured (1.3W).

c) The time required for DNA amplification, i.e. the time for 30 cycles is c.a. 15 min (30 μ l/min) and 7.5 min (60 μ l/min).

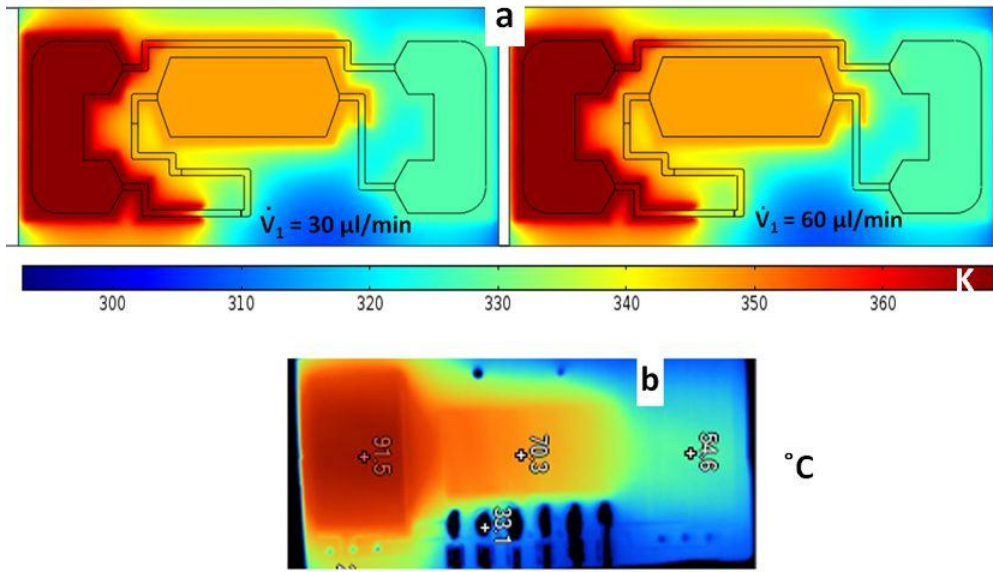


Figure 47 a) The temperature distribution on a cross section at the middle height of the microfluidic channel with the volumetric flow rate equal to i) 30 $\mu\text{l/min}$ and ii) 60 $\mu\text{l/min}$. b) image of the same microdevice using an an IR camera

5.2.3 Static PCR & isothermal amplification microdevices

The calculations started with the initial design, i.e. the design of μheater with a total thickness of 1.5mm. The calculated average temperature vs. time is shown in Fig.48a (green solid line). The duration for a 30-cycle PCR protocol was calculated ~ 90 minutes using as set-points 95 $^{\circ}\text{C}$ and 65 $^{\circ}\text{C}$ respectively. The temperature uniformity, which is critical for the amplification efficiency of PCR as well as for any isothermal amplification method (e.g. LAMP), is quantified by the percentage of the volume of the chamber lying in the acceptable range around the temperature set-point (± 2 $^{\circ}\text{C}$). Two main problems were observed: The PCR duration was long and the temperature uniformity was poor. The next steps were made to deal with the latter problems.

The first step for decreasing the PCR duration was to decrease the thickness of the stack by 800 μm . The decrease of the thickness decreased the thermal mass and this resulted to the decrease of the PCR duration by ~ 30 min (from 90 to 60 min, Fig. 49a). However, the temperature uniformity was still poor (Fig. 48a, green dashed line)

As for the temperature uniformity problem, a Copper (Cu) layer, with thickness of 100 μm , was added between the heaters and the fluidic chamber in order to homogenize the temperature profile due to high thermal conductivity of Cu. After applying the Cu layer, temperature uniformity reached $\sim 100\%$ (Fig. 48c). However, the PCR duration increased from 60 to 76 min (Fig. 48b).

Concluding, according to the numerical calculations as presented in Fig.48, the thickness of the PCB affects greatly the ramping rates. In more details, 30 PCR cycles on thick PCB of 1.6mm thickness lasts 90min whereas on a thinner PCB of 0.8mm thickness the duration is reduced by 30min. In the case of the thin PCB (0.8mm thick) with an external Cu layer the 30-cycle PCR duration is 75min. On the other hand, the temperature uniformity across the heated area is incrementally improved reaching almost 100% when the Cu layer is incorporated. Based on the simulations' findings, the new heaters were realized on a PCB substrate of a 0.8mm thickness with a Cu layer on the outer surface so as to optimize the PCR protocol both in terms of amplification efficiency (increased temperature uniformity) and total duration (faster ramping rates).

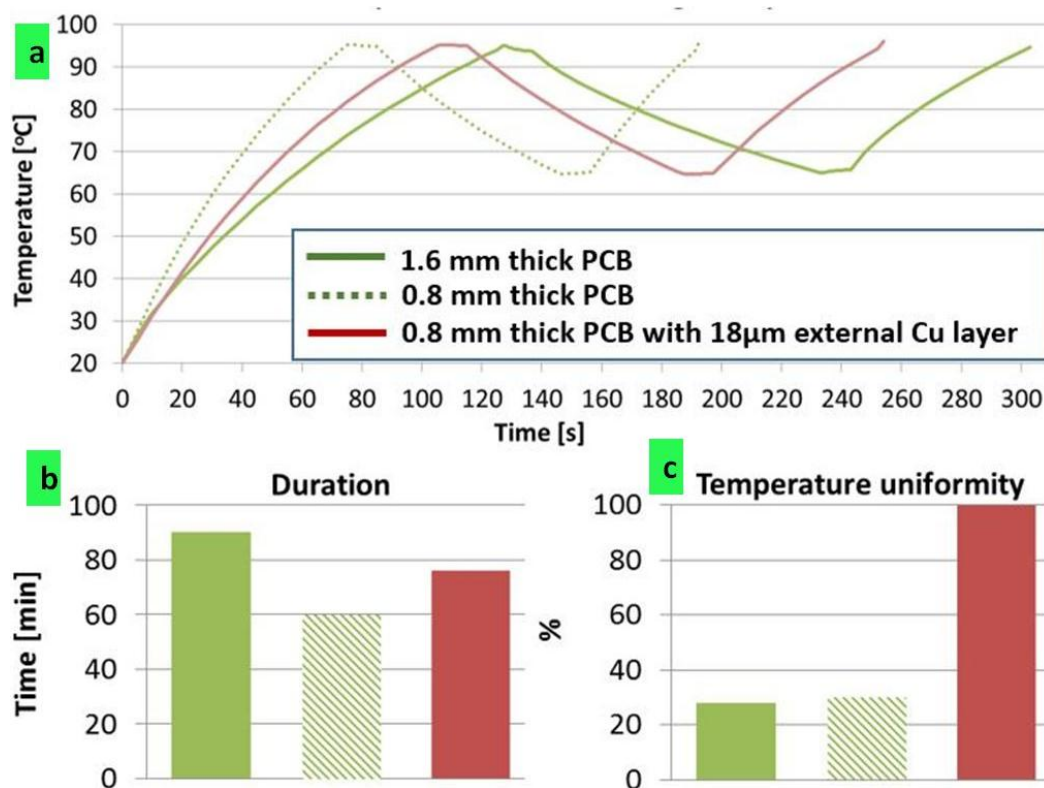


Figure 48 Numerical control results for thick (1.6mm) PCB, thin (0.8mm) PCB and thin PCB with external Cu layer

5.3 Material selection

In many cases the choice of the type of nucleic acid amplification (isothermal vs. non isothermal) as well as the type of fluid motion (static chamber vs. continuous-flow design) drives the choice of the material to be employed for the fabrication of the amplification μ devices, in order to best exploit the advantages of each material for improving the device efficiency and operation.

The materials are carefully chosen, bearing in mind the requirements imposed from the nucleic acid amplification module as well as the other modules to be integrated on the same LoC (i.e. the SAW sensor since its function is susceptible to temperature variations). For the fabrication of the μ -fluidic component of μ -PCR module, polyimide-based dry resist, which is PCB-compatible, is going to be used. Polyimide meets the requirement of a high T_g needed for the thermal cycling (T_g PI>300°C). The patterning of the μ -fluidics will be achieved either by UV-lithography or by means of micromilling. The fabrication of the heaters will be realized in PCB, thus enabling the efficient and simple integration of the two components (microfluidic network-microheaters). Since the aforementioned materials are commercially available, biocompatible, low cost and readily transferable to PCB production line, the process employed is suitable for mass production. Thanks to the low cost and compact technologies involved, the proposed platform is expected to provide a competitive analytical platform for direct application in field settings.

5.4 Fabrication of DNA amplification microdevices

5.4.1 μ heaters

Microheaters are one of the two essential parts of the DNA amplifications microdevices. The aim regarding the microheaters is to be easily, reliably and reproducibly fabricated with a technology readily transferable to mass production.

5.4.1.1 Polyimide-based Microheaters

Several materials were used for the realization of microheaters at a close distance to the microfluidic. In more details, commercially available polyimide/aluminium sheets with

different aluminium thicknesses (Caplinq® Al-metalized polyimide sheet, Goodfellow®), Cu-clad (Pyrallux®, Laminate AP 8545R) and printed circuit board (PCB). In the following section the process is described in more details as well as the reasons why PCB prevailed.

The starting material chosen for microheater fabrication was commercially available polyimide/aluminium sheets (Fig. 49 i) & ii)). The thickness of aluminium was 100nm (or 30nm) and the backing PI sheet had a thickness of 25µm. The first step in the fabrication process was the design of the lithographic masks. The mask designs were based on the simulation designs carried out by Dr. G. Kokkoris and his team. The designs were printed in transparencies, for low cost prototyping. The masks for the microheaters (positive lithography) were designed to provide room temperature resistances of the range of 40-100 Ohms, with 1000 nm or 300 nm aluminum thickness, Fig. 49 iii) shows the design of the aluminum microheaters. The microheaters were patterned by means of photolithography followed by wet etching of Al. In some cases, the metalized film was laminated onto a rigid PCB substrate (Fig. 49 vi)). This material proved hard to be reproducibly processed, because of its low PI thickness and the oxidation of Al.

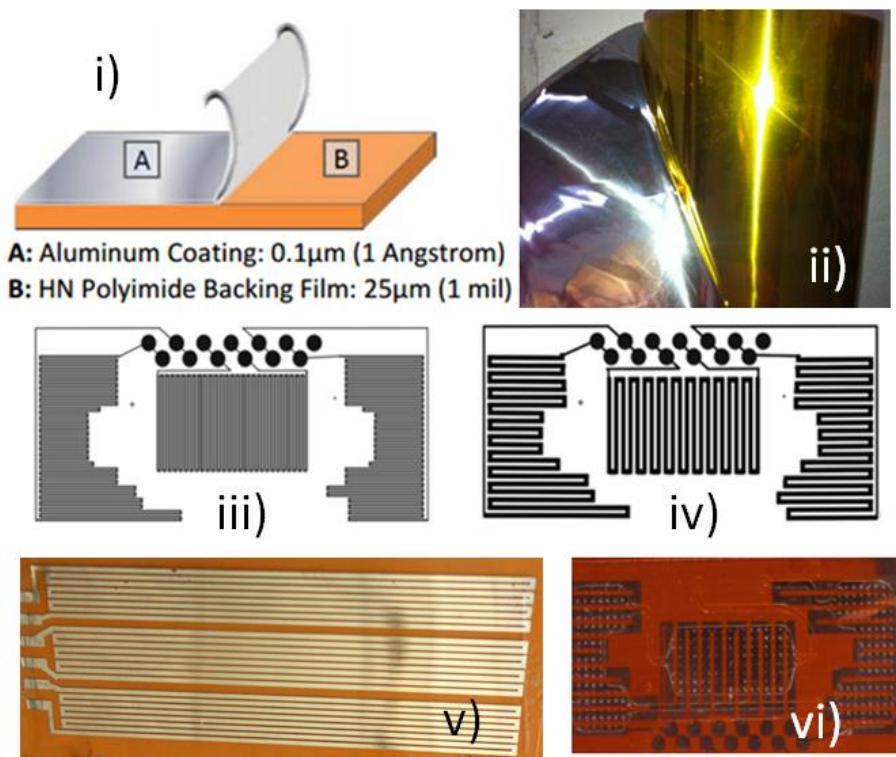


Figure 49 i) & ii) Caplinq® Al-metalized polyimide sheet, lithographic masks for aluminium resistors with iii) 1000 nm Al thickness (Caplinq®), iv) 300 nm Al thickness (Goodfellow®), realised

microheaters on v) plain AL-metalized polyimide sheet vi) AL-metalized polyimide sheet laminated on a rigid PCB substrate

Commercially available polyimide/aluminium sheets with different aluminium thicknesses (Caplinq® Al-metalized polyimide sheet, Goodfellow®), Cu-clad (Pyrallux®, Laminate AP 8545R) were used for the realization of the microheaters. The process flow for each substrate is depicted below.

The software used for the designing of the lithographic masks was CorelDraw®. In the case of the Al-metalized polyimide sheet, the microheaters were patterned by means of photolithography followed by wet etching of Al. Specifically; the AZ® 5214 photoresist was used in a positive lithographic process for the realization of the microheater pattern. Subsequently, the substrates underwent wet Al-etching. Fig. 50 depicts the fabrication process of microheaters on Al-metalized polyimide sheet.

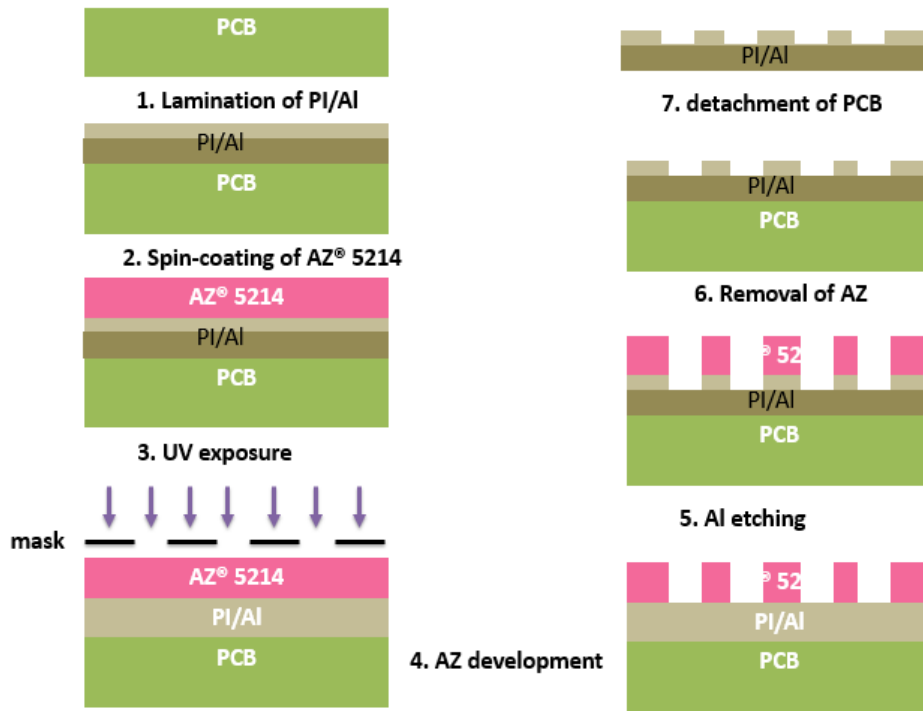


Figure 50 Fabrication process flow of PI/Al microheaters

Respectively for the Cu clad, AZ® 5214 photoresist was spin-coated on top of the Cu surface. After UV exposure followed by AZ development, Cu etching (in commercial FeCl_3 solution) took place. Once the microheater was patterned AZ was removed using ethanol to

reveal the un-etched copper tracks comprising the resistance. Fig. 51 depicts the fabrication process of microheaters on Cu-clad.

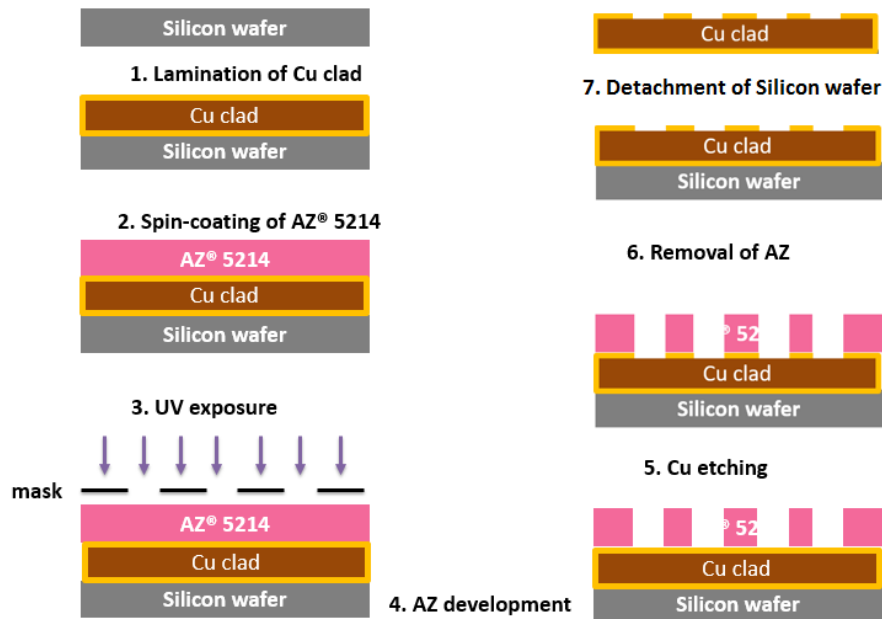


Figure 51 Fabrication process flow of microheaters on Cu clad

Since the processing of the aluminised-polyimide film proved unreliable we moved to an alternative substrate. Another flexible, commercially available substrate for the microheaters fabrication was the Cu-clad (Pyrallux®, Laminate AP 8545R [230]). The aforementioned substrate consists of 100 μm Polyimide backing with 18 μm rolled annealed Cu foil on both sides of PI provided by DuPont™. The desired design of the microheaters was patterned by means of standard photolithography by means of standard photolithography. Fig. 52 shows realized μ heaters on cu clad.

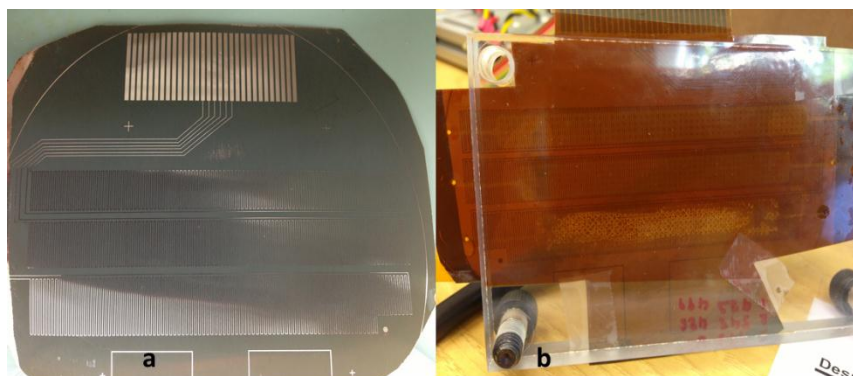


Figure 52 a) realised μ -heaters on cu clad, b) realized μ -device on cu clad under operation

5.4.1.2 PCB microheaters

Due to challenges concerning the Polyimide-based microheaters, embedded Cu microheaters (microresistors) were fabricated on PCB. First the copper resistive microheaters are designed with a PCB design software (Kicad, free software) and realized by major PCB vendors according to our design specifications. They are fabricated in a large number of replicas at a low cost and excellent reproducibility in terms of resistor value accuracy (± 1 Ohm). They have a meandering shape, to maximize their electrical resistance in the space allocated for each thermal zone.

In some cases, -where the footprint of the device is small- a single layer of Cu meandering lines was not sufficient to provide the desired resistor value as specified by the temperature controller, so multilayer PCBs were used providing more cu layers. Therefore, the Cu resistance was spread into three layers in the z-axis, in an industry-common 4-layer Cu PCB stack, (as shown in Fig. 53). The final PCB thickness of the most substrates used was 1.55 mm. We have also designed heaters in thinner substrates with 1mm and 0.8 mm thickness respectively. Another improvement with the PCB heaters is the temperature uniformity. In our latest design we used the bottom layer of Cu not to realize meandering structures but as a solid surface to enhance the temperature uniformity across the heated areas.

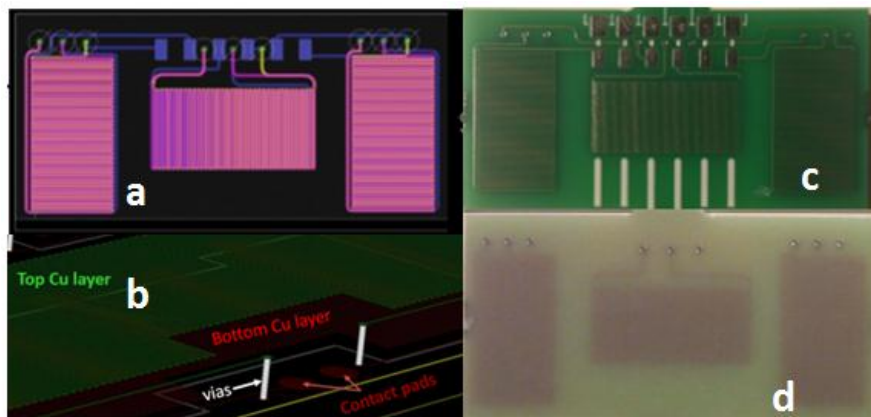


Figure 53 a) schematic of heater, b) 3D representation of multilayer PCB heater, c) backside of realised heater, d) front side of realised heater

5.4.2 Fabrication of DNA amplification μ -devices

Given the results from the numerical simulations and the restrictions of the materials to be used as well as those set from the reactions to be performed within the devices the designs of the μ -devices are drawn using various software such as CorelDraw or Autocad. The files generated can be used for printing the masks used in the photolithography or the CAD files employed in the CNC process as mentioned in subchapter 4.2.1 regarding the patterning methods. As mentioned in the material selection subchapter, the substrate of the microfluidic devices is either polyimide copper clad or PCB. In Fig. 54 the process flow for the fabrication of a μ -device is illustrated.

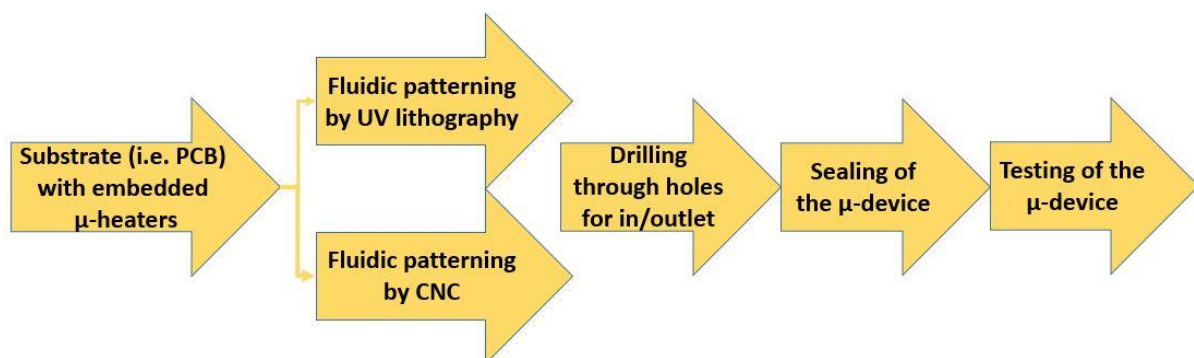


Figure 54 Fabrication process flow of the DNA amplification μ -devices

For the current thesis three different methods namely UV lithography, CNC micromilling and moulding-hot embossing were employed for patterning the desired microfluidic shapes. The designed and fabricated devices consist of the microfluidic network where DNA amplification takes place and resistive microheaters are embedded on the same substrate to facilitate the fabrication and to improve the thermal budget due to reduced distance from the sample. The patterning methods of the microfluidic network are presented in the following paragraphs.

5.4.2.1 UV Lithography

Herein we present the fabrication process of the microfluidic network by means of lithography. The substrate used for the fabrication of the devices is PCB with embedded Cu resistive microheaters. Before starting the process, the substrates are cleaned with acetone, propanol, water and dried with the aid of a pressurised air gun. A dry photoresist is laminated onto the PCB substrate with the aid of a heating roll laminator operated at 85°C -90°C. The photoresist used, Pyralux® PC1025 (Fig. 55), is a commercially available, polyimide-based, flexible, photoimageable dry film product from Dupont®. Due to its composition, it offers excellent bend and crease performance and high resolution. Afterwards, UV exposure (50sec for single layer photoresist) takes place through a photomask. This specific photoresist is negative meaning that after the exposure; the areas that were exposed are hardened, rendering the unexposed areas ready to dissolve during the development stage. The solution used for development is 1% Sodium Carbonate (Na_2CO_3) aqueous solution. Once the development is over, the devices are placed in a furnace or a hot plate for two hours under 160°C. To allow injection of fluid samples, holes are drilled for the microfluidic inlet and outlet using a pedestal drill. Once the inlets/outlet holes are opened, the device is rinsed in order to remove any residues and dried with the aid of a pressurised air gun. In case, there is a need for deeper channels more than one layer of the photoresist can be applied. In case there is a need to cover the bottom surface of the microfluidic network, the photoresist is applied and baked. Following, the above mentioned process takes place. The last step for the device is sealing, in order to form enclosed channels. The sealing process and the materials used are describes in the next section. The process flow followed for the fabrication of μ devices by means of lithography is depicted in Fig. 56.

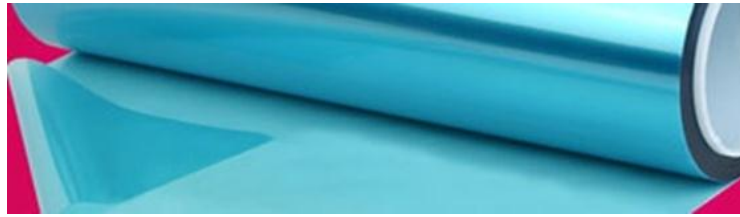


Figure 55 Dry photoresist - Pyralux® PC1025 (Dupont®)

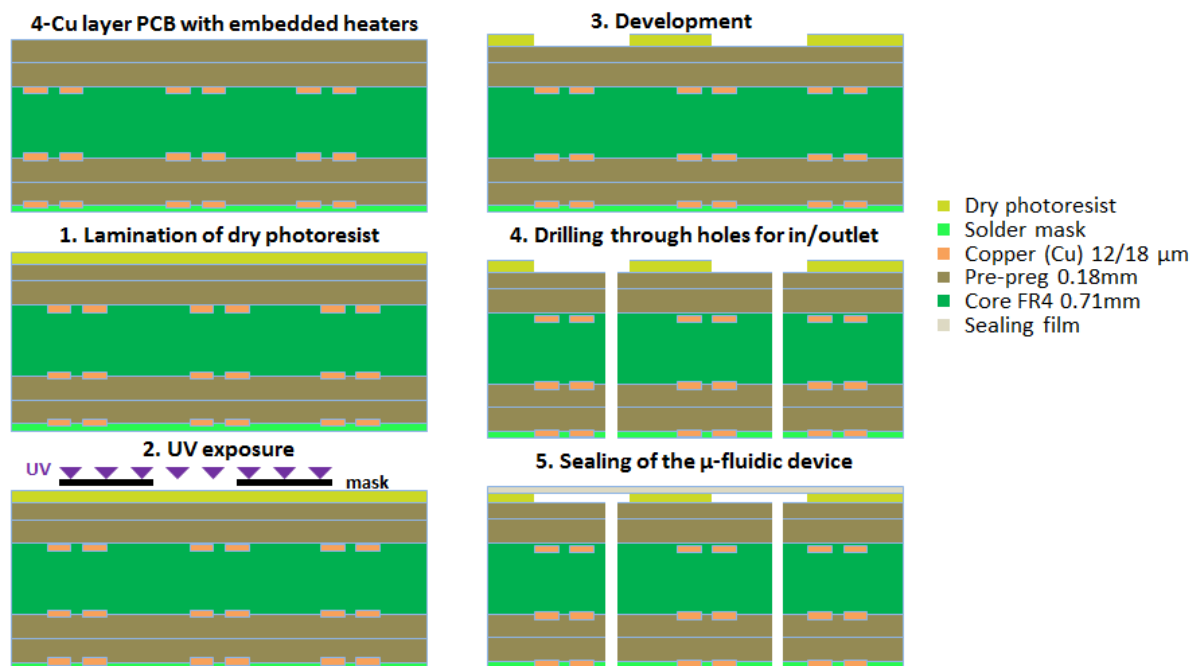


Figure 56 Fabrication process flow of the microfluidic network by means of lithography

5.4.2.2 Computer Numerical Control machining

CNC machining was used both for PCB substrates as well as PMMA substrates in order to pattern the microfluidic network. First the desired microfluidic network was designed using designing software (i.e. Corel Draw®, Autocad®) and then these designs were imported into the specialized software CircuitPro utilized by the LPKF in order to change and or improve any imperfections but mainly to verify the validity of the design (being ready to be fabricated). Once the design was loaded, the substrate was located into the cabinet of the LPKF. The good adherence of the substrate to the milling table is ensured by vacuum. An initial calibration is performed to finalize the correct coordinates (x,y,z) to allow for precise milling. Once all the parameters are set (milling depth, milling step), the automated

patterning process begins. CNC machining also offers the possibility to drill through holes for the inlet and outlet. Subsequently, the patterned fluidics are cleaned with acetone (in case of PMMA substrates we don't use acetone), propanol and water and dried with pressurized air which also assists the removal of any milling residues. The process flow followed for the fabrication of μ devices by means of CNC is depicted in Fig. 57.

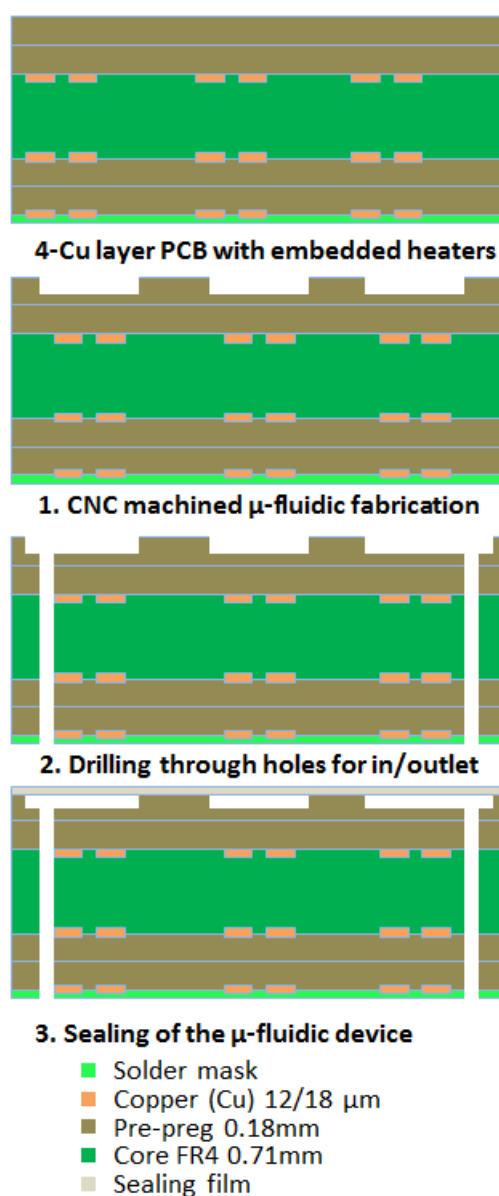


Figure 57 CNC milling process flow

5.5 Sealing of DNA amplification microdevices

As described previously in chapter two sealing process in micro-scale is demanding. Bonding becomes even more challenging when high temperatures are needed for the application devices are fabricated for. Thus we tested numerous materials in order to achieve the desired bonding strength so as the devices withstand the pressure drop accumulated both from the minute dimensions and the elevated temperatures used.

First, we used two different products from American Brittle Inc. namely: 7176 (Fig. 58a) which is a polyimide film double coated with a silicone adhesive. The thickness of the adhesive on each side is 55 μ m and the thickness of the polyimide film backing 25 μ m resulting in a total thickness of 135 μ m. It provides good heat and solvent resistance. The adhesion is stronger on the white film liner side than on the transparent side. The second product tested was 7270 (Fig. 59b) which is a 50 μ m Kapton® tape with a Therm-X silicone thermosetting adhesive system. The thickness of the Kapton backing is 50 μ m and the adhesive's 37.5 μ m resulting to a total thickness of 87.5 μ m. 7270 has a high temperature (180°C) performance. These two products were to seal microfluidic devices. The sealing process involved the use of a laminator operated at 60°C -90°C in order to achieve the optimum bonding strength. Another material used for sealing the microdevices is Clear Polyolefin StarSeal (PCR) (Fig. 59c) from StarLab. This product is typically used for covering multiwall plates and it is suitable for bio-analytical research and PCR compatible. The temperatures it withstands range from -70°C to 110°C. It is single coated with a pressure sensitive acrylate adhesive consisting of a 0.05mm polyolefin film. The seal is supplied on a white paper release liner. This product can be applied by hand or using a laminator (at 90 °C optionally). The main advantage of Clear Polyolefin StarSeal (PCR) is its transparency which enables the monitoring of the interior of the microchannels. Moreover, it has very low auto-fluorescence thus it is compatible with optical measurements.

DuPont™ Pyralux® coverlay (Fig. 59d) composites are constructed of DuPont Kapton® polyimide film, coated on one side with a proprietary B-staged modified acrylic adhesive. Coverlay is used to encapsulate etched details in flexible and rigid-flex multilayer constructions for environmental and electrical insulation. Coverlay is available in a variety of film and adhesive thicknesses. LF0150 has a backing thickness of 127 μ m and adhesive

thickness of 25 μ m. The reason we chose this one is because it provides enough robustness, it does not collapse and it is easy to handle.

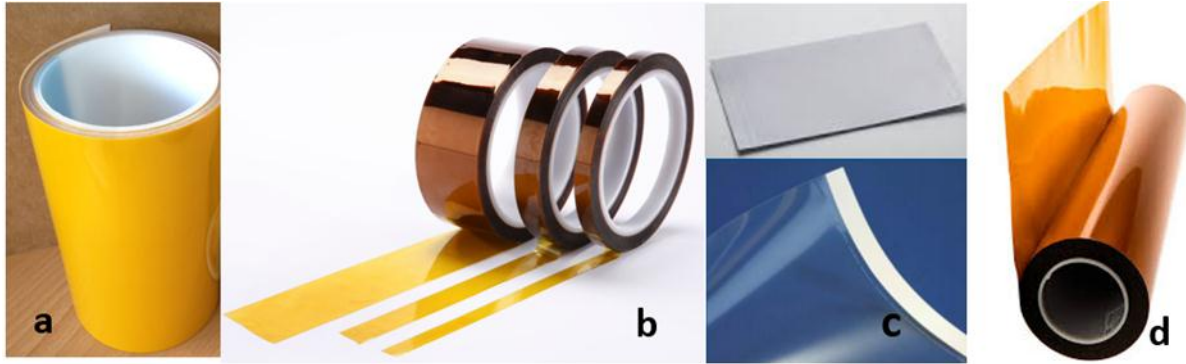


Figure 58 Products used for sealing microfluidic devices: a) Polyimide silicon adhesive tape 7176, b) Kapton with silicon adhesive tape 7270, c) Clear Polyolefin StarSeal (PCR), d) LF Coverlay

5.6 Characterization of DNA amplification microdevices

5.6.1 Electrical characterization of microheaters

The characterization and calibration of the fabricated microheaters took place using a probe station with a heated chuck (Signatone S-1041-D3 Hot chuck) and a Keithley 2400 source-meter controlled by Labview, for sourcing current I and measuring electrical resistance R (see Fig. 59). As for the flexible aluminium or copper microheaters, they were glued on a wafer substrate using thermal paste. The wafer was in-turn tightly attached to a hot plate of controlled temperature under vacuum.

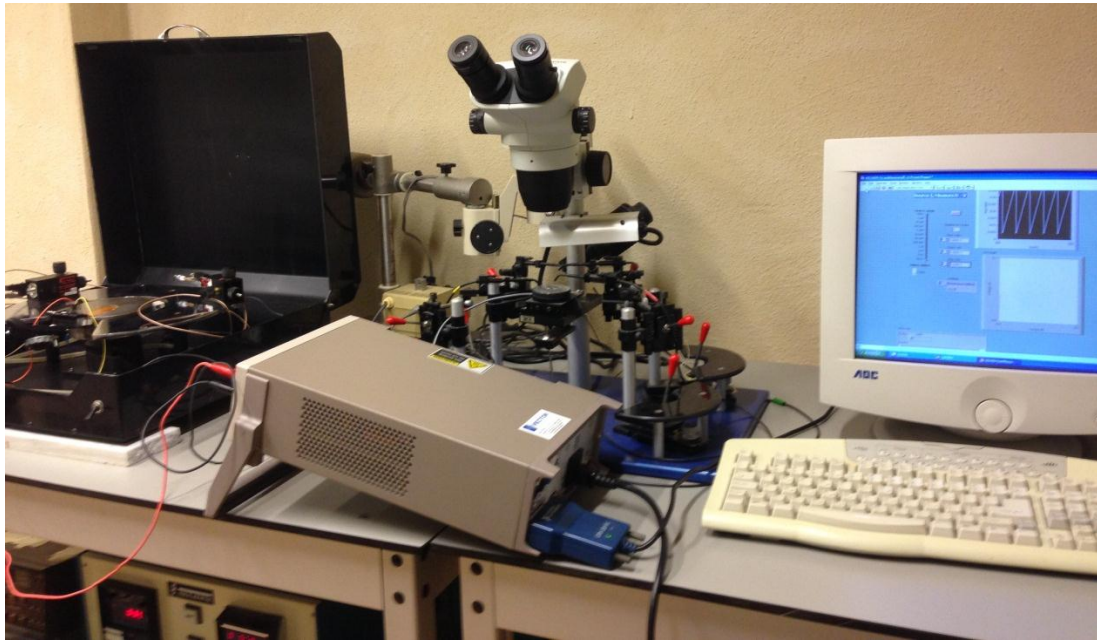


Figure 59 Electrical characterization set-up

An average TCR of $0.0026^{\circ}\text{C}^{-1}$ and $0.0038^{\circ}\text{C}^{-1}$ was estimated for the aluminium resistors with thickness of 300 and 1000 nm, respectively as shown in Fig. 60. and Fig. 61. The experimental TCR value was calculated from the slope (0.151, R_0 : 34 Ohm, 1.086, R_0 : 417 respectively for 300 nm and 1000 nm) of the linear fit. In table 9 and 10 TCR values for different Al thin film is presented [231]

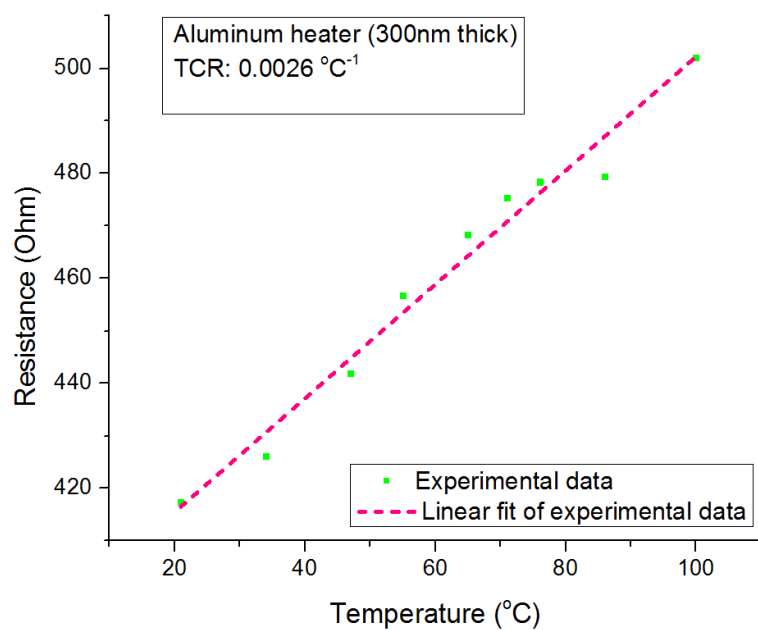


Figure 60 Change in resistance for various temperatures (Al heater 300 nm)

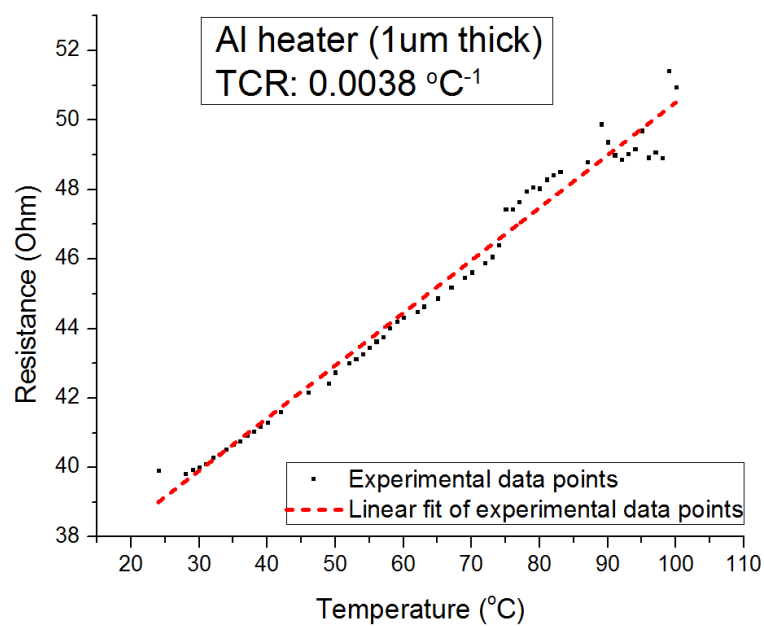


Figure 61 Change in resistance for various temperatures (Al heater 1000 nm)

Table 9 Bibliographic TCR values for different thickness of Al thin films [231]

Aluminum sheet	
Thickness (μm)	TCR ($^{\circ}\text{C}^{-1}$)
0.18	0.0041
0.51	0.0041
1.02	0.0043
1.98	0.0043
bulk	0.0039

Compared to the values found in the table above, there is a deviation of 36% and 11% for the 0.3 μm and 1 μm thick aluminium films, respectively. However, Nancy M. McCurry in her thesis reports a TCR value of $0.00375^{\circ}\text{C}^{-1}$ for 1 μm aluminum thickness [232] which is almost identical to our measurement and R. Belser reports a value of $0.0028^{\circ}\text{C}^{-1}$ for thin Al films [233] which is close to the measure we got for 300 nm Al thickness. In table 10 below theoretical and measured TCR values for Cu and Al films with different thicknesses are depicted [234]

Table 10 Theoretical and measured TCR values for Cu and Al films with different thicknesses

Thickness d_f (nm)	Cu		Al	
	TCR _f (K^{-1}) theoretical	TCR _f (K^{-1}) measured	TCR _f (K^{-1}) theoretical	TCR _f (K^{-1}) measured
200	0.00386	0.00379 ± 0.00014	0.00386	0.00379 ± 0.00009
100	0.00377	0.00382 ± 0.00010	0.00379	0.00370 ± 0.00011
80	0.00376	0.00376 ± 0.00006	0.00378	0.00369 ± 0.00010
60	0.00373	0.00358 ± 0.00004	0.00376	0.00372 ± 0.00009
40	0.00372	0.00361 ± 0.00002	0.00373	0.00355 ± 0.00010
20	0.00369	0.00350 ± 0.00004	0.00358	0.00349 ± 0.00007

Regarding the PCB microheaters with the embedded Cu resistive elements, an average TCR of $0.0035^{\circ}\text{C}^{-1}$ was estimated for Cu resistors as shown in Fig. 62. The experimental TCR value was calculated from the slope (0.057, R_0 : 16 Ohm) of the linear fit. The measured TCR value is in concordance with values ($0.0037^{\circ}\text{C}^{-1}$) reported in literature [234].

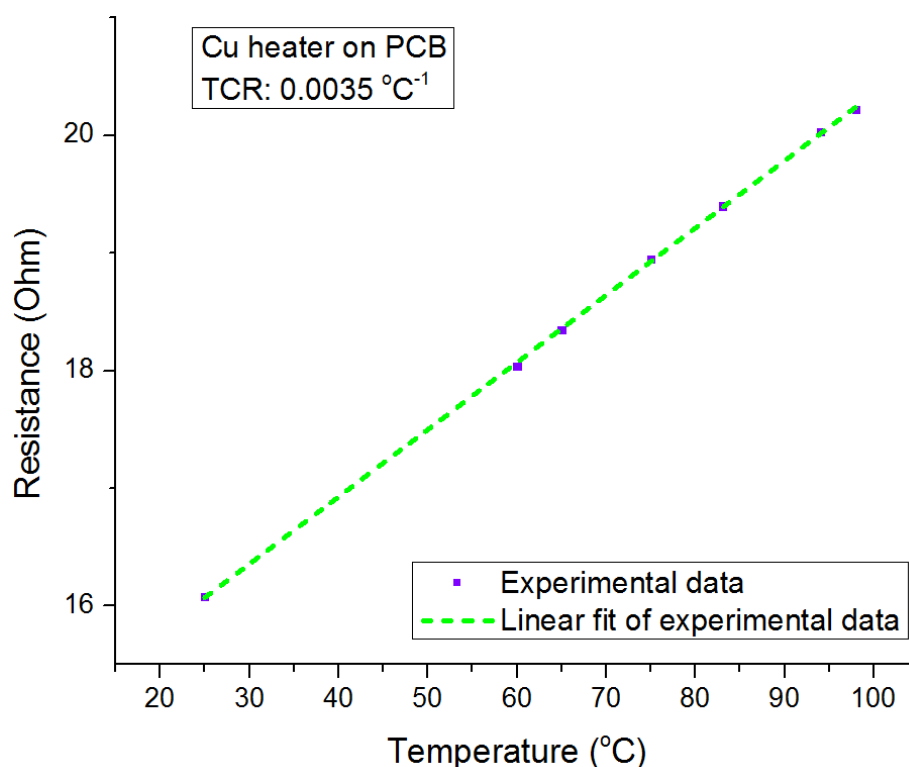


Figure 62 Change in resistance for various temperatures (Cu heater on PCB)

5.6.2 Thermal behaviour of the microdevices

For the evaluation of the thermal behaviour of the microdevice with the integrated copper (Cu) microheaters, we used a thermal camera (InfraRed, IR, Nikon) and a microdevice corresponding to the closed-loop (re-circulating) μPCR (Fig 63). The evaluation was conducted in the Institute of Chemical Engineering Sciences (FORTH, Patras). Two were the main concerns regarding the thermal behaviour of the microdevices: the temperature uniformity across each zone necessary for a PCR reaction step (denaturation, annealing, and extension) and the absence of thermal cross-talk between two neighbouring zones (denaturation-extension, extension-annealing). According to the design of the microheaters in the microdevice, the space between two neighbouring zones is 2.85 mm. This distance was found through numerical calculations sufficient to provide good temperature uniformity in

each zone and thermal independence between neighbouring zones. Thermal images of both sides of the device were obtained. The top layer on both sides of the microdevice is Polyimide (PI), a material of known emissivity equal to 0.97 (literature value [148]). A special paint of known emissivity was used to cover a part of the device surface, from which the emissivity of PI was experimentally determined and verified the accepted (literature) value.

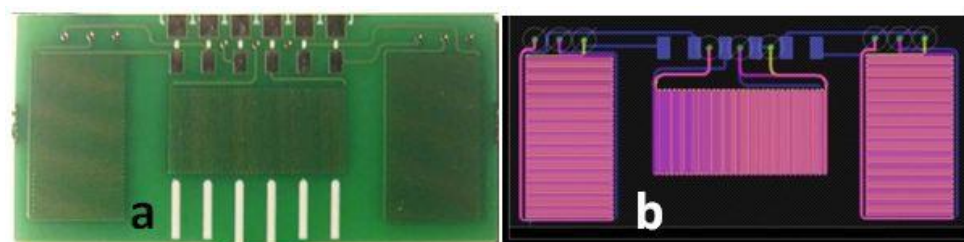


Figure 63 μ PCR device with microheaters integrated in PCB. a) Back side of the device, b) CAD design of the heaters

Temperature uniformity across each zone

Thermal images of the devices were obtained depicting areas of the zones or areas between neighboring zones, as are shown in Figs.64 and 65. We note here that, due to differences in camera focus, only the central part of the image (where the image is on focus) can be reliably used for determining the temperature of the device surface. For example, the color in Fig. 64 is uniform only inside the circle indicated on the image. Therefore, gradients in temperature are expected at the image areas close to the left and right margins. Color uniformity corresponds to temperature uniformity only in the central part of the images, and outside the central area, gradients are considered artificial. The image shown in Fig. 65 depicts part of the back-side of the device, between the extension and denaturation zone. Across this area, three straight lines are drawn and the temperature profiles along these lines are depicted below the image. These temperature profiles are automatically generated by the camera software. According to these profiles, the temperature across the denaturation zone is uniform. The same conclusion cannot be safely drawn for the extension zone, as this area lies outside the camera focus.

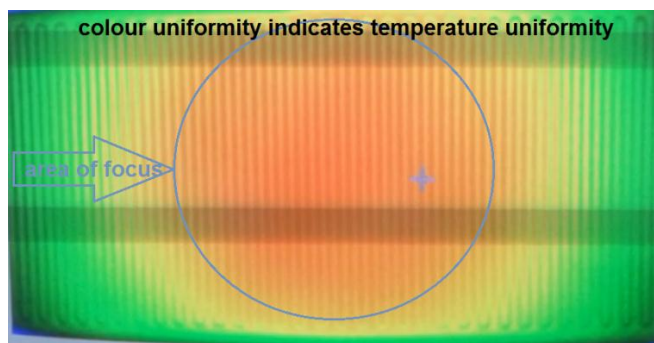


Figure 64 Back-side of the device. A meandering microheater is shown defining the extension zone.

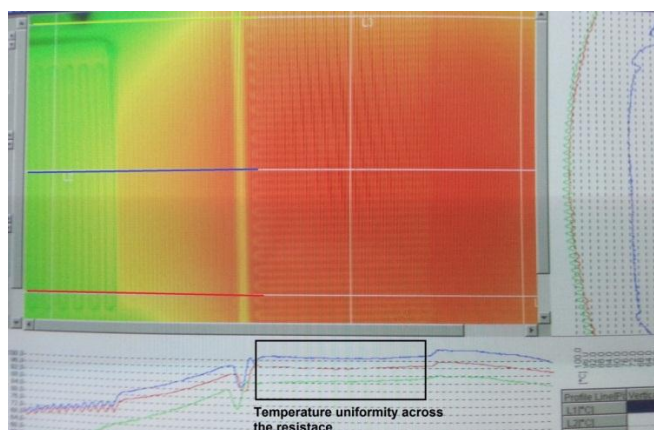


Figure 65 Thermal image of the back-side of the device between the extension and denaturation zones

Thermal cross-talk

From the images in Figs. 66-68, we evaluated the thermal cross-talk between the thermal zones of the μ PCR device. From the temperature profile along line L1, the transition zone between the extension and denaturation zone can be easily derived, as part of the line along which the temperature sharply decreases from 96 °C to 76 °C. The width of the transition zone is 2.85 mm, corresponding exactly to the designed separation between neighboring microheaters. Therefore, one can safely conclude that there is no significant thermal cross-talk between the denaturation and extension zone (Fig. 66). The distance was estimated through its comparison with a known length (width of the microheater copper lines equal to 100 μ m). On both sides of the transition zone, the temperature reaches a plateau value, corresponding to the denaturation temperature (on the right side) and the extension temperature (on the left side). The temperature profile along L1 inside the zones indicates a

small temperature gradient around a middle value ($T \pm 4^\circ\text{C}$). This small gradient was not observed in Fig. 65, where good uniformity was demonstrated. It can be attributed to the proximity of this area to the chip holder shown at the left bottom corner of the image (with large thermal mass at room temperature). The same conclusion regarding the thermal cross-talk can be also drawn from the image of the front side of the device (Fig. 67) which indicates a small (5%) width decrease and similarly, for the extension-annealing zones, given that the width of the transition zone is close to 2.85 mm (see Fig. 68).

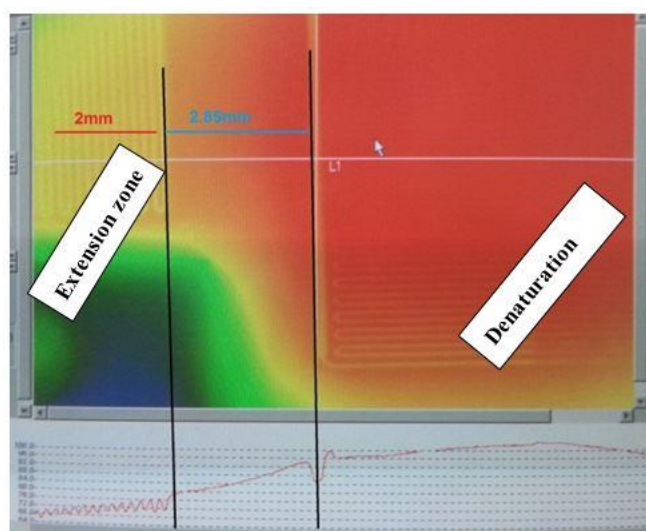


Figure 66 Image of the back-side of the μPCR device. The two black lines denote the extent of the transition zone between the extension and denaturation zone

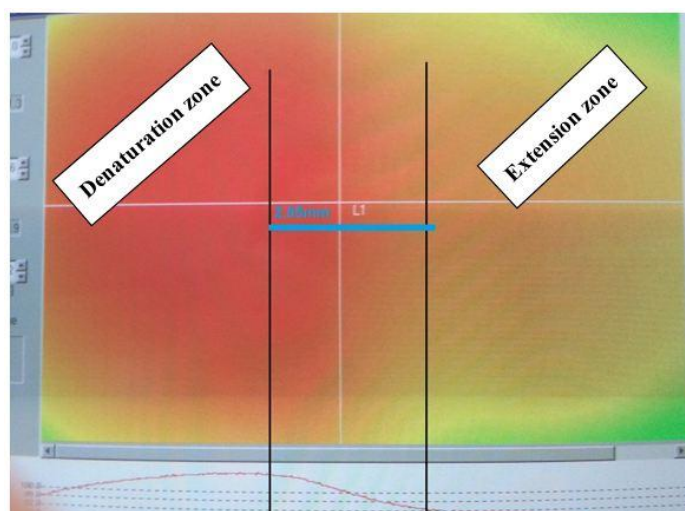


Figure 67 Image of the front side of the μPCR device. The two black lines denote the transition zone between denaturation and extension zone.

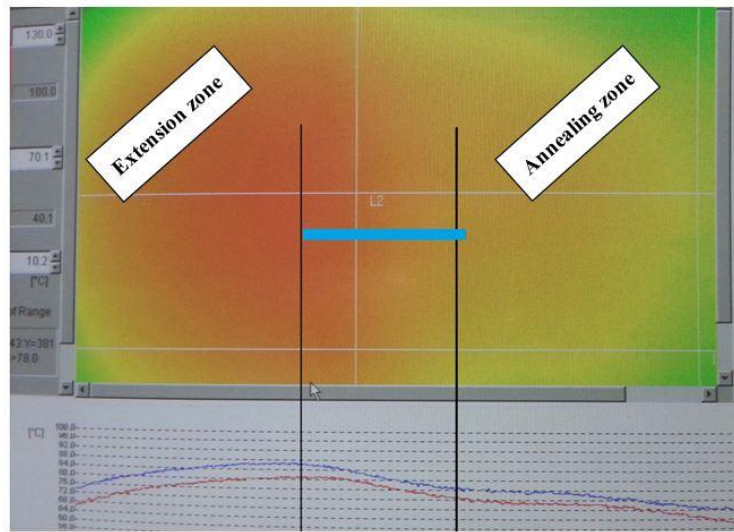


Figure 68 Image of the front side of the device. The two black lines denote the transition between extension and annealing zone

Temperature calibration

The images of the device from the thermocamera were also used for the calibration of the temperatures achieved by means of the microheaters with the temperature control unit. The TCR used in these experiments was $0.0039\text{ }^{\circ}\text{C}^{-1}$. The temperature setpoints for the denaturation, annealing and extension zone were 95°C , 55°C and 72°C respectively. In addition to the thermocamera, a thermocouple was used calibrated with respect to an already calibrated hot-plate. The indications from both instruments (IR camera, thermocouple) are shown in table 12 below and are used for the independent calibration of the temperature on the microdevices

In addition, the TCR value for the copper microresistors can be determined from the comparison between the set-temperatures (controller) and the achieved temperatures (thermocouple). Three set-point temperatures were chosen, relevant to PCR protocols, i.e. the denaturation temperature ($95\text{ }^{\circ}\text{C}$), the extension ($72\text{ }^{\circ}\text{C}$) and the annealing temperature ($55\text{ }^{\circ}\text{C}$), and a TCR value was given as input to the software controlling the microresistors target resistance. For each TCR value, different temperatures were achieved. Using the formula relating the resistance change to the temperature change:

$$\Delta R = R_0 \cdot \text{TCR} \cdot \Delta T$$

a new TCR value was determined, compatible with the correct achieved temperature. From the 9 values of the achieved temperatures shown on Table 11, an average value of TCR was determined for the copper microheaters equal to $0.0034 \pm 0.0002 \text{ }^{\circ}\text{C}^{-1}$. (in good agreement with the experimentally determined value, see 5.6.1).

Table 11 Set-point temperatures and achieved ones (measured with a thermocouple) for different TCRs

T_C (TCR $0.0039^{\circ}\text{C}^{-1}$)	T_{TC} ($^{\circ}\text{C}$)	T_C (TCR $0.0035^{\circ}\text{C}^{-1}$)	T_{TC} ($^{\circ}\text{C}$)	T_C (TCR $0.0032^{\circ}\text{C}^{-1}$)	T_{TC} ($^{\circ}\text{C}$)
55	62	55	59	55	57
72	76	72	70.5	72	64
95	103	95	94	95	88

Table 12 Comparison of the temperatures acquired from the temperature controller, IR camera, and thermocouple

T_C (TCR= $0.0034^{\circ}\text{C}^{-1}$)	T_{IR} ($^{\circ}\text{C}$)	T_{TC} ($^{\circ}\text{C}$)
59	59.5	62
79	78	76
105	103	103

5.6.3 Characterization of Microfluidics

Flow tests were performed by injecting liquid samples in sealed μ -devices with a laboratory syringe pump (Chemyx Inc, Fusion 200). To perform these tests, fluidic interfaces were necessary. More specifically, fluidic interfacing was achieved using a Plexiglas (PMMA) chip holder that was fabricated in-house (see Fig. 69 a) to be compatible with commercially available Upchurch® Nanoport fittings (see Fig. 69 b). Upchurch Scientific® PEEK tubing as well as fused silica tubing are biocompatible and chemically inert to most solvents. Unlike

stainless steel and titanium tubing, PEEK and fused silica tubing are flexible and can be easily cut to desired lengths. Fabricated μ -devices were tested under mild conditions (room temperature, flow rates up to 100 μ l/min) and most of them were found to be leak-tight.

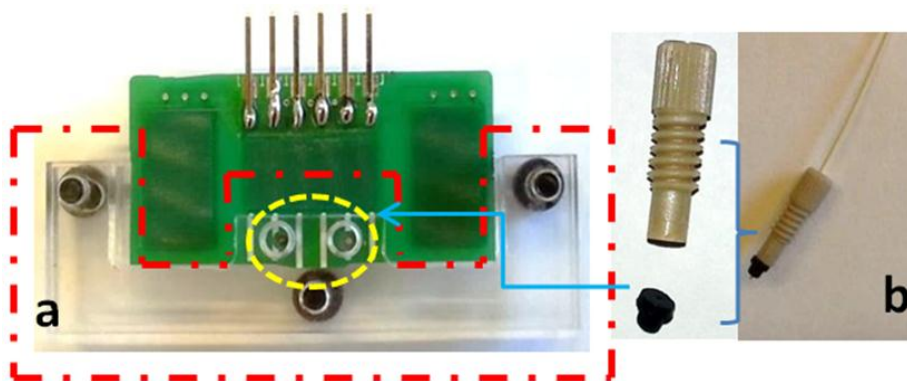


Figure 69 a) custom-made PMMA chip holder, b) Fluidic interconnections (fittings, ferrules, tubing)

The fluidic testing was completed by applying temperature (up to 120°C) either by using a hot plate or the temperature controller unit to provide the heat required. The devices were tested under heat since the amplification methods (most of them) require elevated temperature up to 95°C). Once a μ -device met the leak-tight requirements, it is ready to be used for biological experiments. Another major issue apart from the leak-tightness of the fluidics is the uniform filling of the fluidic network. In some cases, (typically in chamber fluidics) partial (80%) filling of the microchambers was observed. Thus, hydrophilization of the wall surfaces was implemented as remedy. Aqueatic solution of BSA or PEG was used for hydrophilization. These solutions had a dual role, since BSA and PEG can also be used for wall passivation for minimizing adsorption of biomolecules [235, 236]. In order to further enhance the wall passivation BSA and PEG can also be introduced in the reaction sample to provide dynamic passivation.

5.7 Wall passivation of μ -fluidic devices

The adsorption of biomolecules on the surface of microfluidic devices used as bioreactors (e.g. nucleic acid amplification reactor) can heavily/adversely affect the efficiency or even

totally inhibit the biochemical reaction. Biomolecule adsorption is proportional to the surface area. Thus, the higher the surface area, the higher the biomolecule adsorption.

PCB substrates with various surface modifications were tested with respect to their protein adsorption properties. Bovine serum albumin (BSA; fraction V), goat anti-mouse IgG antibody conjugated to horse radish peroxidase (anti-mouse IgG-HRP), and 2,2'-azino-bis(3-ethylbenzothiazoline-6-sulphonic acid) (ABTS) were from Sigma-Aldrich. In addition to the modified substrates, unmodified surfaces were tested for comparison reasons. Frame-Seal incubation chambers (SLF-0601, BioRad, Fig. 70) 15 x 15 mm with 65 μ l capacity were used to demarcate/ define the limits.



Figure 70 Frame-Seal incubation chambers

Surface modifications:

Table 13 shows all the surface modifications tested for reducing biomolecules adsorption on surface walls.

Table 13 List of surface modification

Surface modification			
1	BSA (1%)	6	Pluronic (0.1%)
2	BSA (1%)-baked @95°C 1h	7	Pluronic (0.1%)-baked @95°C 1h
3	PEG-Silane-w. O ₂ Plasma	8	Pluronic (0.1%)-baked @95°C 2h
4	PEG-Silane-w.o. O ₂ plasma	9	Pluronic (0.1%)-baked @160°C 1h
5	O ₂ plasma		

In Fig.71 the process followed for evaluating each modification relatively to hindering biomolecules adsorption is depicted.

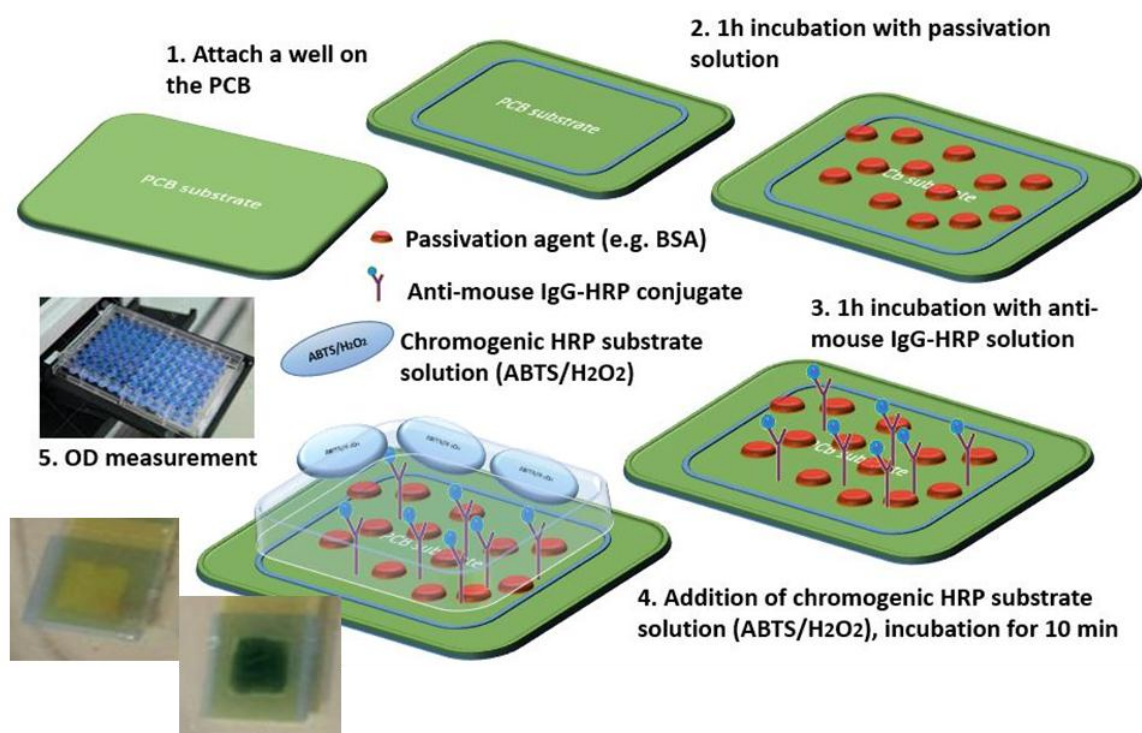


Figure 71 Schematic of the process flow for evaluating each modification relative to hindering biomolecules adsorption

Prior to starting each experiment, the substrates were cleaned with acetone, propanol, DI H₂O, dried with N₂ gun and left on a hot plate at 120°C for 15min. In all cases, the modifying agent was dispensed on the substrate's surface and left for incubation for 1h unless stated differently. Next, the substrates were rinsed with DI H₂O and dried with pressurized air. Subsequently, 100 µl of a 5 µg/ml anti-mouse IgG- HRP solution was placed in each well followed by incubation for 1h. A chromogenic HRP substrate solution (ABTS/H₂O₂) was then added in each well and incubated for 10min and the adsorption of mouse IgG or the absence of it was verified by development or not of green color, respectively (Fig. 72).

In order to quantify the adsorption, the enzymatic reaction was stopped by addition of 50µl of SDS. Then the total volume of the liquid from each chamber was collected and transferred into the wells of a 96-well plate so as to measure the OD at 405nm using an ELISA reader (CVictor3, PerkuElmer, Inc, MA, USA). The results obtained are illustrated on the table in Fig. 73 (color coded, red color indicates heavy adsorption whereas violet color low adsorption).

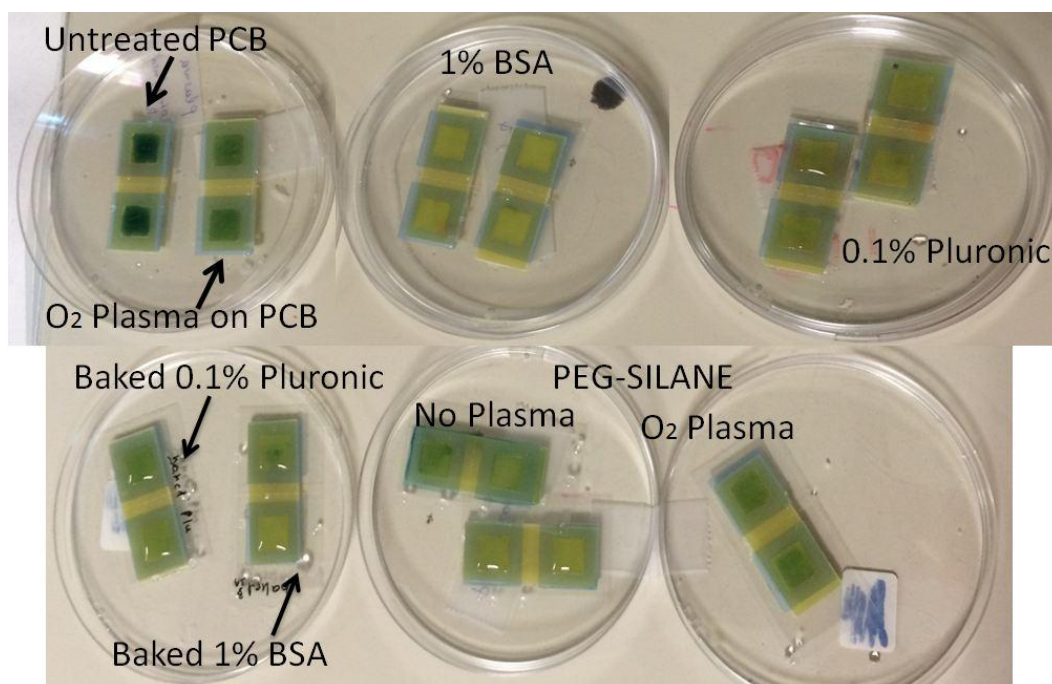


Figure 72 Images of the PCB substrates with different modifications while the reaction is over

A/A	Modification	A/A	Modification	A/A	Modification
1A	PCB UNTREATED	2A	PLURONIC (0.1%)	3A	PEG-SILANE (NO PLASMA)
1B	PCB UNTREATED	2B	PLURONIC (0.1%)	3B	PEG-SILANE (NO PLASMA)
1C	PLASMA ON PCB	2C	PLURONIC (0.1%)	3C	PLURONIC (BAKED 1h@95°C)
1D	PLASMA ON PCB	2D	PLURONIC (0.1%)	3D	PLURONIC (BAKED 1h@95°C)
1E	BSA (1%)	2E	PEG-SILANE	3E	BSA (BAKED 1h@95°C)
1F	BSA (1%)	2F	PEG-SILANE	3F	BSA (BAKED 1h@95°C)
1G	BSA (1%)	2G	PEG-SILANE	3G	NO SAMPLE
1H	BSA (1%)	2H	NO SAMPLE	3H	NO SAMPLE

Figure 73 Table with modifications corresponding to the readings of the OD reader

Plasma surface activation (at 100 mTorr O₂, 100 W) of substrates was conducted in a Nextral Alcatel NE330 reactive ion etching (RIE) with a flow rate of 50 sccm for 1min. PEG-Silane coatings were performed on FR4 and PC1000 substrates. Processes similar to those described in [237] and [238] were followed: The surfaces were plasma activated for 1 min to hydrophilize them in some cases and then immersed for 4 h in 0.5% v/v PEG-Silane anhydrous toluene solution, while 0.08% v/v HCl solution was added as a catalyst. Subsequently, the samples were rinsed with toluene, ethanol and deionized water, and dried with N₂ gun.

BSA coating was achieved by immersing the substrates in a 1% BSA solution for 1h. Respectively, the pluronic (Poly(ethylene glycol)-block-poly(propylene glycol)-block-poly(ethylene glycol), PEG-PPG-PEG, Pluronic®(F-108, Sigma-Aldrich®) – which is a difunctional block copolymer surfactant terminating in primary hydroxyl groups- coating was achieved by 1min immersion of the substrate in a 0.1% Pluronic solution for 1h. In some cases, the BSA and Pluronic modified substrates were baked on a hotplate at 95°C and/or 160°C for 1h.

In Fig. 74 the results obtained regarding biomolecules adsorption on the PCB surface are presented. The best surface passivation was achieved with 1% BSA solution. More specifically, the BSA coating presented only a 13.3% protein adsorption (86.7% reduction of adsorption) whereas a 2h Pluronic treatment and a 1h PEG-Silane (w.o. O₂ plasma) treatment presented 21.4% and 17.1% (reduction of adsorption by 78.6% and 82.9%) respectively .

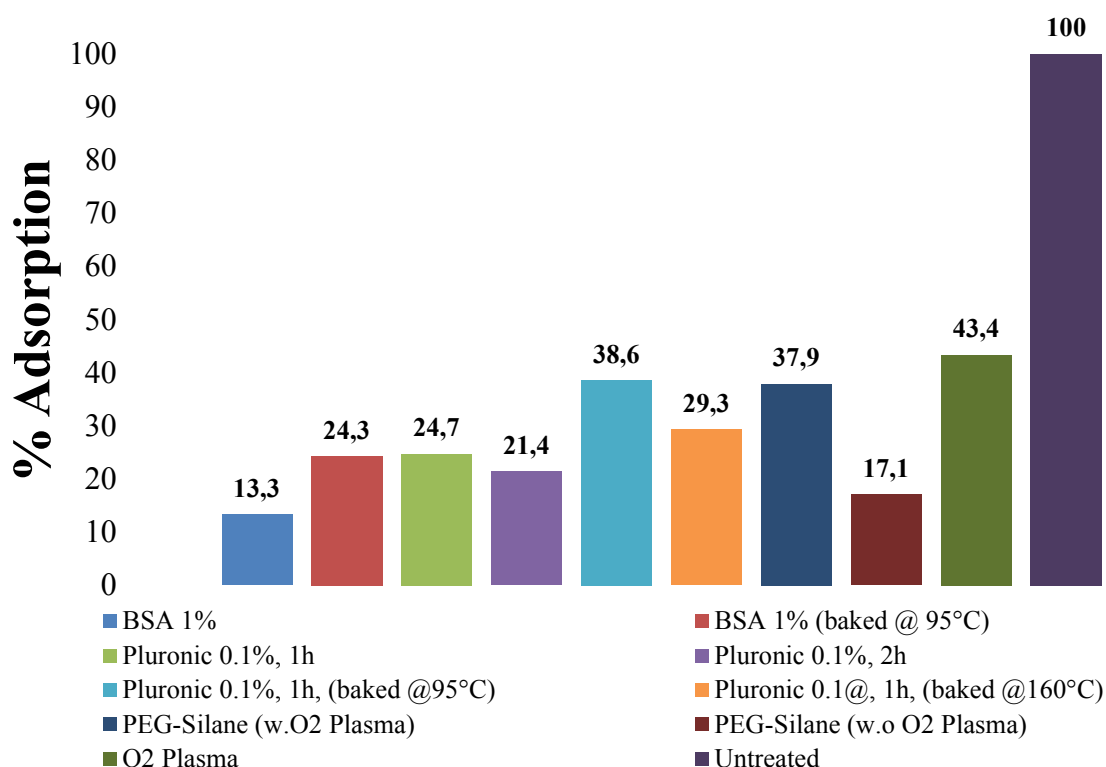


Figure 74 % Protein adsorption on PCB surface implementing various surface modifications. All data were normalized to the adsorption value of the untreated PCB substrate

Since the most promising for results for surface/wall passivation were achieved with 1% BSA solution, the same modification was evaluated in two other substrates, namely the

photosensitive dry film DuPont™ Pyralux® PC 1015 (PC) and the DuPont™ Pyralux® LF coverlay (LF) which are structural and sealing materials respectively for the microreactors developed. PC is a flexible photoimageable dry film solder mask consisting of a specially developed combination of acrylic, urethane, and imide-based material. LF is polyimide-based film, coated on one side with an acrylic adhesive. The results obtained, with 1% BSA passivation are presented in the graph below (Fig. 75). The reduction of protein adsorption on the LF and PC substrates is 60% approximately, whereas for the PCB substrate is 30% higher, reaching almost 87%.

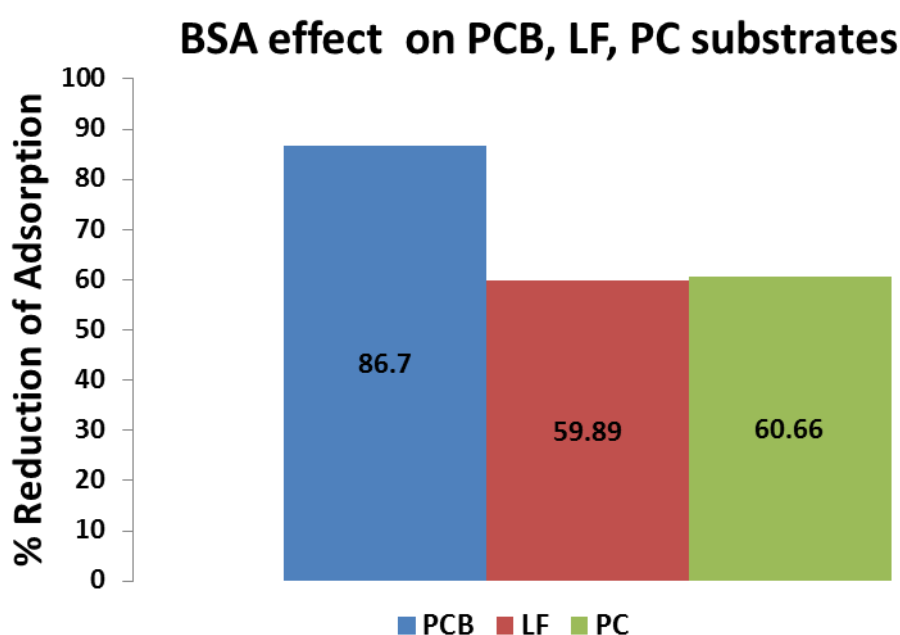


Figure 75 1% BSA solution effect on protein adsorption on different substrates (PCB, LF, PC)

5.8 Conclusions

To sum up for the development of a DNA amplification microdevice numerical calculations are performed to guide the design in terms of energy consumption and temperature uniformity since these two parameters affect the compatibility with LoC platform (especially ones intended for low-resource settings) and the amplification efficiency, respectively. Both the materials and the fabrication methods are compatible with established PCB industry thus rendering the fabrication of the microdevices readily transferable to mass production at a very

low cost. It has to be highlighted that the sealing method proposed (patent pending) it is of extreme importance since it offers a robust and reliable method for irreversibly sealing microdevices where high temperatures and pressure drop is anticipated while in operation. Last, various passivation agents were tested for reducing biomolecules adsorption and it was found that BSA 1% offers the best outcome, thus it can be used in microdevices with high surface/volume ratios to minimize the adsorption and maximize the efficiency of the amplification reaction.

Chapter 6 Evaluation of the DNA amplification microdevices

In this chapter the fabricated devices and their characteristics such as the geometrical design, energy consumption and amplification efficiency are presented. PCR, HDA, RPA and LAMP amplification microdevices are validated with real amplification protocols employing Salmonella genomic DNA and in the case of LAMP-based micro device whole Salmonella cells as DNA template.

6.1 Introduction

In a plethora of cases, nucleic acid amplification is an indispensable tool for the development of diagnostics serving not only the detection but also the identification of genetic disorders, mutations, infectious diseases, and other purposes. Currently, there are numerous nucleic acid amplification methods available which are used in analysing and detecting a small quantity of nucleic acids. The most widely used method is the Polymerase Chain Reaction (PCR). Miniaturized PCR (μ PCR) devices efficiently amplifying DNA can be categorized into static chamber (SC) and continuous flow (CF) devices. The SC devices resemble the conventional thermocyclers at their operation; the sample is static in a chamber (well) and both the device and the sample undergo thermal cycling [239] temperature ramping is required during the operation. On the other hand, in continuous flow (fixed-loop or closed-loop) devices [145], no temperature ramping is required: The sample moves through fixed temperature zones to achieve the required thermal cycling, leading generally to faster DNA amplification and lower power consumption. Moreover, the use of thin (flexible) polymeric films for the fabrication of μ PCR devices or other heated devices [58, 148], and the evolution of the heating elements from external to integrated on chip at a small distance from the DNA sample, allow further reduction in the thermal mass of the devices and as a consequence rapid heating/cooling rates [71, 240, 241] Despite these advantages, a shift towards isothermal methods in microfabricated diagnostics is observed, mainly stemming from their simplicity

and reduced thermal budget. The main advantage of isothermal methods over PCR is the elimination of the need for thermocycling, as the isothermal methods are realized under a stable and constant temperature over time.

Recent advancements in molecular biology have broadened the archery, offering different alternative isothermal methods for DNA amplification [93, 242]. For example, Loop-Mediated Isothermal Amplification (LAMP) [243], Rolling Circle Amplification (RCA) [244], Recombinase Polymerase Amplification (RPA) [130], and Helicase Dependent Amplification (HDA) [169] are some of the isothermal amplification methods that have already been miniaturized. All the aforementioned methods offer exponential amplification of DNA.

The devices presented in this thesis are suitable components for LoC systems offering excellent amplification efficiency since they can be fabricated by low cost, mass production amenable technologies mainly on printed circuit board (PCB) substrates, where copper facilitates the incorporation of on-chip resistive microheaters, defining the thermal zones necessary for DNA amplification methods. The proposed technology has allowed so far the use of copper as structural material for the microfluidic network [49] as well as the integration of microfluidic devices with heterogeneous components such as electronic circuits [245], sensors [246], and microheaters, following the current trend in LoC technology [46].

Throughout this thesis numerous designs for nucleic acid amplification devices were fabricated and evaluated for efficient DNA amplification. In this chapter all the microfluidic devices will be presented. The microdevices include recirculating, static and continuous flow devices for nucleic acid amplification employing both non-isothermal and isothermal protocols. This chapter is divided in subsections each one describing one of the DNA amplification microdevices developed regarding the amplification method (PCR, HDA, RPA and LAMP) and the mode (CF or SC) used. It has to be highlighted that in section 6.4 one of the fastest (2min) ever reported continuous flow μ PCR device is presented with a power consumption of 2.7 W (324 J).

6.2 Closed-loop continuous flow μ -PCR

For a small footprint and flexible regarding the number of thermal cycles on chip DNA amplification, the basic idea was to use of a 3-zone PCR microdevice, consisting of a closed-loop microfluidic network lying at a small distance above 3 integrated resistive heaters that define the 3 zones necessary for PCR. For this design, on-chip pumping was also required to allow re-circulation of the biological samples through the zones. This device consisted of a PCB with 3 embedded microheaters (one for each step of PCR namely denaturation, annealing, extension) a microfluidic network comprising three chambers (μ -posts were added in the chambers in order to prevent the collapse of the sealing film) and channels between the chambers (Fig. 76a). In addition, a microfluidic card with 3 Quake-type valves [247] assisting the recirculation was employed (provided by Jobst Technologies GmbH, Germany). In a later design instead of chambers, we used meandering channels (Fig. 76b), which upon observation tend to fill more uniformly compared to chambers. The number of the thermal cycles is defined by the number of sample re-circulations to be realized using on-chip pumping. Recirculation serves a dual role; apart from the DNA amplification, it would be used to facilitate mixing the reagents and the DNA sample upon insertion within the microfluidic network.

The footprint of a single recirculating device is 18mmx37mm. The depth of the fluidic network was 55 μ m and the volume of each chamber was 4.5 μ l each resulting to a total volume of 15 μ l. Each μ -device can serve PCR protocols with time ratios among the three zones 1:1:1 (the residence time in each zone is the same since the volume of all chambers is identical). The total duration of 30 cycles of the PCR amplification reaction is 15min and 8min with a volumetric flow rate of 30 μ l/min and 60 μ l/min respectively.

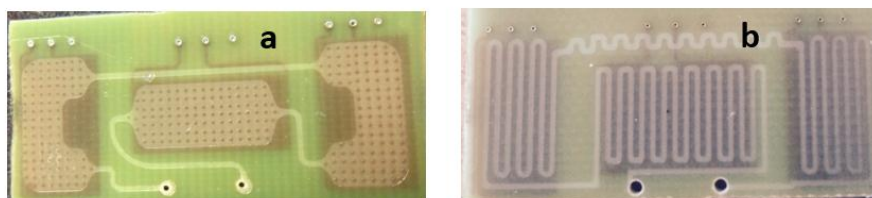


Figure 76 Recirculation μ devices. a) μ -device with chambers, b) μ -device with meandering channels

The embedded copper microheaters were designed and fabricated in three layers in order to achieve the desired resistance values for the temperature controller. The geometry and the

distances between the microheaters were designed following the simulation results in order to achieve adequate temperature uniformity for each zone and to eliminate any thermal cross-talk between the zones. Moreover, the spatial arrangement of the chambers was carefully chosen in order to minimize the power consumption. As for the microfluidic network, it was fabricated by means of photolithography using a dry photoresist directly on top of the PCB (see 5.4.2). The microfluidic card- ensuring sample recirculation- was realized within a 9-layer, credit-card-sized (54mmx85mm), PP/PET substrate (fabricated by Jobst Technologies GmbH, Germany), whereas the Quake-type valves (thin flexible membranes) were made of PDMS. Once the heaters and the microfluidic network were ready, the microfluidic card was attached in order to achieve circular pumping within the heated microchannels, while avoiding the sample to exit the heated substrate through an external pump. Double-sided adhesive O-rings were used in the inlet and outlet to minimize potential leakages. The operation of the Quake-type valves relied on pressurised air/nitrogen or water. Each valve was connected to a channel (underlying the valve) which upon filling was closing the valve.

These devices were designed to be compatible with the LoC platform developed for the European LoveFood project. The LoC serves multiple functions such as bacteria capturing and lysis, DNA purification, DNA amplification and detection using Surface Acoustic Waves. In Fig. 77 the custom-made PMMA docking station (provided by Jobst Technologies GmbH, Germany) for housing all the microfluidic components and the SAW chip -including the recirculating μ -PCR devices- is depicted under operation. Since SAW measurements are affected by heat, the denaturation zone was located as far as possible from the SAW sensor, to prevent any thermal noise which may affect the SAW signal (Fig. 77b).

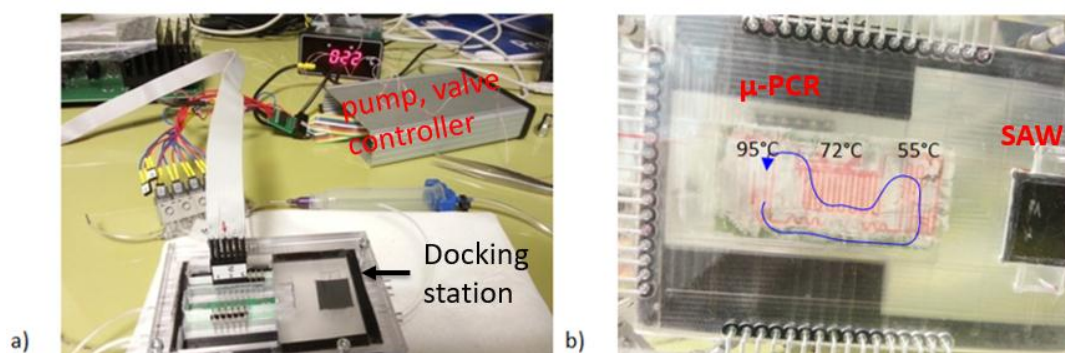


Figure 77 a) Setup for PCR with circular on-chip-pumping. b) Close-up picture of the on-chip pump with integrated μ PCR channel assembled within the docking station and attached by thermal paste to the 3-temperature-zone PCB heater.

The main challenge we faced was the integration of the recirculation card with the 3-zone PCR module. The requirement of pressurized air made this endeavour quite bulky and not very user friendly. The proposed design of closed loop microfluidic network didn't work efficiently due to weak membranes (Quake valves) of the pumping chip causing leakages while performing real amplification protocols. More specifically, the problem was on the membrane close to the denaturation zone (high temperature 95°C approx.).

In case the robustness of the membranes increases in order to withstand the elevated temperatures needed for the PCR reaction, the proposed design is excellent since it offers great flexibility in the number of cycles in a very small and compact footprint suitable for LoC and PoC applications. As an alternative, off-chip recirculation was tested. More specifically, we tried a 3T PCR protocol with off-chip pumping using a small volume peristaltic pump as shown in Fig. 78. No band was observed corresponding to the expected DNA product. Due to the off-chip pumping, the PCR sample outside the μ -device was cooled and reached quickly room temperature thus inhibiting PCR amplification; hence only primer and primer-dimer formations were observed. Exactly the same result was obtained with a conventional thermocycler where in between the extension and the denaturation steps cooling of the sample to room temperature was intentionally imposed. This finding verified the assumption of PCR inhibition due to the sample flow outside the μ -device.

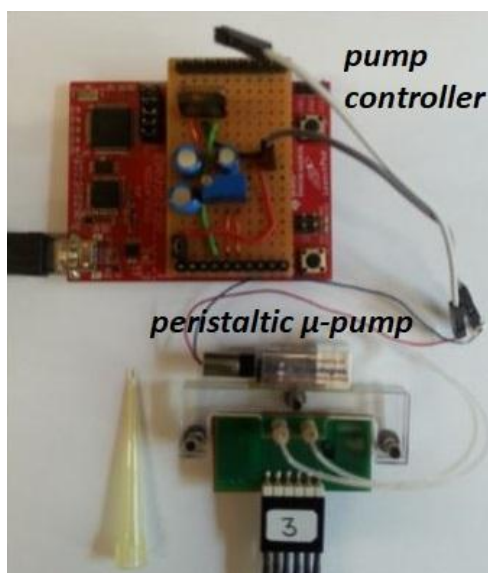


Figure 78 μ -PCR device operating with a peristaltic micropump from Jobst Technologies GmbH, Germany

6.3 Static μ -PCR

Due to the difficulties encountered with the recirculating devices, mentioned in the previous section, it was decided that the μ -devices should be tested in static mode. In static mode the sample is maintained stationary while the μ -heaters were driven by the temperature controlling unit adjust sequentially two temperatures in repeated cycles.

6.3.1 Static μ PCR on PCB

For simplicity, a 2-temperature (2T) PCR protocol –where the annealing and the extension steps are combined- was chosen for amplification of purified genomic *Salmonella* DNA. The 2T protocol was first tested with engraved μ -PCR devices (see Fig. 79a) prior treated with BSA and/or PEG to minimize the adsorption biomolecules which might lead to reduced efficiency. The total volume of such devices was 15 μ l approximately (channel width 0.3mm, depth 0.1mm, length 50 cm). The two temperatures used were 95°C (denaturation) and 62°C (annealing & extension). The residence time in each temperature was within the range from 5sec to 15sec. The total duration of the DNA amplification protocol was 35 minutes for 30 cycles. At the end of the thermal cycling, the sample was collected from which 10 μ l were loaded on agarose gel for evaluation of the efficiency via gel electrophoresis.

Short *Salmonella* DNA template (88bp, 8ng/ μ l and 0.8ng/ μ l) (Fig. 79b) and Genomic *Salmonella* (0.5ng/ μ l) (Fig. 79c) DNA was used as template. One pair of primer design based on the STM4497 gene was selected for the amplification of the 88 bp target gene fragment because of its high specificity, stability and good sensitivity. The target sequence, with a theoretical T_m value of 79.5 °C, was located at 4751059-4751146 of the genomic DNA of *S. Typhimurium* LT2. The set of the primers used in this experiments were for the forward primer 5'-TCCTTTTCCAGATT-ACGCAACAGATACT (28bp, T_m =65.7 °C) and for the reverse primer 5'-TTGGGTTCTGGA-TTTTGTATTATCCTGC (28bp, T_m =65.5 °C).

KAPA2G Fast ReadyMix (KapaBiosystems) kit was used according to supplier's instructions supplemented with 0.75 μ l of BSA (offering dynamic wall passivation to minimize biomolecule adsorption) and 0.75 μ l MgCl₂ for each 25 μ l reaction. Each primer was used at a final concentration of 10 μ M.

Fig. 79b, c show the amplification efficiency achieved for the above mentioned DNA template concentrations used in the PCR mixtures within the static μ -devices. The amplification efficiency of the μ device is 55% of that of the thermocycler (8ng/ μ l), whereas the amplification of 8ng of *Salmonella* DNA is 1.4 times higher compared to that of 0.8ng of *Salmonella* DNA (as it is obtained by comparison of the band intensity was performed with the ImageJ software).

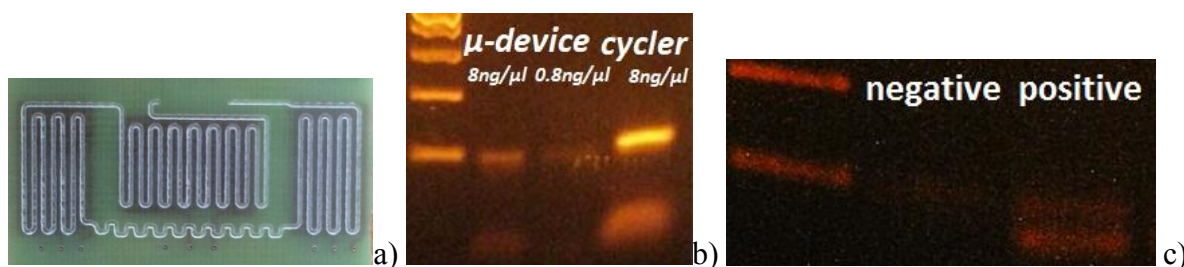


Figure 79 a) Engraved μ -PCR device used in 2T-PCR protocols, b) agarose gel electrophoresis products of on-chip amplification lane 1: DNA ladder, lane 2: on-chip amplification of 8ng short *Salmonella* DNA, lane 3: of 0.8ng, lane 4: thermocycler amplification of 8ng short *Salmonella* DNA, c) agarose gel electrophoresis products of on-chip amplification of negative sample and 0.5ng genomic *Salmonella* DNA

In order to further increase the amplification efficiency, we tried to employ more than 30 cycles. Due to the small volume of the SC DNA amplification μ devices and the sample evaporation at high temperatures, the volume collected after 40 or even 35 cycles was insufficient for gel electrophoresis.

6.3.2 Static PCR on PMMA/PCB

Due to the reduced amplification efficiency within the engraved μ -PCR device we decided to fabricate the μ -fluidic network in PMMA substrate and attach it on top of a PCB μ -heater with the aid of thermally conductive paint or tape in order to ensure excellent thermal conductivity.

Since PCR amplification efficiency heavily depends on the temperature uniformity, new improved PCB μ -heaters were designed. The new design was based on numerical calculation run by Dr. G. Kokkoris team (see 5.2.3)

The DNA amplification device μ -fluidic network (see Fig. 80) consisted of various (4-6) u-shaped chambers in order to perform multiple amplification reactions at a single run. The thickness of the PMMA substrate was 1mm. The width of the fluidics was 2mm and the depth varied from 0.3mm to 0.5mm. The total length of the fluidic channels was between 25-30mm thus leading to a total volume of 25 μ l approximately.

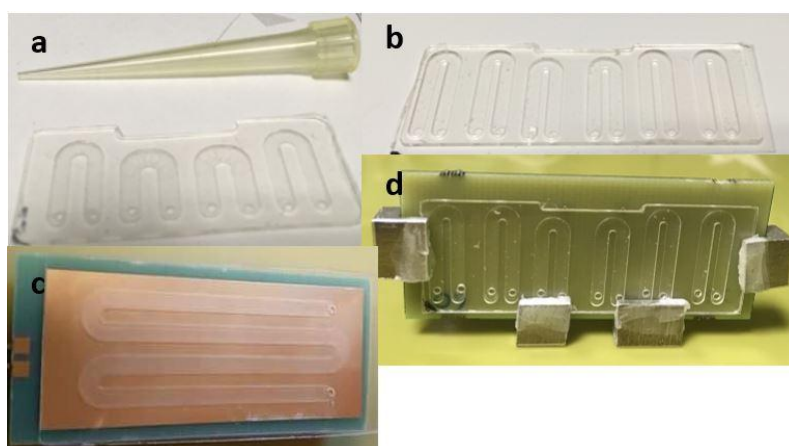


Figure 80 a) PMMA fluidic with 4 u-shaped chambers, b) PMMA fluidic with 6 u-shaped fluidics, c) PMMA fluidic on top of a thin PCB μ -heater with external Cu layer, d) PMMA fluidic attached to a thick PCB μ -heater

In order to further optimise the 2T PCR protocol we run several reactions on a conventional thermocycler to find the optimal temperatures for enhanced amplification efficiency. The DNA template used was purified genomic *Salmonella* DNA. Two set of experiments were performed i) gradient temperature for the denaturation step with temperatures ranging from 81°C to 100°C in steps of 3°C -5°C and constant temperature for the annealing/extension step set at 60°C and ii) constant temperature for the denaturation step set at 95°C and gradient temperature for the annealing extension step ranging from 50°C to 70°C. The duration of each step is 10sec and 30sec for the denaturation and annealing/extension steps respectively. The results obtained are illustrated in Fig. 81. The optimum temperatures for denaturation proved to be in the range of 88°C to 97°C offering an efficiency higher than 80%, whereas for the annealing/denaturation 50°C to 52°C and 60°C offered an efficiency higher than 90%. Apart from the temperature optimization another set of experiments was performed regarding the number of cycles to optimize the amplification efficiency. Five identical reactions were run for 20, 25, 30, 35, 40 cycles respectively as shown in Fig. 82. As expected the amplification efficiency increases with the number of cycles, reaching >80% for 30-40

cycles. Based on these results, we decided to perform the 2T-PCR at 90°C (denaturation) and 60°C (annealing/extension) for optimum T difference employing 40 cycles in order to have increased amplification efficiency. By applying this protocol, we obtain good specificity for the desired product although we lose some efficiency but it's not a significant compromise. Also by using 90°C for the denaturation step, we decrease the temperature difference thus the protocol becomes shorter.

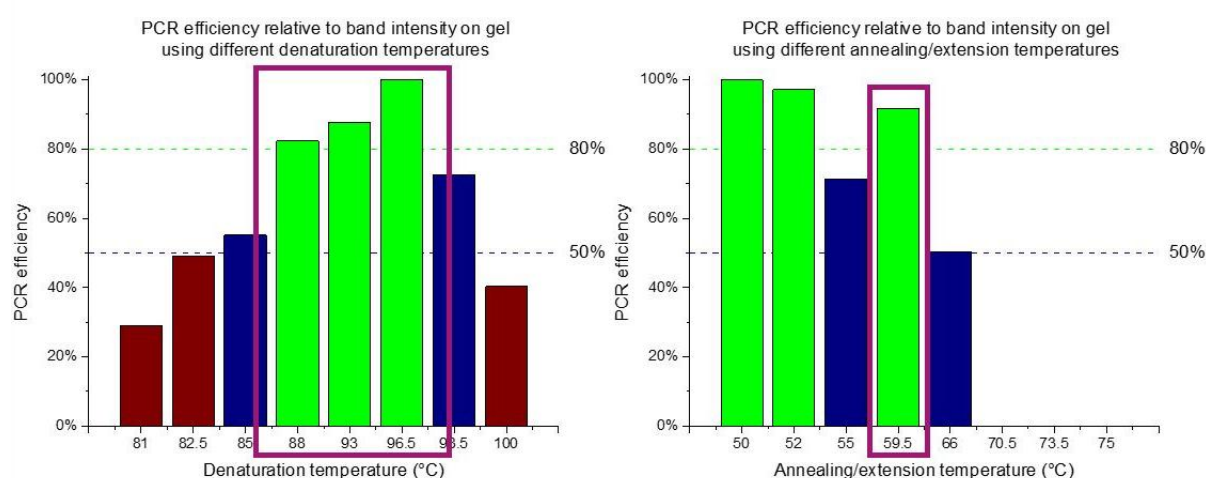


Figure 81 2T-PCR temperatures for optimal amplification efficiency

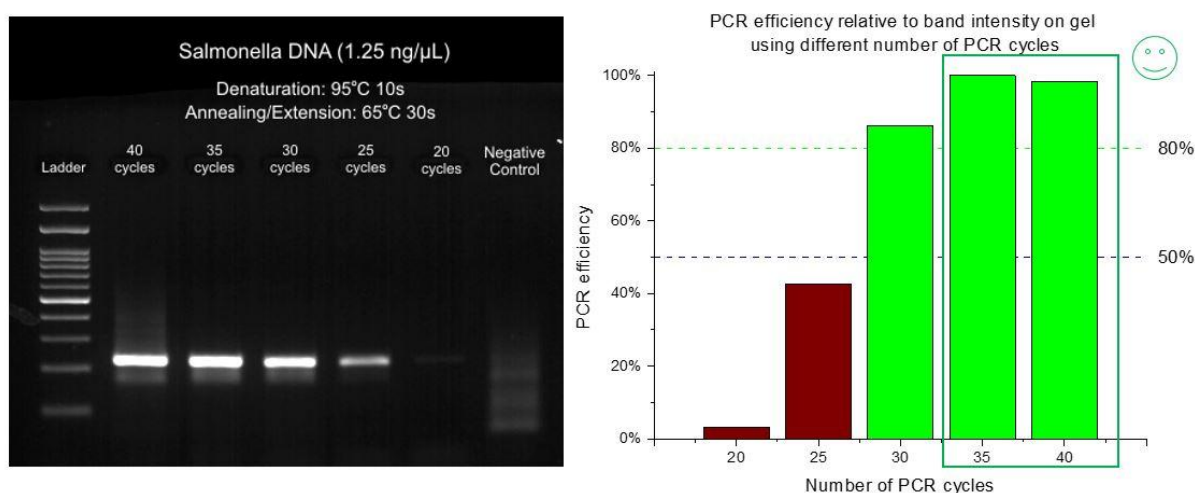


Figure 82 Number of 2T-PCR cycles vs. amplification efficiency

For a successful 2T PCR we had to investigate the ramping rates of the PCB μ -heaters. As an external reference for sensing the temperature we used a Pt resistance temperature detection

(RTD) element. Moreover, a custom-made PMMA chip holder was fabricated and used to enable the injection of fluids. Fig. 83 illustrates the set-up used while running DNA amplification experiment for measuring the actual temperatures with a newly designed heater bearing an external Cu layer for improved temperature uniformity. Below, various ramping protocols are presented (table 14) for the μ -devices.

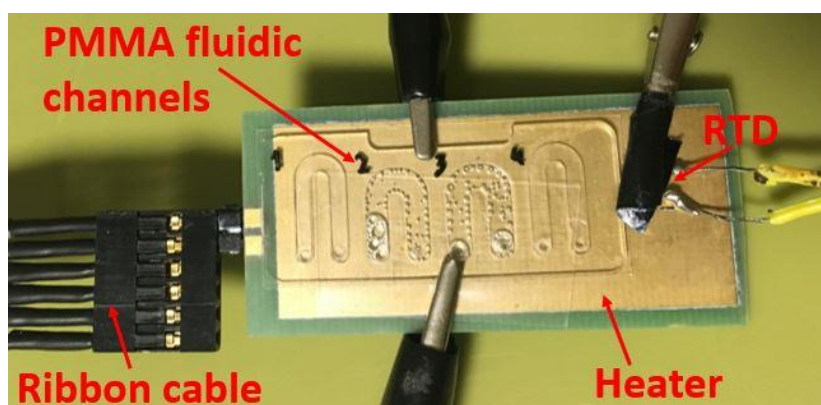


Figure 83 Experimental set-up for temperature measurements

Table 14 Protocols followed for 2T PCR. Setpoints and duration for each step and measured residence time

	Setpoint		Residence time	
	95°C	55°C	T>88°C	T<65°C
Test1 (w/o chip holder)	40s	60s	22s	32s
Test2 (w/o chip holder)	35s	50s	15s	15s
Test3 (w chip holder)	35s	55s	-	-
Test4 (w chip holder)	40s	80s	15s	15s

Through the data collected we measured the ramping rates both for heating and cooling thus concluding which ramping protocols are suited for 2T PCR. The tests were performed both with (w) and without (w/o) chip holder in order to study the effect of the PMMA chip holder (mass added) on the ramping rates. As described above the efficiency of the reaction remains sufficient in a range of temperatures for each step. The effective time (residence time at T> 88°C for denaturation step, and T<65°C for annealing/extension step) was estimated from

each graph for each step. Part of the data corresponding to several PCR cycles for the various ramping protocols is depicted in Fig. 84-87.

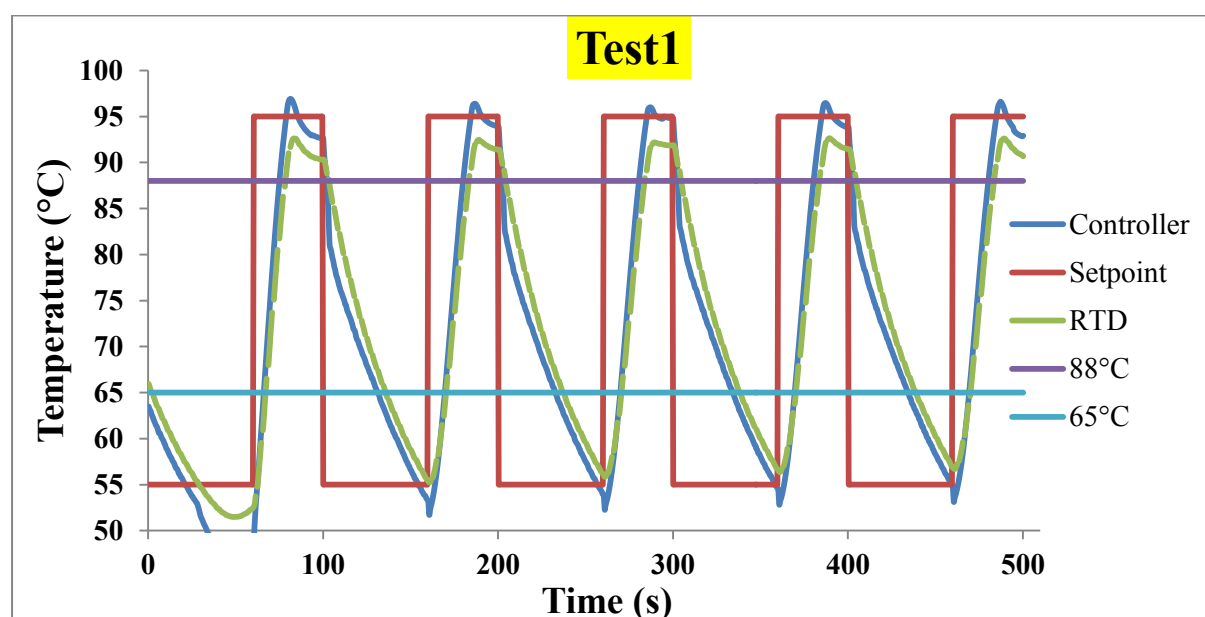


Figure 84 2T-PCR ramping protocol without chip holder (40s@95°C, 60s@55°C)

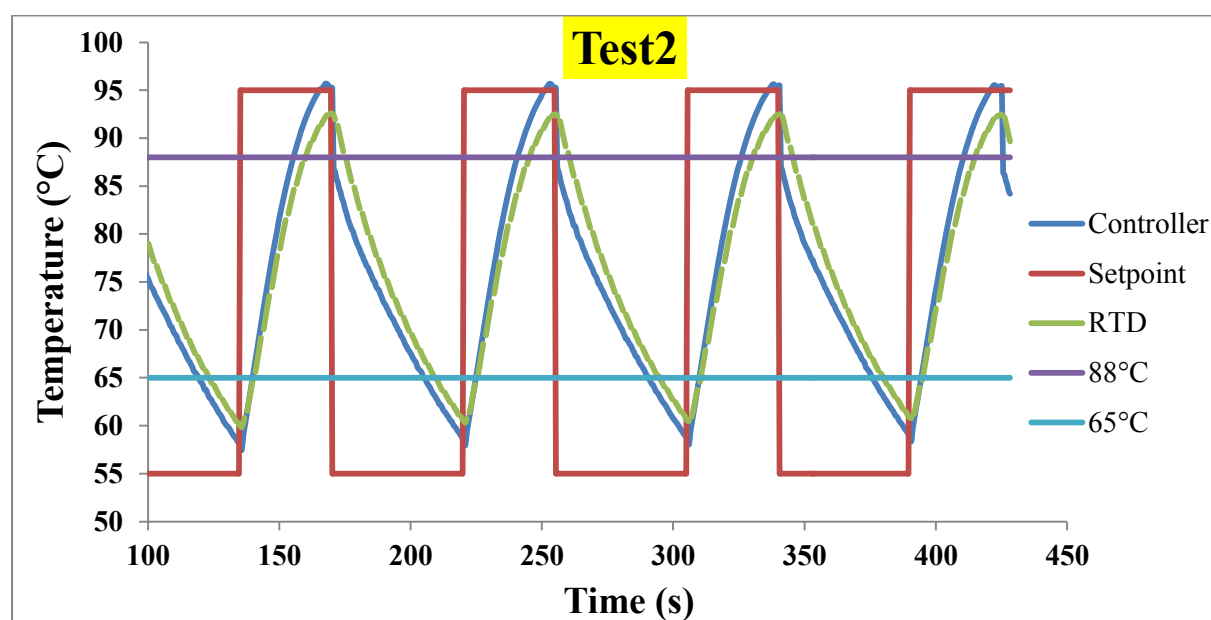


Figure 85 2T-PCR ramping protocol without chip holder (35s@95°C, 50s@55°C)

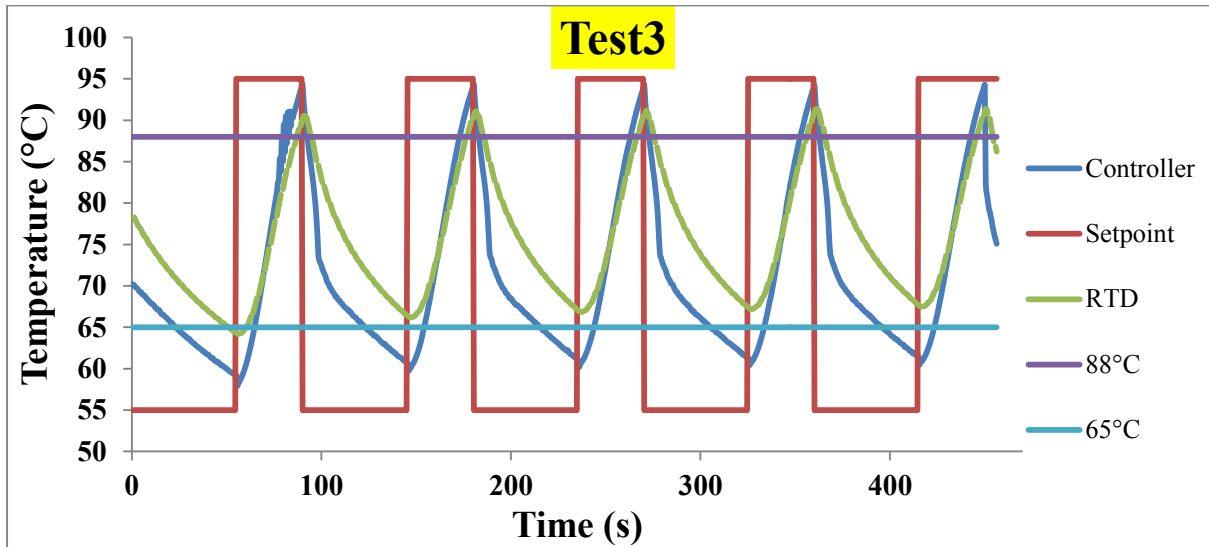


Figure 86 2T-PCR ramping protocol with chip holder (35s@95°C, 55s@55°C)

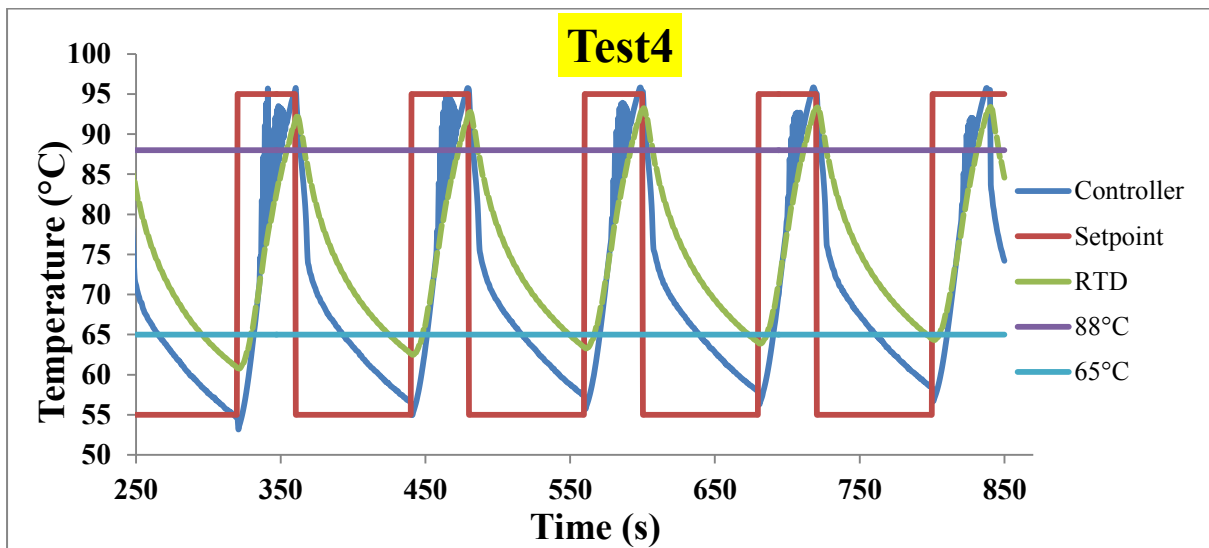


Figure 87 2T-PCR ramping protocol with chip holder (40s@95°C, 80s@55°C)

When the protocol of test 3 was applied, although the μ -device reached the desired temperature for denaturation, the time allocated for the low temperature was not enough. The lowest temperature reached was 67°C which is not a compatible temperature for the 2T PCR we have developed in order to have sufficient amplification. Thus in test4, the duration for each set-point step was increased to 40s and 80s respectively. From the 2 graphs shown in Fig. 86 and Fig. 87 above it is also evident that the whole system is heated as time passes by, which results in small changes in the duration of each step in each cycle.

From the various experiments we conducted, we found out that the whole system comes to equilibrium after the 10th cycle (when the device is exposed to ambient temperature, not enclosed in a ‘box’). Comparing the data obtained from the two sets of experiments (with and without chip holder) we concluded in the following heating and cooling rates presented on Table 15. The heating rate is 45% faster for the set up without the chip holder whereas the cooling rate is 22% faster. The total time for the whole protocol rises 41% when using a PMMA chip holder. Data from Test2 and Test 4 were used for the comparison of the durations since the residence time at each temperature is similar.

KAPA2G Fast ReadyMix (KapaBiosystems) kit was used according to supplier’s instructions. Two pairs of primer design were selected for the amplification of a 117bp and a 228bp target gene fragments because of its high specificity, stability and good sensitivity. The design was based on hilA-iagA gene of *Salmonella* ser Typhi strain Ty2 which can distinguish *Salmonella* species I from other enteric bacteria, including *E. coli*. The target sequence (of the 228bp) has a theoretical T_m value of 72.3 °C.

Table 15 Ramping rates for heating & cooling and duration of 2T-PCR protocols with and without chip holder

Rate	w/o chip holder	w chip holder	%
Heating	1.23°C/s	0.68°C/s	45
Cooling	0.58°C/s	0.45°C/s	22
Duration	3400s	4800s	41

The set of the primers producing the 228bp amplicon used in the experiments were for the forward primer 5'- CTGTTATTTCTGCGTGGATATTTCTTTAG (30bp, T_m=64.5 °C) and for the reverse primer 5'- TATTCAGCGTAAAGAAGATTAACAGCAATAAG (32bp, T_m=64.7°C). The set of the primers producing the 117bp amplicon used in the experiments were for the forward primer 5'- CAACACCTGCAGGATAATCCAATATTATTAAG (32bp, T_m=64.6°C) and for the reverse primer 5'- CTGTTATTTCTGCGTGGATATTTCTTTAG (30bp, T_m=64.4°C). Purified genomic *Salmonella* DNA was used as template. For each 25µl PCR reaction 1µl of DNA template (concentrations ranging from of 1.25ng/µl to 1.25*10⁻³ ng/µl) was added. Each primer was used at a final concentration of 10µM. The DNA

amplification protocol regarding the T-controller is 25s 90°C and 55s at 55°C. The total duration of the DNA amplification was less than 54min. The data log of this experiment was used to calculate the energy requirements (power consumption) of the static PCR protocol for the amplification μ device. Fig. 88 shows part (3 cycles) of the 2-T PCR protocol followed. The blue line corresponds to power consumption whereas the red line to the temperature profile. The energy consumption was calculated by integrating the power consumption given by the data log. The total energy consumption for DNA amplification (following the aforementioned T-protocol) was estimated at 3267 J (<82J per cycle).

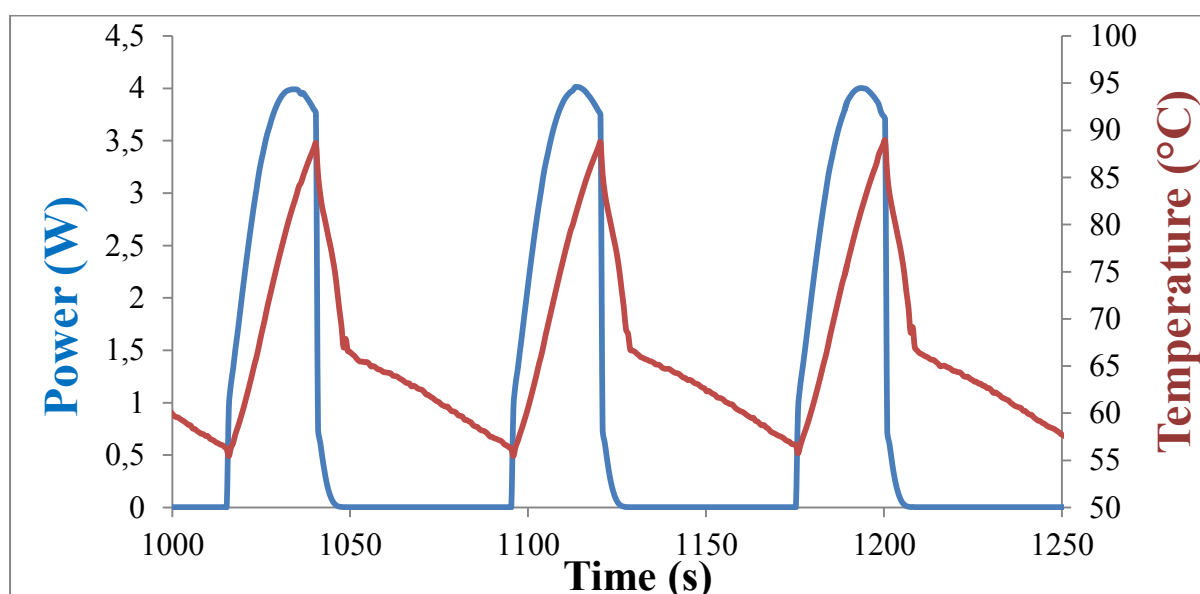


Figure 88 Graph representing the 3 cycles of the 2-T PCR protocol followed. The blue line corresponds to power consumption whereas the red line to the temperature profile

Fig. 89a) shows the agarose gel image comparing the product amplification achieved on chip with the conventional thermocycler. Four reactions were prepared, 2 for each set-up (positive samples, containing DNA and negative samples without DNA). The amplification efficiency within the chip is 90% of that achieved in the thermocycler. Fig. 89b) depicts agarose gel image of various concentrations of genomic DNA template used for on chip amplification. Four reactions with three different DNA concentrations ranging from 1.25 to 1.25×10^{-3} ng/ μ l and one negative sample were loaded in a four chamber PMMA fluidic chip and run simultaneously. The lowest DNA concentration amplified efficiently corresponds to 250 cells.

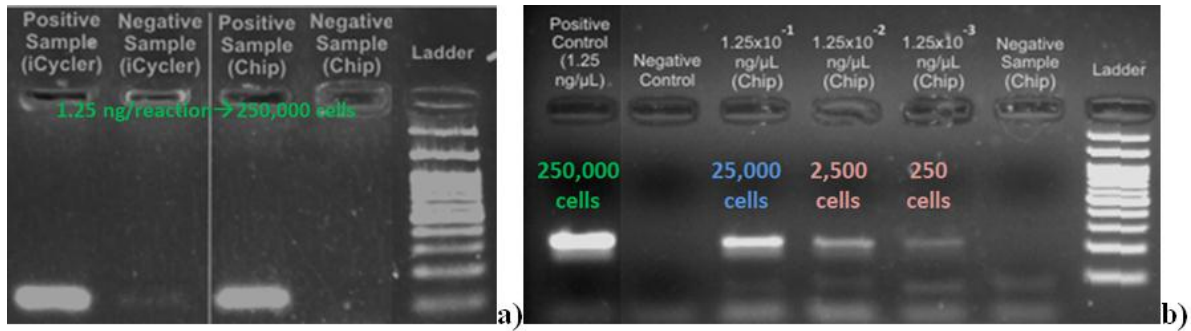


Figure 89 a) agarose gel image comparing the product amplification achieved on chip with the conventional thermocycler, b) agarose gel for various genomic *Salmonella* DNA concentrations

In Fig. 90 below cumulative results for the various PCR reactions performed within the static μ -PCR devices using different DNA template concentrations are presented. The intensities of each band were normalized to the band intensity corresponding to 250.000 cells for a reaction performed on a conventional benchtop thermocycler. The intensity of the bands decreases as the DNA template decreases (on-chip amplification).

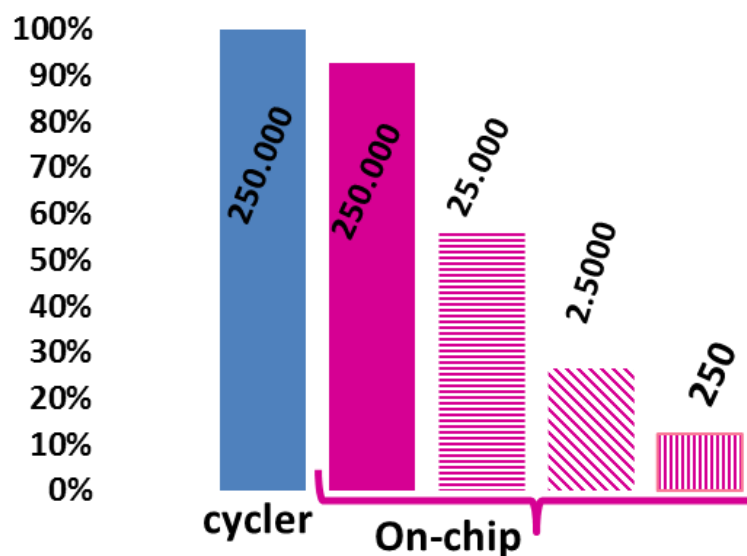


Figure 90 Intensity of bands normalised to the intensity of the band corresponding to 250.000 on the conventional thermocycler.

To sum up, excellent results were obtained with static PCR. Multiple samples were run simultaneously on PMMA fluidics attached to an improved PCB μ -heater with an external Cu layer offering great temperature uniformity which in turn led to better amplification efficiency. In order to improve the static μ -PCR devices, a fan is planned to be employed in

the set-up in order to shorten the duration of the thermal protocol (by increasing the dynamic cooling rate).

6.4 Fixed-loop, continuous flow μ -PCR device

In continuous flow (CF) μ PCR devices, unlike the static chamber, only the injected PCR mixture undergoes thermal cycling (smaller thermal inertia), as it flows across the distinct heated zones corresponding to (2 or 3) temperature steps needed for PCR. Following this approach, rapid NA amplification is achieved (between 120 s and 10 min) and thus the energy requirement is reduced [248], allowing for more energy-efficient devices amenable to portable PoC/PoN systems.

Herein a CF μ PCR device is designed, fabricated and validated for the amplification of 157 bp DNA fragments corresponding to the exon 20 of the BRCA1 gene. We propose the introduction of suitable materials, already established and employed in the PCB industry, nevertheless in a completely different role and application, for the robust sealing of microfluidic devices where both high temperatures (nearly 100 °C) are required and high pressures (in long microchannels) are developed during their operation. The proposed fabrication method includes the use of commercially available polyimide based materials both for sealing of the microdevice. These materials are routinely implemented in the PCB industry as a standard for electrical insulation and environmental protection of the copper structures on PCBs. The introduction of these materials in combination with the formation of embedded resistive microheaters within the PCB [171, 229] renders the herein described integrated microfluidic device for DNA amplification, based on PCR, perfectly suitable and easy to manufacture in large scale and low cost by PCB manufacturers, thus facilitating the commercialization of DNA-based bioanalytical microdevices (G.D. Kaprou *et al.*, Ultrafast, PCB manufacturable, continuous-flow microdevice for DNA amplification, Sensors and Actuators B, submitted)

Chip design

More specifically, a schematic of the (fixed-loop) CF μ PCR device comprising both a microfluidic network and embedded resistive microheaters is depicted in Fig. 91 and is

implemented on commercial PCB substrates. The chip design leverages our previous experience with DNA amplification microdevices regarding the thickness of the substrate, the distance of the microchannel from the microheaters and the spacing between the resistive microheaters in order to ensure good temperature uniformity, fast equilibration of the fluid temperature and low power consumption [52, 171]. The μ PCR device implements by design 30 thermal cycles in total (only a few are shown in magnification in Fig. 91) for the efficient amplification of DNA. Since each PCR cycle comprises three thermal steps in the implemented protocol, three discrete thermal zones are designed.

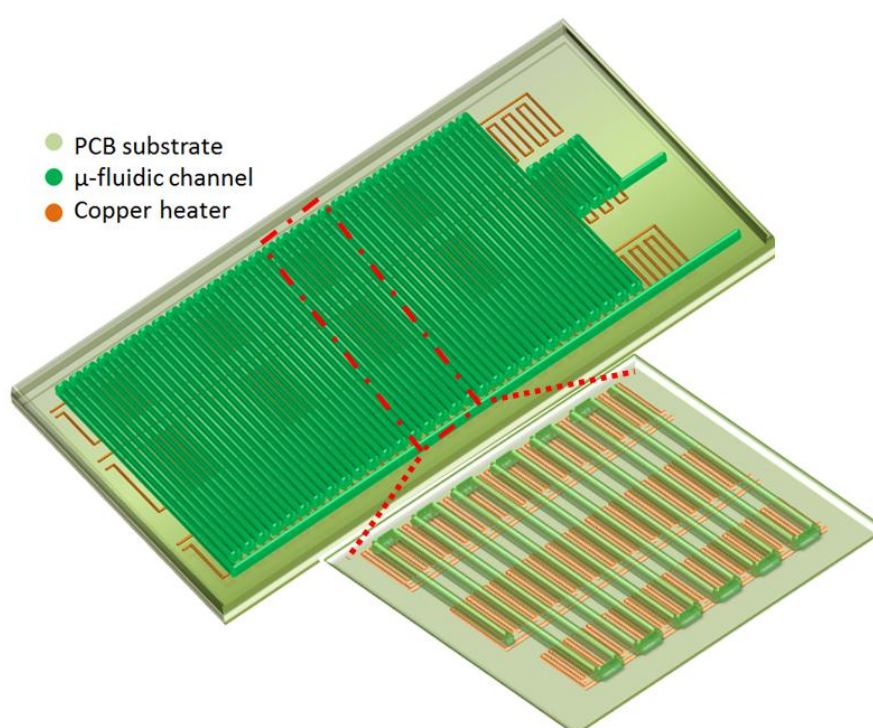


Figure 91 Schematic of a continuous flow μ -PCR device (green: μ -fluidic network, khaki: PCB substrate, orange: Cu μ -resistors)

Each thermal zone is defined by an individual resistive microheater (Fig. 92a), lying at a small distance beneath a part of the meandering microfluidic channel (Fig. 92c). The arclength of the channel above each thermal zone, namely denaturation, annealing, and extension was designed to be 12, 12, and 9.0 mm, respectively. The total length of the meandering microchannel is 1.9 m. As the PCR sample flows continuously across the three PCR temperature zones, it is thermocycled. In order to accommodate PCR protocols with extended residence time for the extension step compared to the denaturation and annealing steps, the channel width for the extension zone was designed double of that for the

denaturation/annealing zones (Fig. 92b), leading to PCR protocols with relative residence time ratios of 1:1:1.5 for denaturation:annealing:extension. Specifically, the channel width corresponding to the denaturation and annealing microfluidic network was designed at 300 μ m, whereas that of the extension at 600 μ m.

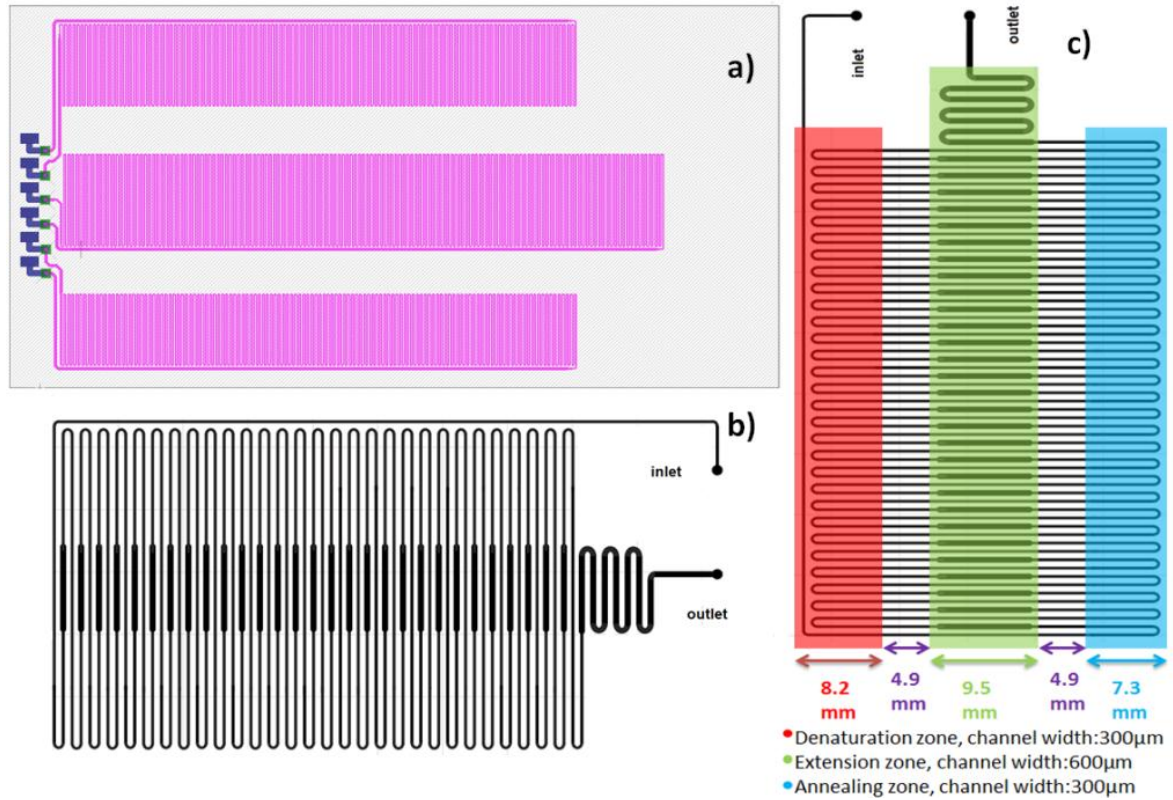


Figure 92 a) Design of the microheaters, b) design of the microfluidic mask, c) design of the μ PCR device comprising the microheaters and the microfluidic network

In addition to the prolonged residence time at the extension zone for each cycle, an extended microchannel at the denaturation zone before the 1st PCR cycle (to ensure the initial unfolding of the double helix of the DNA template), as well as at the extension zone after the 30th cycle (to ensure the final extension of the DNA amplicons) were employed for increased amplification efficiency. The embedded resistive microheaters were designed to be realized in the inner Cu layer (thickness of 18 μ m) of the commercially available PCB substrate. The total thickness of the PCB substrate used is 1.5mm. Copper tracks of 100 μ m in width and of the same spacing were designed in a dense meander in order to provide sufficient electrical resistance for rapid heating as well as to ensure sensitive and accurate temperature control. The total length of the Cu tracks for each heater corresponding to the denaturation, annealing and extension zone is 2.0, 1.9 and 2.4m respectively, yielding an electrical resistance of

approximately 44, 37 and 58 Ohm for the denaturation, annealing and extension microheaters, respectively. The microheaters were designed using Kicad, an open source software suite for electronic design automation (EDA). The designs were sent to a PCB manufacturer (Eurocircuits N.V., Belgium) for the realization of devices in large numbers (see chapter 5.4.1.).

Validation of PCR

Short human DNA template

For the biological evaluation of the fabricated μ PCR devices, a 250bp fragment from the exon 20 of the BRCA1 gene was used (see Fig. 93). For its amplification, a set of primers (Forward: 5'- TCC TGA TGG GTT GTG TTT GG-3' and Reverse: 5'-TGG TGG GGT GAG ATT TTT GTC-3') [249] are employed which produce a 158bp amplicon.

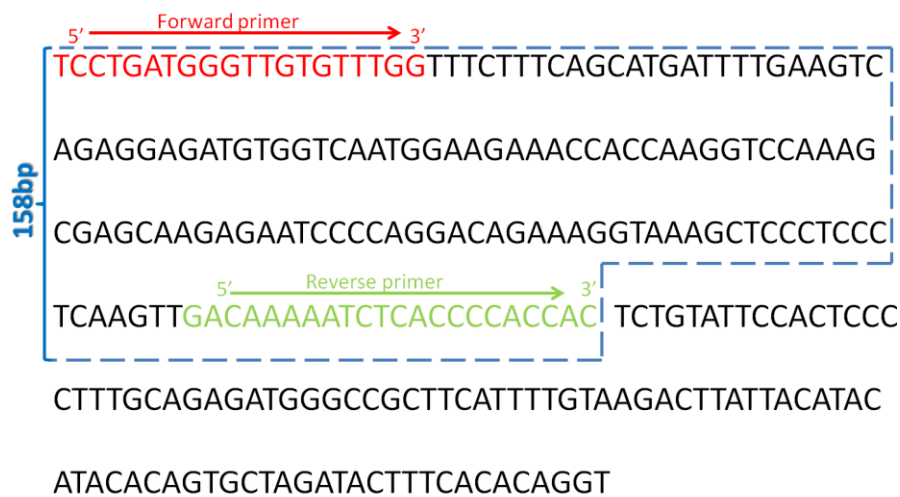


Figure 93 Sequence of the 250-bp DNA fragment from the exon 20 of the BRCA1 gene. Enclosed in the dashed blue lines, the 157bp amplicon is depicted. Forward primer is highlighted in red color whereas the reverse primer in green

PCR amplification was performed according to the manufacturer's instructions (KAPA Biosystems, KAPA 2G Fast Hot Start readymix). 5pmoles of each primer were mixed for short human DNA fragment with KAPA 2G Fast DNA polymerase (KAPABIOSYSTEMS) according to the manufacturer protocol. Each PCR reaction was supplemented with $MgCl_2$ and Bovine Serum Albumin (BSA) to a final concentration of 2.5 mM and 100 μ g/ml, respectively. To avoid adsorption of biological sample on microchannel walls during the actual μ PCR experiments, the blocking agent BSA was added to the μ PCR mixture. 1 μ l of

the short human DNA with a concentration of 0.55ng/ μ l was used per 30 μ l of reaction. 0.55ng of the DNA template correspond to 2×10^9 copies. The amplification protocol used with the conventional thermocycler consisted of 1 min initial denaturation at 95 °C, 30 cycles of 10" denaturation at 95 °C – 10" annealing at 55 °C – 10" extension at 72 °C and a final 1 min extension at 72 °C. PCR products were loaded on a 2% agarose gel stained with ethidium bromide and visualized with an ultraviolet (UV) transilluminator. The 2% agarose gel was prepared by mixing 2 g of agarose (SeaKem LE agarose, CAMBREX) in 100 ml of 0.5 \times TBE (10 \times TBE: 890 mM Tris, 890 mM Boric acid, 20 mM EDTA, pH at 25 °C: 8.0). The solution was heated for 3 min into a microwave and let it cool down. 10 μ l of EtBr (10,000 \times) were added and the gel was casted into the electrophoresis tray. 10 μ l of the collected flow-through amplified DNA were mixed with 6X DNA Loading Dye (Thermo Fischer Scientific Inc.) and loaded on the 2% agarose gel. This dye contains two different dyes (bromophenol blue and xylene cyanol FF) allowing for visual tracking of DNA migration during electrophoresis. Electrophoresis was performed using a Biorad power supply system for 30 min at 100 V. 5 μ l of a 100bp ladder (12 bands, 100-3000bp, 50 μ g, from Nippon Genetics) was used as a reference DNA marker.

μ PCR characterization

Each CF μ -PCR device before used in biological experiments it underwent various characterizations and tests (electrical, thermal, and robustness/sealing). A fabricated continuous flow μ PCR device is shown in Fig. 94, before its sealing for better viewing. The 30 PCR cycles are accommodated by the 30 meanders of the 1.9 m long microchannel and the three microheaters (corresponding to denaturation, annealing and extension) viewed beneath the microchannel as the dark brown zones of the PCB.

For the characterization of the resistive microheaters, their electrical resistance for various temperatures within the range 25-100°C were recorded (see section 5.6.1). As the absolute temperature values achieved on the resistive microheaters are essential for successful and highly efficient PCR reactions, the temperature was independently measured directly on the sealing layer of the device, which is the material in closest contact with the heated DNA sample. Thus, the absolute temperature of each of the three thermal zones above each resistive microheater was measured independently using an external platinum (Pt) thermometer. The absolute temperatures measured with the Pt thermometer were in excellent

agreement with the temperatures set on the resistive microheaters by means of the temperature controller (through the measured TCR value).

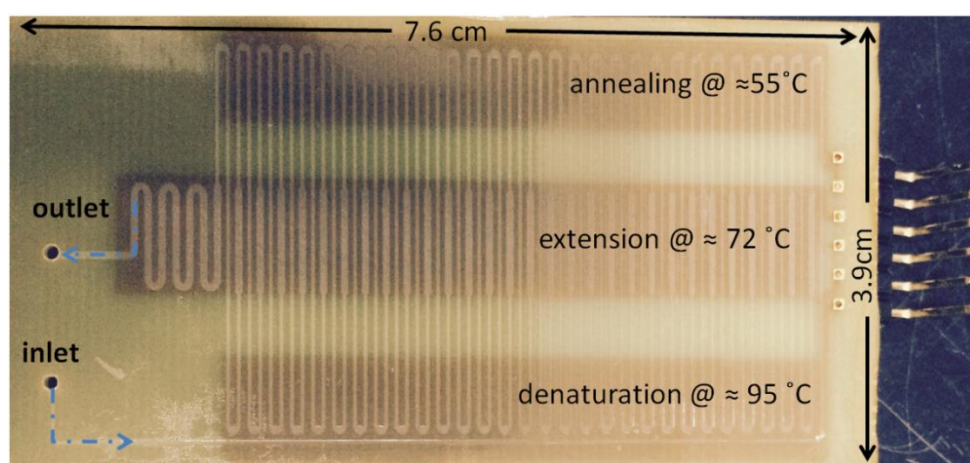


Figure 94 Image of a continuous flow μ PCR device (non-sealed for clearly viewing the microchannel), employing 30 cycles, fabricated on a PCB substrate with embedded microheaters.

Power consumption

Moreover, the characterization of the PCB microheaters was followed by the evaluation of their power consumption for achieving the desirable temperatures for denaturation (95 °C), annealing (55 °C), and extension (72 °C). This involved the use of the custom-made temperature controller unit which records the current, the voltage, and the resulting power consumption for each resistive microheater. For a μ PCR device with a set of PCB microheaters (R_{01} , R_{02} and R_{03}) equal to 44.2 Ohm, 57.2 Ohm and 37 Ohm respectively (R_0 measured at 25°C), the current, the voltage and thus the power consumption were recorded during device operation. Table 16 illustrates the results obtained for each heater after temperature stabilization at the desirable set points. Therefore, the total power consumption during operation of the μ PCR device is 2.7 W, comparable to the power consumption of energy efficient μ PCR devices [250]. The experimentally determined total power consumption is in good agreement with the one calculated (2.3W) through numerical calculations (data not shown) with a deviation less than 15%. This very low power consumption combined with the short total reaction time (as will be shown below) renders it a very efficient μ PCR device with respect to energy requirements (324 J when the microdevice uses a volumetric flow rate of 15 μ l/min).

Table 16 Power requirements of the microheaters for achieving PCR-relevant temperatures

Zone	R_0 (Ohm)	T_0 (°C)	T (°C)	Power (W)
denaturation	44.2	25	95	1.627
extension	57.2	25	72	0.792
annealing	37	25	55	0.246

Regarding the robustness tests, the continuous flow μ -PCR devices were tested under various conditions. In more details, with the aid of a custom made chip holder (enabling the interfacing between the microchannel and the pump), the μ PCR device was connected to a syringe pump and it was tested for flow rates ranging from 1-150 μ L/min, at room temperature, without observing any delamination of the sealing layer. The pressure drop across the microchannel at the flow rate of 100 μ L/min is higher than 12.4 bars, demonstrating that the sealed microdevices were capable of withstanding pressures higher than 12 bars at room temperature. The same tests were performed under elevated temperatures. In more detail, the heaters were set at 95 °C, 55 °C and 72 °C for the denaturation, annealing and extension zones, respectively and flow rates up to 100 μ L/min were used, without any delamination of the sealing layer. The fabricated devices proved to be robust and leak tight even after 1h of operation in these extreme (pressure and temperature) conditions.

Validation of PCR amplification efficiency

The evaluation of the amplification efficiency of the continuous flow μ -PCR device is presented in the following paragraphs. First, the temperature of the resistive microheaters was set to 95 °C, 55 °C and 72 °C for the denaturation, annealing and extension step, respectively. After temperature equilibration of the microheaters (evidenced through their resistance measurement), 30 μ L of reaction mix were introduced in the μ PCR device, flowing through the microchannel at 5 different volumetric flow rates: 2.5, 5, 7.5, 10, 15 and 20 μ L/min. Fig. 95 shows six agarose gel electrophoresis images depicting bands of DNA amplicons obtained at different flow rates. By comparing the bands of amplified products and the DNA ladder

(bands on the left of all images), we verify correct DNA amplification at 157 bp, at flow rates as high as 15 $\mu\text{l}/\text{min}$ (2 min total reaction time), while no amplification is observed at 20 $\mu\text{l}/\text{min}$. The results support successful DNA amplification in the fabricated devices with total amplification time (for 30 PCR cycles) 12, 6, 4, 3 and 2 min, respectively. These amplification times correspond to approximately 21.6, 10.8, 7.2, 5.4 and 3.6 s per PCR, cycle. Conventional benchtop thermocyclers are impossible to achieve such fast cycles, due to limitations in the temperature ramping rates. Typically, more than 30 min are required to perform a 30 cycle PCR reaction depending on the thermocycler's specifications. Indeed, when the same temperature protocol described above was used to perform a PCR reaction in a conventional thermocycler (iCycler™, BIO-RAD), with a residence time of 10 s in each zone/temperature (as recommended for the commercial kit), a 30 cycle PCR was completed in 45 min. The amplicon band intensity obtained with the thermocycler was 4.5% more intense than with the μPCR at a volumetric flow rate of 2.5 $\mu\text{l}/\text{min}$. Therefore, the DNA amplification efficiency of the μPCR (at 2.5 $\mu\text{l}/\text{min}$) is very comparable to that of the thermocycler, at a total reaction time reduced by a factor of 3.75.

Fig. 95 shows six agarose gel electrophoresis images depicting bands of DNA amplicons obtained at six different flow rates. By comparing the bands of amplified products and the DNA ladder (bands on the left of all images), we verify correct DNA amplification at 153 bp, even at flow rates as high as 15 $\mu\text{l}/\text{min}$ (2 min total reaction time). In the present microdevice, PCR reaction can be performed even 22 times faster (at 15 $\mu\text{l}/\text{min}$), nevertheless at the expense of amplification efficiency.

In addition, semi-quantified results can be obtained from the agarose gel images, analyzed by means of imageJ software. The intensity of each amplicon band obtained at different flow rates was normalized to the ladder 200 bp band intensity, and finally relative intensities were obtained with respect to the band intensity corresponding to 2.5 $\mu\text{l}/\text{min}$. The results are presented in Table 17. The results indicate a reduction of the band intensity with increase of the volumetric flow rate, due to reduction of the residence time of the DNA cocktail in each thermal zone. Despite the intensity reduction by almost an order of magnitude (to 19%) at the very high flow rates (15 $\mu\text{l}/\text{min}$), we demonstrate amplification of the DNA (signal above the noise level) at an impressive PCR duration of 2 min. In addition, by extrapolation of the band intensity to the background signal, we believe that DNA amplification is possible with a total duration as small as 96s in a similar μPCR device. This constitutes the CF μPCR device

reported herein one of the fastest ones reported so far in the literature (90 s [145]). Of paramount importance is the fact that this μ PCR is industrially manufacturable and thus can facilitate the way for standardization and commercialization of microfluidic devices implemented in molecular PoC diagnostics.







	$Q = 2.5 \mu\text{l/min}$ Total reaction time: 12 min		$Q = 10 \mu\text{l/min}$ Total reaction time: 3 min
	$Q = 5 \mu\text{l/min}$ Total reaction time: 6 min		$Q = 15 \mu\text{l/min}$ Total reaction time: 2 min
	$Q = 7.5 \mu\text{l/min}$ Total reaction time: 4 min		$Q = 20 \mu\text{l/min}$ Total reaction time: 1.5 min

Figure 95 Images of agarose gels depicting DNA ladder (on the left of each image) and 153 bp DNA amplicons (on the right of each image) from the μ PCR device, operating at different flow rates (2.5–15 $\mu\text{l/min}$). The negative signal (no DNA template in the cocktail) is also shown in one of the images. No amplification was observed with a flow rate of 20 $\mu\text{l/min}$ was used.

Table 17 Residence time in each zone, total PCR duration, 1-cycle duration of the PCR reaction and relative band intensity versus the volumetric flow rate through the μ PCR

Volumetric flow rate ($\mu\text{l/min}$)	Nominal residence time (s)			Total duration (min)	Cycle duration (s)	Band intensity
	Denaturation	Annealing	Extension			
2.5	4.7	4.7	8.9	12	21.6	100
5.0	2.4	2.4	3.6	6	10.8	57
7.5	1.6	1.6	2.6	4	7.2	43
10.0	1.2	1.2	1.8	3	5.4	29
15.0	0.8	0.8	1.2	2	3.6	19

Apart from the short human DNA template the CF μ PCR device was further validated with two different DNA templates.

The CF μ PCR device fabricated by means of lithography was used for the amplification of *Salmonella* genomic DNA. Prior to introducing the PCR cocktail, the microdevice was passivated with BSA 1% for 2h. To avoid adsorption of biological sample on microchannel walls during the actual μ PCR experiments, the blocking agent BSA was also added to the μ PCR mixture. PCR amplification was performed according to the manufacturer's instructions (KAPA Biosystems, KAPA 2G Fast Hot Start readymix). 10pmoles of each set of primers were mixed for plasmid and *Salmonella* DNA fragment respectively with KAPA 2G Fast DNA polymerase (KAPABIOSYSTEMS) according to the manufacturer protocol. Each PCR reaction was supplemented BSA to a final concentration of 2.5 mM and 100 μ g/ml. The amplification protocol used with the conventional thermocycler consisted of 1 min initial denaturation at 95 °C, 30 cycles of 10" denaturation at 95 °C – 10" annealing at 55 °C – 10" extension at 72 °C and a final 1 min extension at 72 °C. The validation of the PCR products was performed as described previously with gel electrophoresis.

Plasmid DNA template

The plasmid pBR322, which is a commonly used cloning vector in *E. coli* containing the genes for resistance to ampicillin and tetracycline, with a size of 4361 bp was used as a DNA template. For its amplification, two set of primers (Forward: 5' - CCA CCA AAC GTT TCG GCG AG-3' and Reverse 198: 5'-GCT GTC CCT GAT GGT CGT CA -3') and Reverse 395 5'-GCCGGCTTCCATTCAGGTCG -3') were employed which produce a 198bp and 395bp amplicon respectively. 1 μ l of the *Salmonella* genomic DNA with a concentration of 0.5ng/ μ l was used per 30 μ l of reaction. 0.23ng of the DNA template correspond to 1.1×10^8 copies. Each PCR reaction was supplemented with $MgCl_2$ and to a final concentration of 2.5 mM.

As shown in Fig.96 representing the gel image of the amplicons produced from the plasmid DNA template. Fig. 96 i) shows the products stemming from the PCR supplemented with one set of primers producing the amplicon of 198bp from the conventional thermocycler (A) and the μ PCR with a flow rate of 2 μ l/min (B,C). Fig. 96ii) shows the products stemming from the PCR supplemented with two set of primers from the μ PCR with a flow rate of 2 μ l/min (A,B),

and the conventional thermocycler (C). For each experiment two wells were loaded on the gel corresponding to two successive effluents collected from the μ PCR device. The use of the two sets of primers gave adequate amplification only for the shortest product (198 bp) (one band is observed) for the μ PCR device, whereas in the thermocycler both products were adequately amplified. The band intensity (198bp amplicon) corresponding to the μ PCR device is 2.7 times higher of that corresponding to the ladder. Compared to the thermocycler the intensity of the band corresponding to the μ PCR device is 40% less.

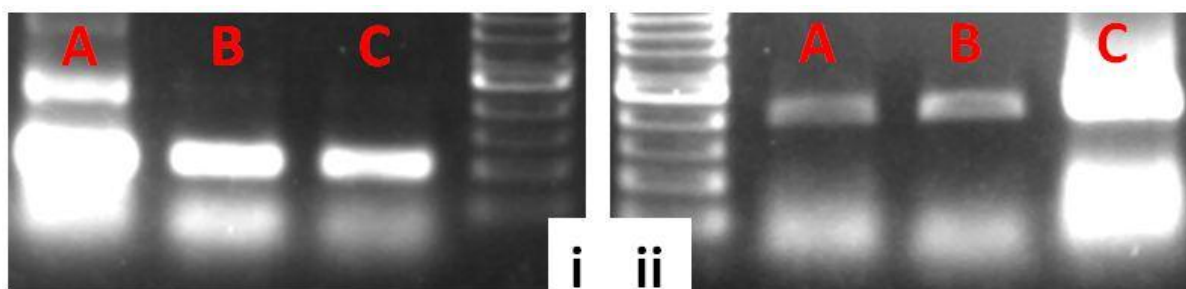


Figure 96 Gel image loaded with PCR products from Plasmid DNA i) supplemented with 1 set of primers, ii) supplemented with two set of primers

Salmonella genomic DNA template

For its amplification, a set of primers (ttrR F: 5'-GGATGATGATACGGCGGTC-3', ttrR R: 5'-CTTCCGCAATTTACGGTTC-3', $T_m=55^\circ\text{C}$ for both) were employed which produce a 455 bp amplicon. 1 μl of the *Salmonella* genomic DNA with a concentration of 0.23 ng/ μl was used per 30 μl of reaction. 0.23 ng of the DNA template correspond to 4.7×10^4 copies.

For *Salmonella* genomic DNA two volumetric flow rates were tested: 1 $\mu\text{l}/\text{min}$ and 3 $\mu\text{l}/\text{min}$. As shown in Fig. 97 representing the gel image of the amplicons loaded from the conventional thermocycler (A), the μ PCR with a flow rate of 1 $\mu\text{l}/\text{min}$ (B,C) and the μ PCR with a flow rate of 3 $\mu\text{l}/\text{min}$ (D,E). For each flow rate two wells were loaded on the gel corresponding to two successive effluents collected from the μ PCR device. The use of the higher volumetric flow rate gave no amplification (no band is observed) whereas, the lower volumetric flow rate gave adequate amplification. The band intensity corresponding to the μ PCR device is 85% of that corresponding to the ladder. Though compared to the thermocycler the intensity of the band corresponding to the μ PCR device is 5 times lower.

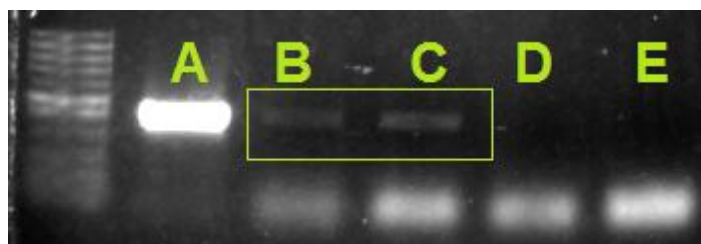


Figure 97 Gel image loaded with PCR products from *Salmonella* genomic DNA amplification

To sum up, in this section we present the design and fabrication of a fast, continuous-flow μ PCR device with integrated resistive heaters, all seamlessly realized on the same PCB substrate. The commercially available materials for the fabrication (patterning and sealing) of the proposed μ PCR chip are PCB compatible and already in use in industrial PCB manufacturing (but for different purposes), thus facilitating the mass production of our chip. The high integrability of microfluidics with other electronic components (such as sensors) offered by the PCB substrate, coupled with the potential of reliable and low cost mass production in the PCB industry, are the main advantages of the proposed chip, thus rendering it an outstanding component for LoC diagnostic systems. Furthermore, the extremely reduced total reaction times (down to 2 min) combined with the reduced power consumption during its operation (2.7 W) suggest that this chip is also suitable for implementation in low-resource settings. The μ PCR chip was validated in terms of real amplifications efficiency using three different DNA templates: short human, plasmid and genomic *Salmonella*. With the short DNA template volumetric flow rates of up to 15 μ l/min could be employed whereas with bigger DNA templates lower flow rates (1-2 μ l/min) gave efficient amplification (with plasmid DNA only one flow rate was used). In the last chapter there is a discussion on how we can improve the amplification efficiency of the μ PCR chip.

6.5 HDA μ -device

Apart from μ -PCR devices (both static and continuous flow), μ -devices for isothermal amplification methods were designed and fabricated. More specifically, low-cost devices for fast DNA amplification [229], focusing on HDA were developed. These devices were implemented in the detection of mutations related to breast cancer as well as *Salmonella* detection. Genetic analysis of mutations in BRCA1 gene that are associated with breast and ovarian cancer is routine in many molecular biology laboratories and most of the detection

methods employed are based on DNA amplification combined with fluorescent labels or gel electrophoresis.

The HDA μ -device consists of the microfluidic network where DNA amplification takes place and the resistive microheaters embedded on the commercially available and low cost PCB substrate. The microfluidic network is patterned by means of computer numerical control (CNC) micromilling (see 5.2.2) for high microchannel depths ($d > 100 \mu\text{m}$), or by UV photolithography of a thin dry photosensitive films (see patterning methods, chapter 4). A meandering microchannel with a total channel length of 65 cm crosses the thermal zone. The width of the meandering microchannel is $500 \mu\text{m}$, while its depth is $100 \mu\text{m}$, thus the microchannel volume is $35 \mu\text{l}$. The chip area is $5.5 \text{ cm} \times 2.5 \text{ cm}$ (Fig. 98b). A schematic inclined view of the device is depicted in Fig. 98a. In more detail, the device has one meandering microheater, embedded within the 1.5 mm -thick PCB, at a distance of $300 \mu\text{m}$ from the top side, where the microchannel was fabricated. The yield of fabricated devices reaches 95% after the patterning process, a percentage reduced to 80% after the sealing. In some cases, clogging of the fluidic network was observed in some areas due to the adhesive layer of the sealing film, thus rendering such devices non-functional. The successful final devices (a representative image is shown in Fig. 98c) have proven to be very reliable and robust, while at operation under elevated temperatures ($T > 95^\circ\text{C}$) and flow rates up to $20 \mu\text{l}/\text{min}$. The power consumption for this amplification microdevice 1.7 W resulting to a total energy consumption of 3060 J (for a 30 min protocol).

For the performance evaluation of the fabricated device, we employed the HDA amplification strategy to amplify a particular gene sequence, i.e., exon 20 of the BRCA1 gene that contains at least two positions where significant mutations occur. The HDA reactions were supplied with a set of primers (Forward: $5' \text{-TGA TGG GTT GTG TTT GGT TTC TTT CAG -3'}$ and Reverse: $5' \text{-ACC TTT CTG TCC TGG GAT TCT CTT GCT -3'}$) that produce a 113 bp fragment and a 157 bp PCR fragment containing the sequence of interest [249] used as template. $25 \mu\text{l}$ of an HDA isothermal amplification reaction prepared according to the manufacturer's instructions (Biohelix, IsoAmp® II Universal tHDA Kit) were loaded in the device and incubated for 15 min (BRCA1) at 65°C .

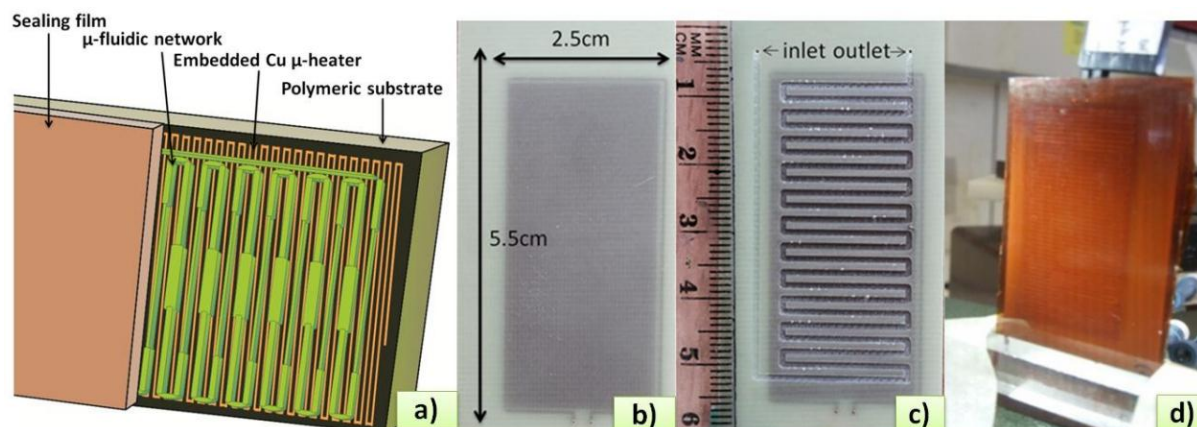


Figure 98 a) Schematic of an inclined view of the isothermal DNA amplification device, showing the discrete layers of the device, b) polymeric substrate with embedded Cu microheaters (before microfluidic patterning), c) fabricated device before sealing (meandering microfluidic network and meandering microheaters), d) fabricated device after sealing

A similar reaction was placed in a bench-top thermocycler under the same conditions. Fig.99 shows the amplified products derived from the microfluidic device and the thermocycler, for BRCA1. Both reactions were performed for 15 min with approximately similar amplification efficiency, as is indicated on Fig. 99.



Figure 99 Gel electrophoresis image depicting the 113 bp fragments amplified in a microfluidic device (lane 1) and in an eppendorf tube placed in a thermocycler (lane 2) using the HDA isothermal method

In addition, another evaluation was performed employing the microdevice with the HDA method using *Salmonella* genomic DNA in order to detect *Salmonella* strains stemming from a 500 bacteria culture after cell lysis and purification step. This is a common procedure used in food safety controls. A different set of primers was used in the second HDA reaction (Forward: 5'- TCCTTTTCCAGATTACGCAACAGATACT-3' and Reverse: 5'- TTGGGTTCTGGATTTTGTATTATCCTGC-3') producing an 88 bp amplicon characteristic of *Salmonella* bacteria. 25μl of an HDA isothermal amplification reaction prepared according to the manufacturer's instructions (Biohelix, IsoAmp® II Universal tHDA Kit) were loaded

in the device and incubated for 90 min at 65°C. In Fig. 100 the amplified products are depicted, which were received from the microdevice after the HDA amplification reaction of the genomic *Salmonella* DNA.



Figure 100 Gel electrophoresis image depicting the 100 bp ladder (lane 1) and the 88 bp fragments amplified in a microfluidic device (lane 2) using the HDA isothermal method

To sum up, in this section the design and fabrication of the HDA amplification microdevices is presented along with its use to efficiently amplify genomic *Salmonella* DNA and short human DNA within 30-90 min. The low power consumption (1.7 W) combined with the mass-amenable and PCB compatible fabrication method of the microdevice renders it a suitable candidate for LoC platforms.

6.6 RPA μ -device

Another ‘hot’ amplification method is RPA. RPA is an isothermal DNA amplification method which shows many advantages over other amplifications methods in terms of speed, portability, accessibility, sensitivity and specificity. Here we present a PCB microdevice for DNA amplification with the RPA method. *Salmonella* genomic DNA was sufficiently amplified with the RPA method at 37°C for 30min. The biochemistry of the technology relies on a combination of polymerases and DNA recombination/repair proteins, including recombinases. The resulting enzyme mixture is active at low temperature (optimum around 37°C) thus enabling the sequence specific recognition of template target sites by oligonucleotide primers, followed by strand-displacing DNA synthesis and thus exponential amplification of the target region within the template [251].

PMMA on PCB RPA microdevice

For RPA amplification method, new PMMA chips were fabricated like the ones depicted in Fig. 101. three meandering/ u-shaped channels were engraved on a 2mm thick PMMA

substrate. The inlets/outlets were drilled so that they are compatible with 100µl tips allowing for direct loading of the sample simply by using a pipette (Fig. 101a).

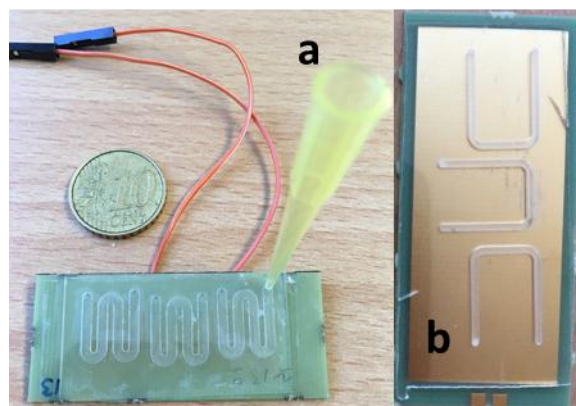


Figure 101 RPA μ-devices: a) 3 U-shaped channels on PMMA, b) 3 meandering channels on PMMA

On-chip DNA amplification using the RPA method was performed by injecting a premix of 48 µl of reagents (TwistAmp® Basic, Twist Dx) and 2µl of purified *Salmonella* DNA (0.5 ng/ul) according to supplier's instructions. The set of primers used was SF GGATCACTAAGCTGTGGATTACCTATTATC and SR CTGTTATTTCTGCGTGGATATTTCTTTAG (30bp each) yielding an amplicon of 195bp. Then in situ heating was performed at 37°C for 30 min using the integrated resistive microheaters. The power consumption of this amplification microdevice is 0.5W resulting to a total energy consumption of 900J (for a 30min protocol). Eventually, 50µl of the amplified product were collected. To analyse the effluents after on-chip DNA amplification, a purification step was implemented employing a clean-up kit (Nucleospin® gel and PCR Clean-up, Macherey-Nagel) and conventional agarose gel electrophoresis of the RPA products. In Fig. 102 lane 1 corresponds to 1ng of DNA /50 µl of reaction (corresponding to 2×10^5 cells).



Figure 102 Agarose gel electrophoresis of on-chip amplified RPA product from 1ng genomic *Salmonella* DNA

PCB-based RPA microdevice

The RPA reaction was also tested on a PCB device patterned with photosensitive dry resist like the one depicted in Fig 103a. Before loading the RPA sample, the interior of the device was passivated with 1% BSA solution to minimise the surface adsorption of biomolecules. The RPA premix was supplemented with 2µl of 1.25 ng/µl of purified *Salmonella* DNA. The set of primers used was the following SF3 GGATCACTAAGCTGTGGATTACCTATTATC (30bp) and SR5 TATTCAGCGTAAAGAAGATTAACAGCAATAAG (32bp) which yields a product of 228bp. The RPA reaction was performed for 1h at 39°C. End-point gel electrophoresis DNA detection was employed for the verification of the correct amplicon (Fig.103b)

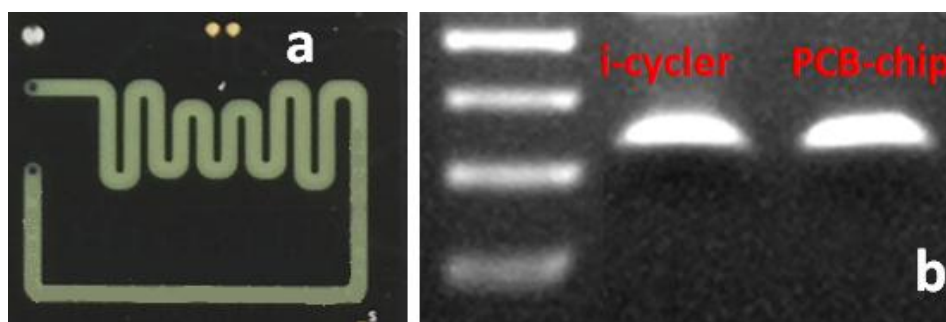


Figure 103 a) meandering PCB amplification device patterned by means of photolithography, b) Gel electrophoresis image depicting the 228 bp RPA amplification product for the conventional thermocycler (left) and the PCB device (right) performed at 39°C for 1h

To sum up, in this section the design and fabrication of the RPA amplification microdevices (PCB-based by means of lithography and PMMA on PCB by means of CNC machining) are presented along with their use to efficiently amplify genomic *Salmonella* DNA and short human DNA within 15-60 min. The low power consumption (0.5 W) combined with the mass-amenable and PCB compatible fabrication method of the RPA microdevices renders them suitable for LoC platforms.

6.7 LAMP µ-device

The last isothermal DNA amplification method used was LAMP. For Lamp amplification method, new devices were fabricated like the ones depicted in Fig. 104. Either three meandering channels with 1 mm width and 0.3 deep (Fig. 104a), or six 5mmx5mm square

type wells 1 mm deep (Fig. 104b) were engraved on a PCB substrate with embedded resistive μ -heaters to accommodate 6 reactions at a time. In addition, three meandering/ u-shaped channels were engraved on a 2 mm thick PMMA substrate (Fig. 104d).

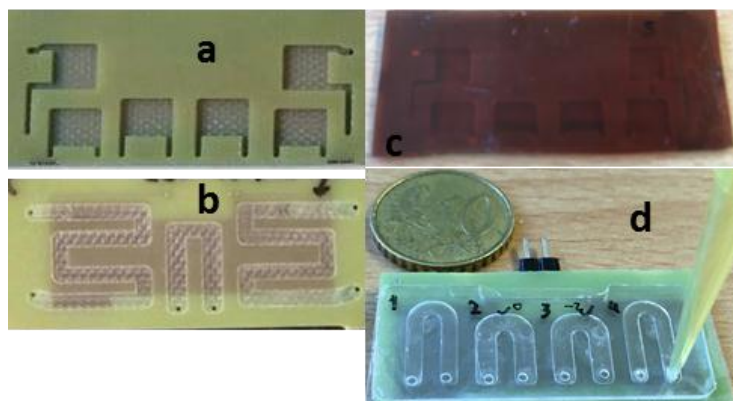


Figure 104 Figure Lamp μ -devices: a) 6 square-shaped wells on PCB substrate, b) 3 meandering engraved channels on PCB substrate, c) 6 square-shaped well device on PCB substrate sealed with kapton adhesive, d) 4 U-shaped channels on PMMA

For the performance evaluation of the fabricated devices, the *Salmonella* invasion gene *invA* was targeted by a set of six primers [252], two outer (F3 and B3), two inner (FIP and BIP) and two loop (Loop-F and Loop-B). F3: CGGCCCGATTTTCTCTGG, B3: CGGCAATAGCGTCA-CCTT, FIP: GCGCGGCATCCGCATCAATATGCCCGGTAAAC-AGATGAGT, BIP: GCGAACGGCGAAGCGTACTGTGCAC-CGTCAAAGGAAC, Loop-F: GGCCTTCAAATC-GGCATCAAT, Loop-B: GAAAGGGAAAGCCAGCTTTACG. The LAMP reagent mix in a total volume of 25 μ l [253] contained 12.5 μ l WarmStart 2x Master Mix (New England BioLabs), 1.8 μ M FIP and BIP, 0.1 μ M F3 and B3, 0.4 μ M Loop-F and Loop-B, and 1 μ l purified *Salmonella* DNA. The 25 μ l Lamp mixture was injected in the chip (using a pipette tip as shown in Fig. 104d) where isothermal DNA amplification was performed at $\sim 65^{\circ}\text{C}$ for 30 min.

PMMA on PCB amplification microdevice

First an engraved PMMA chip was tested with the LAMP method. LAMP products were analyzed using electrophoresis on a 2% agarose gel containing Ethidium bromide and visualized under UV light (see Fig. 105).

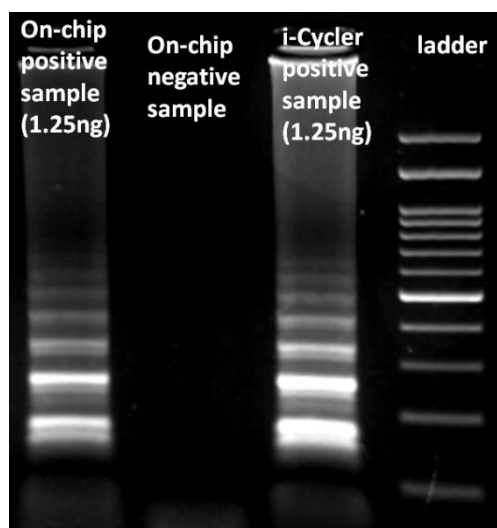


Figure 105 Comparison of LAMP products, lane 1: on-chip positive sample, lane 2: on-chip negative sample, lane 3: i-Cycler positive sample

Following, we tested LAMP efficiency for serial dilutions of the purified *Salmonella* DNA template. In Fig.106a we run simultaneously 4 LAMP reactions (25 μ l total volume) containing various amounts of the DNA template ranging from 1.25×10^{-1} ng to 1.25×10^{-4} ng. The amplification efficiency is excellent even with the lowest DNA concentration tested corresponding to 25 cells verifying the exceptional efficiency of LAMP reaction. More specifically, in Fig 106a, lanes L1, L2, L3 and L4 show the products corresponding to 25.000, 2500, 250 and 25 cells respectively (L5: ladder).

PCB amplification microdevice

Next we evaluated the performance of engraved PCB devices using the same LAMP mixture as mentioned above (see Fig 106b). The engraved channels/chambers on PCB did not show any DNA amplification when used. This is possibly attributed to adsorption of biomolecules thus inhibiting the amplification reaction. The core layer of PCB consists of interwoven glass fibers, hence when engraved channels/chambers are formed, the surfaces of the channels are not smooth [254]. In order to circumvent this issue, the engraved PCB channels/chambers were passivated in order to reduce the adsorption of biomolecules on the walls and surfaces. The same concept can also be used for the PMMA chips in order to have re-usable chips and avoid contamination.

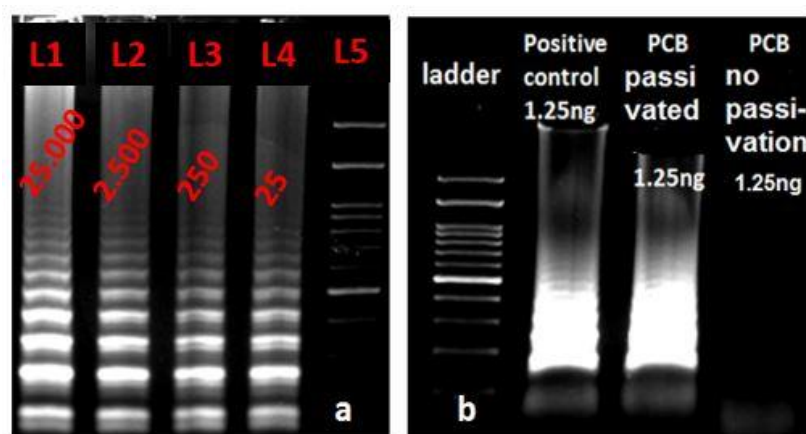


Figure 106 Gel electrophoresis images: a) Comparison of LAMP-on chip products of serial dilutions of *Salmonella* DNA template: lanes L1, L2, L3 and L4 show the products corresponding to 25.000, 2500, 250 and 25 cells respectively, b) LAMP products, lane 1: i-Cycler positive sample, lane 2: on-chip positive sample on passivated PCB, lane 3: on-chip positive sample on untreated PCB

Since LAMP method is a sensitive and rapid isothermal amplification method, we decided to employ it for the integrated LoC. In order to proceed gradually, first we investigated the efficiency of the LAMP with whole lysate instead of purified DNA. Given the fact that thermal lysis was not possible due to the instability of Bst polymerase at elevated temperatures, Triton X-100, a non-ionic detergent commonly used during DNA extraction, was employed for chemical lysis. After performing several tests, it was concluded that a final concentration of 0.004% Triton-X 100 within the LAMP cocktail was sufficient to lyse up to 10^5 cells within 10 min (cells can also be lysed outside the LAMP cocktail with 0.1% - 1% Triton within 5 min) [253].

In addition, in Fig.107 there is a comparison between the conventional i-Cycler and the PMMA chip. Both cell lysis and LAMP amplification took place. Within the chip 2 different final concentrations (0.04% & 0.004%) of Triton were tested. It is evident that there is a small decrease in the amplification efficiency when 0.004% Triton was used. This can be attributed to lower lysis efficiency which in turn affected the LAMP amplification efficiency (Fig. 107 lane 3 & 4). Various small changes in the protocol were also evaluated relative to the temperature and the duration of the LAMP reaction. When new/fresh reagents are employed the amplification efficiency is exceptional even when the reaction takes place for 20min at 63°C instead of 65°C.

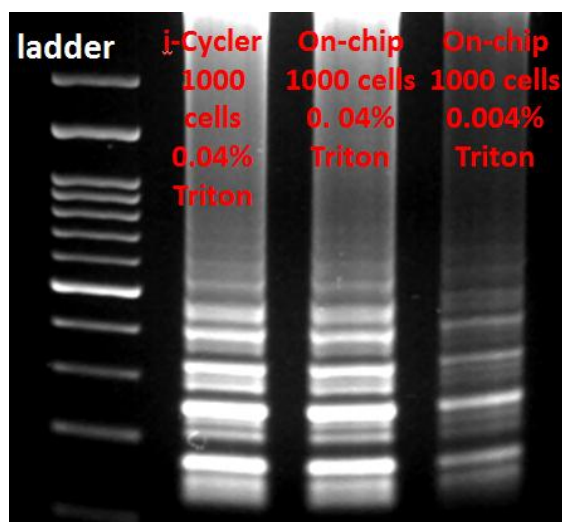


Figure 107 Gel electrophoresis image of DNA amplicons for 1000 cells using 0.04% Triton after 30 min of LAMP performed at 65°C within the i-Cycler (lane 2) for 1000 cells using 0.04% Triton after 30 min of LAMP performed at 65°C within the chip (lane 3), for 1000 cells using 0.004% Triton after 30 min of LAMP performed at 65°C within the chip (lane 4)

To sum up, in this section the design and fabrication of the LAMP amplification microdevices (PCB-based and PMMA on PCB both fabricated by means of CNC machining) are presented along with their use to efficiently amplify genomic *Salmonella* DNA and to perform in the same chamber chemical lysis followed by DNA amplification within 30min. The low power consumption (1.5 W) combined with the mass-amenable and PCB compatible fabrication method of the LAMP microdevices coupled with the extremely robust LAMP amplification method renders them suitable for LoC platforms even for analysing crude samples.

6.8 Conclusions

To sum up, in this chapter four different amplification methods were used for the evaluation of the amplification μ -devices. In more details, PCR method was used both in static chamber as well as in continuous flow μ -devices. As for the isothermal amplification methods, HDA, RPA and LAMP were used for the evaluation of the μ -devices in terms of amplification efficiency. In chapter 8, the integration of such amplification modules in LoCs will be presented for all the isothermal methods tested so far. Table 18 summarizes the DNA amplification microdevices used for efficient DNA amplification.

Table 18 DNA amplification microdevices designed, fabricated and evaluated for efficient DNA amplification

Microdevice	Amplification method	Duration (min)	DNA template	Power consumption (W)	Energy consumption (J)
Continuous flow	PCR	2	Short human (250bp)	2.7	324
Continuous flow	PCR	30	Plasmid (4361 bp)	2.7	4860
Continuous flow	PCR	30	<i>Salmonella</i> genomic	2.7	4860
Continuous flow Closed-Loop	PCR	30	N/A	1,3	2340
Static	PCR	53	<i>Salmonella</i> genomic	W(t)	3267
Static	RPA	15	<i>Salmonella</i> genomic	0.5	450
Static	HDA	30	<i>Salmonella</i> genomic	1.7	3060
Static	LAMP	20	<i>Salmonella</i> genomic & whole cells	1.5	1800

Chapter 7 QCM-D - Surface functionalization for selective DNA capturing

In this chapter surface functionalization agents are investigated in order to provide selective DNA capturing. A comparative study on the selective binding of amplified dsDNA from whole blood samples on functionalized surfaces employing a quartz crystal microbalance with dissipation (QCM-D) without employing any pre-treatment step such as DNA extraction and/or purification, in the presence of the lysed bacterial cells and in a hybridization-free assay is presented. The main outcome of this work on surface functionalization is the use of a blocking solution prior passing the sample over the sensing area which ‘passivates’ the surface and offers better discrimination between positive and negative samples.

7.1 Introduction

Molecular diagnostics have experienced an explosive growth due to the advancements both in molecular biology but also in fabrication technology. PoC testing is a relevant field where simple and portable systems enable diagnostic assays to be performed rapidly and cost-effectively by inexperienced personnel even at low-resource and remote areas at the point of need. NA analysis plays a crucial role in PoC testing, especially in applications such as infectious disease diagnosis. NA extraction, amplification and detection are typically the three primary steps involved in NA testing. Moreover, sample-to-answer concept is desirable in PoC testing platforms, in which NA amplification and detection is accomplished within complex matrices stemming from real crude samples, ideally in less than two steps preferably without pre/post treatment (i.e. purification). PoC testing is hugely facilitated not only by the advent/emergence of neoteric polymerase mutants for NA amplification but also by the microfluidics technology, thus allowing for sample-to answer results even from crude samples [255, 256]. Such results, mostly rely on optical (i.e. fluorescent) or visual detection by naked-eye (i.e. colorimetric, turbidity) [257] of the amplified products. Expensive and complex optical equipment such as lasers and fluorescent probes lacking sufficient sensitivity

frequently leading to false results are the major drawbacks of these methods. DNA acoustic sensor technology, implementing the quartz crystal microbalance with dissipation monitoring (QCM-D), came into light as a substitution to visual or optical detection implemented in PoC diagnostics [258, 259]. The QCM-D approach allows for the real-time detection of binding events (e.g. biomolecule immobilization) at solid/liquid interfaces by simultaneously recording changes in the mass -indicated by the frequency change (ΔF) and the viscoelastic properties of the sample indicated by the energy dissipation (ΔD). Furthermore, the acoustic ratio [dissipation versus frequency change ($\Delta D/\Delta F$)] has been shown to be indicative of the intrinsic viscosity of the immobilized molecules [260], thus providing information on their size, shape [261] and orientation (e.g. flat, protruding modes) [262]. QCM biosensors have been implemented in bacteria [263] and viruses [264] detection as well as in single nucleotide (SNP) [265] and genetically modified organisms (GMO) [266] detection. Recently, a QCM-based method relying on the measurement of the acoustic ratio for the direct detection of dsDNA amplicons without requiring post-PCR purification has been presented for the detection of plant pathogens [267] and breast cancer mutations [259] in pure samples.

In the present work, we investigate the dsDNA acoustic detection methodology in crude, complex samples. A major concern for sample-to-answer biosensors is non-specific macromolecules adsorption, especially in crude samples comprising mixtures of high protein and fat concentrations which in turn might result to potentially high background signal thus hampering the detection sensitivity [268, 269]. Herein, we employ various surface modifications to enhance the selective DNA capturing and minimize fouling from real-world media such as blood-based fluids on the gold surface of a QCM-D sensor.

The strategies implemented in this thesis for surface modification and protein passivation for selective DNA binding on QCM-D device (gold surface) after performing PCR in whole blood involve:

- 1) poly(L-lysine)-graft-poly(ethylene glycol) (PLL-g-PEG) which is a random graft co-polymer with a poly(L-lysine) backbone and poly(ethylene glycol) side-chains. The PLL backbone interacts electrostatically with the substrate since it is positively charged at $\text{pH} < 10$, while the PEG side-chains extend from the surface forming a densely packed polymeric brush. PLL acts as the attracting region for the amplicons whereas PEG (uncharged, hydrophilic) acts as a repellent for the proteins and other biomolecules [270, 271]. The aforementioned strategy was first

demonstrated for DNA detection stemming from whole *Salmonella* Typhimurium cells. The novelty of this concept is the label-free detection based on an acoustic device (QCM-D) and the obliteration of any purification steps prior to the acoustic detection even for complex, real-life samples [272].

2) Functionalization with an avidin-group (neutravidin/streptavidin) – in this case biotinylated primers will be used in order to be complimentary to the avidin group (formation of avidin-biotin complex)- so that the biotinylated amplicons will be attached on the surface. The advantage of NeutrAvidin Protein -which is an avidin derivative with carbohydrates removed- combining numerous key features to provide a biotin-binding protein with exceptionally low non-specific binding properties (compared to o avidin or streptavidin) [273]. The very high affinity of NeutrAvidin for biotin allows biotin-containing molecules (in our case biotinylated amplified DNA) in a complex mixture (PCR mixture using whole blood as DNA template) to specifically bind to avidin.

7.2 Experimental

Chemicals and reagents

Phosphate buffered saline (PBS, P4417) was purchased from Sigma. Whole blood (from healthy donor from the University Hospital of Heraklion) treated with EDTA -acting as an anticoagulant- was used as DNA template in the various PCR reactions. KAPA Blood PCR Kit from KAPABIOSYSTEMS was used to perform the PCR reactions. PLL(25)-g-PEG(2), Biotin PEG Biotin, MW 1000 and Biotin-PEG-NH₂, Biotin PEG amine, MW 20000 were purchased from Nanocs Inc (New York, USA). Streptavidin and NeutrAvidin® biotin-binding protein (A2667) were purchased from Invitrogen. Biotinylated primers and non-biotinylated ones were purchased from Metabion (Germany).

The set of primers employed for the production of the 524bp amplicon from exon 10 of the BRCA2 gene was the F524B: 5' -biotin-ccaccaccacacagaattctgtag-3' and R524: 5' -gcagcaaaccaatggcatac-3'. For the control PCR reactions, a set of primers for *Salmonella* targeting thrA (aspartokinase+homoserine dehydrogenase) house-keeping gene was used. The primer pair used for this gene is: thrAF-B 5'-biotin-GTCACGGTGATCGATCCGGT-3' and thrAR 5'-CACGATATTGATATTAGCCCCG-3'

Quartz crystal microbalance experimental setup and crystal preparation

The acoustic experiments demonstrated in the present work were performed employing the Q-Sense E4 instrument (QSense, Sweden) which includes four sensors that can be utilized in a parallel configuration. Prior to any QCM-D measurement, four gold sensors were plasma (atmospheric) cleaned for 2.50 min at high power using a Harrick Plasma Cleaner. The gold sensors were carefully transferred to the Q-Sense E4 instrument chambers. Each chamber was filled with buffer (BPS or Tris with pH 7.4 depending on the surface modification) with a peristaltic pump. In each experiment, 200 μ l of modification solution was loaded on the sensor under a constant flow of approximately 20 μ l/min followed by buffer rinsing. The PCR reactions loaded over the modification layer were diluted 10-fold in a final volume of 200 μ l. In some experiments, control PCR reactions (without DNA template) were added prior to the PCR sample under investigation. This step is mentioned as passivation throughout the text. Each addition on the sensor was followed by buffer rinsing.

PCR amplification protocol

PCR reactions were set up according to KAPABIOSYSTEMS protocol in a final volume of 25 μ l. 2.5 μ l of whole blood treated with EDTA (16.5ng of DNA approx.) was used as template. The amplification protocol consisted of 3 min initial denaturation at 95 °C, 35 cycles consisted of 30 s denaturation at 95°C, 30 s annealing at 55°C, 30 s extension at 72°C, and 3 min of extension at 72°C. 5 Each of the two primers was at final concentration of 0.2 μ M per 25 μ l reaction. The amplification products were then diluted 10-fold in buffer to a final volume of 200 μ l. The specificity of the PCR products was analyzed and verified by agarose gel electrophoresis.

Acoustic detection protocol

Surface functionalization was performed by injecting 200 μ l of each modification solution followed by buffer rinsing. The PCR reactions were subsequently loaded and rinsed with buffer. In some cases, we incorporated a blocking/passivation step before loading the PCR sample followed by buffer rinsing. The blocking/passivation buffer consists of the PCR reagents excluding primers but containing blood sample. Fig. 108 illustrates the process flow followed for the experiments.



Figure 108 Schematic of the steps followed for the detection of PCR products using whole blood as template sample. A constant flow rate of 20 $\mu\text{l}/\text{min}$ was used for all steps. The sensors can be re-used several times by cleaning the sensors surface by gentle rubbing with a cotton stick. Real time measurements of the amplitude and phase changes were recorded using an Agilent Network Analyzer.

QCM devices operating at 35 MHz were employed to measure the frequency (F) and the dissipation (D) of the wave in the course of the various surface binding events (i.e. the binding of the modification solution and the dsDNA). Acoustic ratio measurements are expressed as $\Delta D/\Delta F$, where ΔF corresponds to the frequency data divided by the overtone number (7th in our case).

7.3 Results and Discussion

In the present work we report for the first time the employment of PCR reactions using whole blood as template sample without any purification step to acquire acoustic measurements (both dissipation and frequency) for DNA-based diagnostic purposes.

In all cases, PCR reactions with whole blood used as DNA template sample (with the two different set of primers corresponding to the BRCA gene and thrA gene) were performed according to the protocol presented in the materials section. An indicative gel image of the PCR reaction performed in duplicates for a positive sample and a negative/control sample is depicted in Fig. 109.

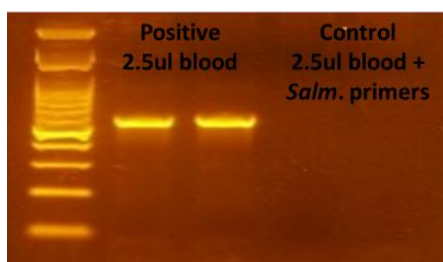


Figure 109 Gel electrophoresis image depicting the 524bp amplicons corresponding to the BRCA gene fragment

In the next paragraphs the results for all modifications regarding the dissipation, the frequency and the acoustic ratio for the positive samples (containing blood and the correct set of primers) and the negative (control samples containing blood but primers corresponding to Salmonella) are presented.

PLL-g-PEG surface functionalization

PLL-g-PEG surface modification with the positively charged PLL chain which is electrostatically bound to the negatively charged gold surface of the sensor and the PEG chains inhibiting the interaction of the proteins with the sensors surface was tested first. The ds DNA, which is negatively charged, it is electrostatically attracted to the PLL chain. Fig 110 shows the working principle of the proposed modification.

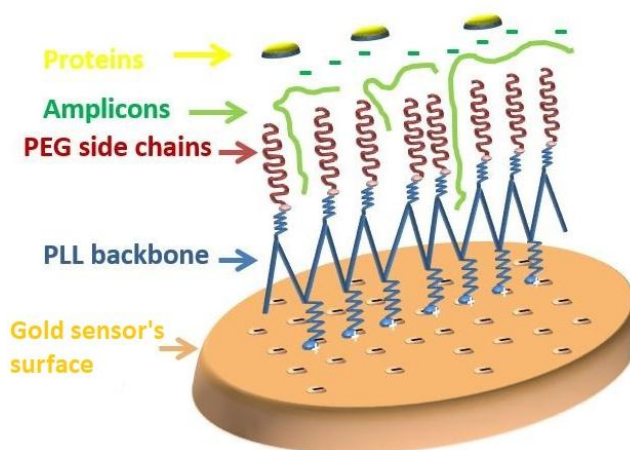


Figure 110 Working principle of the PLL-g-PEG surface modification, enabling the ds DNA to bind/interact with the sensors surface while repelling proteins

In Fig. 111, the results obtained (change in dissipation, frequency and the acoustic ratio) with the PLL-g-PEG (2.5 μ g/ml) modification are presented in bar charts. Although we expected the positive samples to give higher values compared to the negative ones, the results indicate the opposite. More specifically the change in dissipation is 1.5 times higher for the negative samples whereas the change in frequency is 1.2-fold higher. Though these differences are within the error, thus no conclusion could be drawn.

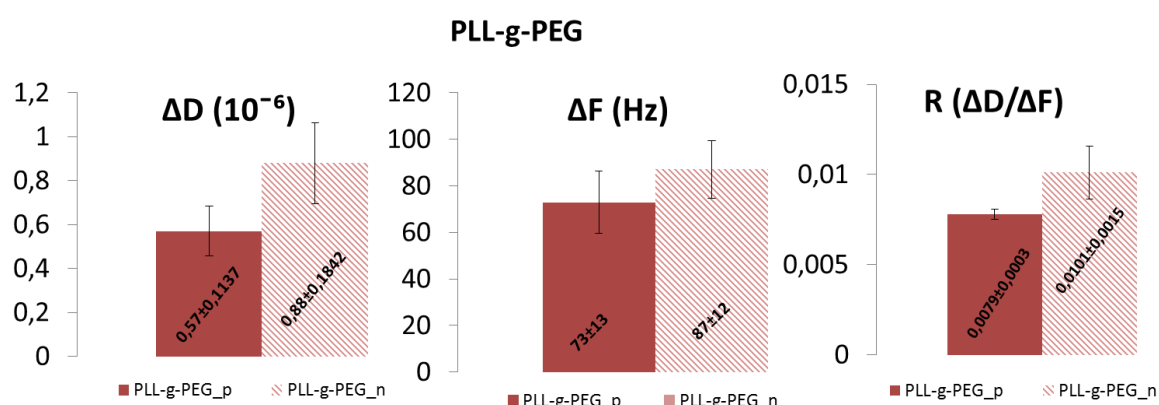


Figure 111 Bar charts showing the measured acoustic signal changes (D and F) and the acoustic ratio ($\Delta D/\Delta F$) caused by the PCR reactions. The bars with the solid colour filling represent the positive samples whereas the bars with the dashed filling represent the negative/control samples.

Avidin surface functionalization

Since the first surface modification relying on electrostatic interactions did not allow for conclusive results, we tried a different modification based on avidin-biotin interactions (as described in the introduction). The working principle followed for these modifications and the steps followed for the detection of the amplification products are illustrated in Fig. 112.

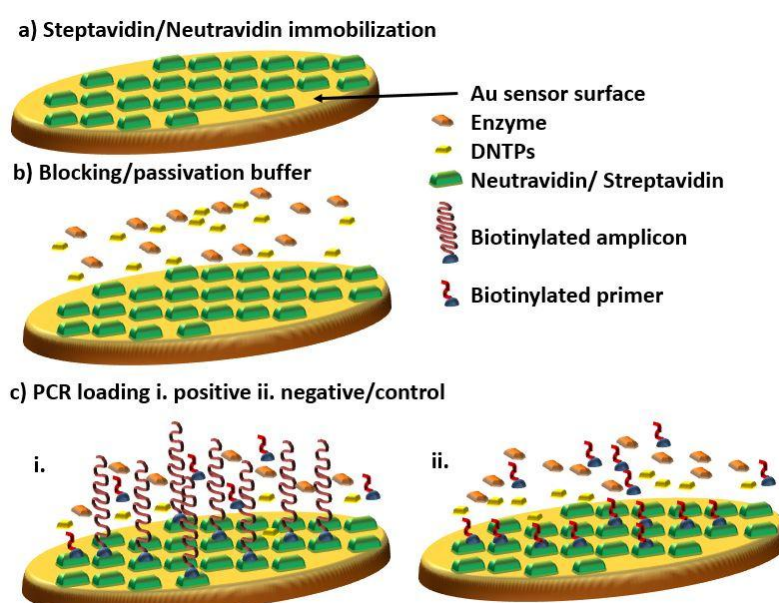


Figure 112 Schematic for the detection scheme followed to verify the presence of amplified DNA targets a) immobilization of streptavidin/neutravidin layer on the sensors surface. b) blocking/passivation buffer is loaded before the introduction of the PCR reactions. c) i. a positive

PCR reaction with ds biotinylated primers and ii. a negative amplification reaction with DNA template but containing biotinylated primers for another target is used as a control.

A typical response of the QCM sensor for the PCR reaction (positive left side and negative right side) is illustrated in Fig. 113. Real time monitoring provides data both for the Dissipation and the frequency changes upon each binding event on the sensors surface. The numbered dashed lines on the plots indicate the addition of a sample (the sample touches the sensing area). More specifically, 1) represents the loading of the modification buffer (in this case neutravidin) followed by PBS buffer rinsing. 2) Indicates the moment when the passivation/blocking buffer was added into the system followed by PBS buffer rinsing. The last step, 3) represents the addition of the PCR reaction followed by PBS buffer rinsing too. The yellow arrows indicate the time points at which we take the differences in order to calculate the frequency and the dissipation changes respectively. Both the frequency and dissipation changes are measured at equilibrium when the rinsing step is completed.

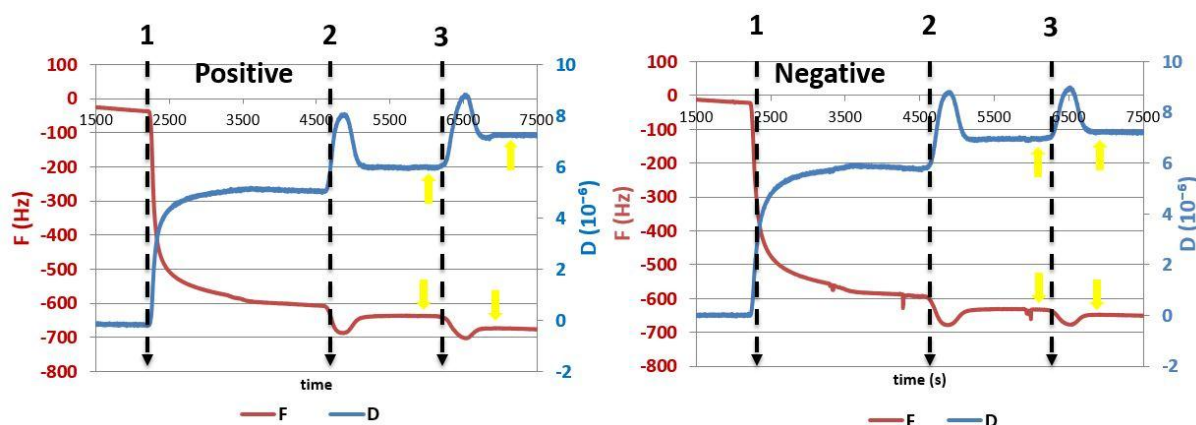


Figure 113 Real time plots of the three basic steps of the assay. (1) Modification solution (Neutravidin (200 $\mu\text{g/ml}$)/Streptavidin (20 $\mu\text{g/ml}$) is added in the sensing system with a flow rate of 20 $\mu\text{l/min}$ followed by rinsing (2) blocking/passivation buffer is added followed by buffer rinsing with a flow rate of 20 $\mu\text{l/min}$ (3) PCR reaction is added followed by buffer rinsing with a flow rate of 20 $\mu\text{l/min}$ leading to dissipation shift of 100 Hz approx. On the left panel results regarding the positive PCR are depicted; the right panel shows the results regarding a negative/control PCR (with blood template, but Salmonella primers) leading to a slight change of 20 Hz approx. in the dissipation signal. The frequency follows the same trend. Note that frequency data is divided by the harmonic number (7th harmonic used, i.e., $F/7$).

As for the streptavidin surface modification, we performed two sets of experiments. The first set is with no passivation/blocking prior to the introduction of the PCR sample and the second set includes the passivation/blocking with the buffer (described in the section of materials). The blocking buffer, which is a PCR reaction without template causes measurable

changes in both frequency and dissipation which can be attributed to the primer-dimers formation (PCR by-products) or the single stranded biotinylated primer present in the reaction. This blocking step enables to measure more precisely the changes on the surface due to the amplified products and minimize the effect of the other ingredients present within the PCR mixture.

The results are presented in bar charts in Fig.114. The blue colour represents the results obtained without blocking whereas the red colour represents the ones with blocking. The solid colour illustrates the positive samples whereas the dashed filling the control samples. Although both the change in dissipation and the frequency is higher for the positive samples in all cases, taking into account the error bars (representing the standard deviation of the measurements) there is an overlap for the experiments performed without blocking. On the other hand, the experiments with blocking give a clearer picture and thus a better discrimination between the positive and the control samples. More specifically, the change in dissipation (ΔD) is almost 7.5-fold higher and the change in frequency is more than 5.8-times higher for the positive samples compared to the control samples respectively. Regarding the acoustic ratio ($\Delta D/\Delta F$), the value corresponding to the positive sample is 1.6 times higher compared to the control.

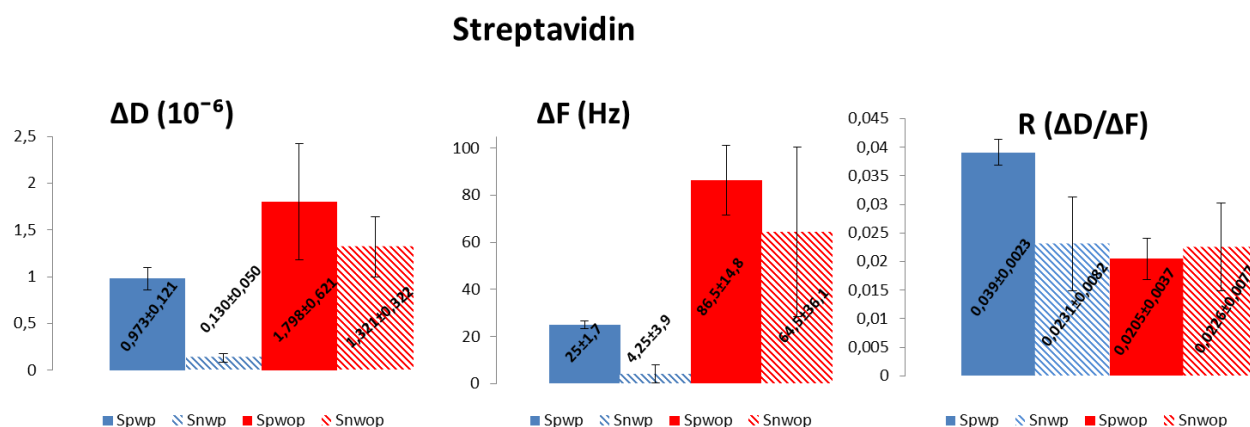


Figure 114 Bar charts showing the measured acoustic signal changes (D and F) and the acoustic ratio ($\Delta D/\Delta F$) caused by the PCR mixture in the QCM sensing system modified with streptavidin. Blue colour represents the experiment with the passivation/blocking (wp) step whereas the red colour without (wop). The solid filling represents the positive samples whereas the dashed one the negative/control samples.

Regarding the neutravidin surface modification, we performed three sets of experiments. The first set is with no passivation/blocking prior to the introduction of the PCR sample, the second set includes the passivation/blocking with the buffer (described in the section of materials) and the third one the use of ten-fold lower blood concentration (0.25 μ l instead of 2.5 μ l whole blood as template). The results are presented in bar charts in Fig. 115. The blue colour represents the results obtained with blocking and 2.5 μ l of whole blood per reaction, the red colour the ones with blocking but with 0.25 μ l whole blood per reaction and the purple colour represents the experiments without blocking while using 2.5 μ l of whole blood per reaction. The solid colour illustrates the positive samples whereas the dashed filling the control samples. Despite the fact that both the change in dissipation and the frequency is higher for the positive samples in all cases, bearing in mind the error bars (representing the standard deviation of the measurements) there is an overlaps for the experiments performed without blocking. On the contrary, the experiments with blocking allow for discrimination between the positive and the control samples. More specifically, the change in dissipation (ΔD) is 7-fold and 3.5-fold higher for 2.5 μ l and 0.25 μ l of template for the positive samples compared to the control samples respectively. As for the frequency change, it is 2-times and 5-times higher for 2.5 μ l and 0.25 μ l of template for the positive samples compared to the control samples respectively. Regarding the acoustic ratio ($\Delta D/\Delta F$), the value corresponding to the positive sample is 3.5 times higher compared to the control for the high blood concentration whereas the low concentration does not follow that trend. The ratio for the control samples give 1.5 times higher value compared to the positive ones.

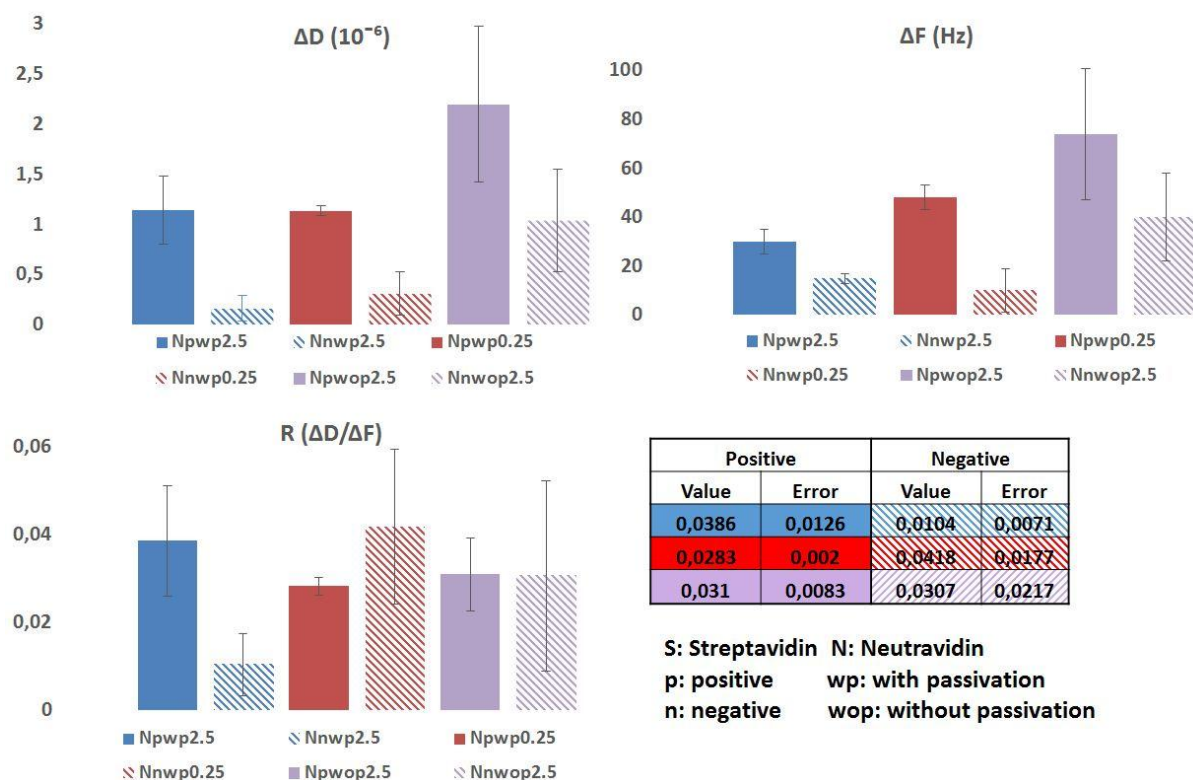


Figure 115 Bar charts showing the measured acoustic signal changes (D and F) and the acoustic ratio ($\Delta D/\Delta F$) caused by the PCR mixture in the QCM sensing system modified with streptavidin. Blue colour represents the experiment with the passivation/blocking (wp) step whereas the purple colour without (wop). Red colour represents the results obtained with the low template concentration of 0.25 μ l per reaction with passivation/blocking step. The solid filling represents the positive samples whereas the dashed one the negative/control samples.

7.4 Conclusions

The purpose of this work was to develop a simple method for rapid detection of unpurified PCR products from whole blood (used as template sample). This method consists of 2 steps (i. sample amplification and ii. acoustic detection) without any purification steps between them. In addition, another advantage of the proposed method is its reliance on a flow through system allowing for real-time monitoring of the surface binding events. The constant liquid flow used decreases also time required for the binding events taking place and thus the signal equilibration compared to static measurements [259].

The use of the blocking buffer improves the obtained results rendering the detection of the desired amplicons in an unpurified sample more efficient and accurate.

The simplicity of the proposed method makes the assay applicable to Lab-on-chip (LoC) applications. Ideally, microfluidics coupled with acoustic devices amenable to miniaturization is the way forward for the realization of LoC platforms. Contrary to the QCM devices which incorporate a large sensing area and thus requiring large sample volumes, SAW devices integrating various microfluidic channels could be extremely attractive for developing LoCs based on acoustic detection assays.

Apart from the three aforementioned surface modifications, we tried several others such as i. Biotin-PEG-Biotin, MW 1000 (in different concentrations) and ii. Biotin PEG amine (NH₂), MW 20000 (in different concentrations). Biotin functionalized polyethylene glycol (PEG-Biotin) is an avidin or streptavidin binding PEG derivative used to modify (biotinylate) material surfaces. In order to draw safe conclusions on these modifications, more experiments need to be performed.

Chapter 8 DNA amplification microdevices in integrated systems

As described in the scope of the present thesis, the ultimate goal is the integration of the developed DNA amplification microdevices in LoC platforms serving in foodborne pathogen detection and disease diagnosis. Towards this goal, numerous integration attempts took place. In this chapter, all these endeavors are described. The highlight of these endeavors is the development of a fast, automated and sensitive LoC platform for Salmonella detection within less than 6 hours based on SAW sensor, where all the pre-treatment steps (cell capturing, lysis and DNA amplification) are performed in a single chamber.

8.1 Introduction

Nucleic-acid-based technology plays a crucial role in accurate diagnosis, thus DNA amplification microdevices are an indispensable component of LoCs/PoCs diagnostics. Towards this goal we developed the microdevices described in the previous chapter. In order to move a step forward, these microdevices had to be integrated in LoC platforms performing more functions such as cell capturing, cell lysis, DNA purification and of course DNA detection. In this chapter all the integrated platform are described in detail. All three isothermal microdevices developed in the present thesis were integrated in LoC platforms and validated with real samples. First, the modular integration of the HDA microdevice with a SAW sensor is described. RPA microdevice was also integrated with cell capturing and lysis, DNA purification, SAW modules. The highlight of the present thesis is the development of an automated, fast and low-power consuming LoC for pathogen detection in dairy products. This platform performs cell capturing, lysis and DNA amplification in a single module and the detection is based on a SAW sensor employing a label-free scheme. The whole process – from sample to answer- is performed in less than 6 hours which is 4 times faster compared to conventional labor-intensive methods used so far. To my knowledge this is the first ever reported LoC platform employing SAW detection coupled with a pretreatment module for

cell capturing, lysis and DNA amplification on a single chip. The commercialization prospects of such a platform are really promising since it is an automated and portable platform for pathogen detection which can have a share in food, environmental and health industries.

8.2 Modular integration of the HDA μ device

Integration with SAW sensor

The results demonstrated in section 6.5 indicate that the developed HDA microdevice is appropriate for performing isothermal amplification of DNA and it is suitable for integration with additional elements such as acoustic sensors for the development of integrated platforms for DNA-based diagnostic applications. For example, a new concept for mutation screening and detection based on acoustic wave sensing was recently proposed [259]. The proposed concept can be realized on a LoC platform through integration of miniaturized acoustic devices (for the detection of mutated DNA) with low-cost microfluidic devices where DNA is first amplified and then digested through reaction with restriction enzymes [58, 59]. Towards this goal, a microfluidic device comprising a meandering microfluidic network (for HDA-based DNA amplification) combined with a split and merge efficient micromixer (SAM) [59] (for enzymatic digestion of DNA) was designed and fabricated via UV lithography as shown in Fig. 116.

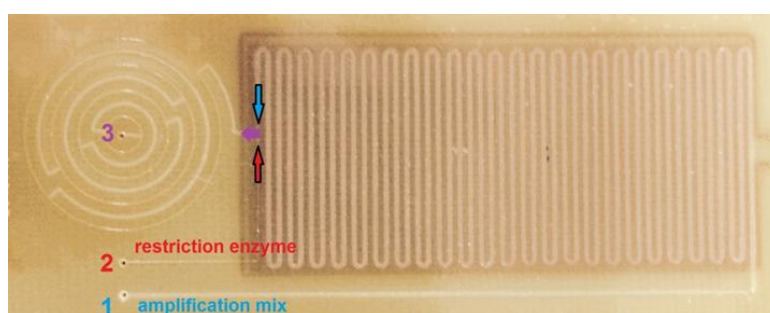


Figure 116 Integrated microfluidic device for DNA amplification and enzymatic digestion

The implementation and evaluation of this concept was realised through the heterogeneous integration of the μ HDA-mixing device with miniaturized acoustic devices as shown in Fig. 117. The heterogeneously integrated platform was used for the detection of DNA from

Mycoplasma. Mycoplasma is linked with several diseases such as the male urogenital tract infection causing male infertility and Mycoplasma pneumonia which is a contagious respiratory infection. The IsoAmp II Universal tHDA kit (Biohelix) and a set of two primers (designed by G. Papadakis) for the 16s rRNA gene of Mycoplasma -producing an 86 bp fragment- were used to perform the experiment and evaluate the platform. One of the two primers was biotinylated to allow binding on the surface of the acoustic device and thus detection. Although the results shown below (acquired by G. Papadakis) are from direct detection of the amplified product, the platform shown in Fig. 117 was used. The integrated microfluidic device allows, in addition to HDA amplification, the introduction of the restriction enzymes (through inlet No.2, Fig. 117) in the micromixer together with the amplified product. Successful hybrid integration of SAW sensor with DNA amplification microdevice using the HDA method is presented. The amplification efficiency between conventional equipment and the integrated platform is comparable.

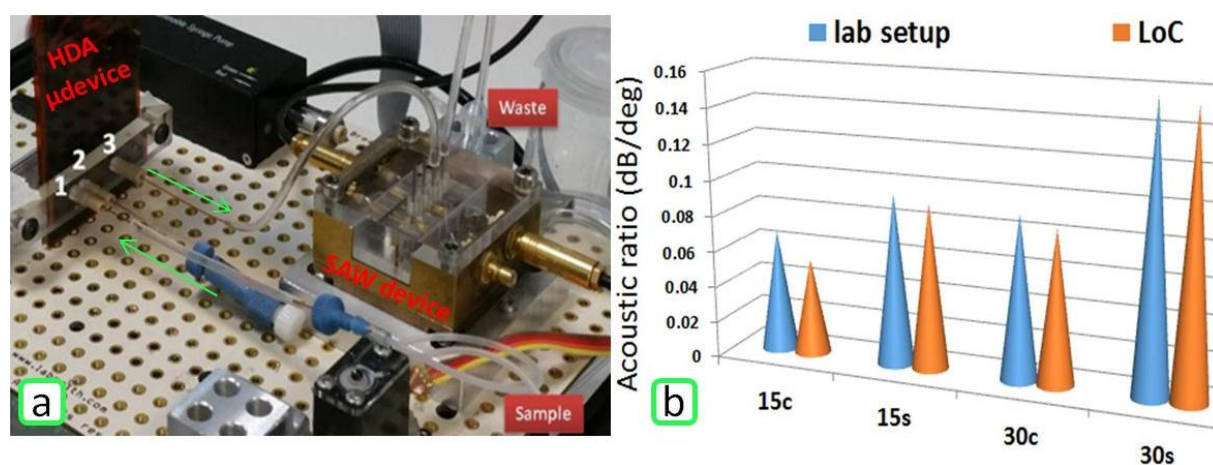


Figure 117 a) Picture of the LoC Green arrows show the direction of liquid flow. The microfluidic device shown has three ports. Port 1 is the inlet to the μ HDA. Port 2 is the inlet for the restriction enzyme, which merges with the outlet of the μ HDA at the entrance of the SAM micro-mixer (see also Fig. 97). Port 2 is closed in this case. Port 3 is the exit from the micro-mixer. The sample starting position and the exit from the acoustic sensor (waste) are also shown labelled in red, b) Graph presenting the comparison of the acoustic ration indicative of the amplification efficiency within the integrated platform and conventional thermocycler. 15c and 30c are the control reactions for 15 and 30 min respectively. 15s and 30s are the samples containing DNA template.

Integration with cell capture, lysis and DNA purification modules: Sample preparation platform

A similar integration strategy can be applied for a LoC platform addressing food related concerns for in situ detection of harmful pathogens such as Salmonella, thus enabling and ameliorating public safety and health.

The modular integrated LoC platform presented herein includes two microfluidic chips on a PMMA substrate and one microfluidic chip on PCB substrate, as presented in Fig. 118. The first two chips comprise the bacteria capture, lysis and DNA purification modules as follows: The first chip (Fig 118 a, i) is a cell capture (developed by Dr. Katerina Tsougeni) and lysis microfluidic chip. Cell capture takes place on immobilized antibodies on oxygen plasma nanotextured polymeric substrates [274]. Due to the high surface area achieved in these innovative chips, a capture efficiency of almost 100% was obtained for concentrations below 10^5 cells/ml. Cell lysis was performed at $\sim 94^\circ\text{C}$ for 13 min, using a PCB-based microheater (described in section 4.1.1) that was attached to the chip allowing for on-chip heating and consequent cell lysis (see Fig. 119b). The second chip (see Fig. 119a, ii) is a DNA purification microfluidic device (developed by Dr. A. Kastania) for removing impurities, which could inhibit DNA amplification or DNA detection. The purification microfluidic chip is designed as a micromixer [58, 275] fabricated via microfabrication processes on polymeric substrate (PMMA) and is plasma micro-nanotextured so that it contains both high surface and high density of -COOH groups on the chip surface. Successful on-chip purification was performed for Salmonella DNA originating from lysed cells that corresponded to <5 cells.

The third chip (amplification module) is a low-cost and fast DNA amplification device for isothermal HDA [171], as described in section 6.5. The proposed device is fabricated by mass production amenable technologies on PCB substrates by means of Computer Numerical Control (CNC) machining. The inner copper layers of the PCB substrate facilitate the incorporation of on-chip resistive microheaters (described in section 5.4.1), necessary for DNA amplification. The overall dimensions of the PCB substrate are 5.5 cm x 2.5 cm. A meandering microchannel with 500 μm width, 100 μm depth and a total channel length of 60 cm crosses the heated zone. The total volume of the CNC-machined device is 30 μl (Fig 118c). In the present design, a single layer of copper with a thickness of 18 μm was used resulting to a resistance value of 30 Ohms for the microheater. The copper layers on the PCB

serve as structural material of the microheaters in order to define the thermal zone needed to achieve both thermal cell lysis and DNA amplification, while they also act as temperature sensors aiding the temperature control during heat-aided reactions.

In Table 19, the protocol steps regarding the validation of the integrated sample preparation LoC are presented. The total operation time starting from loading the sample into the chip until the collection of the amplified DNA is approximately 87 min. Fig. 119 illustrates a schematic of pumps and valves connected to integrated sample preparation LoC described above.

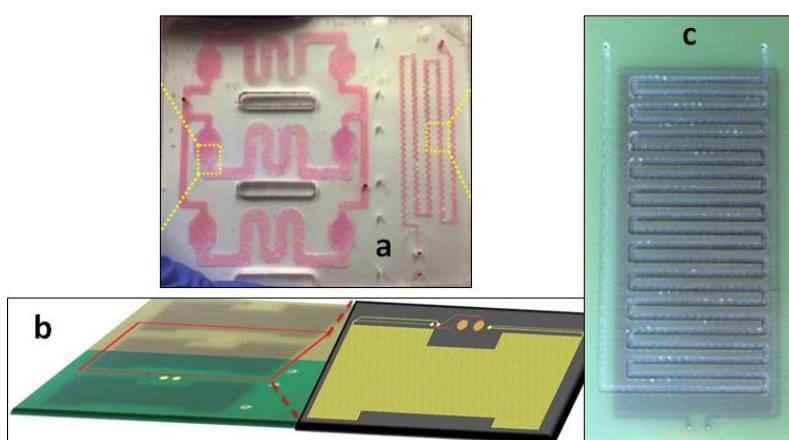


Figure 118 a) Optical image of the cell capture, thermal lysis and DNA purification PMMA module on top of a PCB substrate with 3 embedded heaters, b) design of the PCB microheaters with respect to the cell capture / lysis chip, c) DNA amplification device (μ HDA) with meandering microchannels fabricated by means of CNC

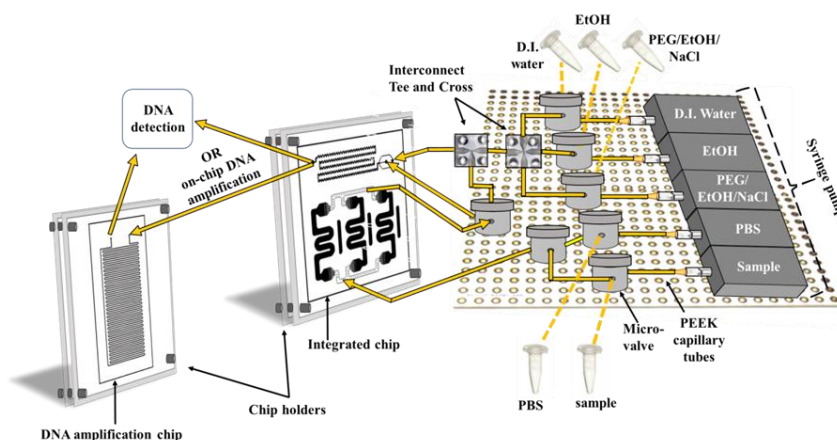


Figure 119 Schematic of pumps and valves connected to integrated sample preparation LoC.

Table 19 Operational protocol of integrated HDA-based lab-on-chip platform

Step	Volume (μ l)	Flow (μ l/min)	Duration (min)	Module
1. Cell capture	100	10	10	Capture / thermal lysis
2. PBS washing	60	10	6	Capture / thermal lysis
3. Cell lysis at 94° C	-	Static	13	Capture / thermal lysis
4. Heating off, wait for $T=T_{\text{room}}$	-	Static	6	Capture / thermal lysis
5. PBS washing	30 (waste) 50 (lysate)	10	5	Capture / thermal lysis
6. Passivation (PEG/EtOH/NaCl)	5	10 per inlet	0.25	Purification
7. DNA capture/purification	50 (lysate) + 50 (PEG/ethanol/NaCl)	10 per inlet	5	Purification
8. Ethanol washing	40-60	20	3	Purification
9. Water elution (DNA collection)	20 (waste) 2*50 (eluted DNA)	20	5	Purification

10. DNA amplification: reagents injection	10 DNA + 20 HDA reagents	20	1.75	DNA amplification
11. Incubation with heating T=65°C	30	static	30	DNA amplification
12. PBS washing	50	20	2.5	DNA amplification

First the evaluation of the bacteria capture, thermal lysis and DNA purification took place using artificially spiked milk with *Salmonella* via off-chip PCR and gel electrophoresis. As shown in Fig. 120 (a-c), thermal cell lysis and DNA purification was successfully performed with milk spiked with *Salmonella* bacteria for (a) 5000, (b) 500 and (c) 100 cells.

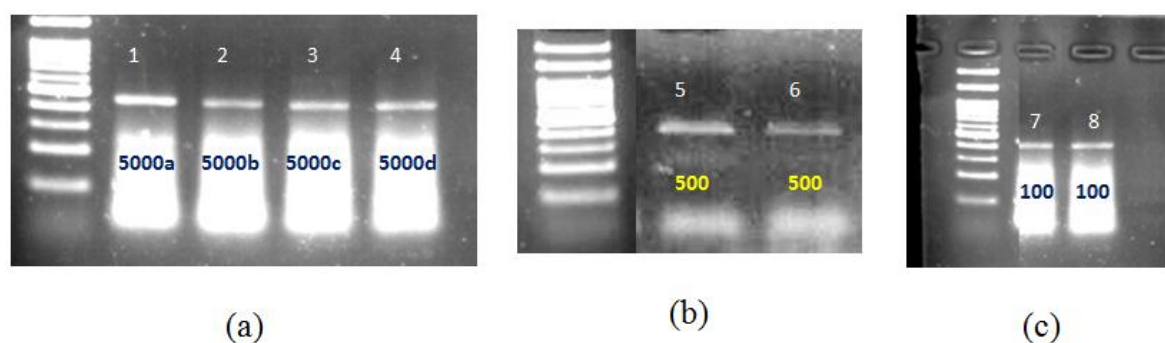


Figure 120 Agarose gel electrophoresis of *Salmonella* products from milk spiked with *Salmonella* bacteria: Off-chip PCR products: (a) Lanes 1 and 2 correspond to cell lysate from 5000 *Salmonella* cells. Lanes 3 and 4 correspond to purified *Salmonella* DNA from fraction of the initial cell lysate of 5000 *Salmonella* cells (1 μ l of sample per 15 μ l of reaction, 40 cycles), (b) Lane 5 corresponds to cell lysate from 500 cells and lane 6 corresponds to purified *Salmonella* DNA from fraction of the initial cell lysate of 500 cells (1 μ l of sample per 15 μ l of reaction, 35 cycles), (c) Lane 7 corresponds to cell lysate from 100 cells and lane 8 corresponds to purified *Salmonella* DNA from fraction of the initial cell lysate of 100 cells (1 μ l of sample per 15 μ l of reaction, 40 cycles).

Subsequently, the evaluation of the whole platform took place by integrating the *Salmonella* bacteria cell capture, lysis, and DNA purification microchip with the HDA amplification

microchip. During the last step, the eluted DNA (from the DNA purification module stemming from the captured and lysed cells from the first module) was injected to the HDA microfluidic chip, where isothermal amplification took place for 30 min at 65 °C. The collected amplified DNA was evaluated via gel electrophoresis. Fig. 121 shows a gel electrophoresis image after on chip HDA Amplification from 500 *Salmonella* cells, indicative of the successful integration of all three modules. The lanes in this figure represent standard sizing ladder (left) and the HDA product (right) from the purified DNA from 500 *Salmonella* cells.

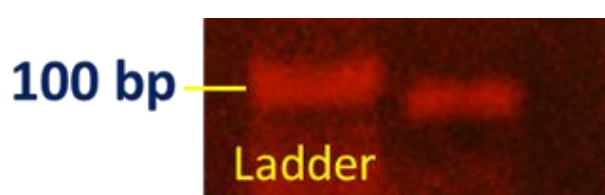


Figure 121 Agarose gel electrophoresis image of on-chip amplified DNA originating from 500 cells after integration of a bacteria cell capture and lysis microchip, the DNA purification microchip and a HDA microchip

Conclusions

To sum up, the proposed integrated Lab-on-Chip platform has all the mandatory performance standards and holds promise for its wide applicability to bacterial detection in food, clinical and water samples. The platform incorporates bacteria capture, lysis, DNA purification, and DNA amplification modules. The validation of the final prototype with *Salmonella* spiked milk was successful and described in detail in the article by K.Tsougeni, *et. al.*, A Modular Integrated Lab-On-a-Chip platform for Fast and Highly Efficient Sample Preparation for Foodborne Pathogen Screening, Sensors and Actuators B (submitted). The cell capture & lysis, the DNA purification, and the DNA amplification were performed successfully in the integrated platform, with *Salmonella* bacteria solutions of 10^5 cell/ml or 5×10^3 cells/ml and with milk spiked with *Salmonella* bacteria of three different concentrations: 5×10^4 cells/ml, 5×10^3 cells/ml, and 10^3 cells/ml (5000 cells, 500 cells and 100 cells in 100 μ l, respectively). The main disadvantage of the proposed platform apart from its relative complexity (use of many external valves and pumps) and modular integration is the limitation posed by the HDA amplification method relatively to the amplicon size (amplification product) which should not exceed 100bp. Thus, the effort for the development of portable and reliable platforms for

performing on-chip bacteria analysis in less than a few hours continued, as will be described in the next section.

8.3 Integrated platform performing RPA and on-chip detection

The two successful attempts regarding the integration of the HDA amplification μ device were followed by the implementation of the RPA method for DNA amplification which was finally selected due to the restrictions on the amplicon size for the validation of the fully integrated LoC platform using real food samples. More specifically, milk spiked with *Salmonella* was tested. More importantly, the platform comprised a SAW biosensing chip for on-chip detection of food-borne pathogens.

The LoC consists of 4 modules i) Cell capturing and Lysis, ii) DNA purification, iii) DNA amplification and iv) DNA acoustic detection via SAW sensor. The modules were assembled in a stack structure to result in a small footprint chip, of the size of a credit card. Apart from the four modules, a custom made instrument enabling the automation of the procedure was developed. The instrument comprised a temperature controller unit for driving the microheaters to the desired temperature (depending on the protocol), a SAW reader and a pump and valve controller for driving the syringe pumps and external valves. A PET microfluidic card (developed by Jobst Technologies) was used for enabling the fluidic interconnection between the various modules. Within this microfluidic card, Quake-type valves were integrated allowing the movement of the fluids towards the desired direction (subsequent module or waste line). On the same μ -fluidic card, PDMS seals were used for creating channels over the surface of the SAW sensor ensuring simultaneously leak-tightness and uniform pressure, thus enabling the acquisition of good and reproducible SAW signal. The detection scheme on the SAW biosensors was based on Neutravidin/Biotin interaction (as described in section 7.2 for QCM-D based detection of DNA). The SAW surface was functionalized with Neutravidin and the amplicons to be detected were created using biotinylated primers in the RPA reaction. Fig. 122, shows all the components comprising the credit card size stack regarding the fluidic module for DNA amplification (122a) fabricated on PMMA attached to the PCB heaters (Fig. 122b) which is glued on the PE credit card sized microfluidic card (Fig. 122c) which assists the interconnection with the cell capture, lysis and

DNA purification modules and the SAW sensor as shown in Fig. 122b and c illustrating the front and back side of the aforementioned stack.

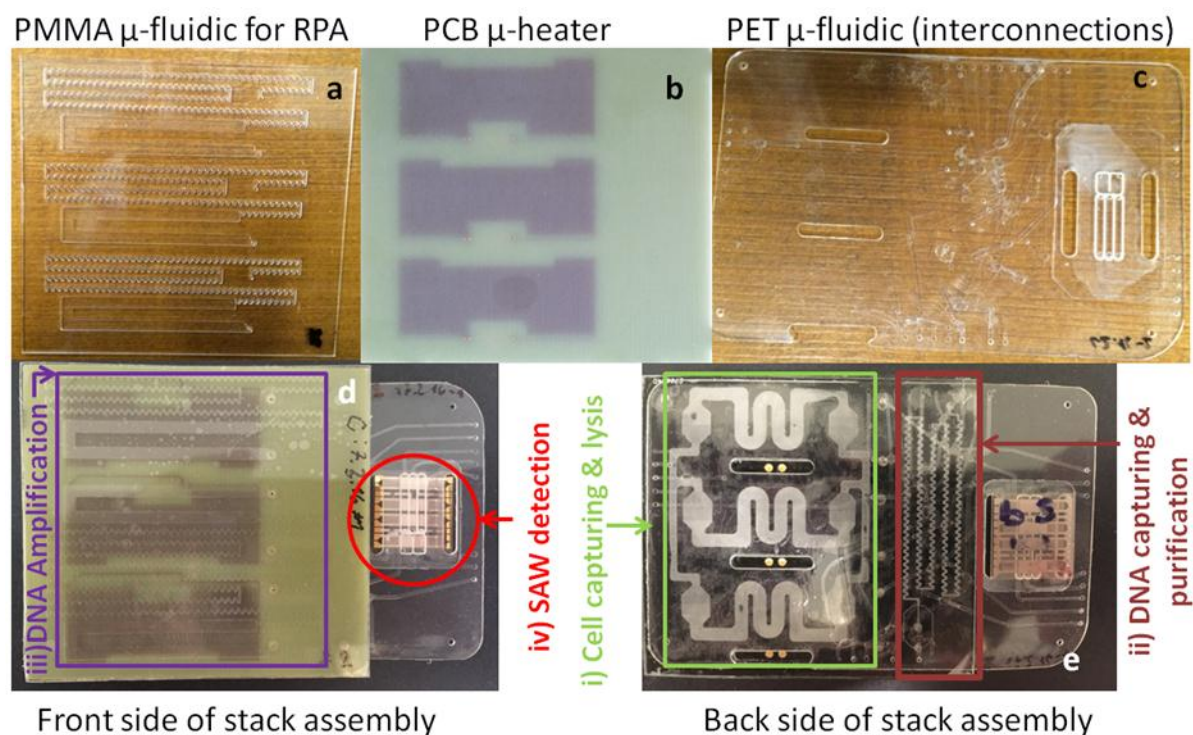


Figure 122 a) 3 μ -fluidic chips for RPA amplification on PMMA, b) PCB substrate with 3 embedded resistive μ -heaters, c) multilayer μ -fluidic card fabricated on PET enabling fluidic interconnections among the 3 modules, d) front side of the stack structure comprising the chips assembled, e) back side of the stack

The total operation time starting from loading the sample into the LoC until the completion of *Salmonella* bacteria detection in dairy products is estimated approximately ~ 130 min. In Table 20 below, the protocol steps regarding the validation of the final LoC are presented.

Table 20 Operational protocol for the LoC validation

Step	Volume (μ l)	Flow (μ l/min)	Duration (min)	Module
1. Cell capture	100	10	10	Capture
2. PBS washing	60		6	Capture
3. Cell lysis at 94° C	50	Static	13	Capture
4. Heating off, wait for $T=T_{room}$	-	Static	6	Capture
5. PBS washing	30 (waste) 50 (lysate)	10	5	Capture
6. Passivation (PEG/ethanol/NaCl)	5	10 per inlet	0.25	Purification
7. DNA capture/purification	50 (lysate)+ 50 (PEG/ethanol/NaCl)	10 per inlet	5	Purification
8. Ethanol washing	40-60	20	3	Purification
9. Water elution (DNA collection)	20 (waste) 2*50 (eluted DNA)	20	5	Purification
10. DNA amplification: reagents injection	10 DNA +40 RPA reagents	20	5	DNA amplification
11. PBS washing	50	20	5	DNA amplification
12. Incubation with heating $T=37^{\circ}\text{C}$	50	static	30	DNA amplification
13. PBS washing	100	20	10	DNA amplification
14. SAW functionalization	200	20	10	SAW biochip
15. PBS washing	200	20	10	SAW biochip
16. DNA detection on SAW	50 sample 100 buffer	50	5	SAW biochip

The first step of the procedure is the capture and thermal lysis of *S. Typhimurium*. After the on-chip functionalization, 100 μ l of the contaminated milk sample were injected in the first module of the LoC (where bacteria's capturing occurs on antibody-functionalized walls) and followed by 60 μ l of washing buffer. Cell lysis was performed at $\sim 94^{\circ}\text{C}$ for 13 min by on-chip heating provided by the PCB resistive μ -heaters. Subsequently, elution was performed with PBS and 50 μ l were pushed towards the waste line and collected, while the successive 50 μ l were pushed through the second module where DNA purification took place. Eventually elution with water was performed with 10 μ l/min per inlet (i.e. 20 μ l/min total volumetric flow). The first 20 μ l were rejected to waste in order to remove traces of Ethanol, the successive 50 μ l were pushed towards the waste line, and 10 μ l were pushed to the next module where DNA amplification took place. More specifically, the RPA method was used

for the DNA amplification. 40 μl of reagents (TwistAmp® Basic, Twist Dx) were injected and 10 μl of purified *Salmonella* DNA coming from the previous module with a flow rate of 15 $\mu\text{l}/\text{min}$. Afterwards, 50 μl of PBS were pushed in order to achieve mixing, and enable the DNA and reagents to reach the chamber where the reaction took place. Then on-chip heating was performed at 37°C for 30 min employing the integrated resistive μ -heaters. Prior to flushing the amplified DNA towards the SAW, a continuous flow of PBS buffer was pumped over the surface of the photoresist-coated SAW biochip at a flow rate of 50 $\mu\text{l}/\text{min}$. The signal was allowed to equilibrate prior to the addition of neutravidin solution (0.5 mg/ml) which was physically adsorbed on the surface. Eventually, 100 μl PBS buffer were pushed towards the next module with a flow rate of 25 $\mu\text{l}/\text{min}$, thus flushing the amplified DNA to the SAW sensor for the final detection. Finally, the amplicons were flushed over the sensor followed by further buffer rinsing. The time required for the detection step was not more than 5min. In Fig. 123 below the acoustic signal of the amplicons on the SAW is depicted. The changes in the amplitude and the phase after the rinsing step are used to calculate the acoustic ratio value that is indicative of the presence or absence of biotinylated *Salmonella* amplicons. The initial neutravidin (sensor's surface functionalization) addition is not shown.

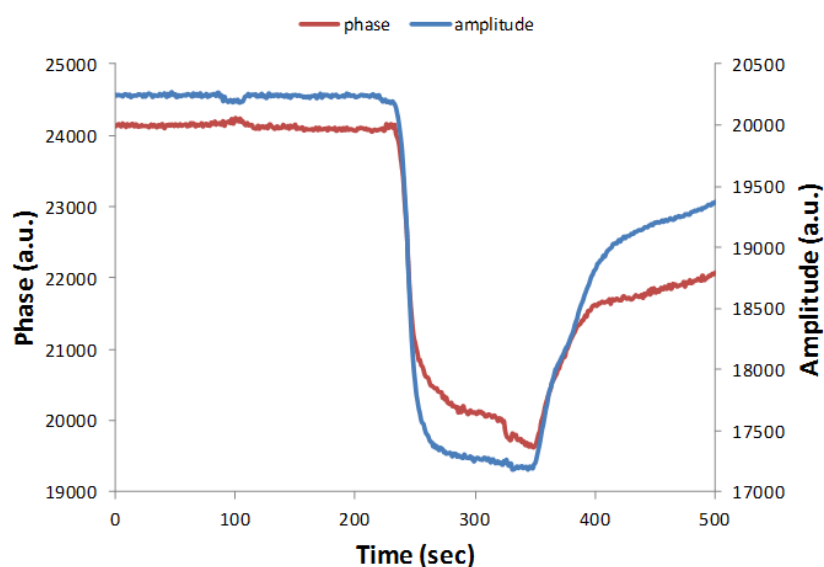


Figure 123 Acoustic monitoring of the RPA reaction addition over the neutravidin modified biochip surface (Data acquired by G. Papadakis)

Although the aforementioned step was automated (no manual steps for valves/pumps), the syringe pumps used for integration were not suitable for accommodating the volumes needed at once. Besides, the injection of the contaminated samples was performed through the

syringe pumps thus making the whole LoC prone to cross contamination. Another difficulty occasionally faced was with the operation of one internal PDMS valve within the μ -fluidic card enabling the interconnections, which often failed, after prolonged exposure to 85% ethanol (required for DNA purification).

8.4 Compact, integrated platform for on-chip sample preparation using the LAMP method and SAW detection

Through the accumulated experience acquired with the previous integration endeavours, coupled with the extremely promising results obtained with the isothermal DNA amplification based on LAMP which proved to be robust and efficient with cell lysates (thus eliminating the need for the DNA purification module), we decided to move forward towards the implementation of LAMP in the integrated LoC platform for food-pathogen detection. Due to the robustness of the LAMP method while performing amplification with cell lysates, the need for DNA purification module was eliminated, thus making the proposed system less complex. In addition, the performance of bacteria capturing, lysis and amplification was attempted in a single chamber. Therefore, the main breakthrough for the proposed integrated platform is the use of a single, compact chip which accommodates all the pre-treatment steps needed before DNA detection on a SAW chip.

In this section, a fully automated micro-nano-bio acoustic platform is presented for the first time. The proposed platform overcomes the limiting factors for implementing integrated platforms and microsystems to food quality control providing ultra-fast, sensitive and cost-effective analysis, complying with the existing legislation framework. The developed platform follows two approaches regarding the pre-treatment of the sample to be analysed. According to the first approach the capturing of the bacteria from milk is based on magnetic immunobeads whereas, the second approach relies on plasma nanotexturing of the chip and efficient antibody immobilization on the surface of the nanotextured walls. In the case of the immunobeads, the capturing step is performed manually using conventional lab equipment outside the LoC whereas in the case of the plasma nanotextured chips all the steps are performed within the LoC. The analysis time for the first approach is 4h whereas for the second approach is 6h. In both cases, the LoC platform accommodates the isothermal amplification of target-DNA in a microfluidic pre-treatment chip employing the LAMP

method, followed by a label-free detection [272] with a surface acoustic wave (SAW) sensor with a planar geometry allowing for easy integration with microfluidics. The instrument developed is common for both approaches comprising a SAW reader, a temperature controller, micropumps and a pump controller.

Regarding the first approach, a micro-nano-bio acoustic system was presented for the sensitive and rapid detection of foodborne pathogens in real samples. This system was developed in parallel with the present thesis. This platform fully integrates for the first time DNA amplification and SAW detection based on a hybridization-free acoustic detection protocol in unpurified samples with the capability of distinguishing between live and dead cells. The analysis time of the proposed system, including the pre-enrichments step, is 4 hours. The fluidics are made of PE and PDMS (Fig. 124a) housed in a custom made PMMA docking station (Fig. 124b) enabling both the fluidic and the electrical communication [253]. A schematic representation of the device surface upon addition of a positive and a negative sample is depicted in Fig. 124c. The results obtained from the validation of the LoC system are presented in Fig. 124d where the normalized amplitude changes for the detection of 10^3 whole *Salmonella* cells is illustrated.

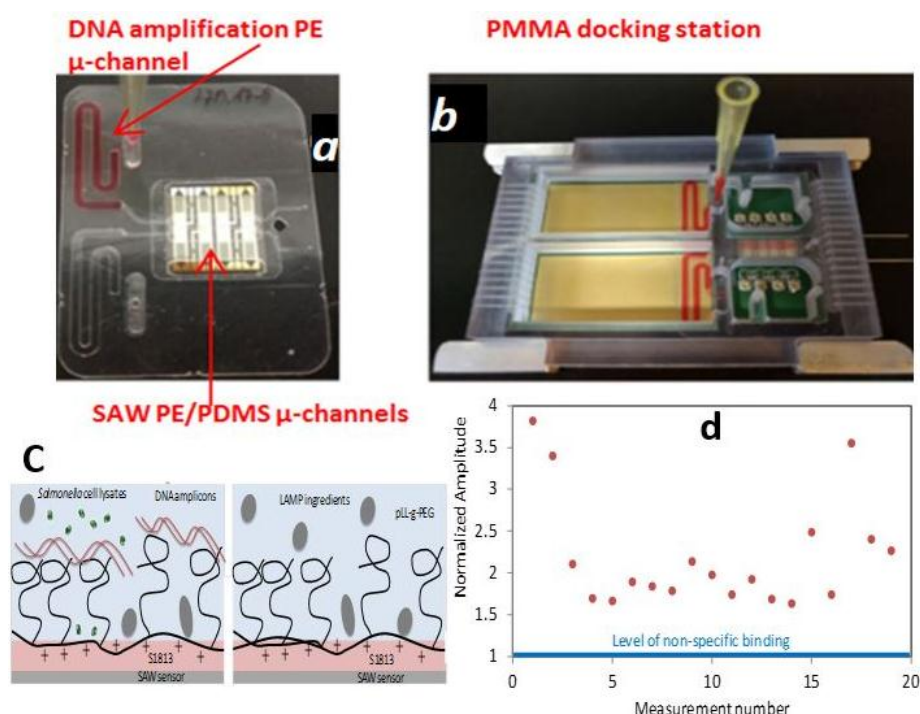


Figure 124 a) the disposable plastic card on top of the SAW biochip with two isothermal DNA amplification micro-chambers; and an extended path at the other end that flows over the 4-sensors of

the acoustic biochip, b) the PMMA docking station housing one acoustic biochip and the plastic card with the 2 amplification chambers. The plastic card lies above a PCB, where a microheater is fabricated for on-chip heating, (c) schematic representation of the device surface upon addition of a positive sample that contains ds DNA amplicons, cell lysates and LAMP ingredients (left); and as before but for a negative sample, i.e., only the LAMP ingredients (right), d) Normalized amplitude changes for the detection of 10^3 whole *Salmonella* cells with the LoC system. Each red point represents one of the 19 acoustic measurements [253].

In the following paragraphs, a detailed description of the second approach will be presented.

Pre-treatment chip description

In more detail, a single, compact PMMA chip was designed and fabricated for the cell capturing, lysis and DNA amplification. The reduction of the number of modules previously used for the sample pre-treatment from three to one made the whole system substantially more user-friendly and less complicated. In other words, the main goal was the fabrication of a chip having a simple design and small footprint combining bacteria capture, lysis and DNA amplification in one single chamber, addressing screening of *Salmonella* in food samples.

The chips comprised a meander-like microchannel and were created on 0.3 mm thick acrylic polymer substrates (Fig. 125). The method chosen for the prototyping was CNC micromilling. The width of the channels is 2.5mm, the total length of the channels is 17.4cm and the depth is 0.15mm (Fig. 125). The volume of the microchannel is 65 μ l.

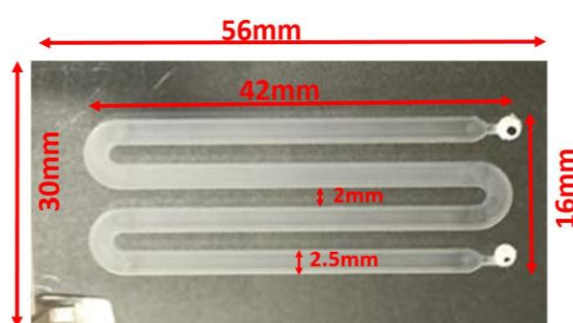


Figure 125 Image of the pre-treatment chip

After structuring the microchannel with micromilling, plasma nanotexturing followed for surface roughening to enhance the antibody binding capacity. Finally, the chips are sealed using a pressure sensitive polyolefin lamination film with silicon-based adhesive. Once the chips are patterned, antibody immobilization and freeze drying takes place for increasing the

self-life of the ready-to use chips. Otherwise, on-chip immobilization can take place prior starting the experiments. More information for on antibody immobilization and plasma treatment can be found in [274].

SAW chip array

A SAW array (16x16 mm) comprising a 4-acoustic channel design was fabricated and provided by SENSEOR SAS & GmbH, France on a ST quartz (YXI/36o) (Fig. 126). Each sensor included patterned 150 nm thick aluminium electrodes followed by a split-finger geometry resulting in an 8 μm electrode period and a 32 μm acoustic wavelength, resulting to an operating frequency of 155 MHz. A waveguiding layer of 1.2 μm thickness was formed by spin coating a S1813 photoresist (Shipley, U.S.) over the entire array. The guiding layer confines the surface acoustic wave energy on the surface and hence improves the gravimetric sensitivity. The resultant evanescent wave has a penetration depth about 150 nm in the media to probe, which is well suited for DNA detection. Next a photolithographic step was performed for opening the electrical pad access after exposure to UV light. Typical insertion losses of the fabricated devices in air were in the 25 dB range. In Fig. 126, a fabricated SAW chip is depicted; the interdigitated (IDT) electrodes are highlighted within the yellow boxes whereas the sensing area is highlighted within the blue box.

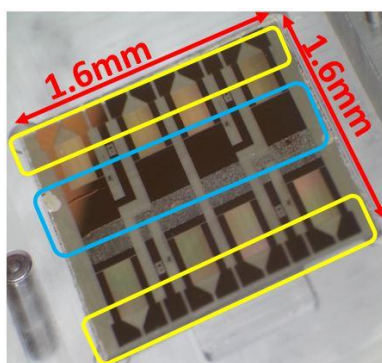


Figure 126 Image of SAW chip, SENSEOR SAS & GmbH, France

Microfluidic Card

The microfluidic cards (Fig. 127) were designed and fabricated by Jobst Technologies GmbH, Germany, from 75 μm thick polyolefin foils structured by a CNC cutter and heat-laminated to a multilayer stack. The microfluidic cards have the size of a credit card. Ultra-narrow low loss seals to the SAW chip of <100 μm seal width were created from MED-6215

silicone (NuSil Technology LLC, USA) serving as channels (highlighted in red) over the sensing area of the SAW sensor. The microfluidic cards were serving as intermediate for the fluidic interconnection of the pre-treatment chip and the SAW sensor (Fig 127 a, b). Fig. 127a and b depict a large and a small microfluidic card respectively which are subsequently connected (in blue are highlighted the points where the actual connection of the fluidics is achieved) to the pre-treatment card (Fig. 127c) resulting to the assembly shown in Fig. 127d. Either O-ring-shaped or rectangular (with the same dimensions as the pre-treatment chip pinched localised at the positions corresponding to the inlet/outlet) double-sided adhesive film was used for ensuring leak-tight connections between the pre-treatment chip and the microfluidic card. In a subsequent more sophisticated design, the pre-treatment chip was also integrated with the microfluidic card on the same substrate (Fig. 127e) thus eradicating any possible misalignment between the chip and the card. Both designs accommodate pipette compatible loading hubs enabling the injection of the sample (highlighted in green).

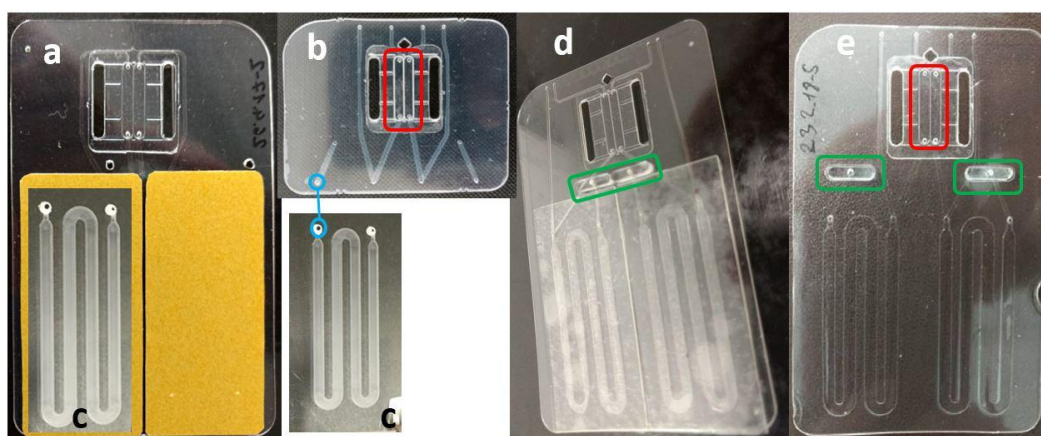


Figure 127 Types of microfluidic cards developed by Jobst Technologies GmbH and assembly with the pre-treatment chips

Docking station

The docking station (Fig.128) was designed and realized by Jobst Technologies GmbH, Germany, by means of precision CNC machining of polycarbonate parts (frame) and PCBs (electrical connections). O-ring-shaped PDMS seals (MED-6215) located on the inlets/outlets of the interface of the docking station with the microfluidic card ensure leak-tightness. The docking station (DS) houses the SAW chip, the Cu resistive microheaters, the fluidic card and the sample pre-treatment chip. In the figure below, the docking station is depicted. More specifically, Fig.128a and Fig.129b show the front and the back side respectively of the

closed DS housing the SAW chip, the μ -heaters, the μ -fluidic card and the pre-treatment chip. Fig.129c and Fig.129d show the two pieces of the interior of the docking station.

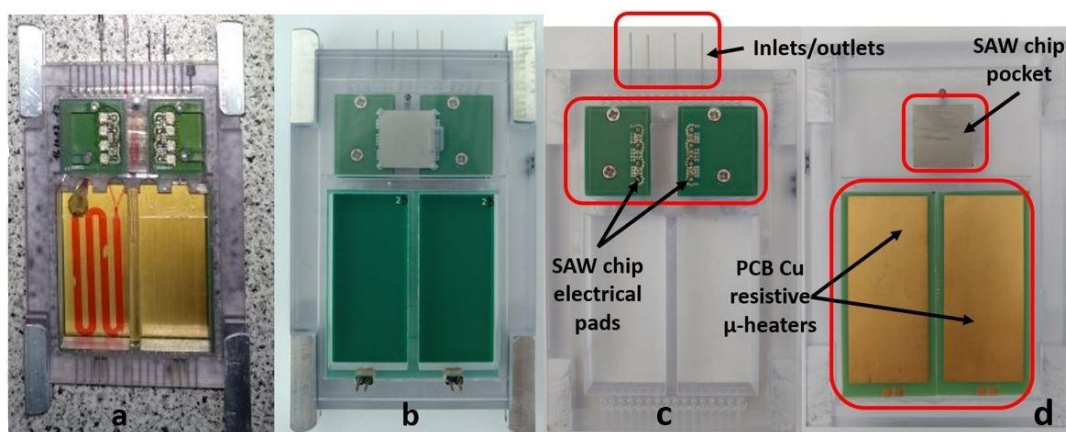


Figure 128 a) Front and b) back side of the docking station developed by Jobst Technologies, GmbH. The sample preparation microfluidic chip is shown with red dye flowing through. c)-d) Two pieces of the opened docking station.

The Cu resistive μ -heaters (Fig. 128d) were fabricated (as described in section 5.4.1) on a 0.8mm thick PCB substrate with total dimensions of 5x5.5 cm². An inner 18 μ m thick Cu layer of the PCB was used for patterning the μ -heater. The Cu tracks follow a meandering-like shape of 200 μ m width to provide the desired electrical resistance (40 Ohm approx.) so as to be compatible with the temperature controller developed. The μ -heaters provide the temperature needed for DNA amplification (through Joule heating). An external copper layer with 18 μ m thickness was used in order to maximize the temperature uniformity across the heating zone and thus improving the amplification efficiency. While in operation, good thermal contact between the μ -heater and the pre-treatment chip is ensured through mechanical pressure (via the 4 aluminium clamps) and thermally conductive paste or tape.

The whole LoC platform is depicted in Fig.129a. The electronics (Fig. 129b, interior of the instrument) to control the integrated platform are developed (with the exception of the temperature controller developed by NCSR “Demokritos”) and assembled by SENSEOR SAS, GmbH France. The electronics comprise a SAW reader, a pump controller, a temperature controller to drive the microheaters, and a power supply. The outer dimensions of the box housing the electronics are of 25 x 25 x 15 cm.

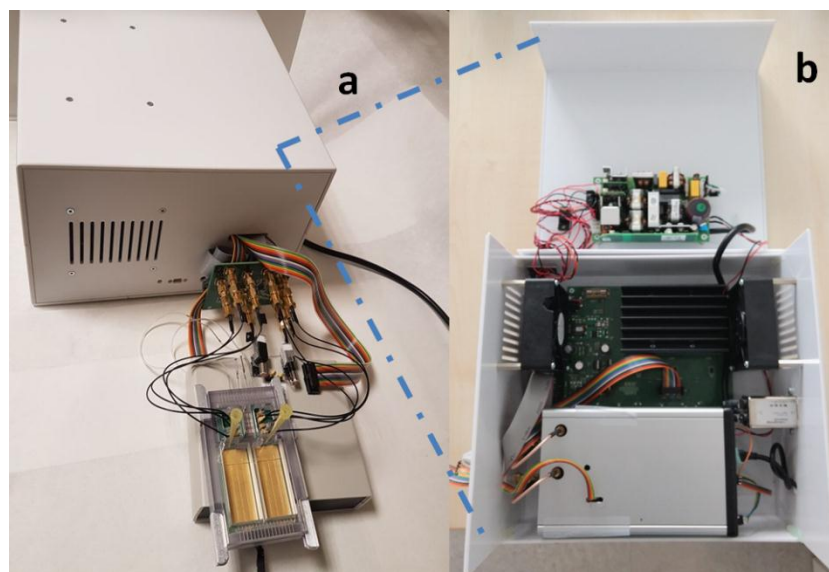


Figure 129 a) LoC platform, b) Picture of the electronic box developed by Sensor SAS, GmbH, France and electronic components inside it

Operation protocol

Fig. 130 presents the operation protocol of the integrated platform regarding the acoustic detection of *Salmonella* bacteria in milk after a short (4h) pre-culturing step. Each step of the procedure is described in more detail below.

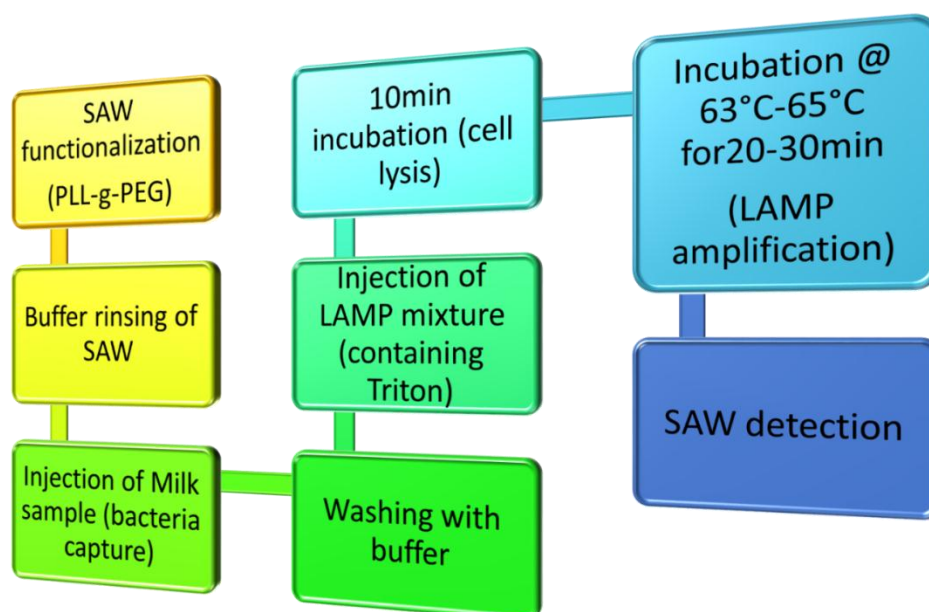


Figure 130 Operation Protocol for the LoC

Surface functionalization of SAW chip and acoustic detection

Surface functionalization was performed by injecting 90 μL of PLL-g-PEG (0.1 mg/mL) in 10mM Tris pH 7.5 followed by buffer rinsing. PLL-g-PEG copolymer can be physically adsorbed onto polymeric materials (such as photoresist) at physiological pH [253, 272]. All steps were performed at a flow rate of 20 $\mu\text{L}/\text{min}$. The surface of the sensor could be cleaned several times by rubbing gently with a cotton stick. Real time amplitude and phase changes were monitored using the electronic measuring system (SAW reader) developed by SENSEOR. Since the SAW functionalization solution should not pass through the functionalized pre-treatment chip, the functionalization of the SAW surface is performed by using a peristaltic pump connected to the waste outlet which withdraws the functionalization solution from the SAW outlet which is connected to a PCR tube (see Fig. 131).

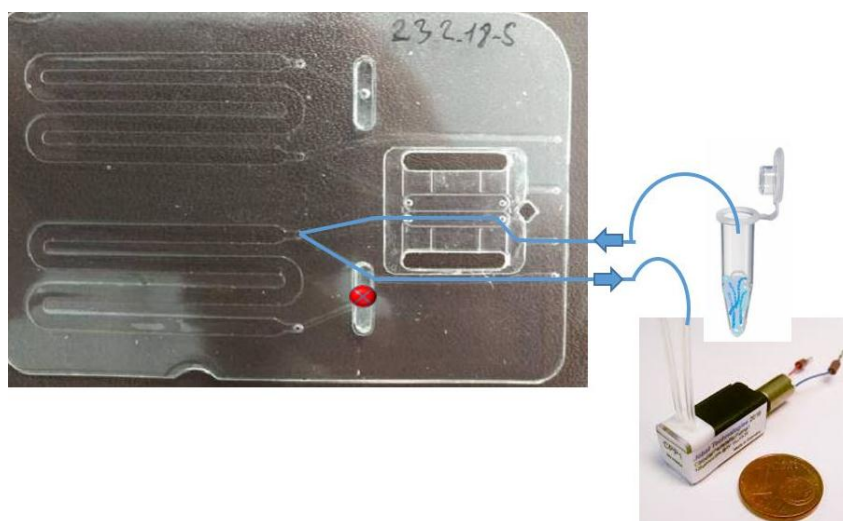


Figure 131 SAW functionalization step

Sample injection step and LAMP amplification protocol

100 μL of the sample are loaded on a pipette tip. The pipette tip is located on the pipette hub attached to the microfluidic card. The sample is then withdrawn with 10 $\mu\text{L}/\text{min}$ using a peristaltic pump which is connected to the waste outlet (Fig. 132) allowing for the bacteria to be specifically captured on the immobilized antibodies on the wall surfaces of the sample preparation chamber. Following 100 μL of buffer are loaded on a pipette tip and withdrawn with a flow rate of 20 $\mu\text{L}/\text{min}$ so as to remove any sample residues which might inhibit either the amplification reaction or hinder the surface acoustic detection.

The *Salmonella* invasion gene *invA* was targeted by a set of six primers [276], two outer (F3 and B3), two inner (FIP and BIP) and two loop (Loop-F and Loop-B). F3: CGGCCCCGATTTTCTCTGG, B3: CGGCAATAGCGTCA-CCTT, FIP: GCGCGGCATCCGCATCAATATGCCCGGTAAAC-AGATGAGT, BIP: GCGAACGGCGAAGCGTACTGTCGCAC-CGTCAAAGGAAC, Loop-F: GGCCTTCAAATC-GGCATCAAT, Loop-B: GAAAGGGAAAGCCAGCTTTACG. The LAMP reagent mix in a total volume of 75 μ l contained 37.5 μ l WarmStart 2x Master Mix (New England BioLabs), 1.8 μ M FIP and BIP, 0.1 μ M F3 and B3, 0.4 μ M Loop-F and Loop-B, and 3 μ l 0.04% Triton-X 100 for lysing the immobilized cells. Chemical lysis with Triton X-100 which is a non-ionic detergent was chosen over thermal lysis given the instability of Bst polymerase at elevated temperatures. 65 μ l from the LAMP mix are loaded on a pipette tip and aspirated through the pre-treatment chip with a peristaltic pump (20 μ l/min) connected to the waste outlet, while the SAW outlet is blocked (Fig. 132). For 10min the chip is left at room temperature for cell lysis and then the temperature is risen to 65°C for 30 min for the DNA amplification. LAMP products were analysed using electrophoresis on a 2% agarose gel containing EtBr and visualized under UV light (Fig. 133).

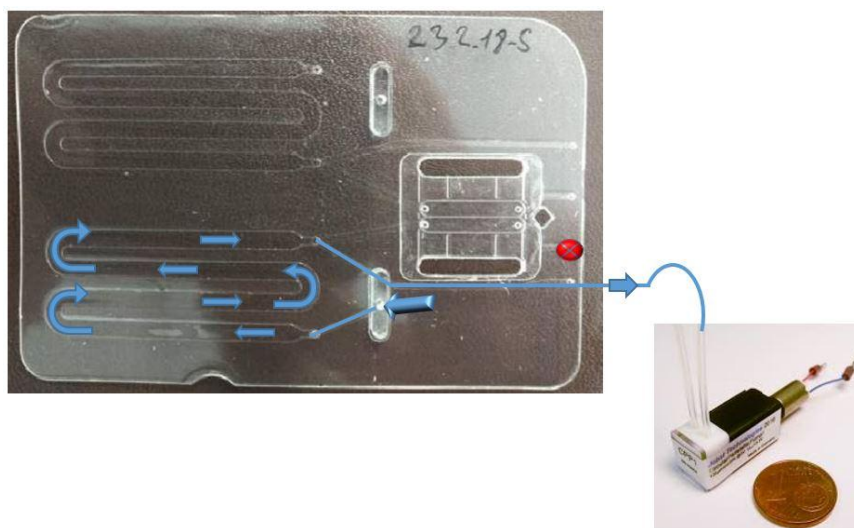


Figure 132 Sample introduction step in the sample preparation chamber

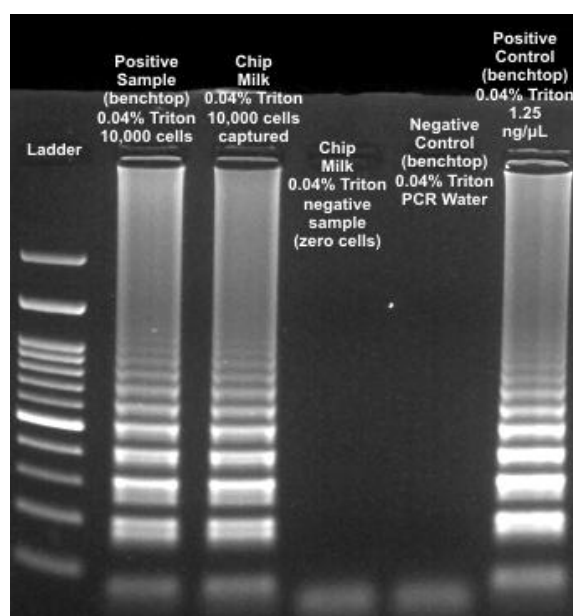


Figure 133 Example of LAMP products analysed by gel electrophoresis: lane1: ladder, lane2 positive benchtop control sample w.cells, lane3: positive on chip sample w.cells, lane 4: negative control sample on chip (no captured bacteria), lane 5: negative benchtop control, lane 6: positive benchtop control w. purified *Salmonella* DNA

Acoustic detection of LAMP amplified product

Once the LAMP amplification is over the system is left for 5min to reach room temperature (acoustic measurements are affected by temperature). Since the SAW sensor was functionalised in the beginning, it is ready to detect the amplified DNA products. The amplified product is withdrawn towards the SAW sensor using a peristaltic pump connected to the SAW outlet with a flow rate of 20 $\mu\text{L}/\text{min}$, while the waste outlet is blocked (Fig. 134). Optionally, a pipette tip can be loaded with buffer and placed on the pipette hub on the pre-treatment module for rinsing. For each experiment, both the amplitude and the phase change is monitored in real time and recorded.

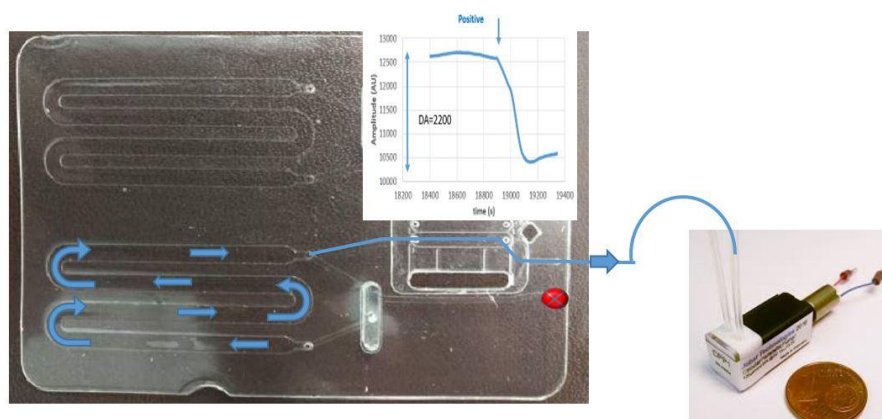


Figure 134 SAW detection step

Amplitude change proved to be more sensitive signal for DNA detection, thus the results presented are based on amplitude change. Moreover, for comparison, the signals recorded (amplitude change) for the examined positive samples were normalized based on the respective changes of negative samples (i.e., without bacteria in the amplification mixture). In Fig. 135, a representative plot of the amplitude change (in dB) for one positive (containing bacteria, red) and one negative (not containing bacteria, green) sample is illustrated. For each experiment, 4 values were recorded corresponding to the 4 channels of the SAW chip. For the positive sample, the change in the amplitude was $0.945 \pm 0.009 \text{ dB}$, whereas for the negative $0.181 \pm 0.004 \text{ dB}$. For each validation experiment, a positive and a negative sample were run through the LoC platform. Each positive signal is divided by the corresponding negative signal. In more details the process followed for data normalization is as follows: first each difference (both for positive and negative samples) was normalized to the reference value corresponding to the signal (functionalised SAW, after letting the system to cool down for 5min due to the temperature applied for performing the LAMP reaction) just before passing the sample over the SAW sensor. Next, all the negative samples were normalized to 1 (error bars set at $1\sigma = 0.45$). Last the positive samples were divided by a value corresponding to the average value of the negative samples. The cumulative normalized signals illustrated in Fig. 136 from several experiments, including both positive and negative samples, show the ratios of positive sample values (AU) over negative values (AU). In more detail, the normalized acoustic signal of 16 measurements is presented. According to the presented data, positive samples in the LoC gave a signal that on average was 2.79 ± 0.99 (AU) times above the control baseline (corresponding to the average value of the signal obtained from the negative samples) normalized to 1.

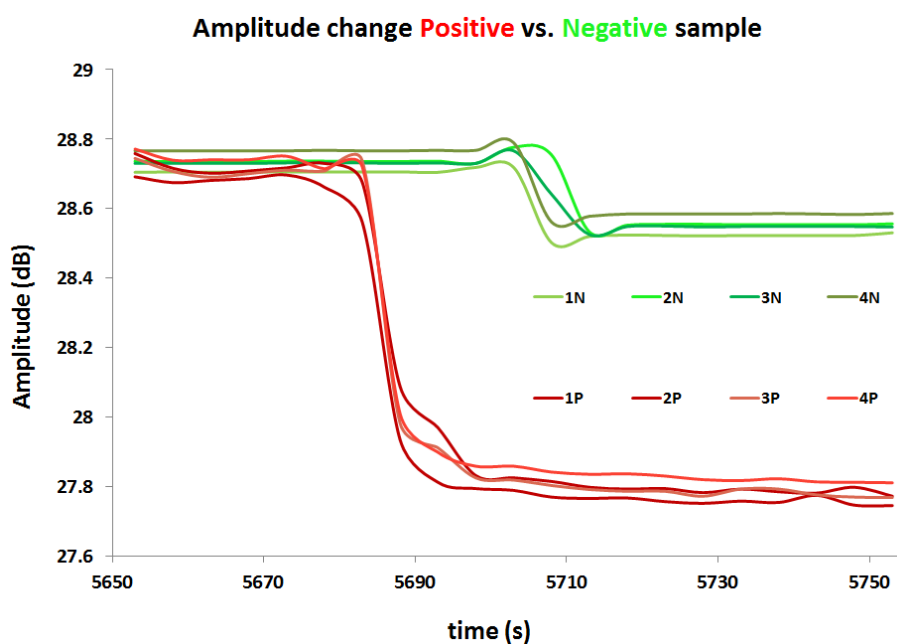


Figure 135 Real-time binding curves of LAMP products flowing sequentially over the 4 channels of the SAW sensors of the LoC. The green and red lines correspond to changes in phase (dB) for the negative and positive samples respectively.

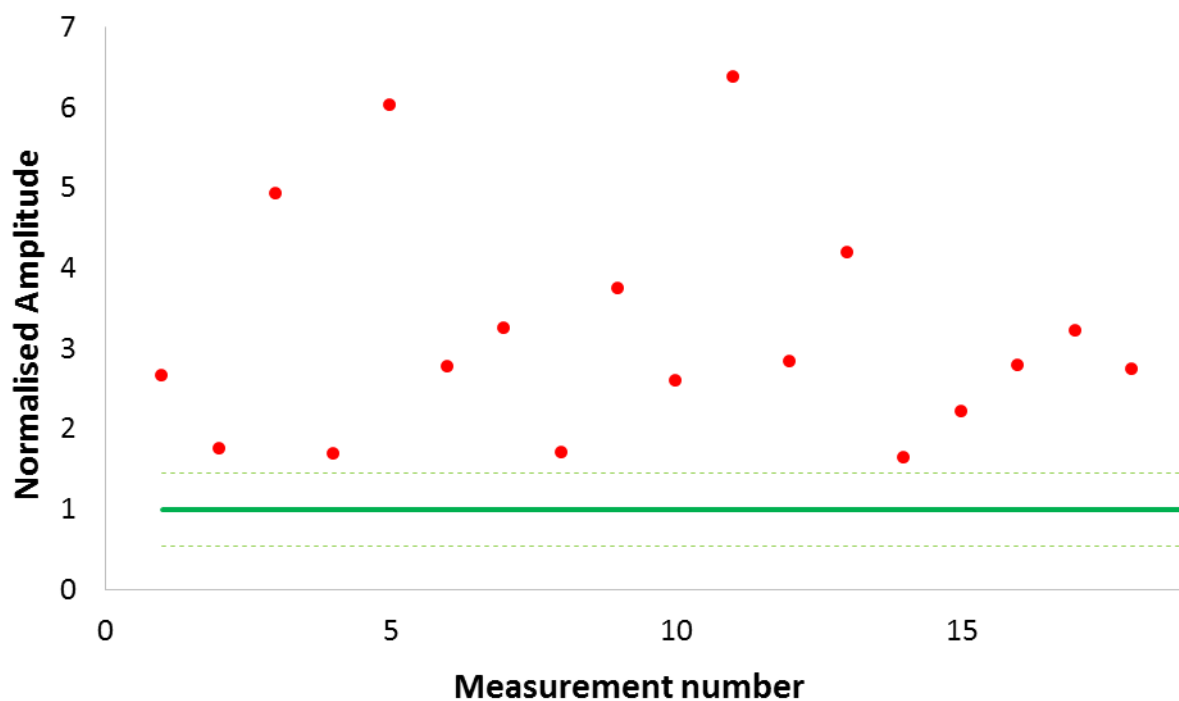


Figure 136 Normalized amplitude changes for the detection of 10^3 whole *Salmonella* cells with the LoC platform. Each red point represents one of the 16 acoustic measurements.

8.5 Conclusions

The validation of the integrated LoC was verified by performing the whole process starting from a short (4h) pre-culturing step, followed by cell capturing and lysis, DNA amplification and acoustic detection of 5-10 starting CFU in 25 ml of whole milk within less than 5h. The implementation of an extremely short pre-enrichment step is doable due to the adequate on-chip capturing efficiency (which can be further improved by using static flow) coupled with the exceptionally high amplification efficiency of the on-chip LAMP method even with whole cell lysates in combination with remarkable performance of the acoustic DNA detection in unpurified complex samples.

The present work demonstrates the first reported fully automated LoC platform combining cell capture and lysis, DNA amplification and acoustic detection. The successful combination of all pre-treatment steps (capture, lysis, amplification) in a single chamber with acoustic detection based on a label-free method, all integrated in a fully automated LoC platform resulting in a sample-to-answer time of only 6h revolutionizes the field of LoCs and promises user-friendly applications in food safety or disease diagnosis.

The combination of the advantages of on-chip pre-treatment steps with the detection power of SAW sensors paves the way to the development of a new product generation for rapid and label-free DNA analysis, addressing not only for food safety but also for point-of-care diagnostics. To sum up, four integrated platforms were presented in this chapter. Table 21 summarizes the integrated platforms presented.

Table 21 Summary of integrated platforms developed

Integrated platforms			
Amplification μ device	Sensor	Extra modules integrated	
HDA	SAW	Micromixer for enzymatic digestion	
HDA	no	Cell capturing and Lysis + DNA purification	
RPA	SAW	Cell capturing and Lysis + DNA purification	
LAMP	SAW	Cell capturing and Lysis	t<6h
LAMP	SAW		t<4h

Chapter 9 Epilogue

In the last chapter we summarize the results obtained throughout this work and we give a glimpse of the future prospects towards the on-going effort for the development of low cost, low power consuming, easy-to-use and automated LoC platforms addressing food safety, healthcare and environmental monitoring. Last, there is a list of publications (patents, papers, conferences) regarding the work conducted in the framework of this thesis.

9.1 Conclusions

The present thesis provides solutions addressing LoC platforms, especially regarding the DNA amplification microdevices which constitute the “heart”, an indispensable and really valuable component of LoCs for DNA-based pathogen detection, since amplified DNA corresponding to the pathogens stemming from minute traces can be easily and reliably detected. Numerous solutions for DNA amplification microdevices employing various amplification methods are presented.

The key features of the developed and evaluated DNA amplification microdevices are:

- The seamless fabrication of DNA amplification microdevices on commercially available PCB substrates with integrated Cu resistive microheaters lying at very close distance to the microfluidic network where the amplification takes place, thus offering great thermal contact and low power consumption.
- The sealing method proposed using a commercially available and PCB compatible polyimide-based coverlay used in an ultimately different way than the manufacturer offering robust and irreversible sealing of microdevices withstanding both high pressure and temperature addressing on of the main challenges of microfluidics industry sealing which inhibits the successful product commercialization.
- The proposed fabrication methods (UV lithography and CNC machining) which are PCB compatible thus allowing for mass production in the PCB industry reliably and with excellent reproducibility at very low cost.

- The possibility of monolithic integration on the PCB substrate, not only of the microfluidic components and the heating elements but also for other electronic components such as sensors.

A cumulative table with the developed and validated DNA amplification microdevices is presented below. For each microdevice, the amplification method, the mode of operation (continuous flow CF or Static chamber SC), the duration of the reaction, the DNA template, the energy consumption and the number of reactions performed using a battery of 10.000mAh with an output voltage of 9V are depicted.

Table 22 Cumulative table with the developed and validated DNA amplification microdevices

mode	Amplification method	Duration (min)	DNA template	no. of reactions 10Ah (9V)
CF	PCR	2	Short human	1000
CF	PCR	30	Plasmid	66
CF	PCR	30	<i>g.Salmonella</i>	66
SC	PCR	53	<i>g.Salmonella</i>	99
SC	RPA	15	<i>g.Salmonella</i>	720
SC	HDA	30	<i>g.Salmonella</i>	105
SC	LAMP	20	<i>g.Salmonella</i>	180

Due to the above mentioned key characteristics of the microdevices, several of them were used in integrated platforms. The highlight of the present thesis is the development of an automated, low cost, and sensitive LoC platform for pathogen detection. The novelty of the proposed LoC system relies on the integration of the aforementioned DNA amplification microdevices with acoustic biosensors incorporated in a Love wave acoustic chip, which is the first time ever reported. Cell capture, cell lysis and DNA amplification are accommodated in a single chip with label-free acoustic detection towards the detection of foodborne pathogens in complex samples (such as *Salmonella* in whole milk). The developed platform offers great sensitivity and rapid diagnosis time (less than 6h) for the detection of *Salmonella* cells in milk.

A cumulative table with the developed integrated LoC platform is presented below:

Table 23 Cumulative table with the developed integrated LoC platforms

Integrated platforms		
Amplification μdevice	Sensor	Extra modules
HDA	SAW	micromixer for enzymatic digestion
HDA	no	Cell capturing and Lysis + DNA purification
RPA	SAW	Cell capturing and Lysis + DNA purification
LAMP	SAW	Cell capturing and Lysis
LAMP	SAW	

Another impressive result of this work was the development of a simple method for rapid detection of unpurified PCR products from whole blood (used as template) on an appropriately functionalized QCM-D device. The proposed method consists of 2 steps (i. sample amplification and ii. acoustic detection) without any purification steps between them. The use of the blocking buffer improves the obtained results rendering the detection of the desired amplicons in an unpurified sample more efficient and accurate. The simplicity of the proposed method makes the assay applicable to Lab-on-chip (LoC) applications. Ideally, microfluidics coupled with acoustic devices amenable to miniaturization and mass production is the way forward for the realization of commercially exploitable LoC platforms. Contrary to the QCM devices which incorporate a large sensing area and thus requiring large sample volumes, SAW devices integrating various microfluidic channels are extremely attractive for developing LoCs based on acoustic detection assays, as it was also demonstrated in this work.

9.2 Suggestions for future work

According to the market forecast, the future in the microfluidics field is bright and it hasn't reached yet its full potential. Thus, our endeavours towards the development of highly efficient microdevices will not cease. The ultimate goal is the development of successful LoC platforms with seamlessly integrated microfluidic devices combining pretreatment modules and sensing elements for the detection of pathogens.

At the moment, we work towards:

- increasing the number of samples processed (chip parallelization) on the fully integrated platform in order to offer a fully integrated and automated platform suitable for multiplexing
- validating the developed platform with more complex, solid matrices (e.g. cheese)
- developing a rapid, fully automated, self-contained and yet industrialized, LoC device enabling operation by non-technical personnel for urinary tract infections (UTI). The proposed system will encompass rapid on-chip DNA amplification and accurate quantification in a single PoC diagnostic chip integrating electrochemical biosensors.

Parts of the present work have been published or are prepared for publication, as follows:

Patents

1. “Method for creating enclosed microfluidic reactors integrated with microheating elements on printed circuit board (PCB)”, A. Tserepi, S. Chatzandroulis, G. Kaprou, G. Kokkoris, K. Ellinas, D. Papageorgiou, GR20180100100,13/03/2018 (pending)
2. “An integrated PCB-based microdevice for sensitive nucleic acid detection, and method for its production” A. Tserepi, S. Chatzandroulis, D. Moschou, G. Kaprou, G. Kokkoris, GR20170100305, 30/06/2017 (pending)

Articles in journals

1. **G.D. Kaprou**, V. Papadopoulos, D.P. Papageorgiou, I. Kefala, G. Papadakis, E. Gizeli, S. Chatzandroulis, G. Kokkoris, A. Tserepi, “Ultrafast, PCB manufacturable, continuous-flow microdevice for DNA amplification”, Sensors and Actuators B, Submitted (08/2018)
2. K. Tsougeni, A.S. Kastania, **G. D. Kaprou**, Michael Eck, Gerhard Jobst, P. N. Petrou, S. E. Kakabakos, D. Mastellos, A. Tserepi and E. Gogolides, “An Integrated Lab-On-a-Chip platform for Fast and Highly Efficient Sample Preparation for Foodborne Pathogen Screening”, Sensors and Actuators B, Submitted (07/2018)

3. G. Papadakis, P. Murasova, A. Hamiot, K. Tsougeni, **G. Kaprou**, M. Eck, D. Rabus, Z. Bilkova, B. Dupuy, G. Jobst, A. Tserepi, E. Gogolides, E. Gizeli, Micro-nano-bio acoustic system for the detection of foodborne pathogens in real samples, *Biosensors and Bioelectronics* (2018) 111, pp. 52-58
4. E. Cunaj, P.S. Petrou, **G.D. Kaprou**, S.E. Kakabakos, E. Gogolides, A. Tserepi, "Stable hydrophilization of FR4 and polyimide-based substrates implemented in microfluidics-on-PCB", *Surface & Coatings Technology* (2018) 334 pp. 292–299
5. **G.D. Kaprou**, G. Papadakis, D.P. Papageorgiou, G. Kokkoris, V. Papadopoulos, I. Kefala, E. Gizeli, A. Tserepi, Miniaturized devices for isothermal DNA amplification addressing DNA diagnostics, *Microsystem Technologies* (2016) 22 (7), pp. 1529-1534.
6. N. Kefala, V. E. Papadopoulos, **G. Karpou**, G. Kokkoris, G. Papadakis, and A. Tserepi, "A labyrinth split and merge micromixer for bioanalytical applications," *Microfluidics and Nanofluidics*, (2015) 19, pp. 1047-1059
7. V.E. Papadopoulos, I.N. Kefala, **G. Kaprou**, G. Kokkoris, D. Moschou, G. Papadakis, E. Gizeli, A. Tserepi, A passive micromixer for enzymatic digestion of DNA, *Microelectronic Engineering* (2014) 124, pp. 42-46

Articles in Conference Proceedings

1. Kefala, V. Papadopoulos, G. Kaprou, G. Kokkoris, G. Papadakis, A. Tserepi, A Passive Micromixer for Bioanalytical Applications, *Proceedings of 4th Micro and Nano Flows Conference* (<http://bura.brunel.ac.uk/handle/2438/9392>).
2. G. Kaprou, G. Papadakis, G. Kokkoris, V. Papadopoulos, I. Kefala, D. Papageorgiou, E. Gizeli, A. Tserepi, Miniaturized devices towards an integrated lab-on-a-chip platform for DNA diagnostics, *Progress in Biomedical Optics and Imaging - Proceedings of SPIE* (2015) 9518, art. no. 95180G, SPIE Microtechnologies 2015
3. K. Tsougeni, A.S. Kastania, G. Kaprou, A. Tserepi, E. Gogolides, Microfluidic sample preparation components for DNA-based food pathogen detection, *20th International Conference on Miniaturized Systems for Chemistry and Life Sciences, MicroTAS 2016*, pp. 681-682

4. M. Filippidou, A. Stamouli, E. Tegou, G. Kaprou, Y. Petrou, A. Tserepi, S. Chatzandroulis, Design and fabrication of a lab-on-a-chip (LOC) incorporating DNA amplification and detection on partially reduced graphene oxide biosensors, 20th International Conference on Miniaturized Systems for Chemistry and Life Sciences, MicroTAS 2016, pp. 1031-1032

Conferences

1. Papadopoulos, V.; Kefala, I.; Kaprou, G.; Kokkoris, G.; Moschou, D.; Papadakis, G.; Gizeli, E.; Tserepi, A., A passive micromixer for enzymatic digestion of DNA, 39th International Conference on Micro & Nano Engineering, London, UK, September 16-19 (2013)
2. Kefala, V. Papadopoulos, **G. Kaprou**, G. Kokkoris, G. Papadakis, A. Tserepi, A Passive Micromixer for Bioanalytical Applications, 4th Micro and Nano Flows Conference, London, UK, 7-10 September 2014
3. **G. Kaprou**, K. Tsougeni, A. Kastania, G. Kokkoris, I. Kefala, V. Papadopoulos, G. Papadakis, E. Gizeli, S. Chatzandroulis, P. Petrou, S.E. Kakabakos, E. Gogolides, A. Tserepi, Microfluidic devices for a lab-on-a-chip platform in food safety control, Israel-Greece Joint Meeting on “Nanotechnology and BioNanoscience”, The David Lopatie Conference Center, Weizmann Institute of Science, 20-23 October 2014, Israel
4. A.S. Kastania, K. Tsougeni, **G. Kaprou**, G. Papadakis, E. Gizeli, A. Tserepi, E. Gogolides, Microfluidic components and integrated Lab on Chip for food safety control, 41st International Conference on Micro and Nano Engineering (MNE), 21-24 September 2015, Hague, The Netherlands
5. **G. Kaprou**, G. Kokkoris, G. Papadakis, V. Papadopoulos, I. Kefala, S. Chatzandroulis, E. Gizeli, A. Tserepi, DNA amplification microdevices towards diagnostic platforms for pathogen detection, Microfluidics Congress, 20-21 October 2015, London, UK
6. **G. Kaprou**, G. Papadakis, G. Kokkoris, V. Papadopoulos, I. Kefala, K. Ellinas, E. Gizeli, A. Tserepi, Miniaturized DNA amplification devices towards Lab-on-a-chip Platforms for DNA diagnostics, 6th International Conference on Micro-Nanoelectronics, Nanotechnologies & MEMs, 4-7 October 2015, Athens, Greece

7. V. Papadopoulos, I. Kefala, **G. Kaprou**, G. Kokkoris, A. Tserepi, Designing microfluidic devices for temperature sensitive biochemical reactions, 6th International Conference on Micro-Nanoelectronics, Nanotechnologies & MEMs, 4-7 October 2015, Athens, Greece
8. E. Gogolides, A. Tserepi, K. Tsougeni, A. Kastania, **G. Kaprou**, G. Kokkoris, S. Chatzandroulis, S. Kakabakos, P. Petrou, E. Gizeli, G. Papadakis, B. Dupuy, A. Hamiot, M. Eck, G. Jobst, Integrated Lab on Chip Platform for Bacteria Screening in Food Safety Control, 5th International Conference from Nanoparticles and Nanomaterials to Nanodevices and Nanosystems (IC4N), 26-30 June 2016, Porto Heli, Greece
9. K. Tsougeni, A.S. Kastania, **G. Kaprou**, A. Tserepi, E. Gogolides, Microfluidic Sample Preparation Components for Food Pathogen Detection, The 20th International Conference on Miniaturized Systems for Chemistry and Life Sciences (MicroTAS), 9-13 October 2016, Dublin, Ireland
10. Kefala, V. E. Papadopoulos, **G. Kaprou**, G. Kokkoris, A. Tserepi, Designing microfluidic devices for DNA amplification, 5th Micro and Nano Flows Conference (MNF 2016), 11-14 September 2016, Milano, Italy
11. E. Gogolides, A. Tserepi, K. Tsougeni, A. Kastania, **G. Kaprou**, Sample Preparation lab on-Chip for Detection of Foodborne Pathogens, 42nd Micro- and NanoEngineering conference (MNE 2016), 19-23 September 2016, Vienna, Austria
12. K. Tsougeni, A.S. Kastania, **G. Kaprou**, A. Tserepi, E. Gogolides, Plasma nanotextured microfluidic sample preparation components for food pathogen detection, iPlasmaNano-VII 2016 Conference, 16-20 October 2016, Vravora, Greece
13. A.S. Kastania, K. Tsougeni, **G. Kaprou**, G. Papadakis, E. Gizeli, A. Tserepi, E. Gogolides, Microfluidic components and integrated Lab on Chip for food safety control, Workshop on Application of Advanced Plasma Technologies in CE Agriculture, 17-21 April 2016, Ljubljana, Slovenia
14. Tserepi, K. Tsougeni, **G. Kaprou**, E. Gogolides, Lab-on-chip for bacteria capture, lysis, and DNA amplification addressing foodborne pathogens, Micro and Nanofluidics Flow 2017, 3-5 July 2017, Paris, France
15. **G.D. Kaprou**, G. Kokkoris, V. Papadopoulos, I. Kefala, C.M. Loukas, S. Chatzandroulis, A. Tserepi, Low-cost, mass-manufacturable, DNA amplification microdevices for diagnostics, 43rd Micro- and Nano Engineering conference (MNE 2017), 18-22 September 2017, Braga, Portugal

16. K. Tsougeni, **G. Kaprou**, C.M. Loukas, A. Tserepi, E. Gogolides, Lab on-chip for bacteria capture, lysis and DNA amplification addressing foodborne pathogens, 43rd Micro- and Nano Engineering conference (MNE 2017), 18-22 September 2017, Braga, Portugal
17. **G. Kaprou**, K. Tsougeni, C.M Loukas, G. Papadakis, A. Hamiot, M Eck, D. Rabus, G. Kokkoris, V. Papadopoulos, B. Dupuy, G. Jobst, E. Gizeli, A. Tserepi, E. Gogolides, Integrated, fast, cost effective, semi-automated Lab on a Chip for foodborne pathogen detection , 44th, Micro- and Nano Engineering conference (MNE 2018), 24-27 September 2018, Copenhagen, Denmark

References

- [1] G. M. Whitesides, "The origins and the future of microfluidics," *Nature*, vol. 442, pp. 368-373, 07/27/print 2006.
- [2] A. J. de Mello, "Focus DNA amplification: does 'small' really mean 'efficient'?", *Lab on a Chip*, vol. 1, pp. 24N-29N, 2001.
- [3] E. K. Sackmann, A. L. Fulton, and D. J. Beebe, "The present and future role of microfluidics in biomedical research," *Nature*, vol. 507, pp. 181-189, 2014.
- [4] A. Manz, N. Graber, and H. M. Widmer, "Miniaturized total chemical analysis systems: A novel concept for chemical sensing," *Sensors and Actuators B: Chemical*, vol. 1, pp. 244-248, 1990/01/01/ 1990.
- [5] S. C. Terry, J. H. Jerman, and J. B. Angell, "A gas chromatographic air analyzer fabricated on a silicon wafer," *IEEE Transactions on Electron Devices*, vol. 26, pp. 1880-1886, 1979.
- [6] A. Husein and R. S. Payne, "MEMS Commercialization: Slow but Steady," in *Transducers '01 Eurosensors XV*, Berlin, Heidelberg, 2001, pp. 1256-1259.
- [7] C. D. Chin, V. Linder, and S. K. Sia, "Commercialization of microfluidic point-of-care diagnostic devices," *Lab on a Chip*, vol. 12, pp. 2118-2134, 2012.
- [8] P. S. Dittrich and A. Manz, "Lab-on-a-chip: microfluidics in drug discovery," *Nature Reviews Drug Discovery*, vol. 5, pp. 210-218, 2006.
- [9] Q. Tu, L. Pang, Y. Zhang, M. Yuan, J. Wang, D. Wang, *et al.*, "Microfluidic Device: A Miniaturized Platform for Chemical Reactions," *Chinese Journal of Chemistry*, vol. 31, pp. 304-316, 2013.
- [10] A. A. S. Bhagat, H. Bow, H. W. Hou, S. J. Tan, J. Han, and C. T. Lim, "Microfluidics for cell separation," *Medical & biological engineering & computing*, vol. 48, pp. 999-1014, 2010.
- [11] D. Di Carlo, "Inertial microfluidics," *Lab on a Chip*, vol. 9, pp. 3038-3046, 2009.
- [12] P. Abgrall and A. M. Gué, "Lab-on-chip technologies: making a microfluidic network and coupling it into a complete microsystem—a review," 0960-1317, 2007.
- [13] J. Gardeniers, R. Tjerkstra, and A. Van den Berg, "Fabrication and application of silicon-based microchannels," in *Microreaction Technology: Industrial Prospects*, ed: Springer, 2000, pp. 36-44.
- [14] C. Iliescu and F. E. Tay, "Wet etching of glass," in *Semiconductor Conference, 2005. CAS 2005 Proceedings. 2005 International*, 2005, pp. 35-44.
- [15] M. N. Exchange.
- [16] J. O. Dennis, F. Ahmad, and H. Khir, "CMOS compatible bulk micromachining," *Advances in Micro/Nano Electromechanical Systems and Fabrication Technologies*, p. 226, 2013.
- [17] "Fabricating MEMS and Nanotechnology."

-
- [18] A. Bagolini, L. Pakula, T. Scholtes, H. Pham, P. French, and P. Sarro, "Polyimide sacrificial layer and novel materials for post-processing surface micromachining," *Journal of Micromechanics and Microengineering*, vol. 12, p. 385, 2002.
- [19] R. Klein, "Material Properties of Plastics," *Laser Welding of Plastics: Materials, Processes and Industrial Applications*, pp. 3-69, 2011.
- [20] R. J. Young and P. A. Lovell, *Introduction to polymers* vol. 2: Chapman & Hall London, 1991.
- [21] I. M. Ward and D. W. Hadley, *An introduction to the mechanical properties of solid polymers*: John Wiley & Sons Ltd.; John Wiley & Sons, Inc., 1993.
- [22] D. K. Armani and C. Liu, "Microfabrication technology for polycaprolactone, a biodegradable polymer," *Journal of Micromechanics and Microengineering*, vol. 10, p. 80, 2000.
- [23] M. Hecke and W. Schomburg, "Review on micro molding of thermoplastic polymers," *Journal of Micromechanics and Microengineering*, vol. 14, p. R1, 2003.
- [24] R. Bartolini, W. Hannan, D. Karlsons, and M. Lurie, "HOLOGRAPHY Embossed Hologram Motion Pictures for Television Playback," *Applied Optics*, vol. 9, pp. 2283-2290, 1970.
- [25] B. Ekstrom, G. Jacobson, O. Ohman, and H. Sjodin, "Microfluidic structure and process for its manufacture," ed: Google Patents, 1994.
- [26] E. Becker, W. Ehrfeld, P. Hagmann, A. Maner, and D. Münchmeyer, "Fabrication of microstructures with high aspect ratios and great structural heights by synchrotron radiation lithography, galvanofarming, and plastic moulding (LIGA process)," *Microelectronic engineering*, vol. 4, pp. 35-56, 1986.
- [27] J. O'Brien, P. Hughes, M. Brunet, B. O'Neill, J. Alderman, B. Lane, *et al.*, "Advanced photoresist technologies for microsystems," *Journal of Micromechanics and Microengineering*, vol. 11, p. 353, 2001.
- [28] Y.-S. Liao, S.-T. Chen, and C.-S. Lin, "Development of a high precision tabletop versatile CNC wire-EDM for making intricate micro parts," *Journal of Micromechanics and Microengineering*, vol. 15, p. 245, 2004.
- [29] M. Farsari, G. Filippidis, S. Zoppel, G. A. Reider, and C. Fotakis, "Efficient femtosecond laser micromachining of bulk 3C-SiC," *Journal of Micromechanics and Microengineering*, vol. 15, p. 1786, 2005.
- [30] C. S. Effenhauser, G. J. Bruin, A. Paulus, and M. Ehrat, "Integrated capillary electrophoresis on flexible silicone microdevices: analysis of DNA restriction fragments and detection of single DNA molecules on microchips," *Analytical Chemistry*, vol. 69, pp. 3451-3457, 1997.
- [31] J. S. Jeon, S. Chung, R. D. Kamm, and J. L. Charest, "Hot embossing for fabrication of a microfluidic 3D cell culture platform," *Biomedical Microdevices*, vol. 13, pp. 325-333, 2011/04/01 2011.
- [32] A. A. Yazdi, A. Popma, W. Wong, T. Nguyen, Y. Pan, and J. Xu, "3D printing: an emerging tool for novel microfluidics and lab-on-a-chip applications," *Microfluidics and Nanofluidics*, vol. 20, pp. 1-18, 2016.

- [33] X. Zhang, X. Jiang, and C. Sun, "Micro-stereolithography of polymeric and ceramic microstructures," *Sensors and Actuators A: Physical*, vol. 77, pp. 149-156, 1999.
- [34] A. K. Au, W. Lee, and A. Folch, "Mail-order microfluidics: evaluation of stereolithography for the production of microfluidic devices," *Lab on a Chip*, vol. 14, pp. 1294-1301, 2014.
- [35] M. P. Lee, G. J. Cooper, T. Hinkley, G. M. Gibson, M. J. Padgett, and L. Cronin, "Development of a 3D printer using scanning projection stereolithography," *Scientific reports*, vol. 5, p. 9875, 2015.
- [36] C. Zhou, H. Ye, and F. Zhang, "A novel low-cost stereolithography process based on vector scanning and mask projection for high-accuracy, high-speed, high-throughput, and large-area fabrication," *Journal of Computing and Information Science in Engineering*, vol. 15, p. 011003, 2015.
- [37] S. H. Park, D. Y. Yang, and K. S. Lee, "Two-photon stereolithography for realizing ultraprecise three-dimensional nano/microdevices," *Laser & Photonics Reviews*, vol. 3, pp. 1-11, 2009.
- [38] C. C. Kai, L. K. Fai, and L. Chu-Sing, *Rapid prototyping: principles and applications in manufacturing*: World Scientific Publishing Co., Inc., 2003.
- [39] S. K. Moon, Y. E. Tan, J. Hwang, and Y.-J. Yoon, "Application of 3D printing technology for designing light-weight unmanned aerial vehicle wing structures," *International Journal of Precision Engineering and Manufacturing-Green Technology*, vol. 1, pp. 223-228, 2014.
- [40] C. B. Williams, J. K. Cochran, and D. W. Rosen, "Additive manufacturing of metallic cellular materials via three-dimensional printing," *The International Journal of Advanced Manufacturing Technology*, vol. 53, pp. 231-239, 2011.
- [41] I. Campbell, D. Bourell, and I. Gibson, "Additive manufacturing: rapid prototyping comes of age," *Rapid prototyping journal*, vol. 18, pp. 255-258, 2012.
- [42] D. F. Weston, T. Smekal, D. B. Rhine, and J. Blackwell, "Fabrication of microfluidic devices in silicon and plastic using plasma etching," *Journal of Vacuum Science & Technology B: Microelectronics and Nanometer Structures Processing, Measurement, and Phenomena*, vol. 19, pp. 2846-2851, 2001/11/01 2001.
- [43] D. J. Guckenberger, T. E. de Groot, A. M. D. Wan, D. J. Beebe, and E. W. K. Young, "Micromilling: A method for ultra-rapid prototyping of plastic microfluidic devices," *Lab on a chip*, vol. 15, pp. 2364-2378, 04/23 2015.
- [44] T. Merkel, M. Graeber, and L. Pagel, "New technology for fluidic microsystems based on PCB technology," *Sensors and Actuators, A: Physical*, vol. 77, pp. 98-105, 1999.
- [45] S. Gaßmann, I. Ibendorf, and L. Pagel, "Realization of a flow injection analysis in PCB technology," *Sensors and Actuators, A: Physical*, vol. 133, pp. 231-235, 2007.
- [46] C. Aracil, F. Perdigones, J. M. Moreno, A. Luque, and J. M. Quero, "Portable Lab-on-PCB platform for autonomous micromixing," *Microelectronic Engineering*, vol. 131, pp. 13-18, 1/5/ 2015.
- [47] N.-T. Nguyen and X. Huang, "Miniature valveless pumps based on printed circuit board technique," *Sensors and Actuators A: Physical*, vol. 88, pp. 104-111, 2/15/ 2001.

-
- [48] J. Li, Y. Wang, E. Dong, and H. Chen, "USB-driven microfluidic chips on printed circuit boards," *Lab on a Chip - Miniaturisation for Chemistry and Biology*, vol. 14, pp. 860-864, 2014.
- [49] A. Wego, S. Richter, and L. Pagel, "Fluidic microsystems based on printed circuit board technology," *Journal of Micromechanics and Microengineering*, vol. 11, pp. 528-531, 2001.
- [50] S. Metz, R. Holzer, and P. Renaud, "Polyimide-based microfluidic devices," *Lab on a Chip - Miniaturization for Chemistry and Biology*, vol. 1, pp. 29-34, 2001.
- [51] E. Mavraki, D. Moschou, G. Kokkoris, N. Vourdas, S. Chatzandroulis, and A. Tserepi, "A continuous flow μ PCR device with integrated microheaters on a flexible polyimide substrate," *Procedia Engineering*, vol. 25, pp. 1245-1248, 2011.
- [52] D. Moschou, N. Vourdas, G. Kokkoris, G. Papadakis, J. Parthenios, S. Chatzandroulis, *et al.*, "All-plastic, low-power, disposable, continuous-flow PCR chip with integrated microheaters for rapid DNA amplification," *Sensors and Actuators, B: Chemical*, vol. 199, pp. 470-478, 2014.
- [53] C. Aracil, F. Perdigones, J. M. Moreno, and J. M. Quero, "BETTS: bonding, exposing and transferring technique in SU-8 for microsystems fabrication," *Journal of Micromechanics and Microengineering*, vol. 20, p. 035008, 2010.
- [54] K. Kontakis, A. Petropoulos, G. Kaltsas, T. Speliotis, and E. Gogolides, "A novel microfluidic integration technology for PCB-based devices: Application to microflow sensing," *Microelectronic Engineering*, vol. 86, pp. 1382-1384, 4// 2009.
- [55] N. Wangler, L. Gutzweiler, K. Kalkandjiev, C. Müller, F. Mayenfels, H. Reinecke, *et al.*, "High-resolution permanent photoresist laminate TMMF for sealed microfluidic structures in biological applications," *Journal of Micromechanics and Microengineering*, vol. 21, p. 095009, 2011.
- [56] L. L. Wu, L. A. Marshall, S. Babikian, C. M. Han, J. G. Santiago, and M. Bachman, "A printed circuit board based microfluidic system for point-of-care diagnostics applications," in *15th International Conference on Miniaturized Systems for Chemistry and Life Sciences (MicroTAS)* 2011, pp. 1819-1821.
- [57] L. L. Wu, S. Babikian, G. P. Li, and M. Bachman, "Microfluidic printed circuit boards," in *Proceedings - Electronic Components and Technology Conference* 2011, pp. 1576-1581.
- [58] V. E. Papadopoulos, I. N. Kefala, G. Kaprou, G. Kokkoris, D. Moschou, G. Papadakis, *et al.*, "A passive micromixer for enzymatic digestion of DNA," *Microelectronic Engineering*, vol. 124, pp. 42-46, 7/25/ 2014.
- [59] I. N. Kefala, V. E. Papadopoulos, G. Karpou, G. Kokkoris, G. Papadakis, and A. Tserepi, "A labyrinth split and merge micromixer for bioanalytical applications," *Microfluidics and Nanofluidics*, vol. 19, pp. 1047-1059, 2015.
- [60] N. Vasilakis, D. Moschou, D. Carta, H. Morgan, and T. Prodromakis, "Long-lasting FR-4 surface hydrophilisation towards commercial PCB passive microfluidics," *Applied Surface Science*, vol. 368, pp. 69-75, 4/15/ 2016.
- [61] A. W. Martinez, S. T. Phillips, M. J. Butte, and G. M. Whitesides, "Patterned Paper as a Platform for Inexpensive, Low-Volume, Portable Bioassays," *Angewandte Chemie International Edition*, vol. 46, pp. 1318-1320, 2007/02/12 2007.

- [62] X. Li, D. R. Ballerini, and W. Shen, "A perspective on paper-based microfluidics: Current status and future trends," *Biomicrofluidics*, vol. 6, p. 011301, 2012/03/01 2012.
- [63] Y. Temiz, R. D. Lovchik, G. V. Kaigala, and E. Delamarche, "Lab-on-a-chip devices: How to close and plug the lab?," *Microelectronic Engineering*, vol. 132, pp. 156-175, 1/25/ 2015.
- [64] C.-W. Tsao and D. L. DeVoe, "Bonding of thermoplastic polymer microfluidics," *Microfluidics and Nanofluidics*, vol. 6, pp. 1-16, 2009.
- [65] A. M. D. Wan, A. Sadri, and E. W. K. Young, "Liquid phase solvent bonding of plastic microfluidic devices assisted by retention grooves," *Lab on a Chip*, vol. 15, pp. 3785-3792, 2015.
- [66] A. E. Mark, A. J. Michael, and K. G. Bruce, "Determining the optimal PDMS–PDMS bonding technique for microfluidic devices," *Journal of Micromechanics and Microengineering*, vol. 18, p. 067001, 2008.
- [67] M. E. Vlachopoulou, A. Tserepi, P. Pavli, P. Argitis, M. Sanopoulou, and K. Misiakos, "A low temperature surface modification assisted method for bonding plastic substrates," *Journal of Micromechanics and Microengineering*, vol. 19, p. 015007, 2009.
- [68] R. Duer, R. Lund, R. Tanaka, D. A. Christensen, and J. N. Herron, "In-plane parallel scanning: a microarray technology for point-of-care testing," *Analytical chemistry*, vol. 82, pp. 8856-8865, 2010.
- [69] A. K. Yetisen, "Point-of-Care Diagnostics," in *Holographic Sensors*, ed: Springer, 2015, pp. 1-25.
- [70] C. Zhang, J. Xu, W. Ma, and W. Zheng, "PCR microfluidic devices for DNA amplification," *Biotechnology Advances*, vol. 24, pp. 243-284, 2006/05/01/ 2006.
- [71] F. Ahmad and S. A. Hashsham, "Miniaturized nucleic acid amplification systems for rapid and point-of-care diagnostics: A review," *Analytica Chimica Acta*, vol. 733, pp. 1-15, 7/6/ 2012.
- [72] J. Sun, Y. Gao, R. J. Isaacs, K. C. Boelte, P. C. Lin, E. M. Boczko, *et al.*, "Simultaneous on-chip DC dielectrophoretic cell separation and quantitative separation performance characterization," *Analytical chemistry*, vol. 84, pp. 2017-2024, 2012.
- [73] M. MacDonald, G. Spalding, and K. Dholakia, "Microfluidic sorting in an optical lattice," *Nature*, vol. 426, pp. 421-424, 2003.
- [74] T. Thorsen, S. J. Maerkl, and S. R. Quake, "Microfluidic large-scale integration," *Science*, vol. 298, pp. 580-584, 2002.
- [75] E. A. Schilling, A. E. Kamholz, and P. Yager, "Cell lysis and protein extraction in a microfluidic device with detection by a fluorogenic enzyme assay," *Analytical chemistry*, vol. 74, pp. 1798-1804, 2002.
- [76] A. H. Free, E. C. Adams, M. L. Kercher, H. M. Free, and M. H. Cook, "Simple specific test for urine glucose," *Clinical chemistry*, vol. 3, pp. 163-168, 1957.
- [77] L. Gervais, N. De Rooij, and E. Delamarche, "Microfluidic chips for point-of-care immunodiagnostics," *Advanced Materials*, vol. 23, 2011.

-
- [78] A. P. Xpress, "Abaxis."
- [79] Cepheid, "GeneXpert® IV."
- [80] C. D. Chin, T. Laksanasopin, Y. K. Cheung, D. Steinmiller, V. Linder, H. Parsa, *et al.*, "Microfluidics-based diagnostics of infectious diseases in the developing world," *Nature medicine*, vol. 17, pp. 1015-1019, 2011.
- [81] P. Yager, T. Edwards, E. Fu, K. Helton, K. Nelson, M. R. Tam, *et al.*, "Microfluidic diagnostic technologies for global public health," *Nature*, vol. 442, pp. 412-418, 2006.
- [82] "Waived Tests-CLIA," 2015.
- [83] i-Micronews_Yole.
- [84] Z. M. Research, "Global Point Of Care Diagnostics Market Set for Rapid Growth to Reach around USD 40.50 Billion by 2022," 2017.
- [85] MarketsandMarkets, "Point-of-Care Diagnostics Market by Products (Glucose, Cardiometabolic Monitoring, & Infectious Disease Testing Kits, Cardiac & Tumor Markers), End Users (Home, Hospitals, Ambulatory Care), Over-the- Counter & Prescription Based - Global Forecast to 2021," 2016.
- [86] M. Intelligence, "Global Point-of-care Diagnostics Market Growth, Trends & Forecasts (2016-2021)."
- [87] K. P. T. Intelligence.
- [88] Yole_Fluidigm.
- [89] K. Loens, T. Beck, D. Ursi, M. Overdijk, P. Sillekens, H. Goossens, *et al.*, "Evaluation of different nucleic acid amplification techniques for the detection of *M. pneumoniae*, *C. pneumoniae* and *Legionella* spp. in respiratory specimens from patients with community-acquired pneumonia," *Journal of microbiological methods*, vol. 73, pp. 257-262, 2008.
- [90] Y. Zhao, S. Park, B. N. Kreiswirth, C. C. Ginocchio, R. Veyret, A. Laayoun, *et al.*, "Rapid real-time nucleic acid sequence-based amplification-molecular beacon platform to detect fungal and bacterial bloodstream infections," *Journal of clinical microbiology*, vol. 47, pp. 2067-2078, 2009.
- [91] J. Jean, D. H. D'souza, and L.-A. Jaykus, "Multiplex nucleic acid sequence-based amplification for simultaneous detection of several enteric viruses in model ready-to-eat foods," *Applied and environmental microbiology*, vol. 70, pp. 6603-6610, 2004.
- [92] N. Ramalingam, T. C. San, T. J. Kai, M. Y. M. Mak, and H.-Q. Gong, "Microfluidic devices harboring unsealed reactors for real-time isothermal helicase-dependent amplification," *Microfluidics and nanofluidics*, vol. 7, p. 325, 2009.
- [93] P. Gill and A. Ghaemi, "Nucleic acid isothermal amplification technologies - A review," *Nucleosides, Nucleotides and Nucleic Acids*, vol. 27, pp. 224-243, 2008.
- [94] V. V. Demidov and N. E. Broude, *DNA amplification: current technologies and applications*: Horizon Bioscience, 2004.
- [95] A. Kornberg and T. A. Baker, *DNA replication* vol. 3: Wh Freeman New York:, 1992.
- [96] J. Kim and C. J. Easley, "Isothermal DNA amplification in bioanalysis: strategies and applications," *Bioanalysis*, vol. 3, pp. 227-239, 2011.

- [97] J. J. Carrino and H. H. Lee, "Nucleic acid amplification methods," *Journal of Microbiological Methods*, vol. 23, pp. 3-20, 1995.
- [98] J. Keer and L. Birch, "Molecular methods for the assessment of bacterial viability," *Journal of Microbiological Methods*, vol. 53, pp. 175-183, 2003.
- [99] L. M. Zanolli and G. Spoto, "Isothermal amplification methods for the detection of nucleic acids in microfluidic devices," *Biosensors*, vol. 3, pp. 18-43, 2012.
- [100] G. T. Walker, M. S. Fraiser, J. L. Schram, M. C. Little, J. G. Nadeau, and D. P. Malinowski, "Strand displacement amplification—an isothermal, in vitro DNA amplification technique," *Nucleic acids research*, vol. 20, pp. 1691-1696, 1992.
- [101] J. C. Detter, J. M. Jett, S. M. Lucas, E. Dalin, A. R. Arellano, M. Wang, *et al.*, "Isothermal strand-displacement amplification applications for high-throughput genomics," *Genomics*, vol. 80, pp. 691-698, 2002.
- [102] P. M. Lizardi, X. Huang, Z. Zhu, P. Bray-Ward, D. C. Thomas, and D. C. Ward, "Mutation detection and single-molecule counting using isothermal rolling-circle amplification," *Nature genetics*, vol. 19, pp. 225-232, 1998.
- [103] W. Zhao, M. M. Ali, M. A. Brook, and Y. Li, "Rolling circle amplification: applications in nanotechnology and biodetection with functional nucleic acids," *Angewandte Chemie International Edition*, vol. 47, pp. 6330-6337, 2008.
- [104] J. Compton, "Nucleic acid sequence-based amplification," *Nature*, vol. 350, p. 91, 1991.
- [105] B. Deiman, P. van Aarle, and P. Sillekens, "Characteristics and applications of nucleic acid sequence-based amplification (NASBA)," *Molecular biotechnology*, vol. 20, pp. 163-179, 2002.
- [106] Y.-J. Jeong, K. Park, and D.-E. Kim, "Isothermal DNA amplification in vitro: the helicase-dependent amplification system," *Cellular and molecular life sciences*, vol. 66, p. 3325, 2009.
- [107] M. Vincent, Y. Xu, and H. Kong, "Helicase-dependent isothermal DNA amplification," *EMBO Reports*, vol. 5, pp. 795-800, 2004.
- [108] O. Piepenburg, C. H. Williams, D. L. Stemple, and N. A. Armes, "DNA detection using recombination proteins," *PLoS Biol*, vol. 4, p. e204, 2006.
- [109] M. Euler, Y. Wang, O. Nentwich, O. Piepenburg, F. T. Hufert, and M. Weidmann, "Recombinase polymerase amplification assay for rapid detection of Rift Valley fever virus," *Journal of clinical virology*, vol. 54, pp. 308-312, 2012.
- [110] T. Notomi, H. Okayama, H. Masubuchi, T. Yonekawa, K. Watanabe, N. Amino, *et al.*, "Loop-mediated isothermal amplification of DNA," *Nucleic acids research*, vol. 28, pp. e63-e63, 2000.
- [111] M. Parida, S. Sannarangaiah, P. K. Dash, P. Rao, and K. Morita, "Loop mediated isothermal amplification (LAMP): a new generation of innovative gene amplification technique; perspectives in clinical diagnosis of infectious diseases," *Reviews in medical virology*, vol. 18, pp. 407-421, 2008.
- [112] N. Kurn, P. Chen, J. D. Heath, A. Kopf-Sill, K. M. Stephens, and S. Wang, "Novel isothermal, linear nucleic acid amplification systems for highly multiplexed applications," *Clinical chemistry*, vol. 51, pp. 1973-1981, 2005.

-
- [113] T. Uemori, H. Mukai, O. Takeda, M. Moriyama, Y. Sato, S. Hokazono, *et al.*, "Investigation of the molecular mechanism of ICAN, a novel gene amplification method," *Journal of biochemistry*, vol. 142, pp. 283-292, 2007.
- [114] F. B. Dean, S. Hosono, L. Fang, X. Wu, A. F. Faruqi, P. Bray-Ward, *et al.*, "Comprehensive human genome amplification using multiple displacement amplification," *Proceedings of the National Academy of Sciences*, vol. 99, pp. 5261-5266, 2002.
- [115] A. Hellani, S. Coskun, A. Tbakhi, and S. Al-Hassan, "Clinical application of multiple displacement amplification in preimplantation genetic diagnosis," *Reproductive biomedicine online*, vol. 10, pp. 376-380, 2005.
- [116] K. Mullis, F. Faloona, S. Scharf, R. Saiki, G. Horn, and H. Erlich, "Specific enzymatic amplification of DNA in vitro: the polymerase chain reaction " in *Cold Spring Harbor symposia on quantitative biology* 1986, pp. 263-273.
- [117] ck12, "The Polymerase Chain Reaction - Advanced."
- [118] H. Erlich, *PCR technology: principles and applications for DNA amplification*: Springer, 2015.
- [119] T. Kojima, Y. Takei, M. Ohtsuka, Y. Kawarasaki, T. Yamane, and H. Nakano, "PCR amplification from single DNA molecules on magnetic beads in emulsion: application for high-throughput screening of transcription factor targets," *Nucleic acids research*, vol. 33, pp. e150-e150, 2005.
- [120] L. An, W. Tang, T. A. Ranalli, H.-J. Kim, J. Wytiaz, and H. Kong, "Characterization of a thermostable UvrD helicase and its participation in helicase-dependent amplification," *Journal of Biological Chemistry*, vol. 280, pp. 28952-28958, 2005.
- [121] M. Vincent, Y. Xu, and H. Kong, "Helicase-dependent isothermal DNA amplification," *EMBO reports*, vol. 5, pp. 795-800, 2004.
- [122] Y. Li, N. Kumar, A. Gopalakrishnan, C. Ginocchio, R. Manji, M. Bythrow, *et al.*, "Detection and species identification of malaria parasites by isothermal tHDA amplification directly from human blood without sample preparation," *The Journal of Molecular Diagnostics*, vol. 15, pp. 634-641, 2013.
- [123] V. Tröger, K. Niemann, C. Gärtig, and D. Kuhlmeier, "Isothermal Amplification and Quantification of Nucleic Acids and its Use in Microsystems," *Journal of Nanomedicine & Nanotechnology*, vol. 6, p. 1, 2015.
- [124] J. Banér, M. Nilsson, M. Mendel-Hartvig, and U. Landegren, "Signal amplification of padlock probes by rolling circle replication," *Nucleic acids research*, vol. 26, pp. 5073-5078, 1998.
- [125] W. Zhao, M. A. Brook, and Y. Li, "Periodic assembly of nanospecies on repetitive DNA sequences generated on gold nanoparticles by rolling circle amplification," *Nanostructure Design: Methods and Protocols*, pp. 79-90, 2008.
- [126] R. Johne, H. Müller, A. Rector, M. Van Ranst, and H. Stevens, "Rolling-circle amplification of viral DNA genomes using phi29 polymerase," *Trends in microbiology*, vol. 17, pp. 205-211, 2009.
- [127] T. Conze, J. Göransson, H. R. Razzaghian, O. Ericsson, D. Öberg, G. Akusjärvi, *et al.*, "Single molecule analysis of combinatorial splicing," *Nucleic acids research*, vol. 38, pp. e163-e163, 2010.

- [128] D. Y. Zhang, W. Zhang, X. Li, and Y. Konomi, "Detection of rare DNA targets by isothermal ramification amplification," *Gene*, vol. 274, pp. 209-216, 2001.
 - [129] T. Murakami, J. Sumaoka, and M. Komiyama, "Sensitive isothermal detection of nucleic-acid sequence by primer generation–rolling circle amplification," *Nucleic acids research*, vol. 37, pp. e19-e19, 2009.
 - [130] S. Lutz, P. Weber, M. Focke, B. Faltin, J. Hoffmann, C. Müller, *et al.*, "Microfluidic lab-on-a-foil for nucleic acid analysis based on isothermal recombinase polymerase amplification (RPA)," *Lab on a Chip - Miniaturisation for Chemistry and Biology*, vol. 10, pp. 887-893, 2010.
 - [131] O. Piepenburg, C. H. Williams, D. L. Stemple, and N. A. Armes, "DNA Detection Using Recombination Proteins," *PLoS Biology*, vol. 4, p. e204, 06/13
- 02/09/received
- 04/18/accepted 2006.
- [132] T. Notomi, "Loop-mediated isothermal amplification," *Nihon rinsho. Japanese journal of clinical medicine*, vol. 65, pp. 957-961, 2007.
 - [133] Y. Mori, K. Nagamine, N. Tomita, and T. Notomi, "Detection of loop-mediated isothermal amplification reaction by turbidity derived from magnesium pyrophosphate formation," *Biochemical and biophysical research communications*, vol. 289, pp. 150-154, 2001.
 - [134] I. Boubourakas, S. Fukuta, and P. Kyriakopoulou, "Sensitive and rapid detection of peach latent mosaic viroid by the reverse transcription loop-mediated isothermal amplification," *Journal of virological methods*, vol. 160, pp. 63-68, 2009.
 - [135] M. C. Giuffrida and G. Spoto, "Integration of isothermal amplification methods in microfluidic devices: Recent advances," *Biosensors and Bioelectronics*, vol. 90, pp. 174-186, 2017/04/15/ 2017.
 - [136] M. A. Northrup, C. Gonzalez, D. Hadley, R. F. Hills, P. Landre, S. Lehew, *et al.*, "A Mems-based Miniature DNA Analysis System," in *Transducers '95* 1995, pp. 764-767.
 - [137] B. Vogelstein and K. W. Kinzler, "Digital PCR," *Proceedings of the National Academy of Sciences*, vol. 96, p. 9236, 1999.
 - [138] Y. Schaerli, R. C. Wootton, T. Robinson, V. Stein, C. Dunsby, M. A. A. Neil, *et al.*, "Continuous-Flow Polymerase Chain Reaction of Single-Copy DNA in Microfluidic Microdroplets," *Analytical Chemistry*, vol. 81, pp. 302-306, 2009/01/01 2009.
 - [139] C. M. Hindson, J. R. Chevillet, H. A. Briggs, E. N. Gallichotte, I. K. Ruf, B. J. Hindson, *et al.*, "Absolute quantification by droplet digital PCR versus analog real-time PCR," *Nature Methods*, vol. 10, p. 1003, 09/01/online 2013.
 - [140] B. Bruijns, A. van Asten, R. Tiggelaar, and H. Gardeniers, "Microfluidic Devices for Forensic DNA Analysis: A Review," *Biosensors*, vol. 6, p. 41, 2016.
 - [141] J. El-Ali, I. R. Perch-Nielsen, C. R. Poulsen, D. D. Bang, P. Telleman, and A. Wolff, "Simulation and experimental validation of a SU-8 based PCR thermocycler chip with integrated heaters and temperature sensor," *Sensors and Actuators A: Physical*, vol. 110, pp. 3-10, 2004/02/01/ 2004.

-
- [142] H.-B. Liu, N. Ramalingam, Y. Jiang, C.-C. Dai, K. M. Hui, and H.-Q. Gong, "Rapid distribution of a liquid column into a matrix of nanoliter wells for parallel real-time quantitative PCR," *Sensors and Actuators B: Chemical*, vol. 135, pp. 671-677, 2009/01/15/ 2009.
- [143] Y. Zhang, Y. Zhu, B. Yao, and Q. Fang, "Nanolitre droplet array for real time reverse transcription polymerase chain reaction," *Lab on a Chip*, vol. 11, pp. 1545-1549, 2011.
- [144] Y. Liu, C. Li, Z. Li, D. Chan Samuel, D. Eto, W. Wu, *et al.*, "On-chip quantitative PCR using integrated real-time detection by capillary electrophoresis," *ELECTROPHORESIS*, vol. 37, pp. 545-552, 2016/02/01 2015.
- [145] M. U. Kopp, A. J. De Mello, and A. Manz, "Chemical amplification: Continuous-flow PCR on a chip," *Science*, vol. 280, pp. 1046-1048, 1998.
- [146] P. J. Obeid and T. K. Christopoulos, "Continuous-flow DNA and RNA amplification chip combined with laser-induced fluorescence detection," *Analytica Chimica Acta*, vol. 494, pp. 1-9, 2003/10/08/ 2003.
- [147] H. Qi, X. Wang, T. Chen, X. Ma, and T. Zuo, "Fabrication and characterization of a polymethyl methacrylate continuous-flow PCR microfluidic chip using CO₂ laser ablation," *Microsystem Technologies*, vol. 15, pp. 1027-1030, 2009/07/01 2009.
- [148] D. Moschou, N. Vourdas, G. Kokkoris, G. Papadakis, J. Parthenios, S. Chatzandroulis, *et al.*, "All-plastic, low-power, disposable, continuous-flow PCR chip with integrated microheaters for rapid DNA amplification," *Sensors and Actuators B: Chemical*, vol. 199, pp. 470-478, 8// 2014.
- [149] A. C. Hatch, T. Ray, K. Lintecum, and C. Youngbull, "Continuous flow real-time PCR device using multi-channel fluorescence excitation and detection," *Lab on a Chip*, vol. 14, pp. 562-568, 2014.
- [150] D. J. Sadler, R. Changrani, P. Roberts, C. Chia-Fu, and F. Zenhausern, "Thermal management of BioMEMS: temperature control for ceramic-based PCR and DNA detection devices," *IEEE Transactions on Components and Packaging Technologies*, vol. 26, pp. 309-316, 2003.
- [151] Z. Chen, S. Qian, W. R. Abrams, D. Malamud, and H. H. Bau, "Thermosiphon-Based PCR Reactor: Experiment and Modeling," *Analytical Chemistry*, vol. 76, pp. 3707-3715, 2004/07/01 2004.
- [152] B. Minqiang, M. Tracy, E. Graham, S. W. James, and G. R. E. Alan, "Design and theoretical evaluation of a novel microfluidic device to be used for PCR," *Journal of Micromechanics and Microengineering*, vol. 13, p. S125, 2003.
- [153] W. Wei, L. Zhi-Xin, L. Rong, L. Shu-Hai, X. Ai-Dong, and Y. Yong-Jun, "Droplet-based micro oscillating-flow PCR chip," *Journal of Micromechanics and Microengineering*, vol. 15, p. 1369, 2005.
- [154] O. Frey, S. Bonneick, A. Hierlemann, and J. Lichtenberg, "Autonomous microfluidic multi-channel chip for real-time PCR with integrated liquid handling," *Biomedical Microdevices*, vol. 9, pp. 711-718, 2007/10/01 2007.
- [155] J. Nie, Y. Zhao, and N. Peng, "Multichannel oscillatory-flow PCR micro-fluidic chip with controllable temperature gradient," *Microsystem Technologies*, vol. 21, pp. 41-48, 2015/01/01 2015.

- [156] L. Zhang, B. Ding, Q. Chen, Q. Feng, L. Lin, and J. Sun, "Point-of-care-testing of nucleic acids by microfluidics," *TrAC Trends in Analytical Chemistry*, vol. 94, pp. 106-116, 2017/09/01/ 2017.
- [157] M. Safavieh, M. K. Kanakasabapathy, F. Tarlan, M. U. Ahmed, M. Zourob, W. Asghar, *et al.*, "Emerging Loop-Mediated Isothermal Amplification-Based Microchip and Microdevice Technologies for Nucleic Acid Detection," *ACS Biomaterials Science & Engineering*, vol. 2, pp. 278-294, 2016/03/14 2016.
- [158] Seung J. Oh, Byung H. Park, Jae H. Jung, G. Choi, D. C. Lee, D. H. Kim, *et al.*, "Centrifugal loop-mediated isothermal amplification microdevice for rapid, multiplex and colorimetric foodborne pathogen detection," *Biosensors and Bioelectronics*, vol. 75, pp. 293-300, 2016/01/15/ 2016.
- [159] J. T. Connelly, J. P. Rolland, and G. M. Whitesides, "'Paper Machine' for Molecular Diagnostics," *Analytical Chemistry*, vol. 87, pp. 7595-7601, 2015/08/04 2015.
- [160] T.-H. Kim, J. Park, C.-J. Kim, and Y.-K. Cho, "Fully Integrated Lab-on-a-Disc for Nucleic Acid Analysis of Food-Borne Pathogens," *Analytical Chemistry*, vol. 86, pp. 3841-3848, 2014/04/15 2014.
- [161] G. Choi, J. H. Jung, B. H. Park, S. J. Oh, J. H. Seo, J. S. Choi, *et al.*, "A centrifugal direct recombinase polymerase amplification (direct-RPA) microdevice for multiplex and real-time identification of food poisoning bacteria," *Lab on a Chip*, vol. 16, pp. 2309-2316, 2016.
- [162] L. A. Tortajada-Genaro, S. Santiago-Felipe, M. Amasia, A. Russom, and A. Maquieira, "Isothermal solid-phase recombinase polymerase amplification on microfluidic digital versatile discs (DVDs)," *RSC Advances*, vol. 5, pp. 29987-29995, 2015.
- [163] S. H. Chung, C. Baek, V. T. Cong, and J. Min, "The microfluidic chip module for the detection of murine norovirus in oysters using charge switchable micro-bead beating," *Biosensors and Bioelectronics*, vol. 67, pp. 625-633, 2015/05/15/ 2015.
- [164] S. J. Reinholt, A. Behrent, C. Greene, A. Kalfe, and A. J. Baeumner, "Isolation and Amplification of mRNA within a Simple Microfluidic Lab on a Chip," *Analytical Chemistry*, vol. 86, pp. 849-856, 2014/01/07 2014.
- [165] K. Pardee, A. A. Green, M. K. Takahashi, D. Braff, G. Lambert, J. W. Lee, *et al.*, "Rapid, Low-Cost Detection of Zika Virus Using Programmable Biomolecular Components," *Cell*, vol. 165, pp. 1255-1266, 2016/05/19/ 2016.
- [166] H. Y. Heo, S. Chung, Y. T. Kim, D. H. Kim, and T. S. Seo, "A valveless rotary microfluidic device for multiplex point mutation identification based on ligation-rolling circle amplification," *Biosensors and Bioelectronics*, vol. 78, pp. 140-146, 2016/04/15/ 2016.
- [167] M. Kuhnemund, D. Witters, M. Nilsson, and J. Lammertyn, "Circle-to-circle amplification on a digital microfluidic chip for amplified single molecule detection," *Lab on a Chip*, vol. 14, pp. 2983-2992, 2014.
- [168] T. Konry, I. Smolina, M. Yarmush Joel, D. Irimia, and L. Yarmush Martin, "Ultrasensitive Detection of Low-Abundance Surface-Marker Protein Using Isothermal Rolling Circle Amplification in a Microfluidic Nanoliter Platform," *Small*, vol. 7, pp. 395-400, 2011/02/07 2010.

-
- [169] M. Mahalanabis, J. Do, H. Almuayad, J. Y. Zhang, and C. M. Klapperich, "An integrated disposable device for DNA extraction and helicase dependent amplification," *Biomedical Microdevices*, vol. 12, pp. 353-359, 2010.
- [170] S. Huang, J. Do, M. Mahalanabis, A. Fan, L. Zhao, L. Jepeal, *et al.*, "Low Cost Extraction and Isothermal Amplification of DNA for Infectious Diarrhea Diagnosis," *PLOS ONE*, vol. 8, p. e60059, 2013.
- [171] G. Kaprou, G. Papadakis, D. Papageorgiou, G. Kokkoris, V. Papadopoulos, I. Kefala, *et al.*, "Miniaturized devices for isothermal DNA amplification addressing DNA diagnostics," *Microsystem Technologies*, vol. 22, pp. 1529-1534, 2016.
- [172] J. West, B. Karamata, B. Lillis, J. P. Gleeson, J. Alderman, J. K. Collins, *et al.*, "Application of magnetohydrodynamic actuation to continuous flow chemistry," *Lab on a Chip*, vol. 2, pp. 224-230, 2002.
- [173] O. Lazcka, F. J. D. Campo, and F. X. Muñoz, "Pathogen detection: A perspective of traditional methods and biosensors," *Biosensors and Bioelectronics*, vol. 22, pp. 1205-1217, 2/15/ 2007.
- [174] D. P. Chandler, "Advances towards integrated biodetection systems for environmental molecular microbiology," *Current issues in molecular biology*, vol. 4, pp. 19-32, 2002.
- [175] C. Lui, N. C. Cady, and C. A. Batt, "Nucleic acid-based detection of bacterial pathogens using integrated microfluidic platform systems," *Sensors*, vol. 9, pp. 3713-3744, 2009.
- [176] D. Ivnitski, D. J. O Neil, A. Gattuso, R. Schlicht, M. Calidonna, and R. Fisher, "Nucleic acid approaches for detection and identification of biological warfare and infectious disease agents," *Biotechniques*, vol. 35, pp. 862-869, 2003.
- [177] M. S. Green, R. D. Balicer, D. Cohen, I. Wiser, and J. Zenilman, *Risk assessment and risk communication strategies in bioterrorism preparedness*: Springer, 2007.
- [178] J. E. Bennett, R. Dolin, and M. J. Blaser, *Principles and practice of infectious diseases*: Elsevier Health Sciences, 2014.
- [179] C. Sensen and H. S. Mohtashim, "Biosensors-on-chip: a topical review," *Journal of Micromechanics and Microengineering*, vol. 27, p. 083001, 2017.
- [180] T. Vo-Dinh and B. Cullum, "Biosensors and biochips: advances in biological and medical diagnostics," *Fresenius' journal of analytical chemistry*, vol. 366, pp. 540-551, 2000.
- [181] L. C. Clark and C. Lyons, "Electrode systems for continuous monitoring in cardiovascular surgery," *Annals of the New York Academy of sciences*, vol. 102, pp. 29-45, 1962.
- [182] P. D'Orazio, "Biosensors in clinical chemistry," *Clinica Chimica Acta*, vol. 334, pp. 41-69, 2003.
- [183] I. E. Tothill, "Biosensors developments and potential applications in the agricultural diagnosis sector," *Computers and Electronics in Agriculture*, vol. 30, pp. 205-218, 2001.
- [184] J. Wang, *Analytical electrochemistry*: John Wiley & Sons, 2006.

- [185] K. R. Rogers and M. Mascini, "Biosensors for field analytical monitoring," *Field Analytical Chemistry & Technology*, vol. 2, pp. 317-331, 1998.
- [186] S. Laschi, M. Fránek, and M. Mascini, "Screen-printed electrochemical immunosensors for PCB detection," *Electroanalysis*, vol. 12, pp. 1293-1298, 2000.
- [187] M. Yang, M. E. McGovern, and M. Thompson, "Genosensor technology and the detection of interfacial nucleic acid chemistry," *Analytica Chimica Acta*, vol. 346, pp. 259-275, 1997.
- [188] E. Paleček, "Past, present and future of nucleic acids electrochemistry," *Talanta*, vol. 56, pp. 809-819, 2002.
- [189] D. Ivnitski, I. Abdel-Hamid, P. Atanasov, and E. Wilkins, "Biosensors for detection of pathogenic bacteria," *Biosensors and Bioelectronics*, vol. 14, pp. 599-624, 1999.
- [190] P. M. Milos, "Emergence of single-molecule sequencing and potential for molecular diagnostic applications," *Expert review of molecular diagnostics*, vol. 9, pp. 659-666, 2009.
- [191] V. M. Ugaz, R. D. Elms, R. C. Lo, F. A. Shaikh, and M. A. Burns, "Microfabricated electrophoresis systems for DNA sequencing and genotyping applications: current technology and future directions," *Philosophical Transactions of the Royal Society of London A: Mathematical, Physical and Engineering Sciences*, vol. 362, pp. 1105-1129, 2004.
- [192] P. Gascoyne, J. Satayavivad, and M. Ruchirawat, "Microfluidic approaches to malaria detection," *Acta tropica*, vol. 89, pp. 357-369, 2004.
- [193] P. Liu and R. A. Mathies, "Integrated microfluidic systems for high-performance genetic analysis," *Trends in biotechnology*, vol. 27, pp. 572-581, 2009.
- [194] T. Kubik, K. Bogunia-Kubik, and M. Sugisaka, "Nanotechnology on duty in medical applications," *Current pharmaceutical biotechnology*, vol. 6, pp. 17-33, 2005.
- [195] K. Ramanathan and B. Danielsson, "Principles and applications of thermal biosensors," *Biosensors and Bioelectronics*, vol. 16, pp. 417-423, 2001.
- [196] V. Ferrari and R. Lucklum, "Overview of acoustic-wave microsensors," *Piezoelectric transducers and applications*, pp. 39-59, 2008.
- [197] M. J. Vellekoop, "Acoustic wave sensors and their technology," *Ultrasonics*, vol. 36, pp. 7-14, 1998/02/01/ 1998.
- [198] Z. Xu and Y. J. Yuan, "Implementation of guiding layers of surface acoustic wave devices: A review," *Biosensors and Bioelectronics*, vol. 99, pp. 500-512, 2018/01/15/ 2018.
- [199] M. Ferrari, *BioMEMS and Biomedical Nanotechnology: Volume IV: Biomolecular Sensing, Processing and Analysis* vol. 4: Springer Science & Business Media, 2007.
- [200] R. Lucklum, C. Behling, and P. Hauptmann, "Gravimetric and non-gravimetric chemical quartz crystal resonators," *Sensors and Actuators B: Chemical*, vol. 65, pp. 277-283, 2000.
- [201] E. Gizeli, N. J. Goddard, C. R. Lowe, and A. C. Stevenson, "A Love plate biosensor utilising a polymer layer," *Sensors and Actuators B: Chemical*, vol. 6, pp. 131-137, 1992/01/01/ 1992.

-
- [202] G. Kovacs, G. Lubking, M. Vellekoop, and A. Venema, "Love waves for (bio)-chemical sensing in liquids," in *Ultrasonics Symposium, 1992. Proceedings., IEEE 1992*, 1992, pp. 281-285.
- [203] J. Du, G. Harding, J. A. Ogilvy, P. Dencher, and M. Lake, "A study of Love-wave acoustic sensors," *Sensors and Actuators A: Physical*, vol. 56, pp. 211-219, 1996.
- [204] X. Ding, P. Li, S.-C. S. Lin, Z. S. Stratton, N. Nama, F. Guo, *et al.*, "Surface acoustic wave microfluidics," *Lab on a Chip*, vol. 13, pp. 3626-3649, 2013.
- [205] G. Papadakis, J. M. Friedt, M. Eck, D. Rabus, G. Jobst, and E. Gizeli, "Optimized acoustic biochip integrated with microfluidics for biomarkers detection in molecular diagnostics," *Biomedical Microdevices*, vol. 19, p. 16, 2017/03/29 2017.
- [206] K. Mitsakakis and E. Gizeli, "Detection of multiple cardiac markers with an integrated acoustic platform for cardiovascular risk assessment," *Analytica Chimica Acta*, vol. 699, pp. 1-5, 2011/08/05/ 2011.
- [207] S. Krishnamoorthy, A. A. Iliadis, T. Bei, and G. P. Chrousos, "An interleukin-6 ZnO/SiO₂/Si surface acoustic wave biosensor," *Biosensors and Bioelectronics*, vol. 24, pp. 313-318, 2008/10/15/ 2008.
- [208] M. Perpeet, S. Glass, T. Gronewold, A. Kiwitz, A. Malavé, I. Stoyanov, *et al.*, "SAW Sensor System for Marker-Free Molecular Interaction Analysis," *Analytical Letters*, vol. 39, pp. 1747-1757, 2006/07/01 2006.
- [209] K. Saha, F. Bender, and E. Gizeli, "Comparative Study of IgG Binding to Proteins G and A: Nonequilibrium Kinetic and Binding Constant Determination with the Acoustic Waveguide Device," *Analytical Chemistry*, vol. 75, pp. 835-842, 2003/02/01 2003.
- [210] D. Matatagui, D. Moynet, M. J. Fernández, J. Fontecha, J. P. Esquivel, I. Gràcia, *et al.*, "Detection of bacteriophages in dynamic mode using a Love-wave immunosensor with microfluidics technology," *Sensors and Actuators B: Chemical*, vol. 185, pp. 218-224, 2013/08/01/ 2013.
- [211] D. Matatagui, L. J. Fontecha, J. M. Fernández, I. Gràcia, C. Cané, P. J. Santos, *et al.*, "Love-Wave Sensors Combined with Microfluidics for Fast Detection of Biological Warfare Agents," *Sensors*, vol. 14, 2014.
- [212] F. Fournel, E. Baco, M. Mamani-Matsuda, M. Degueil, B. Bennetau, D. Moynet, *et al.*, "Love wave biosensor for real-time detection of okadaic acid as DSP phycotoxin," *Sensors and Actuators B: Chemical*, vol. 170, pp. 122-128, 2012/07/31/ 2012.
- [213] K. Mitsakakis, A. Tserepi, and E. Gizeli, "Integration of Microfluidics With a Love Wave Sensor for the Fabrication of a Multisample Analytical Microdevice," *Journal of Microelectromechanical Systems*, vol. 17, pp. 1010-1019, 2008.
- [214] K. Mitsakakis, A. Tsortos, and E. Gizeli, "Quantitative determination of protein molecular weight with an acoustic sensor; significance of specific versus non-specific binding," *Analyst*, vol. 139, pp. 3918-3925, 2014.
- [215] K. Mitsakakis, S. Sekula-Neuner, S. Lenhert, H. Fuchs, and E. Gizeli, "Convergence of Dip-Pen Nanolithography and acoustic biosensors towards a rapid-analysis multi-sample microsystem," *Analyst*, vol. 137, pp. 3076-3082, 2012.
- [216] I. Gammoudi, V. Raimbault, H. Tarbague, F. Moroté, C. Grauby-Heywang, A. Othmane, *et al.*, "Enhanced bio-inspired microsensor based on

- microfluidic/bacteria/love wave hybrid structure for continuous control of heavy metals toxicity in liquid medium," *Sensors and Actuators B: Chemical*, vol. 198, pp. 278-284, 2014/07/31/ 2014.
- [217] F. Zhang, S. Li, K. Cao, P. Wang, Y. Su, X. Zhu, *et al.*, "A Microfluidic Love-Wave Biosensing Device for PSA Detection Based on an Aptamer Beacon Probe," *Sensors*, vol. 15, 2015.
- [218] LPKF.
- [219] Fluke.
- [220] F. A325sc.
- [221] Flir.
- [222] I. Corporation.
- [223] LabSmith.
- [224] G. miniplus3.
- [225] peqStar.
- [226] iCycler.
- [227] B.-R. Electrophoresis.
- [228] B.-I. SYSTEMS.
- [229] G. Kaprou, G. Papadakis, G. Kokkoris, V. Papadopoulos, I. Kefala, D. Papageorgiou, *et al.*, "Miniaturized devices towards an integrated lab-on-a-chip platform for DNA diagnostics," in *Progress in Biomedical Optics and Imaging - Proceedings of SPIE*, 2015, p. 95180G.
- [230] Dupont.
- [231] F. AvilÉS, O. Ceh, and A. I. Oliva, "PHYSICAL PROPERTIES OF AU AND AL THIN FILMS MEASURED BY RESISTIVE HEATING," *Surface Review and Letters*, vol. 12, pp. 101-106, 2005/02/01 2005.
- [232] N. M. McCurry, "Aluminum temperature coefficient of resistance vs. grain structure," 1993.
- [233] R. B. Belser and W. H. Hicklin, "Temperature Coefficients of Resistance of Metallic Films in the Temperature Range 25° to 600°C," *Journal of Applied Physics*, vol. 30, pp. 313-322, 1959/03/01 1959.
- [234] A. I. Oliva and J. M. Lugo, "Measurement of the Temperature Coefficient of Resistance in Metallic Films with Nano-thickness," *International Journal of Thermophysics*, vol. 37, p. 35, 2016/02/10 2016.
- [235] J. H. Park, T. N. Sut, J. A. Jackman, A. R. Ferhan, B. K. Yoon, and N.-J. Cho, "Controlling adsorption and passivation properties of bovine serum albumin on silica surfaces by ionic strength modulation and cross-linking," *Physical Chemistry Chemical Physics*, vol. 19, pp. 8854-8865, 2017.
- [236] M. Kanoatov and S. N. Krylov, "DNA Adsorption to the Reservoir Walls Causing Irreproducibility in Studies of Protein–DNA Interactions by Methods of Kinetic Capillary Electrophoresis," *Analytical Chemistry*, vol. 83, pp. 8041-8045, 2011/10/15 2011.

-
- [237] S. Lan, M. Veiseh, and M. Zhang, "Surface modification of silicon and gold-patterned silicon surfaces for improved biocompatibility and cell patterning selectivity," *Biosensors and Bioelectronics*, vol. 20, pp. 1697-1708, 2005/03/15/ 2005.
- [238] E. Cunaj, P. S. Petrou, G. D. Kaprou, S. E. Kakabakos, E. Gogolides, and A. Tserepi, "Stable hydrophilization of FR4 and polyimide-based substrates implemented in microfluidics-on-PCB," *Surface and Coatings Technology*, vol. 334, pp. 292-299, 2018/01/25/ 2018.
- [239] K. Shen, X. Chen, M. Guo, and J. Cheng, "A microchip-based PCR device using flexible printed circuit technology," *Sensors and Actuators B: Chemical*, vol. 105, pp. 251-258, 3/28/ 2005.
- [240] S. Haeberle and R. Zengerle, "Microfluidic platforms for lab-on-a-chip applications," *Lab on a Chip - Miniaturisation for Chemistry and Biology*, vol. 7, pp. 1094-1110, 2007.
- [241] D. Mark, S. Haeberle, G. Roth, F. Von Stetten, and R. Zengerle, "Microfluidic lab-on-a-chip platforms: Requirements, characteristics and applications," *Chemical Society Reviews*, vol. 39, pp. 1153-1182, 2010.
- [242] P. J. Asiello and A. J. Baeumner, "Miniaturized isothermal nucleic acid amplification, a review," *Lab on a Chip - Miniaturisation for Chemistry and Biology*, vol. 11, pp. 1420-1430, 2011.
- [243] X. Fang, Y. Liu, J. Kong, and X. Jiang, "Loop-mediated isothermal amplification integrated on microfluidic chips for point-of-care quantitative detection of pathogens," *Analytical Chemistry*, vol. 82, pp. 3002-3006, 2010.
- [244] L. Mahmoudian, N. Kaji, M. Tokeshi, M. Nilsson, and Y. Baba, "Rolling circle amplification and circle-to-circle amplification of a specific gene integrated with electrophoretic analysis on a single chip," *Analytical Chemistry*, vol. 80, pp. 2483-2490, 2008.
- [245] A. Wu, L. Wang, E. Jensen, R. Mathies, and B. Boser, "Modular integration of electronics and microfluidic systems using flexible printed circuit boards," *Lab on a Chip*, vol. 10, pp. 519-521, 2010.
- [246] D. Moschou, N. Vourdas, M. K. Filippidou, V. Tsouti, G. Kokkoris, G. Tsekenis, *et al.*, "Integrated biochip for PCR-based DNA amplification and detection on capacitive biosensors," *Progress in Biomedical Optics and Imaging - Proceedings of SPIE*, vol. 8765, 2013.
- [247] M. A. Unger, H.-P. Chou, T. Thorsen, A. Scherer, and S. R. Quake, "Monolithic Microfabricated Valves and Pumps by Multilayer Soft Lithography," *Science*, vol. 288, p. 113, 2000.
- [248] V. E. Papadopoulos, G. Kokkoris, I. N. Kefala, and A. Tserepi, "Comparison of continuous-flow and static-chamber μ PCR devices through a computational study: the potential of flexible polymeric substrates," *Microfluidics and Nanofluidics*, vol. 19, pp. 867-882, 2015.
- [249] P. A. Vorkas, K. Christopoulos, C. Kroupis, and E. S. Lianidou, "Mutation scanning of exon 20 of the BRCA1 gene by high-resolution melting curve analysis," *Clinical Biochemistry*, vol. 43, pp. 178-185, 2010.

- [250] K. Shen, X. Chen, M. Guo, and J. Cheng, "A microchip-based PCR device using flexible printed circuit technology," *Sensors and Actuators, B: Chemical*, vol. 105, pp. 251-258, 2005.
- [251] TwistDx_RPA.
- [252] S. Chen, F. Wang, J. C. Beaulieu, R. E. Stein, and B. Ge, "Rapid Detection of Viable Salmonellae in Produce by Coupling Propidium Monoazide with Loop-Mediated Isothermal Amplification," *Applied and Environmental Microbiology*, vol. 77, pp. 4008-4016, 02/16/received 04/10/accepted 2011.
- [253] G. Papadakis, P. Murasova, A. Hamiot, K. Tsougeni, G. Kaprou, M. Eck, *et al.*, "Micro-nano-bio acoustic system for the detection of foodborne pathogens in real samples," *Biosensors and Bioelectronics*, vol. 111, pp. 52-58, 2018/07/15/ 2018.
- [254] A. Morgan, "Developments in Glass Yarns and Fabric Constructions," *The PCB Magazine*, pp. 78-88, 2014, March.
- [255] W. Lu, J. Wang, Q. Wu, J. Sun, Y. Chen, L. Zhang, *et al.*, "High-throughput sample-to-answer detection of DNA/RNA in crude samples within functionalized micro-pipette tips," *Biosensors and Bioelectronics*, vol. 75, pp. 28-33, 2016/01/15/ 2016.
- [256] Z. Zhang, M. B. Kermekchiev, and W. M. Barnes, "Direct DNA Amplification from Crude Clinical Samples Using a PCR Enhancer Cocktail and Novel Mutants of Taq," *The Journal of Molecular Diagnostics*, vol. 12, pp. 152-161, 2010.
- [257] N. Tomita, Y. Mori, H. Kanda, and T. Notomi, "Loop-mediated isothermal amplification (LAMP) of gene sequences and simple visual detection of products," *Nature Protocols*, vol. 3, p. 877, 04/24/online 2008.
- [258] G. Papadakis, A. Tsortos, A. Kordas, I. Tiniakou, E. Morou, J. Vontas, *et al.*, "Acoustic detection of DNA conformation in genetic assays combined with PCR," *Scientific Reports*, vol. 3, p. 2033, 06/19/online 2013.
- [259] G. Papadakis and E. Gizeli, "Screening for mutations in BRCA1 and BRCA2 genes by measuring the acoustic ratio with QCM," *Analytical Methods*, vol. 6, pp. 363-371, 2014.
- [260] A. Tsortos, G. Papadakis, K. Mitsakakis, K. A. Melzak, and E. Gizeli, "Quantitative Determination of Size and Shape of Surface-Bound DNA Using an Acoustic Wave Sensor," *Biophysical Journal*, vol. 94, pp. 2706-2715, 2008.
- [261] A. Tsortos, G. Papadakis, and E. Gizeli, "On the Hydrodynamic Nature of DNA Acoustic Sensing," *Analytical Chemistry*, vol. 88, pp. 6472-6478, 2016/06/21 2016.
- [262] D. Milioni, A. Tsortos, M. Velez, and E. Gizeli, "Extracting the Shape and Size of Biomolecules Attached to a Surface as Suspended Discrete Nanoparticles," *Analytical Chemistry*, vol. 89, pp. 4198-4203, 2017/04/04 2017.
- [263] J. Cai, C. Yao, J. Xia, J. Wang, M. Chen, J. Huang, *et al.*, "Rapid parallelized and quantitative analysis of five pathogenic bacteria by ITS hybridization using QCM biosensor," *Sensors and Actuators B: Chemical*, vol. 155, pp. 500-504, 2011/07/20/ 2011.

-
- [264] S.-R. Hong, H.-D. Jeong, and S. Hong, "QCM DNA biosensor for the diagnosis of a fish pathogenic virus VHSV," *Talanta*, vol. 82, pp. 899-903, 2010/08/15/ 2010.
- [265] G. Papadakis, A. Tsortos, F. Bender, E. E. Ferapontova, and E. Gizeli, "Direct Detection of DNA Conformation in Hybridization Processes," *Analytical Chemistry*, vol. 84, pp. 1854-1861, 2012/02/21 2012.
- [266] I. Mannelli, M. Minunni, S. Tombelli, and M. Mascini, "Quartz crystal microbalance (QCM) affinity biosensor for genetically modified organisms (GMOs) detection," *Biosensors and Bioelectronics*, vol. 18, pp. 129-140, 2003/03/01/ 2003.
- [267] G. Papadakis, N. Skandalis, A. Dimopoulou, P. Glynos, and E. Gizeli, "Bacteria Murmur: Application of an Acoustic Biosensor for Plant Pathogen Detection," *PLOS ONE*, vol. 10, p. e0132773, 2015.
- [268] S. Sheikh, D. Y. Yang, C. Blaszykowski, and M. Thompson, "Single ether group in a glycol-based ultra-thin layer prevents surface fouling from undiluted serum," *Chemical Communications*, vol. 48, pp. 1305-1307, 2012.
- [269] C. Blaszykowski, S. Sheikh, and M. Thompson, "Surface chemistry to minimize fouling from blood-based fluids," *Chemical Society Reviews*, vol. 41, pp. 5599-5612, 2012.
- [270] G. L. Kenausis, J. Vörös, D. L. Elbert, N. Huang, R. Hofer, L. Ruiz-Taylor, *et al.*, "Poly(l-lysine)-g-Poly(ethylene glycol) Layers on Metal Oxide Surfaces: Attachment Mechanism and Effects of Polymer Architecture on Resistance to Protein Adsorption," *The Journal of Physical Chemistry B*, vol. 104, pp. 3298-3309, 2000/04/01 2000.
- [271] R. Schlapak, D. Armitage, N. Saucedo-Zeni, W. Chrzanowski, M. Hohage, D. Caruana, *et al.*, "Selective protein and DNA adsorption on PLL-PEG films modulated by ionic strength," *Soft Matter*, vol. 5, pp. 613-621, 2009.
- [272] G. Papadakis, P. Palladino, D. Chronaki, A. Tsortos, and E. Gizeli, "Sample-to-answer acoustic detection of DNA in complex samples," *Chemical Communications*, vol. 53, pp. 8058-8061, 2017.
- [273] Y. Hiller, J. M. Gershoni, E. A. Bayer, and M. Wilchek, "Biotin binding to avidin. Oligosaccharide side chain not required for ligand association," *Biochemical Journal*, vol. 248, pp. 167-171, 1987.
- [274] K. Tsougeni, G. Papadakis, M. Gianneli, A. Grammoustianou, V. Constantoudis, B. Dupuy, *et al.*, "Plasma nanotextured polymeric lab-on-a-chip for highly efficient bacteria capture and lysis," *Lab on a Chip*, 2016.
- [275] A. S. Kastania, K. Tsougeni, G. Papadakis, E. Gizeli, G. Kokkoris, A. Tserepi, *et al.*, "Plasma micro-nanotextured polymeric micromixer for DNA purification with high efficiency and dynamic range," *Analytica Chimica Acta*, vol. 942, pp. 58-67, 2016/10/26/ 2016.
- [276] Chen, S.; Wang, F.; Beaulieu, J. C.; Stein, R. E.; Ge, B., "Rapid detection of viable *Salmonellae* in produce by coupling propidium monoazide with loop-mediated isothermal amplification," *Appl. Environ. Microbiol.*, vol. 77, pp. 4008–4016, 2011.